Science of Climate Change

Volume 4.2
2024

https://scienceofclimatechange.org

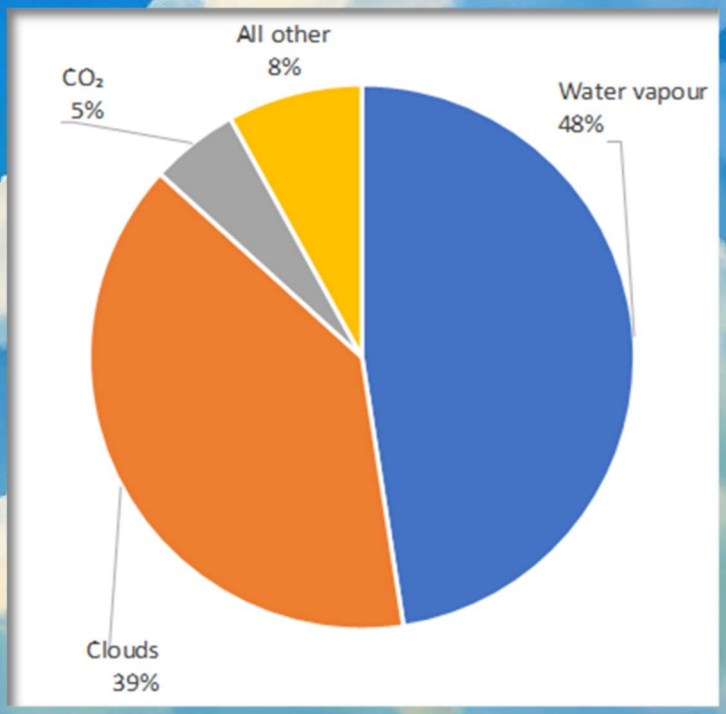

Published by: Klimarealistene (Org.no.995314592)

ISSN2703-9080(print) ISNN2703-9072(online)

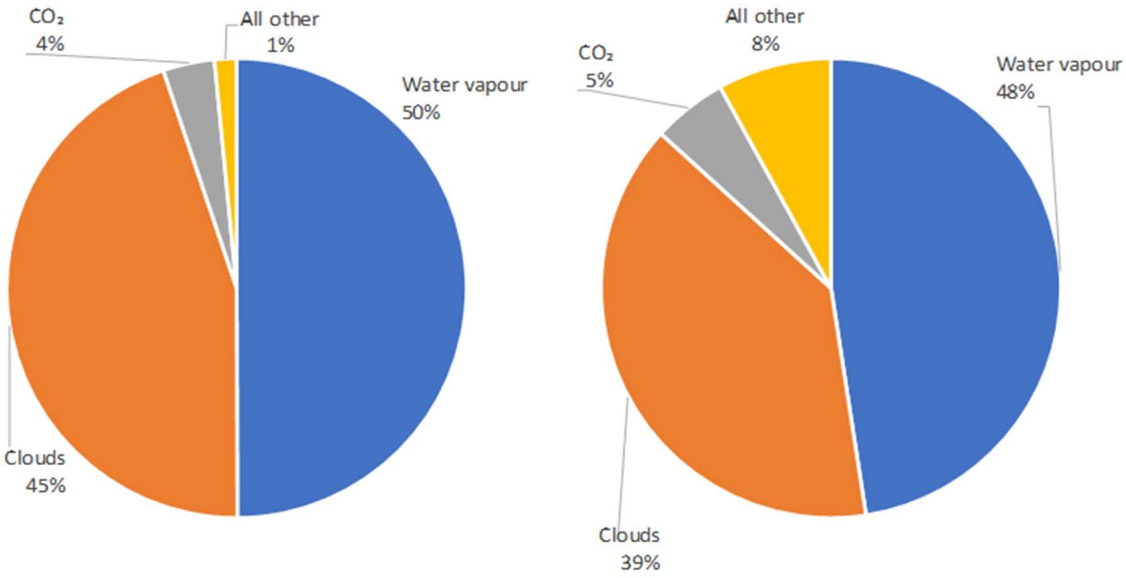

*Figure 24: Contribution of the greenhouse drivers to the LW radiation fluxes, **(left)** downwelling and **(right)** outgoing.*

.

From Demetris Koutsoyiannis:
Relative Importance of Carbon Dioxide and Water in the Greenhouse Effect: Does the Tail Wag the Dog?

SCIENCE OF CLIMATE CHANGE

Volume 4.2

December 2024

ISSN 2703 9072

A digital version of this volume is available: https://doi.org/10.53234/scc202412/02

Published by: Klimarealistene (Org. no. 995 314 592)
Michelets vei 8 B, 1366 Lysaker Norway

Table of Content

Preface

The Journal Science of Climate Change is a non-profit venture, hosted and supported by the Norwegian Klimarealistene (KR – Climate Realists). Also, other climate organizations and their members support the journal with qualified publications or their engagement as co-editors and reviewers.

The objective of this journal was and is, to publish – different to many other journals – also peer reviewed scientific contributions, which contradict the often very unilateral climate hypotheses of the IPCC and thus, to open the view to alternative interpretations of climate change.

In 2021 SCC started in the classical format publishing two volumes. Since 2022 it is operating as Open Access Journal with very moderate publication fees, with a new layout and new website. In 2022 three volumes and in 2023 five volumes could be published, consisting of research and review articles, of essays, discussion papers, conference summaries and book reviews.

Within less than three years SCC could develop to an internationally recognized Journal of Climate Sciences presenting alternative views for a much broader discussion and understanding of climate phenomena. This success is essentially due to the dedicated engagement of the previous Chief Editors, in the founding phase, *Geir Hasnes*, and from October 2022 to December 2023 by Prof. Jan Erik Solheim, strongly supported by Dr. Stein Bergsmark.

The Scientific Board of Klimarealistene and the Editorial Board of SCC would like to thank them all for their unprecedented engagement, the good cooperation within the board and their further advice.

The new Editorial Board tries to continue the previous successful work and at the same time to gain further experts on the wide field of climate sciences, who can strengthen the editorial work and who are well known representatives of their countries and/or organizations. This should also contribute to a closer exchange and cooperation between different scientists and nations.

Ole Henrik Ellestad
(KR's Scientific Board)

Hermann Harde
(SCC's Editorial Board)

Editorial

Volume 4 consists of two regular issues, Vol. 4.1 and 4.2. An additional issue, Vol. 4.3, contains all presentations on the CLINTEL Climate Conference in Prague. Vol. 4.4 is planned for contributions of the Climate Conference 2024 in Mölndal, Sweden.

This issue, Vol. 4.2, starts with an article of *Dai Ato*, who has rigorously examined the impacts of sea surface temperature (SST) and fossil fuels on the atmospheric CO_2 level using a multivariate regression analysis. This study demonstrates that the independent determinant of the annual increase in atmospheric CO_2 concentration was SST, which shows strong predictive ability, while human CO_2 emissions are irrelevant.

Moritz Büsing has investigated the ageing of weather station housings with its influence on the temperature measurements. Due to many different state-of-the-art homogenization algorithms, which are adding up each time a weather station is renovated, renewed, or replaced, this results in a substantial systematic error. An in-depth analysis of the weather station data sets (homogenized and non-homogenized) confirms the presence of this systematic error. Corrections reduce the calculated warming of the land surface temperatures since 1880 from 1.43 °C to 0.83 °C. An estimate of a less conservative correction even suggests only 0.41 °C.

Demetris Koutsoyiannis discusses the relative importance of CO_2 and water for the greenhouse effect, using a detailed atmospheric radiative transfer model. He derives macroscopic relationships of downwelling and outgoing longwave radiation with their respective partial derivatives. From this he infers that CO_2 doesn't contribute more than 4% – 5% to the greenhouse effect, while water and clouds dominate with a contribution of 87% – 95%. The minor effect of carbon dioxide is confirmed by the small, non-discernible effect of the recent escalation of atmospheric CO_2 concentration from 300 to 420 ppm. This effect is quantified at 0.5% for both downwelling and outgoing radiation.

Frans Schrijver studies the impact of global greening in terms of gross primary production on the natural atmospheric CO_2 level. The total mass of CO_2 in the atmosphere is equal to the yearly uptake of CO_2 (down flux), multiplied by the average time, CO_2 remains in the atmosphere (residence time). The biological processes of photosynthesis and respiration are by far the most important components of the fluxes to and from the atmosphere. Since preindustrial times the down flux has increased by 29% and the residence time by 16%. Together they fully explain the recent CO_2 rise, without assuming different behaviors for human-generated CO_2 compared to natural CO_2 and without the need for an ad-hoc model with multiple residence times.

In a debate paper *Ad Huijser* presents his view of greenhouse feedbacks, which he explains as "intrinsic properties of the Planck feedback parameter." From this he concludes that climate feedbacks are not effects induced by forcings, but constitute our climate. So, independent from the origin of a disturbance, our climate will always respond according to the Planck feedback parameter, which he just sees as difference between the surface feedback parameter and the sum of climate feedbacks.

Finally, this issue contains a note from *Zdirad Žák* to a comment of F. Engelbeen on historical data of E.-G. Beck. Due to a consistency of Beck's and Callendar's data Žák asks: Has not already come the time to change our mind about a background level of 280 ppm?

We hope that the above contributions will stimulate our readers to a further critical discussion of climate science, and we wish interesting reading.

Hermann Harde
(Editor-in-chief)

Research Article

Multivariate Analysis Rejects the Theory of Human-caused Atmospheric Carbon Dioxide Increase: The Sea Surface Temperature Rules

Dai Ato

Independent researcher, Osaka, Japan

ORCID:0000-0002-6049-5039

Klimarealistene
Vollsveien 109
1358 Jar, Norway
ISSN: 2703-9072

Correspondence: ato.dai1@wind.ocn.ne.jp

Vol. 4.2 (2024)

pp. 1-15

Abstract

The impact of certain factors on the changes in atmospheric carbon dioxide (CO_2) concentrations has yet to be elucidated. In particular, the impacts of sea surface temperature (SST) on the balance of CO_2 emissions and absorption in the atmosphere and the human use of fossil fuels have not been rigorously compared. In this study, the impact of each factor was examined using multivariate analysis. Publicly available data from prominent climate research and energy-related organizations were used. Multiple linear regression analysis was performed using the annual changes in atmospheric CO_2 levels for each year as the objective variable. The SST and human emissions for each year were the explanatory factors. After 1959, the model using the SST derived from NASA best represented the annual CO_2 increase (regression coefficient $B = 2.406$, $P < 0.0002$, model $R^2 = 0.663$, $P < 7e\text{-}15$). However, human emissions were not a determining factor in any of the regression models. Furthermore, the atmospheric CO_2 concentration predicted, using the regression equation obtained for the SST derived from UK-HADLEY centre after 1960, showed an extremely high correlation with the actual CO_2 concentration (Pearson correlation coefficient $r = 0.9995$, $P < 3e\text{-}92$). The difference was 1.45 ppm in 2022. In conclusion, this study is the first to use multiple regression analysis to demonstrate that the independent determinant of the annual increase in atmospheric CO_2 concentration was SST, which showed strong predictive ability. However, human CO_2 emissions were irrelevant. This result indicates that atmospheric CO_2 has fluctuated as natural phenomenon, regardless of human activity.

Keywords: human emission; global warming; climate change; ice core; Jaworowski; CLINTEL

Submitted 2024-03-15, Accepted 2024-07-14. https://doi.org/10.53234/SCC202407/19

1. Introduction

Since the establishment of the Intergovernmental Panel on Climate Change (IPCC), endorsed by Margaret Thatcher (Thatcher, [1]), the “so-called” global consensus that human emissions of carbon dioxide (CO_2) are the primary cause of global warming, has been said to be growing. Nowadays, the term "global warming" has been replaced by the term "climate change.” Beginning in 1990, the IPCC has published reports every few years. The latest version of the sixth report (IPCC, [2]) stated that humanity's impact on climate change is certain.

This argument has been also refuted by skeptics. In recent years, starting with the Global Warming Petition Project [3,4], the Nongovernmental International Panel on Climate Change (NIPCC) was established in 2007 (later the International Conference of Climate Change, Singer, [5]).

Furthermore, the Global Climate Intelligence Group (CLINTEL, [6]) and more than 90 Italian scientists [7] have denied the impact of humans on climate change. They share the belief that being pessimistic about the impact of increased anthropogenic CO_2 emissions is unnecessary. Among these beliefs, the rejection of the anthropogenic theory by John Clauser, Nobel laureate in Physics in 2022, is significant (Clauser, [8]).

The main indicators used in the climate change debate include atmospheric CO_2, human emissions, and land and sea surface temperatures. The accuracy of these temperature measurements has been debated since the early 1990s because of the differences between the data from meteorological satellites, observation balloons and the values of surface measurements [4,5,9]. For measurements recorded at the ground surface, issues have arisen related to the objectivity of the error correction, especially those caused by the heat island effect [4,5,9]. Thus, no realistic consensus exists on the extent of global warming.

Regarding the other main indicator, CO_2, the assumptions that its atmospheric levels have risen consistently since the post-industrial revolution and that this is due to human emissions are also controversial. High-precision measurements began at Mauna Loa, Hawaii, in 1959. However, a discrepancy exists between the ice core reproduction and the chemical method used for measuring atmospheric CO_2 concentrations before that time. Jaworowski noted that the historical figures of atmospheric CO_2 were underestimated by 30%–50% owing to various limitations of the ice core reconstruction method (Jaworowski, [10,11]). Jaworowski also strongly criticized the link between data from Hawaii since 1959 and the data reconstructed from the ice core [10,11,12]. The results of the analysis of radioisotopes have indicated defects in shifting the age of atmospheric constituents [10,11,13]. Jaworowski further noted [10] that the time required to release gas from the ice core could cause a huge discrepancy, by referring to a study of Stauffer et al. [14]. Furthermore, Beck [15] compiled and published data from many papers on CO_2 measurements using direct chemical methods. Recently, Yndestad [16] argued that atmospheric CO_2 concentrations are governed by the lunar node cycle.

The ocean is a huge reservoir of CO_2 and a major contributor to the global CO_2 cycle because of solubility changes with temperature. Therefore, depending on the temperature, CO_2 release into the atmosphere or CO_2 absorption occurs during both the day and the seasonal cycle. According to the National Aeronautics and Space Administration (NASA) Earth Observatory, annual emissions and absorption are approximately 330 gigatons for oceanic sources. The terrestrial biological origin of CO_2 is considered to be 440 gigatons absorbed by photosynthesis and 440 gigatons emitted by respiration [17]. However, precisely evaluating annual fluctuations is difficult because the amount of CO_2 fixed by organisms involves an increase in the total amount of organisms themselves. Volcanic emissions are considered stable. Human CO_2 emissions reached approximately 37 gigatons by 2021 (International Energy Agency (IEA), [18]). This should be considered much less than the amount released and absorbed by oceans and organisms. Based on this information, whether the increased atmospheric CO_2 values in recent years are attributable, at least partially, to human activity, and to what extent remain unclear. Therefore, the impact of human emissions on atmospheric CO_2 concentrations was statistically analyzed using multiple regression analysis. And if the human activity is responsible, it must be reflected in the analysis.

2. Methods

2.1 Data and evaluation periods

The indicators for each year were atmospheric CO_2, CO_2 emissions, and sea surface temperature (SST). Publicly available data from prominent climate research and energy-related organizations worldwide were used. Data from the National Oceanic and Atmospheric Administration (NOAA) were used to determine atmospheric CO_2 values [19]. The latest global SST data were derived from the University of Alabama in Huntsville (version 6.0, UAH-SST) (lower troposphere globe ocean data as a surrogate) (Spencer et al, [20,21]), HADLEY Centre (version HAD-SST4, HAD-

SST) [22,23], and NASA-Goddard Institute for Space Studies (GISS, version GISTEMP v4, GISS-SST) [24,25]. UAH-SST data were derived only from meteorological satellites. Because the UAH-SST data are provided monthly, the annual averages of the global sea temperature were calculated. The reason to use UAH data as SST surrogate is that meteorological satellite provides unbiased data all over the world and the temperature in the atmosphere above the ocean strongly reflects the SST. In fact, UAH-SST shows similar temperature trends and results of the analysis like the other SSTs, as described in the Results section. Each SST data until 2022 was available.

Based on the availability of data, the statistical analysis was divided into two periods, after 1979 and after 1959, depending on the starting year for each measurement. The UAH-SST was limited to the period after 1979.

Highly accurate measurements of CO_2 concentrations started being recorded on Hawaii in 1959 [19]. This data until 2022 is available. Data from the International Energy Agency (IEA, [18]) and Our World in Data (OWID, [26]) were used to determine human emissions. These data until 2021 were available. The IEA data were analyzed only from 1979 to 2021, whereas the OWID data were analyzed from 1959 to 2021 and from 1979 to 2021. The reason for this division is that publicly available CO_2 emission data from the IEA are only available for the period after 1971. Data before 1970 required registration and the payment of a fee (US$ 610 as of October 2023). Hopefully, all people worldwide will facilitate the viewing of the same results using publicly available data using inexpensive and widely used spreadsheet applications such as Microsoft® Excel. Therefore, OWID data were used in the analysis after 1959. The consistency of the IEA and OWID data is discussed in the Statistics and Results sections.

Thus, the combinations of data used were as follows:

- After 1979: IEA and OWID for human emissions; UAH, HADLEY, and GISS for SST.
- After 1959: OWID for human emissions; HADLEY and GISS for SST.

2.2 Statistical analysis

EZR Version 1.61 (Kanda (2013) [27]) and Microsoft® Excel were used for analysis. The Pearson correlation test was used to analyze the correlations for each indicator.

The steps of the analysis were as follows:

1. For the period between 1979 and 2021, we assessed the Pearson correlation of UAH-SST and emissions data obtained by the IEA against the annual CO_2 concentration increase.
2. For the period between 1979 and 2021, a multiple linear regression analysis was performed with the annual atmospheric CO_2 concentration increase as the objective variable and UAH-SST and IEA emissions as explanatory variables. Based on these results, which are discussed in more detail in the Results section, an analysis using more data and years was performed.
3. Correlations and differences between the SSTs of each agency (UAH, HADLEY, and GISS) were assessed with data up to 2021 using linear regression.
4. The correlations and differences between the IEA and OWID CO_2 emissions data were assessed.
5. For the period between 1979 and 2021, multiple linear regression analysis was performed with the annual atmospheric CO_2 concentration increase as the objective variable, and SST and CO_2 emissions as explanatory variables.
   As discussed in more detail in the Results section, similar multiple linear regression analysis results were obtained for UAH, HADLEY, and GISS for SSTs; IEA and OWID for CO_2 emissions; and for any combination. Subsequently, the following analyses were conducted.
6. For the period between 1959 and 2021, multiple linear regression analysis was similarly conducted using the annual atmospheric CO_2 concentration increase as the objective variable.

HADLEY or GISS for SST and OWID CO_2 emissions were used as the explanatory variables. The results of the multiple regression analyses were similar for each SST. However, each emission was strongly correlated to the HAD-SST and GISS-SST. The possibility of multicollinearity due to this phenomenon and the interpretation of the results are discussed in the APPENDIX.

7. Based on the results of the multiple linear regression analysis, the atmospheric CO_2 concentrations after 1979 and 1959 were predicted from the SST and compared with the actual NOAA data.

The calculation was performed as follows:

$$[\Delta CO_2]_i = B \times T_i + Co\,, \tag{1}$$

where $[\Delta CO_2]_i$ is the annual CO_2 concentration increase in the atmosphere, B is the regression coefficient for the SST, T_i is the SST of each year and Co is the constant of the regression model. As described in the Results section, the only statistically significant factor for the objective variable was SST and not human emissions. Therefore, the annual increase in atmospheric CO_2 concentration can be estimated using the above equation. Subsequently, the CO_2 concentrations were predicted as:

$$[CO_2]_n = \sum_{i=x}^{n} [\Delta CO_2]_i + C_{st}\,, \tag{2}$$

where $[CO_2]_n$ is the predicted atmospheric CO_2 concentration, and C_{st} is the actual value of the atmospheric CO_2 concentration in the starting year. For example, the predicted atmospheric CO_2 concentration in 2022 is the sum of the estimated annual increase during 1979–2022 and the actual atmospheric CO_2 concentration in 1978.

A P value of ≤ 0.05 was considered statistically significant (two-sided).

3. Results

Step 1: Figure 1 shows the correlation of UAH-SST (a) and IEA emissions (b) with the annual atmospheric increase in CO_2 concentration. A linear correlation is shown, with correlation coefficients of $r = 0.749$, $P < 8e\text{-}9$ for UAH-SST and $r = 0.581$, $P < 5e\text{-}5$ for emissions.

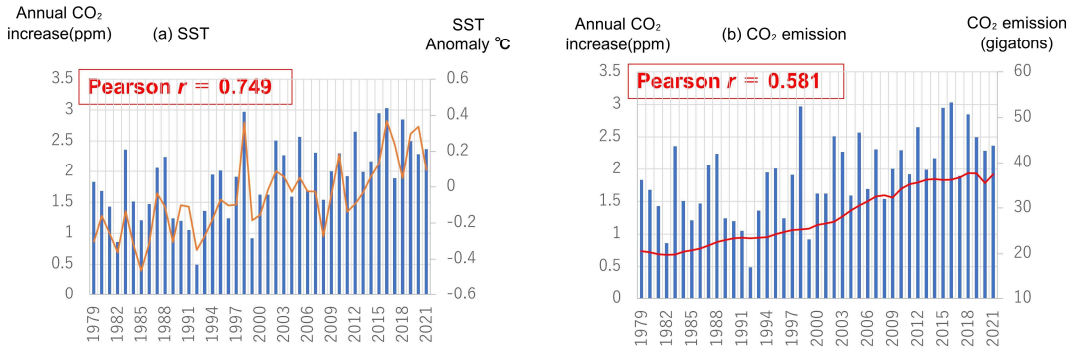

Figure 1. Comparison between annual increase in atmospheric CO_2 concentration and (a) SST, (b) anthropogenic CO_2 emissions:
(a) SST: sea surface temperature (orange line, right vertical axis) derived from the University of Alabama in Huntsville, Blue bar (left vertical axis): annual CO_2 increase derived from National Oceanic and Atmospheric Administration, SST anomaly "0" is the average through 1991 – 2020, horizontal axis: year
(b) anthropogenic CO_2 emission derived from International Energy Agency (red line, right vertical axis), Blue bar (left vertical axis): annual CO_2 increase derived from National Oceanic and Atmospheric Administration, horizontal axis: year

Step 2: Table 1 shows the results of the multiple linear regression analysis with the annual CO_2 change in concentration as the objective variable. Only UAH-SST was a significant explanatory factor (regression coefficient $B = 1.964$, $P < 4e\text{-}5$, model $R^2 = 0.571$, $P < 5e\text{-}8$). IEA CO_2 emission was not ($B = 0.013$, $P = 0.35$).

Table 1. Results of multiple linear regression analysis for annual increase in atmospheric CO_2 concentrations as objective variable.

Model R^2 = 0.571	*B*	*t*	*P*
Constant	1.660 (ppm)	4.068	< 0.0003
SST	1.964 (ppm/℃)	4.661	< 4e-05
CO_2 emission	0.013 (ppm/Gt)	0.949	0.348

B: regression coefficient (value of B in the equation (1)), t: result of t-test, SST: sea surface temperature derived from the University of Alabama in Huntsville, CO_2 emission derived from International Energy Agency

Step 3: Figure 2 (a, b) shows plots of three types of SST. From 1979 to 2022 (a), each SST was strongly correlated, and the slopes of the linear regression equation were similar. The results were similar from 1959 to 2022 (b).

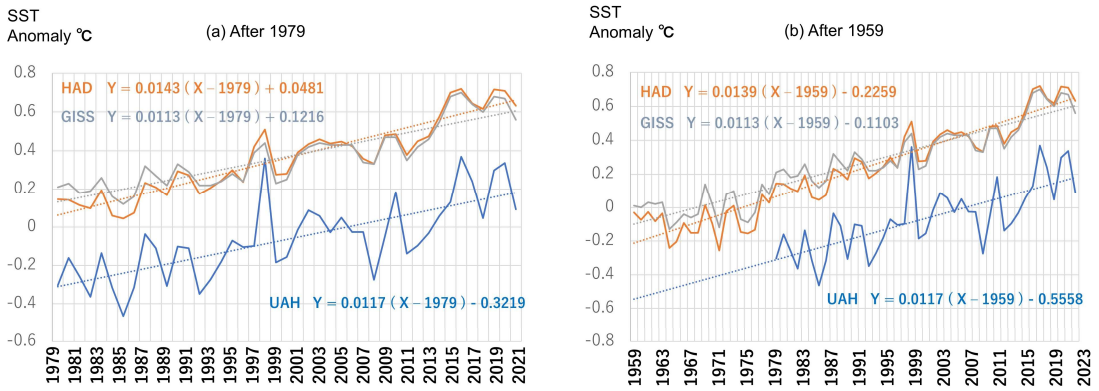

Figure 2. Comparison between SSTs: UAH - University of Alabama in Huntsville (blue line); HAD - Hadley centre (orange line): GISS - Goddard Institute for Space Studies (gray line). All SSTs are the difference from the average (UAH: 1991 – 2020, HAD: 1961-1990, GISS: 1951-1980). Horizontal axis: year, note that Y in the linear regression equation means SST anomaly, X means year. (a) after 1979, Pearson correlation coefficient, UAH vs HAD r = 0.892, P < 5e-16; UAH vs GISS r = 0.888, P < e-15, (b) after 1959, Pearson correlation coefficient, HAD vs GISS r = 0.993, P < 8e-59.

Step 4: Figure 3 shows the strong correlation between the IEA and OWID emissions ($r = 0.9996$, $P < 2e\text{-}75$). The slopes of the linear regression were almost identical (0.446 for IEA and 0.454 (Gt / year) for OWID).

Step 5: Table 2 shows the results of the multiple linear regression analysis of the data after 1979. All data combinations yielded similar results. SST was consistently a strong independent determinant of annual CO_2 concentration increases but not human emissions. Moreover, no significant difference was found in the explanatory power of each SST using either emission type. In this step of the analysis, the combination of the IEA and UAH-SST data provided the most accurate predictions of the annual increases in CO_2 levels, and the explanatory power of the regression model was model $R^2 = 0.571$ ($P < 5e\text{-}8$), as described in Step 2. The analysis using the OWID instead of the IEA CO_2 emission data produced similar results in each regression model. The results of Steps 4 and 5 showed that the use of only OWID CO_2 emissions was appropriate after 1959.

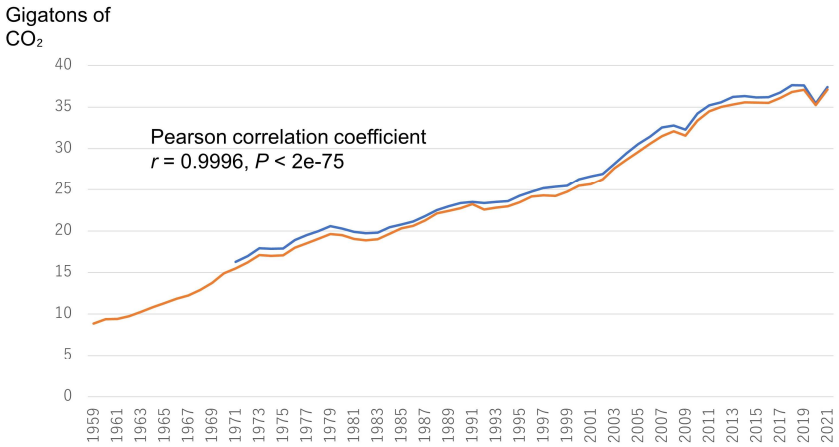

Figure 3. CO_2 emissions data of IEA and OWID. IEA - International Energy Agency (blue line), OWID - Our World In Data (orange line), horizontal axis: year.

Table 2. Results of multiple linear regression analysis for annual increase in atmospheric CO_2 concentrations as objective variable after 1979

	IEA emission			OWID emission		
	R^2=0.5711	B	P	R^2=0.5702	B	P
	Constant	1.660	<0.0003	Constant	1.688	<0.0002
UAH	UAH-SST	1.964	<4e-5	UAH-SST	1.977	<4e-5
	IEA emission	0.013	0.348	OWID emission	0.012	0.372
	R^2=0.5038	B	P	R^2=0.5058	B	P
	Constant	1.505	<0.002	Constant	1.522	<0.002
HAD	HAD-SST	2.834	<0.0008	HAD-SST	2.894	<0.0006
	IEA emission	-0.023	0.356	OWID emission	-0.025	0.314
	R^2=0.506	B	P	R^2=0.5076	B	P
	Constant	1.136	<0.005	Constant	1.156	<0.004
GISS	GISS-SST	3.155	<0.0007	GISS-SST	3.230	<0.0006
	IEA emission	-0.014	0.517	OWID emission	-0.017	0.458

B - regression coefficient (value of B in equation (1)), IEA - International Energy Agency, OWID - Our World In Data, SST - Sea surface temperature, UAH - University of Alabama in Huntsville, HAD - Hadley centre, GISS - Goddard Institute for Space Studies. Unit for constant is ppm, unit for SST is ℃, unit for emission is gigatons, note that the units for each B is the same as Table 1.

Step 6: Table 3 shows the results of the multiple linear regression analysis of the data from 1959. Similar to the above results, both SST data sources were independent determinants of the annual increase in CO_2 levels, but CO_2 emissions were not. Furthermore, the explanatory power of the regression models exceeded that of the models derived from the UAH-SST and IEA data after 1979. Both SST data sources produced similar results, including the explanatory power of the models. However, in terms of R^2, GISS-SST slightly outperformed HAD-SST (model R^2=0.663, P<7e-15).

Table 3. Multiple linear regression analysis for annual CO_2 increase as objective variable after 1959. Meaning of symbols and units of B, see Table 1 and 2.

R^2 = 0.6559	B	P
Constant	1.143	<0.0002
HAD-SST	2.006	<0.0003
OWID emission	0.0017	0.918

R^2 = 0.6628	B	P
Constant	0.953	<0.0002
GISS-SST	2.406	<0.0002
OWID emission	0.0027	0.863

Step 7: Thus, the annual increase in atmospheric CO_2 concentrations can be explained using the SST as follows:

$$Annual\ CO_2\ increase = 1.964 \times UAH\text{-}SST + 1.660 \text{ (after 1979)}$$

$$Annual\ CO_2\ increase = 2.006 \times HAD\text{-}SST + 1.143 \text{ (after 1959)}$$

$$Annual\ CO_2\ increase = 2.406 \times GISS\text{-}SST + 0.953 \text{ (after 1959)}$$

Based on these equations, the atmospheric CO_2 concentration was predicted using the UAH-SST data after 1979 (values of the model using IEA data were selected according to the higher R^2), starting from the NOAA data in 1978. For HAD-SST and GISS-SST, CO_2 concentrations after 1960 were predicted using the 1959 NOAA data as the starting point. The results are shown in Figure 4(a, b, c).

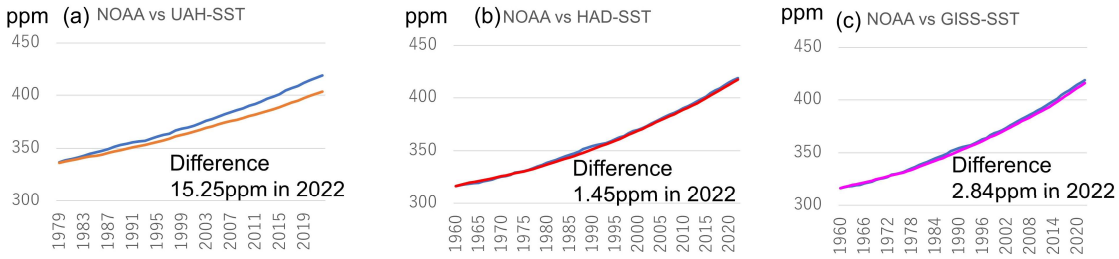

Figure 4. Measured and predicted CO_2 concentrations: (a) NOAA (all blue lines) vs UAH-SST (orange), (b) NOAA vs HAD-SST (red), (c) NOAA vs GISS-SST (purple), horizontal axes: year

The Pearson correlations between the predicted CO_2 concentrations and the NOAA measurements for each SST were as follows:

UAH-SST (1979～2022) $r = 0.9995$, $P <$ 4e-64

HAD-SST (1960～2022) $r = 0.9995$, $P <$ 3e-92

GISS-SST (1960～2022) $r = 0.9997$, $P <$ 7e-99

Each showed a very strong correlation.

The smallest error in 2022 was 1.45 ppm, which was predicted by HAD-SST, based on the analysis of data from the period starting in 1959.

4. Discussion

To the best of our knowledge, this is the first use of multiple regression analysis to demonstrate that SST has been the determinant of the annual changes in atmospheric CO_2 concentrations and that anthropogenic emissions have been irrelevant in this process, by head-to-head comparison. Furthermore, this study supports existing studies on the strong correlation between preceding global temperature changes and changes in atmospheric CO_2 concentrations (Harde, [28], Koutsoyiannis et al, [29], Salby et al, [30], Stallinga et al. [31]). Those results of this study are reasonable considering the total amount of CO_2 cycling on Earth. The annual CO_2 cycle includes 330 gigatons from oceanic sources, 440 gigatons from terrestrial sources, and 37 gigatons from human emissions, including recent years (NASA, [17], IEA, [18]). The CO_2 emitted by all the sources is used in photosynthesis and by the animals, both terrestrial and marine, that benefit from it. Furthermore, there has been a recent research reporting particularly of thermally induced CO_2 emissions from soil respiration in the tropical areas [Salby et al, [30]]. If the increase in atmospheric CO_2 were entirely caused by mankind, it would have been reflected in the multiple regression analysis, by cancelling the effect of SST (e.g. $B =$ 0.0613, $P < 0.05$ for OWID emissions; non-significant for HAD-SST, note that these values are obtained by univariate analysis.).

If the analysis in this study is incorrect, that is, if the results are artifacts, then all the data for each SST are fatally wrong, the CO_2 measurements since 1959 are fatally wrong, or both. Moreover, these data would be coincidentally incorrect. The emissions data being grossly erroneous is unlikely.

In this study, the data published by organizations with international reputations were used. The CO_2 concentrations on Hawaii were measured using trusted methods and are consistent with worldwide data (Figure 5) (NOAA, [32]). As such, the assumption that the most objective measure of air and ocean temperatures results from meteorological satellites, which can assess a wide range of areas, is reasonable. Among the UAH-SST, HAD-SST, and GISS-SST datasets used in this study, UAH-SST data are more sensitive and show a wider range of fluctuation (Figure 2). However, all datasets exhibit similar upward slopes. Furthermore, the Pearson correlation between HAD-SST and GISS-SST or UAH-SST was also high, at approximately 0.9. For the data from 1979 and later, the results of multiple linear regression analysis were similar for all three SST datasets, regardless which was used. The slopes of the HAD-SST and GISS-SST increases were similar when considering the analysis from 1959 onward. The explanatory power of the multiple regression analysis was stronger for HAD-SST and GISS-SST after 1959 than for UAH-SST after 1979. Therefore, as SST has been the main determinant of the CO_2 cycle between the ocean and the atmosphere, this indicates a causal relationship and its extent.

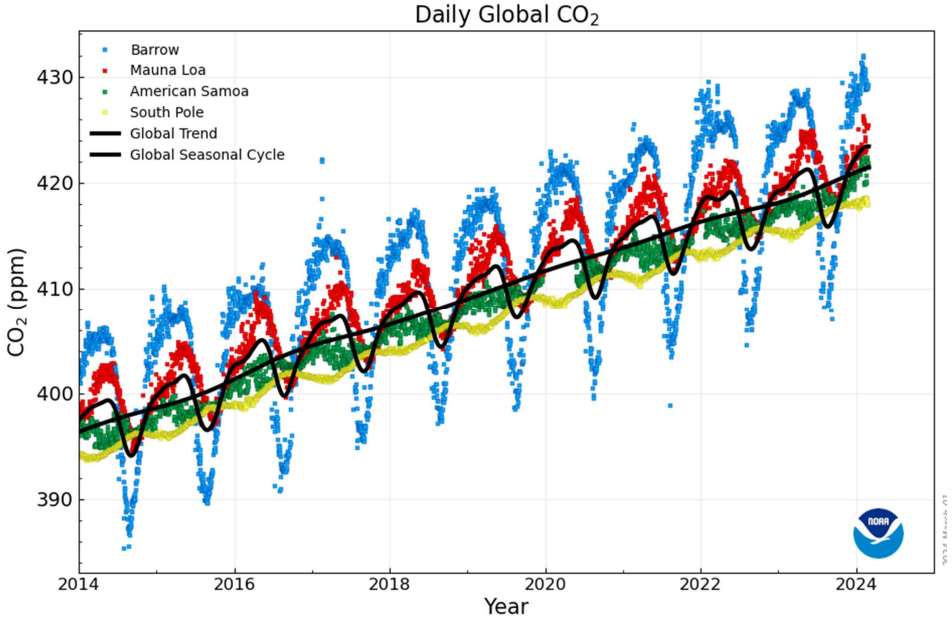

Figure 5. Recent Global CO_2 Trend: Image from National Oceanic and Atmospheric Administration.

Figure 1(a) illustrates this phenomenon. In 1992, the year of the global cold snap caused by the Pinatubo eruption, the atmospheric CO_2 concentration increased 0.49 ppm. If all the human emissions of the year had stayed in the atmosphere, they would have risen by approximately 3 ppm. In contrast, in 1998 and 2016, when El Niño warmed the world, the CO_2 concentration increased 2.97 and 3.05 ppm, respectively, showing a six-fold difference (3 divided by 0.5=6). Additionally, the emissions in these years were 23.4, 25.3, and 36.2 gigatons (IEA, [18]), respectively. Human emissions in 1992 and 1998 differed by only 8%. Moreover, the emissions in 2016 were only 1.56 times higher (36.2 divided by 23.4). These data suggest that the main factor governing the annual increase in atmospheric CO_2 concentration is the SST rather than human emissions, as confirmed by the results of the multiple linear regression analysis in this study. The results of this study are also consistent from a perspective of carbon isotope that the increase in the atmospheric CO_2 is originated from the ocean. As Spencer [33] pointed out in 2009, the ^{13}C concentration in the ocean is lower than in the atmosphere.

The atmospheric CO_2 concentration predicted using the UAH-SST dataset using the regression equation deviated the most from the NOAA-measured data as of 2022 (Figure 4a, b, c). In contrast, the HAD-SST and GISS-SST data from 1959 onward produced an accurate approximation. This result is reasonable because of the increased accuracy of the model in the regression analysis. HADLEY and GISS contain approximately 20 years more of data with good fit with the increase in atmospheric CO_2, which will consequently increase the explanatory power of the multiple regression analysis model. For HAD-SST and GISS-SST, the CO_2 values predicted using the model obtained with data only since 1979 were 30.8 and 21.1 ppm in 2022, respectively, which are overestimations compared with the measured CO_2 concentrations.

The results of this study also indicate that recent concentrations and increases in atmospheric CO_2 are not abnormally high as they are natural phenomena. The reasons why modern CO_2 concentrations have been said to be abnormally high (or the highest in one million years) are as follows: The atmospheric CO_2 concentration reconstructed using ice cores was approximately 280 ppm at the time of the Industrial Revolution, and the subsequent rise in CO_2 levels chronologically coincided with an increase in human activity. However, this theory has some fundamental limitations. As mentioned in the Introduction, reasonable arguments exist against the theory that modern CO_2 concentrations are abnormally high. Jaworowski pointed out [10,11] that ice core reconstructions of CO_2 concentrations were underestimated by 30–50%. Phenomena that support the argument by Jaworowski on the ice core method have been observed in the atmosphere, even in recent years. Although humanity is releasing vast amounts of methane, atmospheric methane concentrations have declined twice since the 21st century (Figure 6) (NOAA, [34]). If all human emissions of methane remain in the atmosphere, they would have to rise by more than 115 ppb per year in the 21st century and beyond (human emissions more than 0.3 gigatons (NASA, [35]), 1ppb ≅ 0.0026 gigatons). This indicates that natural fluctuations are far more powerful than human emissions in terms of the influence on atmospheric methane levels.

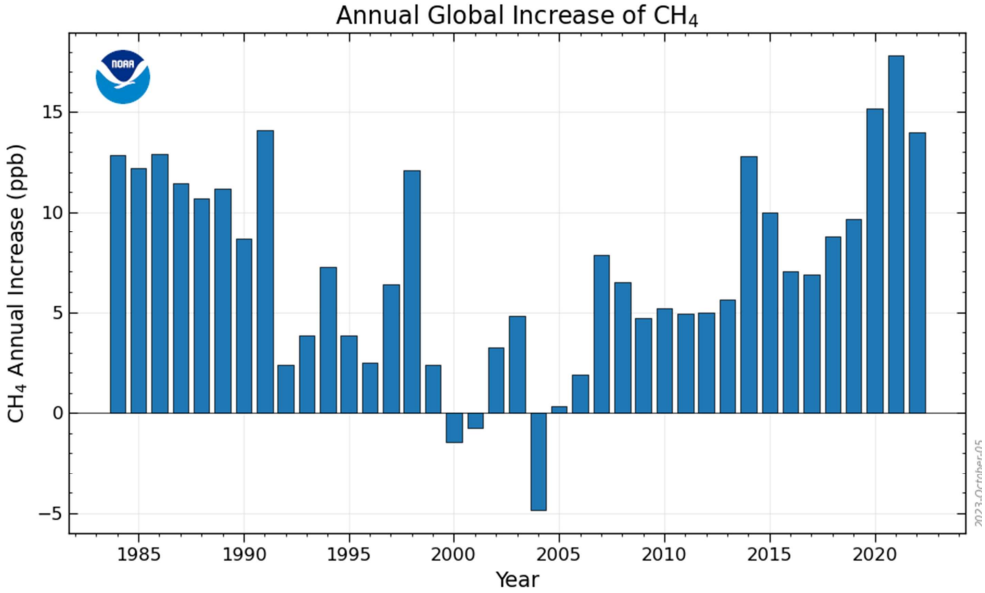

Figure 6. Recent atmospheric concentration of methane. Iimage taken from NOAA.

Furthermore, this contradicts the estimates that atmospheric methane concentrations have increased by approximately 1000 ppb since the Industrial Revolution (Figure 7) (IPCC, [36]). This fact supports the point made by Jaworowski [10,11] regarding the deficiencies in the reproduction method using ice cores, particularly with respect to the reproduced concentrations of the atmospheric components. Beck [15] compiled chemical measurements and reported that the pre-1958 values of atmospheric CO_2 concentration were several tens ppm higher than those reproduced in ice cores. The results of this study are consistent with those of these reports.

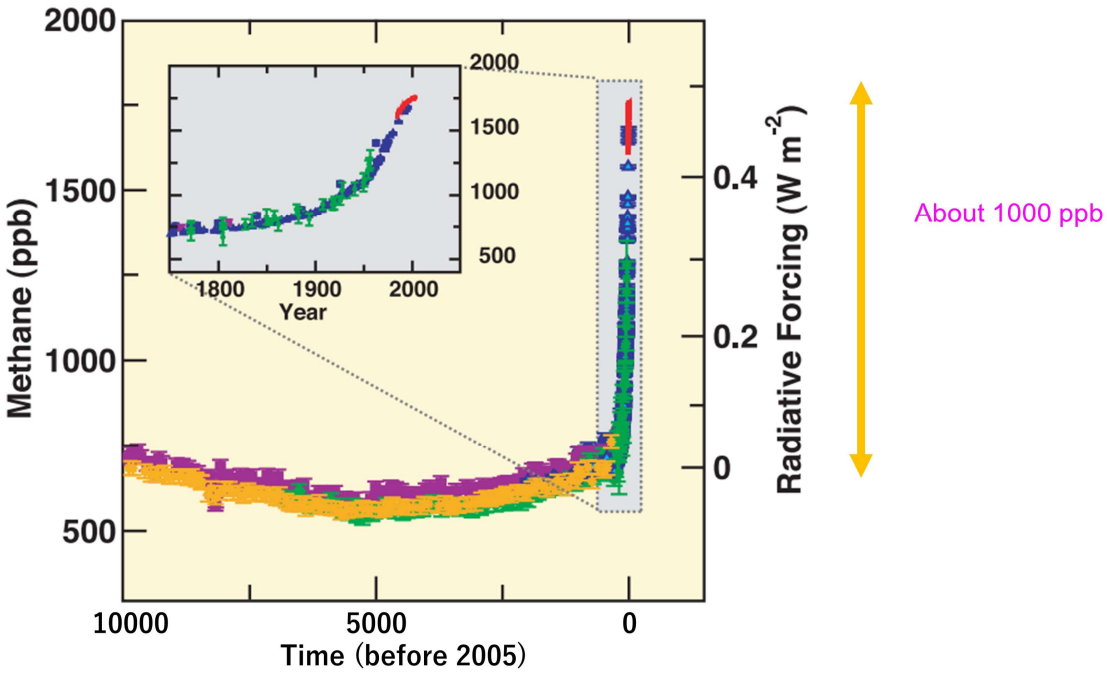

Figure 7. Reconstruction of atmospheric methane concentration. Image taken from the IPCC Fourth Assessment Report, Summary for Policymakers.

There are strengths and limitations in this study. This study involved a correlational analysis, which cannot identify direct causality. In addition, the effects of terrestrial organisms and volcanoes were not evaluated. These two indicators are difficult to precisely assess from year to year, unlike the CO_2 concentration measurements in Hawaii or human emissions.

However, as SST is a strong determinant of the CO_2 cycle between the ocean and the atmosphere, the assumption is reasonable that this is some proof of causality and its degree of influence. The results of the post-1959 analysis suggest that terrestrial organisms and volcanic activity may have been responsible for approximately 35% of the residual power in the regression model, which could not be explained by SST. Nevertheless, the accuracy of the CO_2 concentration predicted using each SST dataset (including the constants in the regression models) suggests that little improvement in the explanatory power can be expected.

All the results of the multiple linear regression analysis in this study could only be wrong if all the data in each SST dataset, if all the CO_2 measurements from Hawaii, or all of them are coincidentally similarly fatally wrong.

5. Conclusions

The global SST has been the main determinant of annual increases in atmospheric CO_2 concentrations since 1959. No human impact was observed. This result indicates that human efforts to curb CO_2 emissions have been, at least in the past, meaningless. Moreover, the theory that modern global warming and climate change are caused by human-emitted CO_2 is also wrong, irrelevantly to the credibility of the story that modern warming and climate change are occurring more dramatically than those in the past.

Funding

The author did not receive any funding of the work.

Declaration of competing interest

The author declares no conflict of interest. Dai Ato, an autonomous and private researcher, authored this article as an academic activity based on the guaranteed right of freedom in an academy for the Japanese (Article 23) and the Supreme Law provided in Article 98 of the Constitution of Japan.

Data Availability

The data set used in this study is available as a supplemental file (Ato, 2024 [37]).

Chief-Editor: Prof. H. Harde, **Guest-Editor**: Prof. P. Stallinga; **Reviewers**: anonymous.

Acknowledgements

The author appreciates all the institutes and the researchers for providing the data and the knowledge related to this study.

Appendix

Discussion of the results about the high correlation between SSTs and human emissions

As shown in Appendix Table 1, HAD-SST or GISS-SST and emissions were highly correlated at the coefficient of approximately 0.9. On the other hand, it is slightly lower than 0.7 for UAH-SST and each emission.

Appendix Table 1. Pearson correlation coefficient between each indicator.
All abbreviations refer to the main text.

1979~2021	UAH-SST	HAD-SST	GISS-SST	IEA	OWID
Annual CO_2 Increase	r = 0.749, P = 7.46e-9	r = 0.702, P = 1.55e-7	r = 0.708, P = 1.12e-7	r = 0.581, P = 4.33e-5	r = 0.578, P = 4.98e-5
UAH-SST	---	r = 0.892, P = 1.03e-15	r = 0.886, P = 2.73e-15	r = 0.680, P = 5.33e-7	r = 0.679, P = 5.45e-7
HAD-SST	---	---	r = 0.984, P = 2.76e-32	r = 0.894, P = 6.52e-16	r = 0.895, P = 5.98e-16
GISS-SST	---	---	---	r = 0.872, P = 2.69e-14	r = 0.874, P = 2.1e-14
IEA	---	---	---	---	r = 0.999, P = 1.17e-62
1959~2021	UAH-SST	HAD-SST	GISS-SST	IEA	OWID
Annual CO_2 Increase	---	r = 0.810, P = 9.29e-16	r = 0.814, P = 5.03e-16	---	r = 0.753, P = 1.1e-12
HAD-SST	---	---	r = 0.993, P = 1.87e-57	---	r = 0.926, P = 1.64e-27
GISS-SST	---	---	---	---	r = 0.919, P = 2.73e-26

Furthermore, the correlation coefficient for CO_2 increase is consistently higher with SST than with emissions.

And in the analysis of Step 2 (after 1979), only UAH-SST was the explanatory factor in the multiple regression analysis. The Variance Inflation Factor (VIF) in this case is 1.86 in both IEA and OWID (Appendix Table 2).

Appendix Table 2. Variance inflation factors in the multiple regression analysis Annual CO_2 increase is the objective factor. All abbreviations refer to the main text.

	OWID	IEA
UAH-SST	<1979~2021> 1.86	<1979~2021> 1.86
HAD-SST	<1979~2021> 5.02 <1959~2021> 7.03	<1979~2021> 5.00
GISS-SST	<1979~2021> 4.22 <1959~2021> 6.41	<1979~2021> 4.17

The same analysis was performed (Step 5) using HAD-SST and GISS-SST in the post-1979 analysis, and the results of the multiple regression analysis were also similar. And the VIF was about 4 to 5 (Appendix Table 2).

Thus, at least as an interpretation of the results from the post-1979 analysis, the human emissions were not significant factor because of the high explanatory power of each SST.

Furthermore, the results were essentially the same in the post-1959 analysis (Step 6).

Again, even in the post-1979 analysis, when emissions have clearly increased than before, only SSTs independently explained the annual increase of CO_2. Even during this period, human emissions did not predict the annual CO_2 increase. Therefore, it is inevitable that the same result was obtained including the period of much smaller emissions from 1959 to 1978 (27.30 ± 6.25 gigatons for after 1979, and 13.70 ± 3.43 gigatons between 1959 and 1978, OWID data).

And because the VIF is 6.4~7 in the entire period (Appendix Table 2), the results of the multiple regression analysis are considered reasonable and valid.

The predictive power of CO_2 concentrations by SST after 1959 (Step 7) also supports this interpretation and the results of this study.

For reference, correlation diagrams of each indicator since 1959 are shown below.

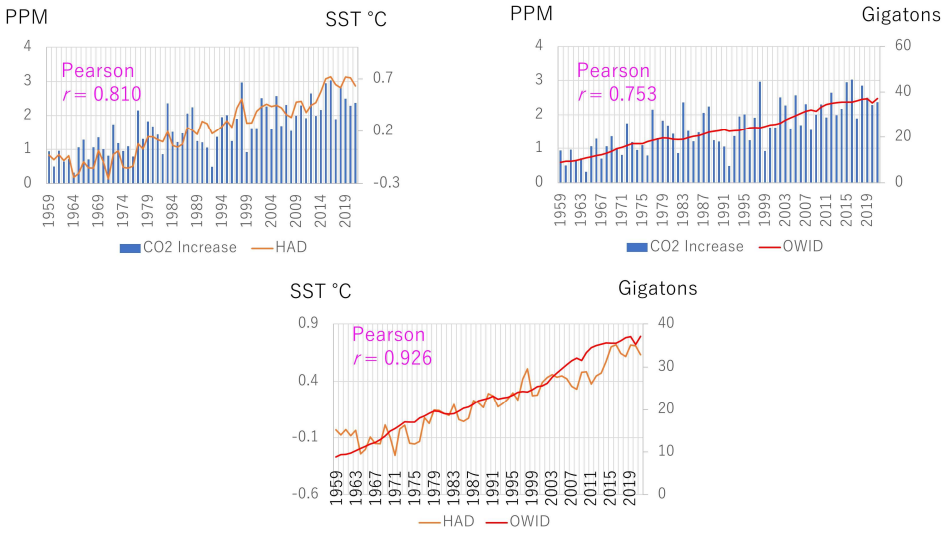

Appendix Figure. HAD-SST, human emissions, CO_2 increase between 1959 and 2021

References

1. M. Thatcher, 2002: Statecraft: Strategies for a Changing World
2. Sixth Assessment Report (AR6), IPCC, 2021: V. Masson-Delmotte, P. Zhai, A. Pirani et al.: Climate Change 2021: The Physical Science Basis. Contribution of Working Group I to the Sixth Assessment Report of the Intergovernmental Panel on Climate Change, Cambridge University Press.
3. Oregon Institute of Science and Medicine, Year: *Global Warming Petition Project* http://www.petitionproject.org/index.php
4. A. B. Robinson, N. E. Robinson, W. Soon, 2007: *Environmental Effects of Increased Atmospheric Carbon Dioxide*, Journal of American Physicians and Surgeons (2007) 12, pp. 79-90, http://www.petitionproject.org/review_article.php
5. Singer S.F., 2008: Nature, Not Human Activity, Rules the Climate: Summary for Policymakers of the Report of the Nongovernmental International Panel on Climate Change, Chicago, IL: The Heartland Institute, 2008. https://yosemite.epa.gov/oa/EAB_Web_Docket.nsf/Filings%20By%20Appeal%20Number/5E65BBBD50EED79A85257416005ACE06/$File/Exhibit...32.pdf
6. GLOBAL CLIMATE INTELLIGENCE GROUP: World Climate Declaration, *There is no climate emergency,* https://clintel.org/world-climate-declaration/
7. Clima, una petizione controcorrente, 2019: https://opinione.it/cultura/2019/06/19/redazione_riscaldamento-globale-antropico-clima-inquinamento-uberto-crescenti-antonino-zichichi/?altTemplate=Stampa&fbclid=IwAR1YAoqulAKKXJTY-uzRfSEaX-G6NRpVOckp3nVE7iiTAgOQu8DMHGUxRnE
8. Clauser J. F., 2023: Nobel Prize Winner Dr. John F. Clauser signs the Clintel World Climate Declaration https://clintel.org/nobel-prize-winner-dr-john-f-clauser-signs-the-clintel-world-climate-declaration/
9. Christy J.R., Goodridge J.D., 1995: *Precision global temperatures from satellites and urban warming effects of non-satellite data*, Atmospheric Environment, Volume 29, Issue 16, p. 1957-1961. https://doi.org/10.1016/1352-2310(94)00240-L
10. Jaworowski Z., Segalstad T.V., Hisdal V., 1992: *Atmospheric CO_2 and global warming: a critical review*. 2nd edition, 1992 https://www.researchgate.net/publication/307215789_Atmospheric_CO2_and_global_warming_a_critical_review_2nd_edition
11. Jaworowski Z., Segalstad T.V., Ono N., 1992: *Do glaciers tell a true atmospheric CO_2 story?* The Science of The Total Environment 114(12):227-284 https://doi.org/10.1016/0048-9697(92)90428-U
12. Neftel A., Moor E., Oeschger H., Stauffer B., 1985: *Evidence from polar ice cores for the increase in atmospheric CO_2 in the past two centuries*, Nature volume 315, pages 45–47(1985), https://www.nature.com/articles/315045a0
13. Craig H., Chou C. C., Welhan J. A., Stevens C. M., Engelkemeir A., 1988: *The Isotopic Composition of Methane in Polar Ice Cores*, Science 16 Dec 1988:Vol. 242, Issue 4885, pp. 1535-1539, https://www.science.org/doi/10.1126/science.242.4885.1535
14. Stauffer B., Berner W., Oeschger H., Schwander J., 1981: *Atmospheric CO_2 history from ice core studies,* Zeitschr. für Gletcherkunde und Glaziol.,1981, 17: 1-15.

15. Beck E-G, 2022: *Reconstruction of Atmospheric CO_2 Background Levels since 1826 from direct measurements near ground*, Science of Climate Change, Vol 2.2 (2022) pp.148-211, https://doi.org/10.53234/scc202112/16

16. Yndestad H., 2022: *Lunar Forced Mauna Loa and Atlantic CO_2 Variability*. Science of Climate Change, Vol. 2.3 (2022) pp. 258-274, https://doi.org/10.53234/scc202212/13

17. NASA earth observatory: *The Carbon Cycle*, https://earthobservatory.nasa.gov/features/CarbonCycle

18. International Energy Agency: *Greenhouse Gas Emissions from Energy Highlights*, https://www.iea.org/data-and-statistics/data-product/greenhouse-gas-emissions-from-energy-highlights Accessed on 27, August 2023

19. NOAA Global Monitoring Laboratory: *Trends in Atmospheric Carbon Dioxide,* https://gml.noaa.gov/ccgg/trends/data.html Accessed on 27, August 2023

20. Spencer, R.W., Christy, J.R. Braswell, W.D., 2017: *UAH Version 6 global satellite temperature products: Methodology and results.*, Asia-Pacific J Atmos Sci 53, 121–130 (2017). https://doi.org/10.1007/s13143-017-0010-y

21. Spencer R.: *Latest Global Temps* https://www.drroyspencer.com/latest-global-temperatures/ Accessed on 27, August 2023

22. Kennedy, J. J., Rayner, N. A., Atkinson, C. P., Killick, R. E., 2019.: *An ensemble data set of sea-surface temperature change from 1850: the Met Office Hadley Centre HadSST.4.0.0.0 data set.* Journal of Geophysical Research: Atmospheres, 124. https://doi.org/10.1029/2018JD029867

23. Met Office Hadley Centre observations datasets: Accessed on 24, September 2023, https://www.metoffice.gov.uk/hadobs/hadsst4/data/download.html

24. Lenssen, N., Schmidt G., Hansen J., Menne M., Persin A., Ruedy R., Zyss D., 2019: *Improvements in the GISTEMP uncertainty model.*, J. Geophys. Res. Atmos., 124, no. 12, 6307-6326, https://doi.org/10.1029/2018JD029522

25. NASA Goddard Institute for Space Studies: *GISS Surface Temperature Analysis (v4),* Accessed on 24, September 2023 https://data.giss.nasa.gov/gistemp/graphs_v4/

26. Data on CO_2 and Greenhouse Gas Emissions by Our World in Data https://github.com/owid/co2-data Accessed on 2, September 2023

27. Kanda Y., 2013: *Investigation of the freely available easy-to-use software 'EZR' for medical statistics*, Bone Marrow Transplantation 2013: 48, 452–458, https://doi.org/10.1038/bmt.2012.244

28. Harde H., 2023: *About Historical CO_2-Data since 1826: Explanation of the Peak around 1940*, Science of Climate Change, Vol. 3.2 (2023) pp. 211-218, https://doi.org/10.53234/scc202304/21

29. Koutsoyiannis D., Kundzewicz Z. W., 2020: *Atmospheric Temperature and CO_2: Hen-Or-Egg Causality?* Sci 2020, 2(4), 83, https://doi.org/10.3390/sci2040083

30. Salby M., Harde H., 2022: *Theory of Increasing Greenhouse Gases*, Science of Climate Change, Vol. 2.3 (2022) pp. 212-238, https://doi.org/10.53234/scc202212/17

31. Stallinga P., Khmelinskii I., 2018: *Analysis of Temporal Signals of Climate*, Natural Science, 2018, Vol. 10, (No. 10), pp: 393-403,

https://www.scirp.org/pdf/NS_2018101510264849.pdf,
https://doi.org/10.4236/ns.2018.1010037

32. NOAA Global Monitoring Laboratory: *Trends in Atmospheric Carbon Dioxide, Recent Global CO_2 Trend*
https://gml.noaa.gov/ccgg/trends/gl_trend.html
33. Spencer R., 2009: *Increasing Atmospheric CO_2: Manmade…or Natural?*
https://www.drroyspencer.com/2009/01/increasing-atmospheric-co2-manmade%E2%80%A6or-natural/
34. NOAA Global Monitoring Laboratory: *Trends in Atmospheric Methane,*
https://gml.noaa.gov/ccgg/trends_ch4/ Accessed on 30, October 2023
35. NASA earth observatory: *Methane Matters,*
https://earthobservatory.nasa.gov/features/MethaneMatters
36. The Intergovernmental Panel on Climate Change, 2007: *IPCC Fourth Assessment Report, Summary for Policymakers,*
https://www.ipcc.ch/site/assets/uploads/2018/02/ar4-wg1-spm-1.pdf
37. D. Ato, 2024: Data set used in this study available as supplemental Excel file
https://note.com/api/v2/attachments/download/4b813ffc78de8018b7d28d4478ca6650

OPEN ACCESS

Klimarealistene
Vollsveien 109
1358 Jar, Norway
ISSN: 2703-9072

Correspondence:
Moritz.Buesing@gmail.com

Vol. 4.2 (2024)

pp. 16-35

Systematic Error in Global Temperatures due to Weather Station Ageing

Moritz Büsing

Augsburg, Germany

Abstract

The white paint or white plastic of the housings of weather stations ages, which leads to increased absorption of solar radiation and to increased temperature measurements. This alone would be a small error. However, many different state-of-the-art homogenization algorithms repeatedly add this small value each time a weather station is renovated, renewed, or replaced, which results in a substantial systematic error.

This error occurs, because steps in the temperature data series are corrected as if they were permanent, but this is not always the case, particularly not in case of weather station ageing and renewal.

An in-depth analysis of the weather station data sets (homogenized and non-homogenized) confirmed the presence of this systematic error, proved the existence of statistically significant ageing effects, and allowed the author to quantify the size of the ageing effects.

The effect of the ageing effects on the temperature curves is quantified by adding the ageing functions to the temperature data points in the intervals between homogenizations. This corrected data base is analyzed using the GISTEMP tool.

Here it is shown that a reduction of the temperature change between the decades 1880-1890 and 2010-2020 also reduces the objective temperature increase from 1.43 °C to 0.83 °C (Confidence Interval 95 %: [0.46 °C; 1.19 °C]).

Keywords: Temperature anomaly; ageing; weather stations; homogenization; land surface temperatures.

Submitted 2024-02-10, Accepted 2024-08-20. https://doi.org/10.53234/scc202407/21

1. Introduction

Several institutions have performed surface temperature analyses, such as GISTEMP from the Goddard Institute for Space Studies (GISS), and HadCRUT from the Hadley Centre for Climate Prediction and Research. A data homogenization step is performed before or during these analyses. The homogenization algorithms differ in the way they detect the time and size of stepwise changes in the data series, but they are very similar - often almost identical, regarding how the detected steps are corrected. See Venema et al. 2018 for an authoritative overview of the often-ingenious homogenization methods, algorithms and related literature.

There are many different such algorithms (e.g. ACMANT, HOMER, MASH), but this work mainly addresses the corrections as they are applied by the "pairwise algorithm" (Menne et al. 2009) from the National Centers for Environmental Information (NCEI) of the National Oceanic and Atmospheric Administration (NOAA), because this covers most of the other algorithms. Furthermore, the excellent documentation and data availability by GISS and NCEI NOAA made it

particularly easy to reproduce their results, and finally adjust them.

Homogenization consists of removing non-climate related changes in temperature, especially stepwise changes in temperature measurements related to using different types of weather stations, different instrumentation, different housings, different recording methods and/or different locations. The data series are homogenized by adjusting the past data such that the data series becomes continuous and shows a homogenous trend with the other highly correlated weather stations. This means when there is an upwards step in the data series, then all the past data are increased by the size of the step. When there is a downwards step in the data series then all the past data are decreased by the size of the step.

These stepwise corrections are applied equally to all adjusted data. This means that the same offset is applied to all data before a step. This is correct for changes in instrumentation, type of weather station or location, however, a systematic error occurs when this is applied to temporary steps in the data series.

Ageing effects change the temperature measurements continuously until the effect is saturated. When the station is cleaned, repainted, or the housing is replaced, then there is a downwards step. But this step is temporary, because the ageing effects return within a few years and then reach saturation again (see Figure 1).

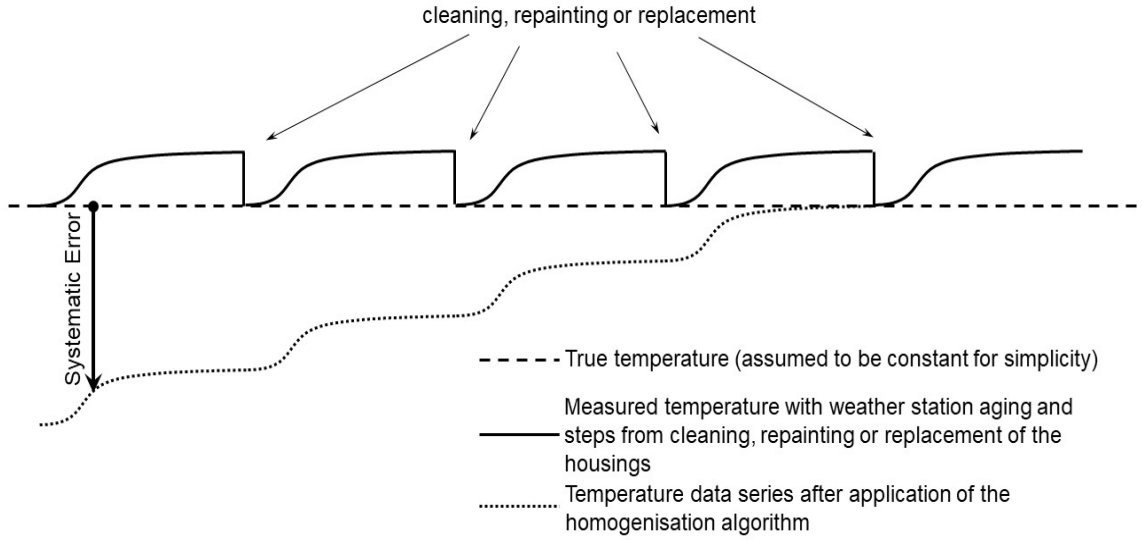

Figure 1: Sketch of the principle of the systematic error in the homogenization algorithm, when applied to non-permanent steps in the data series.

Most causes of large stepwise temperature changes, such as changes in instrumentation, type of weather station or location, coincide with cleaning, repainting, or replacing the housing of the weather stations.

2. Material and Methods

2.1 Systematic error due to ageing effects

The white paint or white plastic of the housings of weather stations age and become dirty which leads to slightly higher temperature measurements. This phenomenon was analyzed by a group at the Istituto Nazionale die Ricerca Metrologica in Turin, Italy (Lopardo et al. 2013). Their research determined the effect on the maximum daily, minimum daily and mean temperature effect of five years of ageing. The maximum daily temperature changes by an average of 0.46 °C, and the

minimum daily temperature does not change. The data from another pair of stations, one which was one year old and the other three years old, show an average change of the maximum daily temperature of 0.49 °C within two years. This suggests substantial scatter that cannot be quantified here due to the different time intervals.

The data from a third pair of weather stations, one new and one which was one year old, show no change of the maximum daily temperature. The minimum daily temperature is unchanged; therefore, the total mean change can be conservatively assumed to be 0.46 °C / 2 = 0.23 °C for the five-year interval.

The reason for the comparatively large change of the maximum daily temperatures and the absence of change of the minimum daily temperatures, is presumably the change of the albedo of housing of the weather stations. The albedo has a large effect when the housing is exposed to direct or indirect sunlight and smaller effect when the housing is not exposed to sunlight. In theory there should even be a small cooling effect during the night, which has apparently been too small to measure in this study. Note: this change in albedo can happen in the visible spectrum, but also outside of the visible spectrum: in the infrared spectrum and the ultraviolet spectrum. Therefore, not all of these changes of the albedo are visible with the naked eye.

The ageing effect is continuous but cleaning, repainting, or replacing the housings of weather stations leads to a downward step of 0.23 °C. This step is too small in order to be reliably detected by the homogenization algorithms. Therefore, most such events do not lead to an over-correction of the time series data. However, if a larger step occurs, then the full step is corrected, including over-correcting the ageing effect. Each time a stepwise correction is applied by the homogenization algorithm, regardless of it being an upwards or a downwards step, the ageing effect of 0.23 °C is added. For example, if there are 5 stepwise corrections of the data from a weather station, then there are 5 successive downward over-corrections of the past data, leading to a false overall temperature trend of 5*0.23 °C = 1.15 °C (Note: This calculation is only for the explanation of the effect. The worldwide average effect size per homogenization step is determined in the following chapters without the input from Lopardo et al. (2013).

2.2 Existence of the systematic error in the NOAA weather station basis

Reverse engineering the homogenized temperature data set “ghcnm.tavg.qcf.dat” and the non-homogenized data set “ghcnm.tavg.qcu.dat” provided by NCEI NOAA (Menne et al. 2018), results in an average of 7.2 stepwise homogenizations per 140 years of recordings or roughly once in 19 years. This is confirmed by the documentation of the homogenization (Menne et al. 2009) which states an average interval between 15 and 20 years, and therefore validates the reverse engineering method. Since the reverse engineered interval is on the high end of the documented range, the correction described below is conservative.

There is no mention of a sub-algorithm addressing ageing effects or other non-permanent steps in the documentation of the homogenization algorithms. But there may be an undocumented correction.

An in-depth analysis of the detected homogenizations confirmed the absence of a correction for non-permanent steps during the homogenization process. Nevertheless, the corrections in the following analysis are only applied to those time periods between homogenizations without a negative trend in the differences between raw data and homogenized data, i.e., 98.6 % of the detected 82,622 stepwise homogenizations, in order to be conservative (81,465 stepwise homogenizations remain).

2.3 The size of the ageing effects

The size of the ageing effect was derived from a study with a small dataset (Lopardo et al. 2013) that does not allow for a statistical analysis, and which may not be representative for different climates around the world. Fortunately, this effect can also be extracted from the two NCEI NOAA datasets that contain measured temperatures from 27,107 land-based weather stations around the world by searching for the comparably increased temperature gradient starting one year after a homogenization step.

The ageing effects were analyzed for 4 time periods, because the pigments in the paint and the materials changed over time. The boundaries between these time periods are somewhat arbitrary because the uses of different technologies overlapped. Nevertheless, this separation into time periods should improve the analysis:

- 1880-1909: Paint with zinc sulphide and lead chromate pigments
- 1910-1959: Paint with barium sulphate pigments
- 1960-1989: Paint with titanium dioxide pigments
- 1990-2020: Plastic with titanium dioxide pigments

For each calendar year the temperature gradient is calculated as the difference between the current year and the previous year (wherever both data points are available). Then these gradients during each calendar year from several weather stations were averaged in 4 separate groups, depending on the year after the last stepwise homogenization at each weather station. For example, for 1990 to 2020:

a) average gradient 1st year after a step
b) average gradient 2nd to 13th year after a step
c) average gradient 14th to 35th year after a step
d) average gradient after the 35th year after a step

In a second loop, the average gradient of the interval c) was subtracted from each point in the intervals a), b) and d). These differences display the different phases of ageing:

a) No initial ageing in the first year or first two years
b) "Early" ageing effect
c) Reference period
d) "Late" ageing effect

Here, the same phenomenon becomes apparent as with the tests documented by Lopardo et al. (2013). There is no statistically significant ageing effect during the first year. This may be caused by an initial bleaching effect and/or by remaining chemical buffering of the photocatalytic ageing.

Then a statistically significant ageing effect occurs during the years 2 to 13 followed by saturation of the ageing effect. The mean ageing effect starts to increase again after 35 years (possibly heavier degradation of the paint or plastic).

2.4 Correction of the homogenized weather station data

First both data sets "ghcnm.tavg.qcf.dat" and "ghcnm.tavg.qcu.dat" were loaded into a program.

All the weather stations that are not part of "ghcnm.tavg.qcf.dat" were removed from "ghcnm.tavg.qcu.dat".

The differences between each pair of temperature data points were calculated.

The differences were compared for each month in successive years. If there is missing data (i.e. temperature = -9999) or the difference in differences is less than 0.1 °C, then the comparison bracket is expanded to the next year. Once the difference in differences exceeds 0.1 °C a stepwise correction is detected.

The ageing effect was removed from the data set by adding the ageing effect functions to each point of the dataset. The number of years since the last homogenization step is calculated. Then the gradient of the correction function is assigned to each data point based on the calendar year and on the number of years since the last homogenization. These gradients are integrated backwards in time in order to identify the offsets for the correction. These offsets are added to each data point of the homogenized dataset resulting in the corrected dataset.

3. Results

3.1 Ageing Functions

The phases of ageing were analyzed for each of the time periods by evaluating the datasets from 27,107 weather stations compiled by NOAA according to the methods described in the previous chapter. The mean ageing effects were determined, and the confidence intervals (CI) were calculated:

- 1880-1909: There is a clear early ageing effect (0.01605 °C/yr CI(95 %) [0.00779 °C/yr; 0.02521 °C/yr]). The mean values show a late ageing effect; however, it is not statistically significant. Only the early ageing effect will be corrected.

- 1910-1959: The early ageing effect is shortened to 5 years (0.02303 °C/yr CI(95 %) [0.01652 °C/yr; 0.02954 °C/yr]). There is a late ageing effect starting at 35 years that is statistically significant (0.01054 °C/yr CI(95 %) [0.00001 °C/yr; 0.02107 °C/yr]).

- 1960-1989: There seems to be no detectable early ageing effect despite good data quality. This is possibly due to the high UV-resistance and high UV-absorption of the titanium dioxide pigments. Alternatively, there may be a slow ageing effect without saturation, which makes the selection of a reference period impossible. There is a clear late ageing effect starting at 25 years that is statistically significant (0.00884 °C/yr CI(95 %) [0.00136 °C/yr; 0.01632 °C/yr]). Only the late ageing effect will be corrected.

- 1990-2020: There are clearly detectable statistically significant early ageing (0.00921 °C/yr CI(95 %) [0.00602 °C/yr; 0.01241 °C/yr]) and late ageing effects (0.01409 °C/yr CI(95 %) [0.00643 °C/yr; 0.02174 °C/yr]). The plastic matrix is prone to discoloration despite the high UV-resistance of the titanium dioxide pigments.

The explanations above assume that a stepwise homogenization always coincides with cleaning, repainting, or replacing the housing of a weather station. However, this may not always have been the case. Therefore, multiple variants were analyzed with various probabilities of coincidence. This showed an approximately linear relationship between the step size and magnitude of the correction, and also an approximately linear relationship between the probability of coincidence and magnitude of the correction. Therefore, determining a "mixed" ageing function that includes both the magnitude and the probability of coincidence is sufficient. The ageing functions displayed in Figure 2 overleaf are therefore "mixed" ageing functions that consist of the steeper "true" ageing functions reduced by an unknown probability of coincidence. This unknown probability of coincidence also increases the scatter.

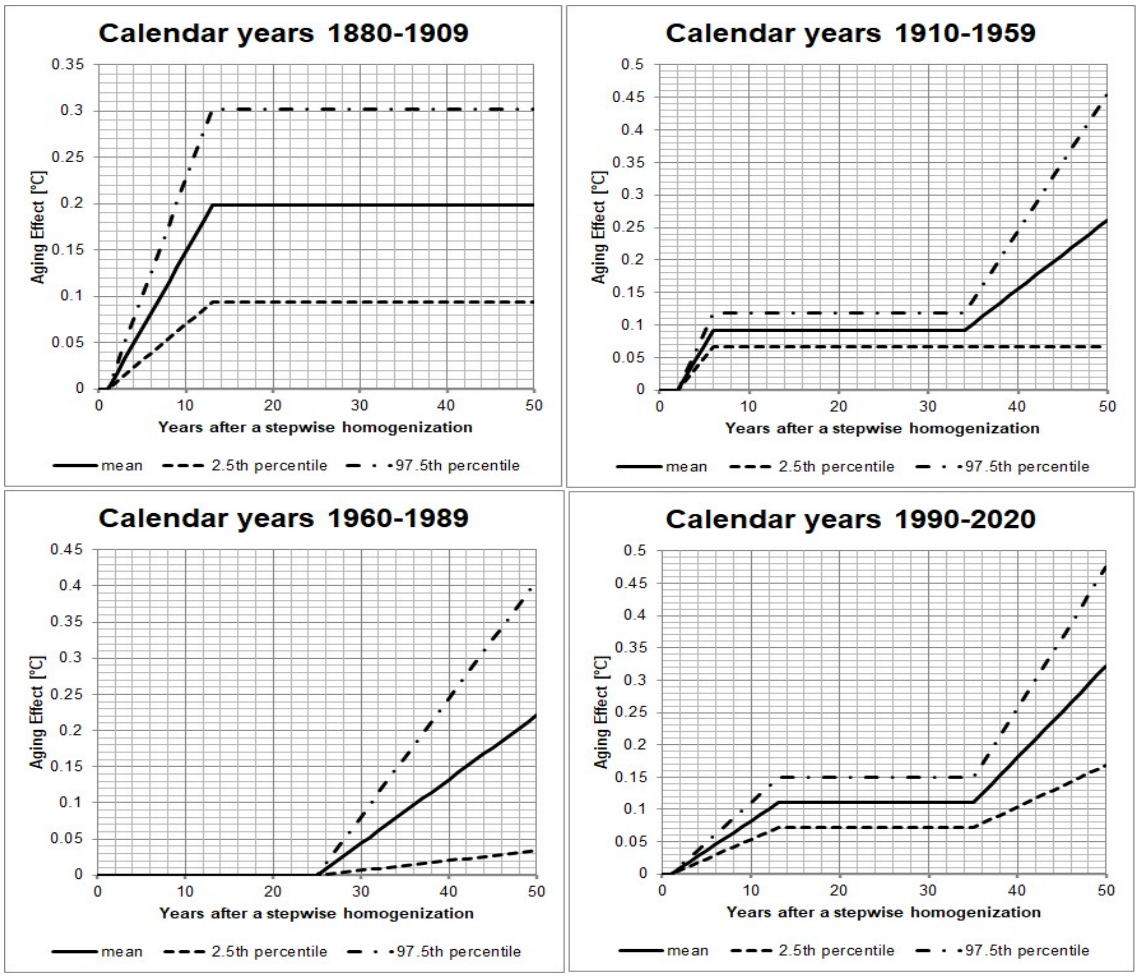

Figure 2: Graphs of the ageing effect functions for the different time periods.

3.2 Example: Weather Station Hamburg-Fuhlsbüttel

The following tables (Table 1-4) show a shortened example of the methods applied for this study. Only the data from the month of July is shown for brevity, but this process is applied to all months for the analysis performed in this study. Please note: In Tables 1, 2 and 4, the entries are marked in yellow, where homogenization steps occur.

At each homogenization step the differences between the non-homogenized dataset and the homogenized dataset changes. This is detected by calculating the Difference of Differences to the same month in the previous year. Then the number of years since each homogenization event, and the beginning of the dataset are counted.

This is done for all weather stations. Then the average change in temperature per year and the scatter is calculated for all weather stations that have data within each time interval with the same number of years from the previous homogenization step. These averages are compared to the averages of the reference period during which the ageing effect is assumed to be zero (conservative assumption). This difference is the ageing effect.

These differences in average, the scatter, and the number of applicable weather stations are used to calculate the mean and the confidence intervals of the ageing functions.

Note: The homogenization steps are approximately randomly distributed in time between the thousands of weather stations. Therefore, autocorrelation can be excluded.

The slope of the ageing functions of each time period is applied according to the year since each previous homogenization event. This is integrated backwards in order to determine the cumulative ageing effect. The cumulative ageing effect is added to the original homogenized dataset in order to get the corrected homogenized dataset.

Note: The difference between the homogenized dataset and the corrected dataset can be larger than the difference between the homogenized dataset and the non-homogenized dataset. This means that a correct homogenization taking the ageing effect into account, can lead to even less overall warming trend than the non-homogenized dataset. The differences between the non-homogenized dataset and the homogenized dataset are also discussed at length in the documentation of Menne et al. (2018).

Table 1: Processed Data from Weatherstation Hamburg-Fuhlsbüttel interval 1880 to 1909. Homogenization steps are marked in yellow.

Year	Non-Homo-genized July	Homo-genized July	Diffe-rence between Datasets	Difference of Differences to previous year	Years since Ho-mogeniza-tion	Ageing effect per year	Cumula-tive ageing effect	Corrected Homo-genized July
	[°C]	[°C]	[°C]	[°C]	[yrs]	[°C/yr]	[°C]	[°C]
1881	18.00	17.38	-0.62	NA	0	0	1.17	18.55
1882	17.50	16.88	-0.62	0	1	0.0161	1.17	18.05
1883	17.50	16.88	-0.62	0	2	0.0161	1.16	18.04
1884	18.50	17.88	-0.62	0	3	0.0161	1.14	19.02
1885	17.30	16.68	-0.62	0	4	0.0161	1.12	17.80
1886	16.10	15.48	-0.62	0	5	0.0161	1.11	16.59
1887	17.90	17.28	-0.62	0	6	0.0161	1.09	18.37
1888	14.40	13.78	-0.62	0	7	0.0161	1.08	14.86
1889	16.20	15.58	-0.62	0	8	0.0161	1.06	16.64
1890	15.40	14.78	-0.62	0	9	0.0161	1.04	15.82
1891	17.12	16.18	-0.94	-0.32	0	0	1.03	17.21
1892	15.58	14.64	-0.94	0	1	0.0161	1.03	15.67
1893	17.64	16.70	-0.94	0	2	0.0161	1.01	17.71
1894	18.45	17.51	-0.94	0	3	0.0161	1.00	18.51
1895	16.84	15.90	-0.94	0	4	0.0161	0.98	16.88
1896	17.56	16.62	-0.94	0	5	0.0161	0.96	17.58
1897	16.12	15.18	-0.94	0	6	0.0161	0.95	16.13
1898	14.22	13.22	-1.00	-0.06	0	0	0.93	14.15
1899	18.39	17.39	-1.00	0	1	0.0161	0.93	18.32
1900	18.37	17.37	-1.00	0	2	0.0161	0.91	18.28
1901	19.37	18.37	-1.00	0	3	0.0161	0.90	19.27
1902	15.51	14.51	-1.00	0	4	0.0161	0.88	15.39
1903	16.85	15.85	-1.00	0	5	0.0161	0.87	16.72
1904	17.65	16.65	-1.00	0	6	0.0161	0.85	17.50
1905	18.34	17.34	-1.00	0	7	0.0161	0.83	18.17
1906	17.73	16.73	-1.00	0	8	0.0161	0.82	17.55
1907	15.19	14.19	-1.00	0	9	0.0161	0.80	14.99
1908	18.10	17.10	-1.00	0	10	0.0161	0.79	17.89
1909	15.76	14.76	-1.00	0	11	0.0161	0.77	15.53

Table 2: Processed Data from Weatherstation Hamburg-Fuhlsbüttel interval 1910 to 1959. Homogenization steps are marked in yellow.

Year	Non-Homo-genized July	Homo-genized July	Diffe-rence between Datasets	Difference of Differences to previous year	Years since Ho-mogeniza-tion	Ageing effect per year	Cumula-tive ageing effect	Corrected Homo-genized July
	[°C]	[°C]	[°C]	[°C]	[yrs]	[°C/yr]	[°C]	[°C]
1910	16.51	15.51	-1.00	0	12	0	0.75	16.26
1911	18.62	17.62	-1.00	0	13	0	0.75	18.37
1912	19.40	18.40	-1.00	0	14	0	0.75	19.15
1913	15.96	14.96	-1.00	0	15	0	0.75	15.71
1914	19.23	18.23	-1.00	0	16	0	0.75	18.98
1915	16.47	15.47	-1.00	0	17	0	0.75	16.22
1916	16.51	15.51	-1.00	0	18	0	0.75	16.26
1917	17.78	16.78	-1.00	0	19	0	0.75	17.53
1918	17.24	16.24	-1.00	0	20	0	0.75	16.99
1919	15.38	14.38	-1.00	0	21	0	0.75	15.13
1920	17.89	17.07	-0.82	0.18	0	0	0.75	17.82
1921	17.77	16.95	-0.82	0	1	0	0.75	17.70
1922	16.07	15.25	-0.82	0	2	0.023	0.75	16.00
1923	18.92	18.10	-0.82	0	3	0.023	0.73	18.83
1924	17.16	16.34	-0.82	0	4	0.023	0.71	17.05
1925	19.57	18.75	-0.82	0	5	0.023	0.68	19.43
1926	18.98	18.16	-0.82	0	6	0.023	0.66	18.82
1927	18.54	17.72	-0.82	0	7	0	0.64	18.36
1928	17.22	16.40	-0.82	0	8	0	0.64	17.04
1929	17.43	16.61	-0.82	0	9	0	0.64	17.25
1930	17.50	16.68	-0.82	0	10	0	0.64	17.32
1931	17.47	16.65	-0.82	0	11	0	0.64	17.29
1932	19.59	18.77	-0.82	0	12	0	0.64	19.41
1933	18.95	18.13	-0.82	0	13	0	0.64	18.77
1934	19.08	18.26	-0.82	0	14	0	0.64	18.90
1935	16.54	16.41	-0.13	0.69	0	0	0.64	17.05
1936	17.60	17.47	-0.13	0	1	0	0.64	18.11
1937	17.40	17.27	-0.13	0	2	0.023	0.64	17.91
1938	16.82	16.69	-0.13	0	3	0.023	0.62	17.31
1939	17.82	17.69	-0.13	0	4	0.023	0.59	18.28
1940	16.66	16.21	-0.45	-0.32	0	0	0.57	16.78
1941	19.62	19.17	-0.45	0	1	0	0.57	19.74
1942	16.14	15.69	-0.45	0	2	0.023	0.57	16.26
1943	17.66	17.21	-0.45	0	3	0.023	0.55	17.76
1944	18.07	17.62	-0.45	0	4	0.023	0.52	18.14
1945	17.82	17.37	-0.45	0	5	0.023	0.50	17.87
1946	18.13	17.68	-0.45	0	6	0.023	0.48	18.16
1947	17.73	17.53	-0.20	0.25	0	0	0.45	17.98
1948	16.78	16.58	-0.20	0	1	0	0.45	17.03
1949	16.59	16.39	-0.20	0	2	0.023	0.45	16.84
1950	16.82	16.62	-0.20	0	3	0.023	0.43	17.05
1951	16.44	16.24	-0.20	0	4	0.023	0.41	16.65
1952	16.51	16.31	-0.20	0	5	0.023	0.39	16.70
1953	17.70	17.50	-0.20	0	6	0.023	0.36	17.86
1954	14.91	14.71	-0.20	0	7	0	0.34	15.05
1955	17.96	17.76	-0.20	0	8	0	0.34	18.10
1956	17.20	17.00	-0.20	0	9	0	0.34	17.34
1957	17.64	17.44	-0.20	0	10	0	0.34	17.78
1958	16.60	16.40	-0.20	0	11	0	0.34	16.74
1959	18.78	18.58	-0.20	0	12	0	0.34	18.92

Table 3: Processed Data from Weatherstation Hamburg-Fuhlsbüttel interval 1960 to 1989

Year	Non-Homo-genized July	Homo-genized July	Diffe-rence between Datasets	Difference of Differences to previous year	Years since Ho-mogeniza-tion	Ageing effect per year	Cumula-tive ageing effect	Corrected Homo-genized July
	[°C]	[°C]	[°C]	[°C]	[yrs]	[°C/yr]	[°C]	[°C]
1960	15.69	15.49	-0.20	0	13	0	0.34	15.83
1961	15.54	15.34	-0.20	0	14	0	0.34	15.68
1962	14.55	14.35	-0.20	0	15	0	0.34	14.69
1963	17.18	16.98	-0.20	0	16	0	0.34	17.32
1964	16.83	16.63	-0.20	0	17	0	0.34	16.97
1965	14.76	Missing	Missing	Missing	18	0	0.34	Missing
1966	15.99	15.79	-0.20	0	19	0	0.34	16.13
1967	17.62	17.42	-0.20	0	20	0	0.34	17.76
1968	16.30	16.10	-0.20	0	21	0	0.34	16.44
1969	18.49	18.29	-0.20	0	22	0	0.34	18.63
1970	16.08	15.88	-0.20	0	23	0	0.34	16.22
1971	17.37	17.17	-0.20	0	24	0	0.34	17.51
1972	17.69	17.49	-0.20	0	25	0	0.34	17.83
1973	17.92	17.72	-0.20	0	26	0.0088	0.34	18.06
1974	14.91	14.71	-0.20	0	27	0.0088	0.33	15.04
1975	18.38	18.18	-0.20	0	28	0.0088	0.32	18.50
1976	18.90	18.70	-0.20	0	29	0.0088	0.31	19.01
1977	16.34	16.14	-0.20	0	30	0.0088	0.30	16.44
1978	15.72	15.52	-0.20	0	31	0.0088	0.30	15.82
1979	14.90	14.70	-0.20	0	32	0.0088	0.29	14.99
1980	15.77	15.57	-0.20	0	33	0.0088	0.28	15.85
1981	16.32	16.12	-0.20	0	34	0.0088	0.27	16.39
1982	18.36	18.16	-0.20	0	35	0.0088	0.26	18.42
1983	19.38	19.18	-0.20	0	36	0.0088	0.25	19.43
1984	15.70	15.50	-0.20	0	37	0.0088	0.24	15.74
1985	17.02	16.82	-0.20	0	38	0.0088	0.23	17.05
1986	17.38	17.18	-0.20	0	39	0.0088	0.23	17.41
1987	16.82	16.62	-0.20	0	40	0.0088	0.22	16.84
1988	17.32	17.12	-0.20	0	41	0.0088	0.21	17.33
1989	17.39	17.19	-0.20	0	42	0.0088	0.20	17.39

Table 4: Processed Data from Weatherstation Hamburg-Fuhlsbüttel interval 1990 to 2023. Homogenization steps are marked in yellow.

Year	Non-Homo-genized July	Homo-genized July	Diffe-rence between Datasets	Difference of Differences to previous year	Years since Ho-mogeniza-tion	Ageing effect per year	Cumula-tive ageing effect	Corrected Homo-genized July
	[°C]	[°C]	[°C]	[°C]	[yrs]	[°C/yr]	[°C]	[°C]
1990	16.37	16.17	-0.20	0	43	0.0064	0.19	16.36
1991	18.96	18.76	-0.20	0	44	0.0064	0.18	18.94
1992	18.79	18.59	-0.20	0	45	0.0064	0.18	18.77
1993	15.95	15.75	-0.20	0	46	0.0064	0.17	15.92
1994	21.88	21.68	-0.20	0	47	0.0064	0.16	21.84
1995	19.97	19.77	-0.20	0	48	0.0064	0.16	19.93
1996	16.14	15.94	-0.20	0	49	0.0064	0.15	16.09
1997	18.06	17.86	-0.20	0	50	0.0064	0.15	18.01
1998	16.07	15.87	-0.20	0	51	0.0064	0.14	16.01
1999	19.14	18.94	-0.20	0	52	0.0064	0.13	19.07
2000	15.91	15.71	-0.20	0	53	0.0064	0.13	15.84
2001	18.73	18.73	0.00	0.2	0	0	0.12	18.85
2002	17.63	17.63	0.00	0	1	0.0092	0.12	17.75
2003	19.39	19.39	0.00	0	2	0.0092	0.11	19.50
2004	16.32	16.32	0.00	0	3	0.0092	0.10	16.42
2005	18.33	18.33	0.00	0	4	0.0092	0.09	18.42
2006	21.85	21.85	0.00	0	5	0.0092	0.08	21.93
2007	16.96	16.96	0.00	0	6	0.0092	0.07	17.03
2008	18.53	18.53	0.00	0	7	0.0092	0.06	18.59
2009	18.39	18.39	0.00	0	8	0.0092	0.06	18.45
2010	20.89	20.89	0.00	0	9	0.0092	0.05	20.94
2011	16.71	16.71	0.00	0	10	0.0092	0.04	16.75
2012	17.10	17.10	0.00	0	11	0.0092	0.03	17.13
2013	18.88	18.88	0.00	0	12	0.0092	0.02	18.90
2014	20.37	20.37	0.00	0	13	0.0092	0.01	20.38
2015	17.80	17.80	0.00	0	14	0	0.00	17.80
2016	18.35	18.35	0.00	0	15	0	0.00	18.35
2017	16.85	16.85	0.00	0	16	0	0.00	16.85
2018	19.80	19.80	0.00	0	17	0	0.00	19.80
2019	18.20	18.20	0.00	0	18	0	0.00	18.20
2020	15.95	15.95	0.00	0	19	0	0.00	15.95
2021	19.45	19.45	0.00	0	20	0	0.00	19.45
2022	18.00	18.00	0.00	0	21	0	0.00	18.00
2023	17.75	17.75	0.00	0	22	0	0.00	17.75

3.3 Corrected Temperature Curves

New corrected homogenized temperature data sets were generated by introducing upwards corrections by applying the ageing functions to the reverse engineered stepwise homogenizations (see Figure 2).

The surface temperature analysis tool provided by GISS (GISTEMP Team 2021) was used with the original data set provided by NCEI NOAA and the corrected homogenized temperature data sets (see Figure 3).

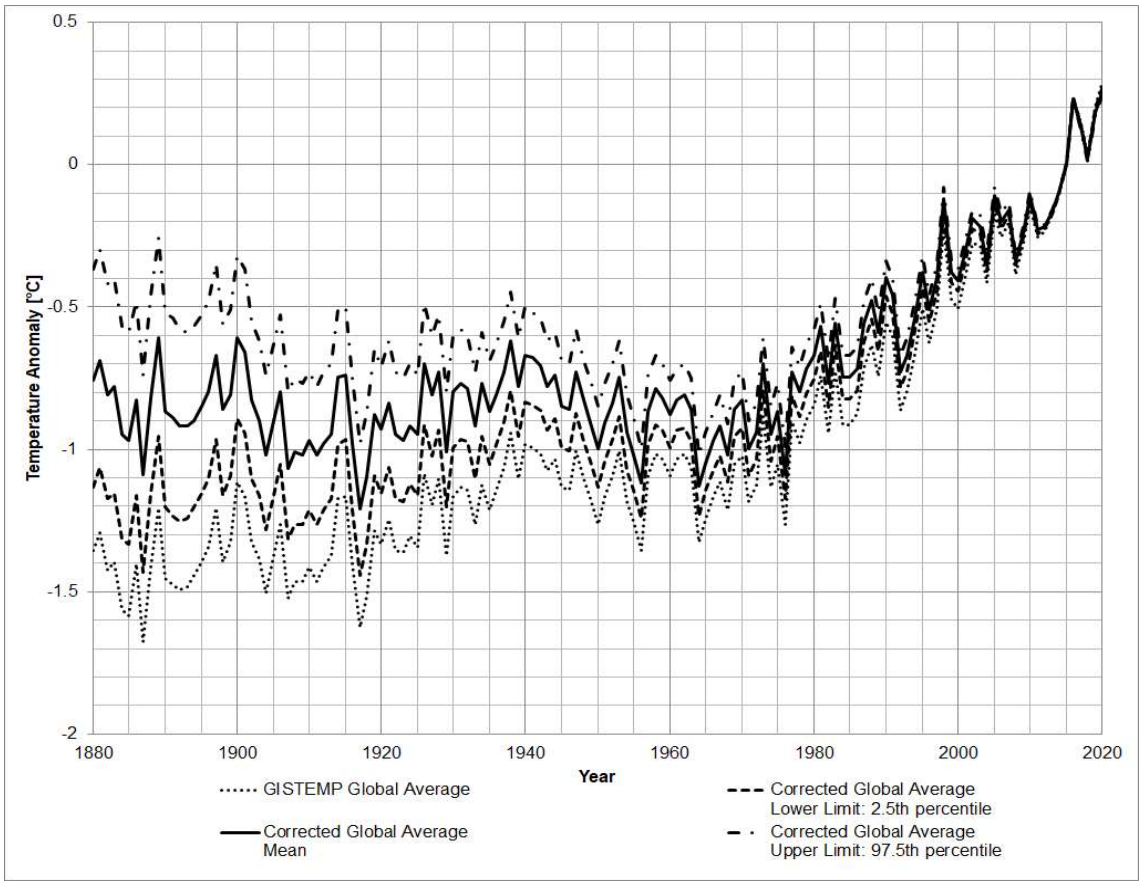

Figure 3: Global yearly land surface temperature anomalies calculated with the original homogenized weather station temperature dataset provided by GISS (dotted line) the 2.5th percentile corrected homogenized weather station temperature dataset (dashed line), mean corrected dataset (solid line) and 97.5th percentile corrected dataset (dashed-dotted line). The base period between 2010 and 2020 is selected in order to visualize the upwards correction of the past data.

4. Discussion

4.1 Discussion of conservative assumptions

This correction of the systematic error of over-correcting the ageing effect leads to a temperature difference between the decades 1880-1890 and 2010-2020 that is reduced by 42 % compared to the original GISTEMP data:

- Original temperature difference (GISTEMP): 1.43 °C
- Corrected temperature difference: 0.83 °C CI (95 %) [0.46 °C; 1.19 °C]

This analysis was performed with the following conservative assumptions:

- The ageing effect during the reference period is assumed to be exactly zero. However, if there is a remaining small ageing effect, then this amount is missing from the ageing functions of all periods. Assuming an undetectably small 0.002 °C/yr, then this would reduce the temperature difference between the decades 1880-90 to 2010-20 by a further 0.26 °C.
- Only the detectable homogenization steps were corrected. Whenever a cause for a permanent upwards step in the temperature record coincides with a temporary downwards step of similar size (±0.2 °C) then this results in an undetectable self-homogenization. The number of these self-homogenized steps is estimated by fitting a normal distribution to the bimodal distribution of the sizes of the 81,465 detected homogenizations resulting in roughly 22,000 missed self-homogenizations. This means, that the size of the corrections could be increased by 27 %. These undetected self-homogenizations also have an effect on the apparent warming rate of the reference period.
- The ageing effects in each time period and for each weather station are assumed to be not statistically independent. This means that the same percentile correction is applied to all time periods and to all weather stations for each of the three correction curves. This maximizes the width of the confidence interval of the final result. A better approach would be to perform a Monte Carlo analysis combining randomly selected percentiles and analyzing the resulting ensemble statistically. However, the author does not have the computing resources for such an analysis. This would result in substantially narrower confidence intervals (approximately ½), but in the same approximate mean value.

Removing the conservative assumptions according to these estimates, reduces the corrected mean temperature difference to 0.41 °C. This also results in a near perfect fit with the UAH satellite data (difference in trend: 0.02 °C; correlation coefficient R: 0.972). This is a comparatively poorly substantiated estimate that indicates the need for further research.

4.2 Discussion of the impact of CO_2

The original and the corrected climate curves were compared with the base 2 logarithms of the CO_2 concentrations since 1880 (Etheridge et al. 1988, Tans and Keeling 2021) in order to determine the transient climate sensitivities. Least square fits result in the following maximum values for the sensitivities per doubling of the CO_2 concentration (assuming no other causes for the warming):

- GISTEMP: up to 3.02 °C
- Corrected mean: up to 1.85 °C
- Less conservative estimate: up to 1.04 °C

The coefficients of determination R^2 were calculated, which indicate up to which proportion the base 2 logarithms of the CO_2 concentrations predict the variation of the temperature data sets:

- GISTEMP: up to 92 %
- Corrected mean: up to 73 %
- Less conservative estimate: up to 36 %

The changes in the simplified maximum transient climate sensitivities indicate that the true equilibrium climate sensitivities are probably smaller than previously thought. Despite their simplicity, these changes of the coefficients of determination R^2 indicate that CO_2 causes a smaller proportion of the climate change than previously thought. These findings may have to be taken into consideration when developing climate models for simulations of the future.

The temperature trends of the corrected datasets are smaller than previously thought. These may affect the results of a multitude of sensitivity analyses in numerous scientific fields such as geology, biology, economics and social studies among others. This could mean that many sensitivities

are higher than expected. For example, the evaluation of tree ring data or other proxies needs to be recalibrated.

5. Validation

5.1 Validation with satellite data

The results were compared with global land lower troposphere temperature anomalies based on satellite data. There are multiple different satellite data series that show different trends. The data series by Spencer et al. (2021) provided by the University of Alabama in Huntsville (UAH) was selected, because its temperature trends had the best validation with independent data sources, especially data from radiosondes (Christy et al. 2018). These data were averaged for each year and plotted in Figure 4 together with the results mentioned above.

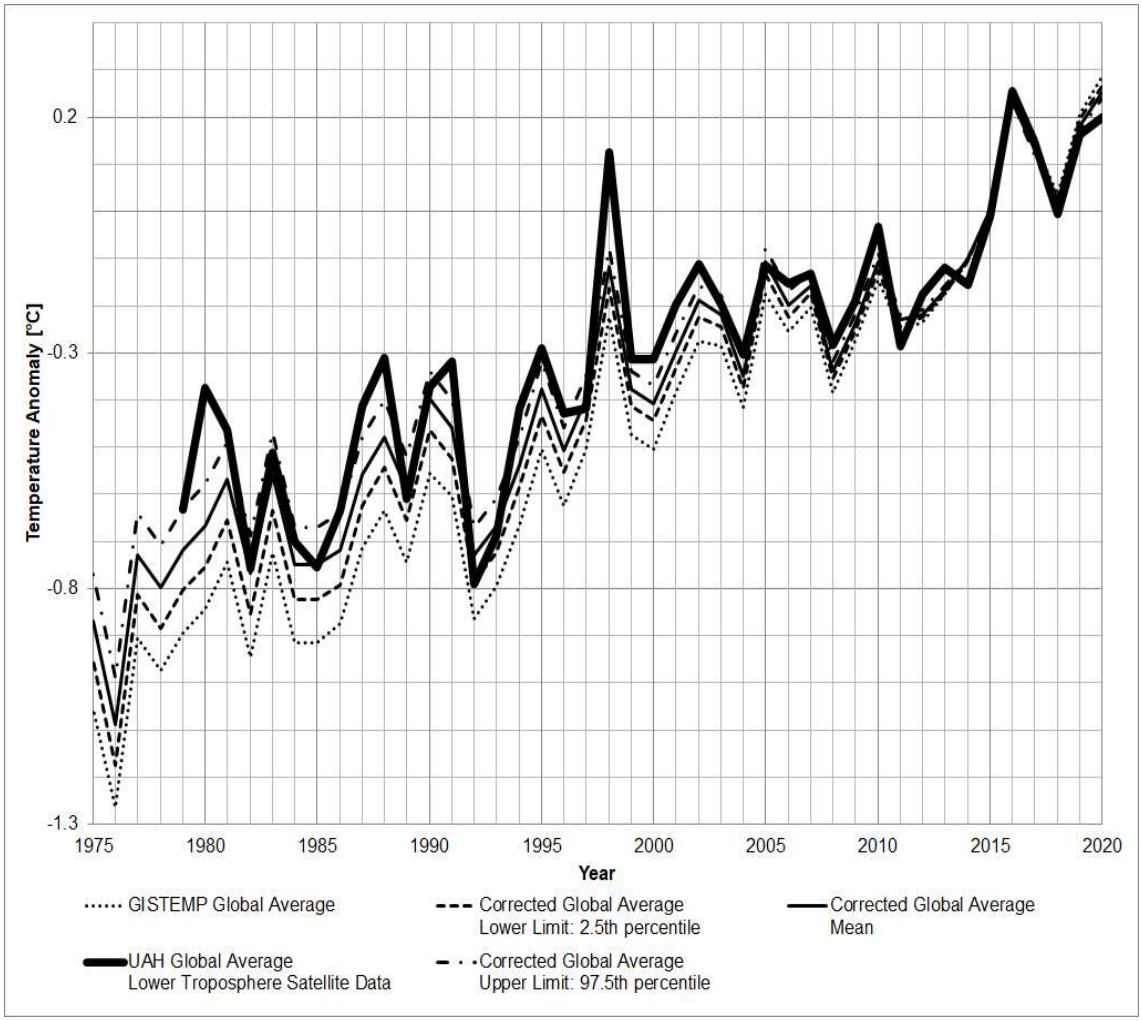

Figure 4: Global yearly land surface temperature anomalies provided by GISS (dotted line) the 2.5th percentile corrected dataset (dashed line), mean corrected dataset (solid line) and 97.5th percentile corrected dataset (dashed-dotted line). The global average temperature anomaly of the lower troposphere over land based on UAH satellite data (bold line).

The corrections were also compared with another satellite dataset by Mears and Wentz 2021 provided by Remote Sensing Systems (RSS). This dataset was chosen for a conservative comparison because it shows a particularly high warming trend (see Figure 5).

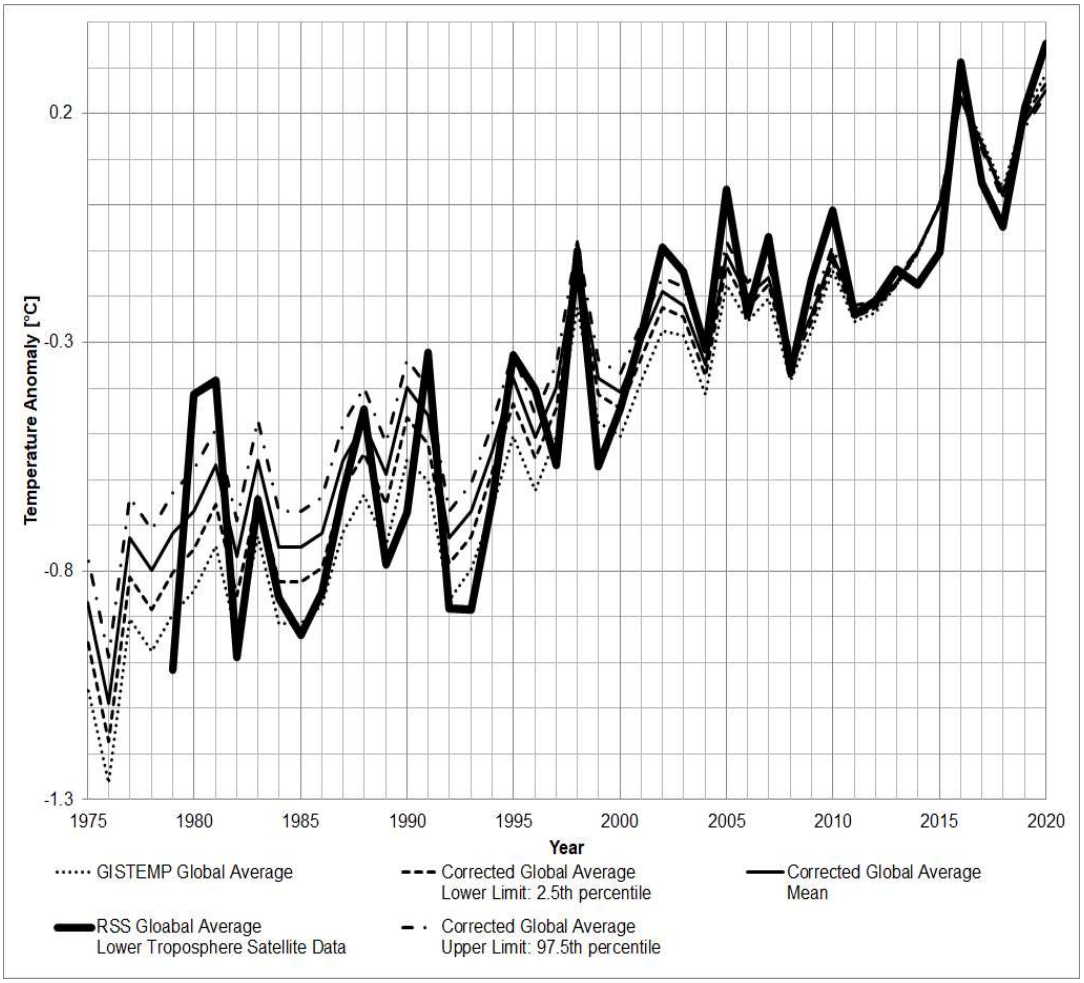

Figure 5: Global yearly land surface temperature anomalies provided by GISS (dotted line) the 2.5th percentile corrected dataset (dashed line), mean corrected dataset (solid line) and 97.5th percentile corrected dataset (dashed-dotted line). The global average temperature anomaly of the lower troposphere over land based on RSS satellite data (bold line).

The correlation coefficients R of the temperature data series from 1979 to 2020 between the UAH dataset and the other datasets are:

- GISTEMP: 0.950
- Corrected 2.5th percentile: 0.958
- Corrected Mean: 0.964
- Corrected 97.5th percentile: 0.970

The correlation coefficients R of the temperature data series from 1979 to 2020 between the RSS dataset and the other datasets are:

- GISTEMP: 0.934
- Corrected 2.5th percentile: 0.939
- Corrected Mean: 0.943
- Corrected 97.5th percentile: 0.946

The correlation coefficients with both satellite datasets from UAH and RSS suggest that the corrected 97.5th percentile dataset is the best fit. As expected, the calculation of the corrected mean was too conservative. The truth is probably closer to the estimate of the corrected mean with less conservative assumptions.

6. Validation by simplified analysis

The methods used above may introduce some kind of bias, that is currently not known, due to the explicit and implicit assumptions that were made during the analysis. Therefore, two more simplified analyses were tried, with fewer assumptions, in order to validate the discovered effect. These analyses are not suitable for quantifying the "correct" amount of temperature change, but they show the qualitative tendency of the corrections that need to be made.

6.1 Removing affected data

The first simplified method consists of removing the temperature anomaly data points that fall into those time periods after each homogenization step where the aging functions have the steepest slopes, and where the effect of the homogenization step is the largest for each weather station. This means that the data from years 0 to 12 and 31 to end after each homogenization step are removed. The data from the years 13 to 30 remain.

Using the GISTEMP tool may allow determining the "true" Global average anomaly, but this may also introduce some hidden bias. Therefore, the simply averaged anomalies of all weather stations were calculated.

Three simple analysis results were compared:

a) The temperature anomaly by simply averaging all weather station anomalies after homogenization (This is the reference).
b) The temperature anomaly by simply averaging all weather station anomalies before homogenization, skipping the data spanning the homogenization steps.
c) The temperature anomaly by simply averaging all weather station anomalies, but removing the data from those years, where the ageing has the largest effect. The data from the years 13 to 30 after each homogenization step remain.

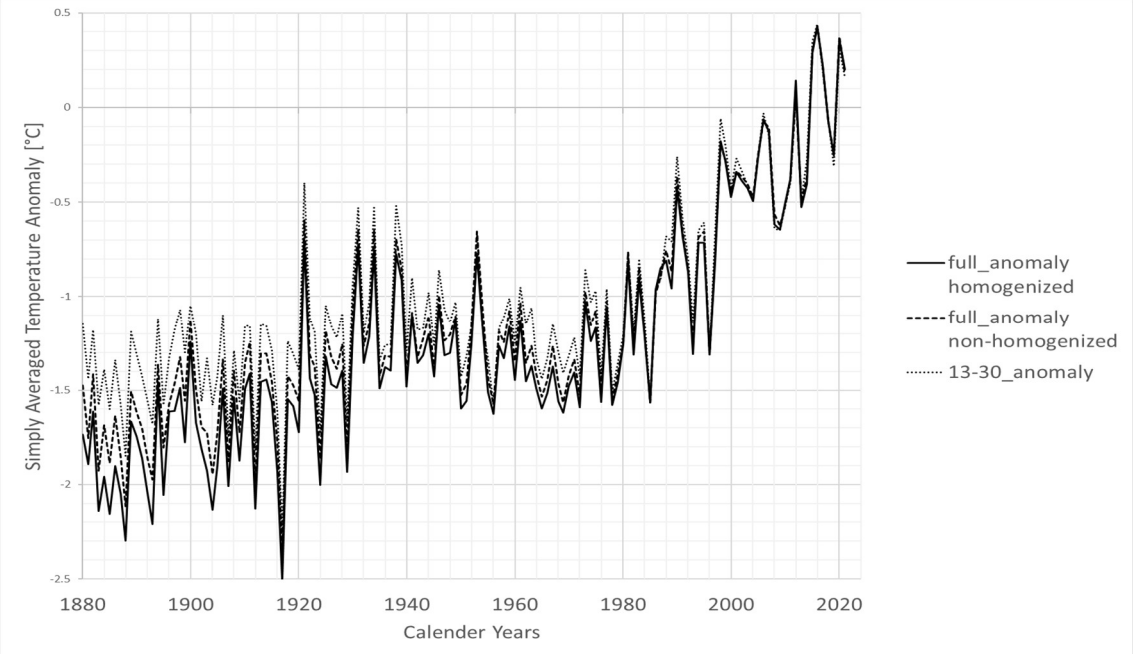

Figure 6: Simply averaged Global temperature anomalies from the NOAA data set; after homogenization (solid line), without homogenization (dashed line), with only the data from years 13 to 30 after each homogenization step (dotted line)

This simple average of the anomalies shows a larger warming trend than the area-weighted-average data from GISTEMP (see Figure 6):

a) Full data set homogenized: 1.94 °C warming.
b) Data set non-homogenized (and year 0 removed): 1.67 °C warming.
c) Data from years 13-30: 1.43 °C warming.

The anomaly from the years 13-30 after each homogenization step shows 0.51 °C less warming than the homogenized full data set.

However, the ageing during the interval between 13 years and 30 years remains as an error. Furthermore, what was described as "self-homogenization" in chapter 4.1 remains in the data set. This analysis method also does not allow for statistical evaluations.

6.2 Averaging national absolute temperatures

Because of these problems remaining with simply removing data, a third analysis approach was tried:

It was considered that analyzing anomalies "bakes in" any trend error due to ageing or any other cause. One should rather use absolute temperatures, because thermometers are precision instruments that are calibrated on a regular basis. However simply averaging the absolute worldwide temperature measurements would introduce a new bias: The changes in numbers and distributions of weather station locations around the world.

When looking at the NOAA data base, one can see the following trends in weather station location densities: At first, most weather stations were located in Europe and Northern America, which are comparatively cool and moderate regions. Then many more weather stations were introduced in the rest of the world, especially in warmer countries in the beginning of the 20th century. The numbers increased in the comparatively cold Soviet Union and its allies in the middle of the 20th century. Towards the end of the 20th century, the numbers of weather stations in Northern America and western Europe further increased, but the numbers in the former Soviet Union and its allies decreased drastically. All these non-climate related trends have a large impact on the averaging of the absolute weather station temperature data.

Massively different results were observed when averaging the global absolute temperatures, depending on the intervals in which data is deleted (see Figure 7).

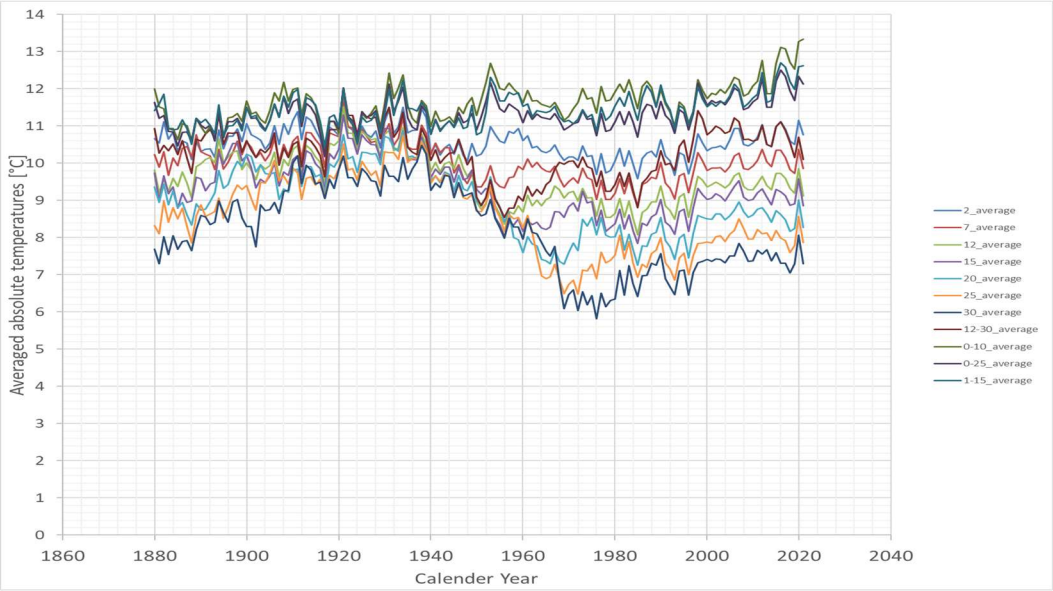

Figure 7: Simply averaged global absolute temperatures for a few variations of deleted data after each homogenization step. "2_" means that everything below and including year 2 after each homogenization step is deleted. "12-30" means that everything below and including 12 years and above 30 years is deleted.

These curves are a side product from the analysis described in the previous chapter, and are otherwise meaningless, however they do show the extremely high sensitivity of the global average absolute temperatures to seemingly neutral changes in the database. It appears that weather stations in cold locations have on average substantially longer intervals between homogenization events, than those in warm locations.

Therefore, it was tried to eliminate the effect of different trends in weather station densities in different regions, by averaging the absolute temperatures and the temperature anomalies in each region and comparing the results. Luckily, the weather station data is tagged by a letter code for the countries in which they are located.

The absolute temperatures and temperature anomalies were calculated for the following 29 countries, which were selected for having the most complete data sets for the past 140 years:

Netherlands, Portugal, South Korea, New Zealand, South Africa, Uruguay, Uzbekistan, USA, Iceland, Germany, China, Brazil, Egypt, Turkey, India, Australia, United Kingdom, France, Spain, Italy, Austria, Ireland, Hungary, Japan, Morocco, Poland, Sweden, Tunesia, Ukraine.

Then the difference was calculated between the temperature anomaly and the absolute temperature of each country. Finally, the trends of these differences were calculated (see Table 5 and Figure 8):

Table 5: Trends of differences between national averaged temperature anomalies and absolute temperatures

	Trend of the differences per year [°C/yr]
Netherlands	0.0064
Portugal	0.0168
South Korea	0.0062
New Zealand	-0.0064
South Africa	0.0042
Uruguay	0.0030
Uzbekistan	0.0144
USA	0.0137
Iceland	0.0242
Germany	0.0087
China	0.0477
Brazil	-0.0064
Egypt	-0.0023
Turkey	0.0137
India	-0.0051
Australia	0.0035
United Kingdom	0.0007
France	0.0122
Spain	-0.0011
Italy	-0.0064
Austria	-0.0047
Ireland	0.0109
Hungary	0.0015
Japan	-0.0042
Morocco	-0.0036
Poland	-0.0107
Sweden	0.0055
Tunesia	0.0048
Ukraine	0.0174

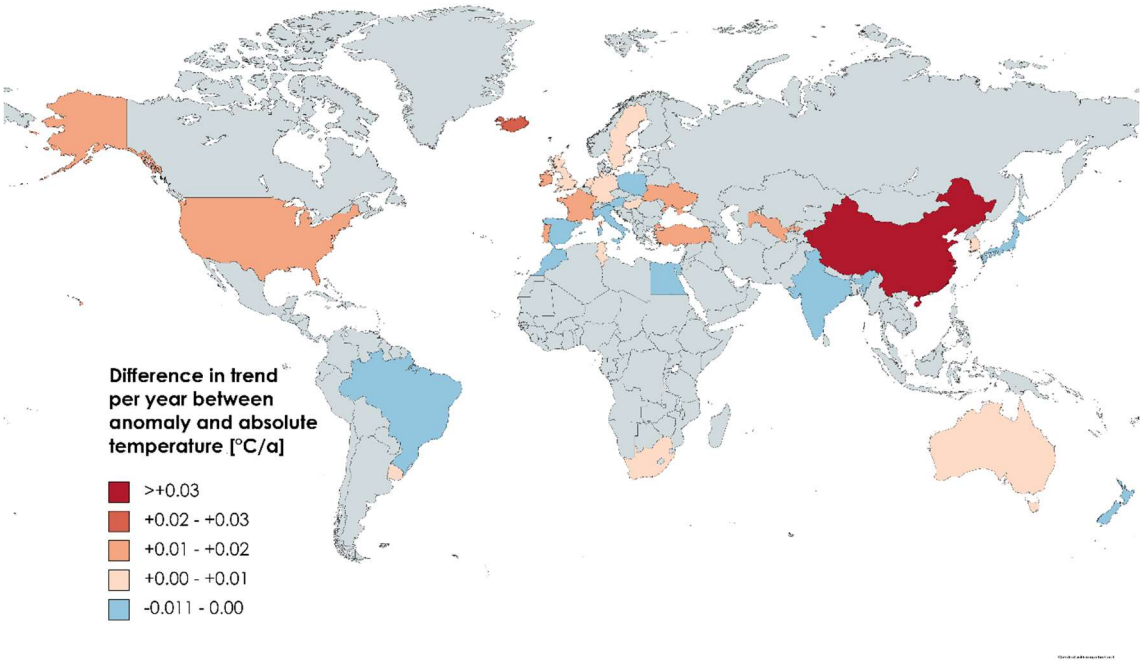

Figure 8: Plot of the trends of the differences between national averaged temperature anomalies and absolute temperatures for the selected countries.

These data were analyzed statistically:

- Lower bound 95 % confidence interval: 0.00137 °C/yr
- Mean: 0.00568 °C/yr
- Upper bound 95 % confidence interval: 0.00999 °C/yr

For 141 years, this leads to the following differences between the warming trends of the absolute temperatures and the temperature anomalies:

- Lower bound 95 % confidence interval: 0.19 °C
- Mean: 0.80 °C
- Upper bound 95 % confidence interval: 1.41 °C

This means that analyzing the anomalies overestimates the warming by a statistically significant amount.

This analysis still includes a bias for the trends in weather station locations within each country, but there is no reason to assume, that all of these 29 countries have the same bias. While one might argue that there were cooling biases for the absolute temperatures in China and USA due to high densities in the highly populated coastal areas and lower densities in the cooler inland regions in the beginning of the data sets, a reverse bias could be argued for South Africa, Australia, Tunesia and Japan. There is little bias to be expected from locations such as the United Kingdom, Ireland, Iceland, Netherlands and Portugal, due to the small sizes and maritime climates.

7. Conclusion

The approximate average ageing effects were extracted directly from the temperature datasets provided by NOAA. Furthermore, the results are validated qualitatively by satellite data and alternative analysis methods. Therefore, there is a high level of confidence in the trend of the results of this study. However, the changes of the quantified values due to the corrections may be small due to several conservative assumptions.

The corrections reduce the calculated warming of the land surface temperatures since 1880 from 1.43 °C to 0.83 °C. An estimate of a less conservative correction even suggests only 0.41 °C.

Especially the need of a reference period during the analysis makes it impossible to determine the ageing effects during the reference period itself. Therefore, alternative sources for the size of the ageing effects, or other causes of non-permanent steps in the datasets should be researched.

This additional research should determine the effect of direct sunlight, wind speeds, climate zone on various different types of weather stations that have been used in the past. This research should also be expanded to weather stations on the sea.

There may be other causes of temporary steps in the data series that are over-corrected by the homogenization algorithms. It is conceivable that thermometers have a tendency to drift more often towards higher temperatures than to lower temperatures between calibration events, because of corrosion, cold temperature crystallization, and cold temperature alloying of the probe material. The existence of a tendency should be researched.

Funding

Self-funded

Guest-Editor: Stein Storlie Bergsmark; Reviewers: Anonymous.

Acknowledgements

I would like to thank the GISTEMP-team for making their data and software so easily accessible.

References

Büsing, M., 2021. *Supplemental materials for preprint: Correction of Systematic Error in Global Temperature Analysis Related to Ageing Effects*. Open Science Framework Project. Uploaded on 2021-10-29. https://doi.org/10.17605/OSF.IO/XP78Y

Christy, J.R., Spencer, R.W., Braswell, W.D., Junod, R., 2018. *Examination of space-based bulk atmospheric temperatures used in climate research.* International Journal of Remote Sensing 39, 2018 - Issue 11, https://doi.org/10.1080/01431161.2018.1444293

Etheridge, D.M., G.I. Pearman, and F. de Silva. 1988. *Atmospheric trace-gas variations as revealed by air trapped in an ice core from Law Dome, Antarctica*. Ann. Glaciol. 10:28-33

GISTEMP Team, 2021. *GISS Surface Temperature Analysis (GISTEMP)*, version 4. NASA Goddard Institute for Space Studies. Dataset accessed 2021-09-24 at https://data.giss.nasa.gov/gistemp/

Lopardo, G., Bertiglia, F., Curci, S., Roggero, G., Merlone, A., 2013. *Comparative analysis of the influence of solar radiation screen ageing on temperature measurements by means of weather stations*. Int. J. Climatol. 34: 1297–1310 (2014), https://doi.org/10.1002/joc.3765

Mears, C. A., Wentz, F. J., 2021. *Remote Sensing Systems Air Temperature Time Series*. Version 4.0, Lower Troposphere, Land, RSS_Monthly_MSU_AMSU_Channel_TLT_Anomalies_Land_v04_0.txt, Accessed on 2021-10-02 at https://www.remss.com

Menne, M. J., Williams, C. N., Gleason, B.E., Rennie, J. J, Lawrimore, J. H., 2018. *The Global Historical Climatology Network Monthly Temperature Dataset*. Version 4. J. Climate, in press. https://doi.org/10.1175/JCLI-D-18-0094.1 Data accessed on 2021-09-24 at https://www.ncei.noaa.gov/products/land-based-station/global-historical-climatology-network-

monthly

Menne, M.J., Williams, C.N., Vose, R.S., 2009. *The U.S. Historical Climatology Network Monthly Temperature Data*. Version 2. Bull. Amer. Meteorol. Soc. 90, 993-1007, https://doi.org/10.1175/2008BAMS2613.1

Spencer, R.W., Christy, J.R., Braswell, W.D., 2021. *UAH Temperature Dataset*. Version 6.0, Lower Troposphere, Land, uahncdc_lt_6.0.txt, Accessed on 2021-09-27 at https://www.nsstc.uah.edu/data/msu/v6.0/tlt/

Tans, P., Keeling, R., 2021. *CO_2 monthly mean data*. NOAA/GML (gml.noaa.gov/ccgg/trends/) and Scripps Institution of Oceanography (scrippsco2.ucsd.edu/). Accessed on 2021-10-10 at https://gml.noaa.gov/ccgg/trends/data.html

Venema, V., Trewin, B., Wang, X., Szentimrey, T., Lakatos, M., Aguilar, E., Auer, I., Guijarro, J. A., Menne, M., Oria, C., 2018. *Guidance on the homogenization of climate station data*. Version 2. EarthArXiv. https://doi.org/10.31223/osf.io/8qzrf

Glossary

CI	Confidence Interval (usually 95% between 2.5th percentile and 97.5th percentile)
GISS	Goddard Institute for Space Studies
GISTEMP	Global land and sea surface temperatures compiled by GISS
HadCRUT	Global land and sea surface temperatures compiled by Hadley Centre for Climate Prediction and Research
Homogenization	Process of removing non-climate related changes in temperature data
NCEI	National Centers for Environmental Information (in USA)
NOAA	National Oceanic and Atmospheric Administration (in USA)
R^2	coefficient of determination (statistical parameter)
RSS	Remote Sensing Systems (provides satellite data sets)
Saturated	A process does not continue to increase an output value beyond a saturation limit despite further increase of an input value.
UAH	University of Alabama in Huntsville (provides satellite temp. data sets)

OPEN ACCESS

Klimarealistene
Vollsveien 109
1358 Jar, Norway
ISSN: 2703-9072

Correspondence:
dk@itia.ntua.gr

Vol. 4.2 (2024)
pp. 36-78

Relative importance of carbon dioxide and water in the greenhouse effect: Does the tail wag the dog?

Demetris Koutsoyiannis

Department of Water Resources and Environmental Engineering, School of Civil Engineering, National Technical University of Athens, Zographou, Greece

Abstract

Using a detailed atmospheric radiative transfer model, we derive macroscopic relationships of downwelling and outgoing longwave radiation which enable determining the partial derivatives thereof with respect to the explanatory variables that represent the greenhouse gases. We validate these macroscopic relationships using empirical formulae based on downwelling radiation data, commonly used in hydrology, and satellite data for the outgoing radiation. We use the relationships and their partial derivatives to infer the relative importance of carbon dioxide and water vapour in the greenhouse effect. The results show that the contribution of the former is 4% – 5%, while water and clouds dominate with a contribution of 87% – 95%. The minor effect of carbon dioxide is confirmed by the small, non-discernible effect of the recent escalation of atmospheric CO_2 concentration from 300 to 420 ppm. This effect is quantified at 0.5% for both downwelling and outgoing radiation. Water and clouds also perform other important functions in climate, such as regulating heat storage and albedo, as well as cooling the Earth's surface through latent heat transfer, contributing 50%. By confirming the major role of water on climate, these results suggest that hydrology should have a more prominent and more active role in climate research.

Keywords: Greenhouse effect; longwave radiation; water vapour; carbon dioxide; evaporation radiative forcing

Submitted 2024-09-22, Accepted 2024-10-28. https://doi.org/10.53234/scc202411/01

A good rule of thumb to keep in mind is that anything that calls itself 'science' probably isn't.

J.R. Searle (1984)

1. Introduction

A notable feature of the current period is that the classical value of science as the pursuit of the truth, independently of other interests, is gradually being abandoned (Koutsoyiannis and Mamassis, 2021). People pride themselves on being scientists and activists at the same time (Koutsoyiannis, 2020b), while calls for political actions to "save the planet", including enhanced global governance, are published even in scientific journals (e.g. Biermann et al., 2012). While common perception promotes the idea of science-based policies and politics, the reality is the exact opposite, i.e., politics-based science. For it is self-evident that by mixing science and politics the end product is politics. A relevant example is provided by the high-profile journal *Nature*, which declares that it is "committed to supporting the research enterprise"[1], but admits being involved in politics and proclaims that this is the right thing (Howe, 2020; Nature Editorial, 2023),

[1] Nature, Editorial Values Statement, https://www.nature.com/nature/editorial-values-statement (accessed 27 March 2024).

even though it is recognized that this affects scientific credibility and causes loss of confidence in science (Lupia, 2023; Zhang, 2023). Another relevant example is the campaign of a famous learned society, the American Geophysical Union (AGU), related to the USA 2024 election.[2]

It is thus natural to wonder if articles published in scientific journals promote the truth or political aims, perhaps hiding or distorting the truth, and even reversing cause and effect (Koutsoyiannis, 2021; Koutsoyiannis et al. 2022a,b, 2023). Gradually, by repetition and accumulation, distorted information becomes dominant among the scientific community and the public. In contrast, studies providing information different from the dominant tend to be suppressed (the current study serves as an example—see Supplementary Information).

Seeking truth may have been even more difficult due to a recent development, the appearance of artificial intelligence (AI) bots, which certainly affects common opinion, as well as scientific perception and advancement. Assuming that AI bots more or less reflect the common perception in the scientific community and the general public, Microsoft Bing's chatbot was asked the following question:

> *Which gas determines the greenhouse effect on Earth?*

The bot provided the following answer[3]:

> *The greenhouse effect is the process through which heat is trapped near Earth's surface by substances known as 'greenhouse gases.' These gases consist of carbon dioxide, methane, ozone, nitrous oxide, chlorofluorocarbons, and water vapor. Water vapor, which reacts to temperature changes, is referred to as a 'feedback', because it amplifies the effect of forces that initially caused the warming. Scientists have determined that carbon dioxide plays a crucial role in maintaining the stability of Earth's atmosphere. If carbon dioxide were removed, the terrestrial greenhouse effect would collapse, and Earth's surface temperature would drop significantly, by approximately 33°C (59°F).*

A literature search reveals that the chatbot essentially (and selectively) reproduces the following statements by Lacis et al. (2010), in which the atmospheric CO_2 is presented as the principal control knob governing Earth's temperature:

> *Noncondensing greenhouse gases, which account for 25% of the total terrestrial greenhouse effect, thus serve to provide the stable temperature structure that sustains the current levels of atmospheric water vapor and clouds via feedback processes that account for the remaining 75% of the greenhouse effect. Without the radiative forcing supplied by CO_2 and the other noncondensing greenhouse gases, the terrestrial greenhouse would collapse, plunging the global climate into an icebound Earth state.* […]
>
> *If the global atmospheric temperatures were to fall to as low as $T_S = T_E$* [where $T_E = 255$ K is the global mean effective temperature] *the Clausius-Clapeyron relation would imply that the sustainable amount of atmospheric water vapor would become less than 10% of the current atmospheric value.*

Interestingly, while Lacis et al. recognize a high contribution of water vapour and clouds, they regard them as results of feedback processes of the CO_2 control knob. Moreover, the estimate of 75% they provide is too low, as we will see below.

On the other hand, Koutsoyiannis and Vournas (2024) recently examined longwave radiation observations extending over a century-long period and found that the observed increase of the atmospheric carbon dioxide concentration ([CO_2]; from 300 to 420 ppm) has not altered, in a discernible manner, the greenhouse effect, which remains dominated by the quantity of water vapour in the atmosphere. Naturally, given the uproar about the enhancement of the greenhouse effect

[2] AGU, This November Stand Up For Science, https://sciencevotesthefuture.org/ (accessed 27 Oct. 2024).

[3] It also provided references to: climate.nasa.gov; britannica.com; britannica.com

due to human emissions by fossil fuel combustion, this finding appeared surprising to many. Some (including a knowledgeable reviewer of Koutsoyiannis and Vournas, 2024) postulated that this would be expected for the downwelling longwave (LW) radiation flux, which was the subject of Koutsoyiannis and Vournas (2024), but this would not be the case for the outgoing radiation, where the effect of [CO_2] increase would be substantial. However, no long data series exist to verify such a conjecture and hence this question was not investigated in Koutsoyiannis and Vournas (2024), whose scope was to make inference based on data.

Hence the following research questions are raised:

1. Are Lacis et al. right about the importance of CO_2 in the greenhouse effect, and is it meaningful to state that without it the terrestrial greenhouse would collapse? Or is the effect of CO_2 negligible as Koutsoyiannis and Vournas (2024) claimed, and that of H_2O dominant?
2. Is the role of H_2O as a greenhouse gas limited to the downwelling LW flux or does it extend also to the outgoing LW flux?

We will examine these questions below, noting that the first one refers to a fictitious case (removal of atmospheric CO_2) for which no empirical data can exist. Rather, paleoclimatic studies and geological facts suggest that CO_2 existed, mostly in much higher concentrations than today, in most periods of Earth's history (see its evolution during the Phanerozoic in Koutsoyiannis, 2024a), and also before oxygen appeared in the atmosphere. Also, the second question cannot be studied on a purely empirical basis, as no long-term data exist. For systematic satellite measurements of outgoing LW flux have only been made in the 21st century. Therefore, to study these questions we need to resort to theoretical arguments and analyses. We will do this by applying the established greenhouse theory and by enrolling standard models, without considering doubts that have been cast on the validity of the theory or alternative hypotheses (e.g. Nikolov and Zeller, 2017, Miskolczi, 2023). In applying this theory, we will follow a macroscopic approach, without discussing the details of the physical processes related to radiation and the physical mechanisms thereof. The reader interested in the latter may find relevant critical discussions in Harde (2013, 2014, 2017) and Clark (2024).

Human CO_2 emissions are 4% of the total (Koutsoyiannis et al., 2023) but there are also human H_2O emissions over the terrestrial part of Earth of a comparable percentage (Peachey, 2006; Sherwood et al., 2018; Li et al., 2024). Specifically, according to Koutsoyiannis (2020a) the quantity of evaporation and transpiration over land is 91 400 km^3/year. According to the Food and Agriculture Organization of the United Nations[4], the human water withdrawal in 2010, including the evaporation from reservoirs, was 4 300 km^3/year, of which 69% and 19% were for agricultural and industrial use, respectively. Considering the fact that almost all agricultural and a large part of industrial water are evaporated, and taking into account the increasing trend in water withdrawal, with simple calculations we may conclude that the current human addition to the natural water cycle over land is about 4%. One could speculate that each of these 4% additions might influence the climate to a degree comparable to that percentage, but the reasons that only the influence of CO_2 is investigated and highlighted by the scientific community, being regarded as a control knob of climate (even though H_2O is much stronger as a greenhouse gas) are not scientific.

We may note, though, that the percentage of human H_2O emissions becomes much lower, of the order of 1%, if we also consider the evaporation over oceans, where there is no human intervention. However, it appears reasonable for this estimate of human water emissions to consider only the terrestrial part of Earth, because of the high local variability and the small residence time of atmospheric water. Indeed, the mean residence time of atmospheric water is a few days (specifically, 12 250 km^3 / (522 700 km^3/year) = 0.023 years = 8.6 d, where the total volume of liquid

[4] Water use – AQUASTAT - FAO's Global Information System on Water and Agriculture https://www.fao.org/aquastat/en/overview/methodology/water-use (accessed 19 February 2024).

water in the atmosphere, 12 250 km^3, was taken as the average atmospheric water content, 24.0 kg/m^3, as estimated from the ERA5 Reanalysis (see explanation about ERA5 in Section 3) over the globe for the period 1950-2023, while the atmospheric inflow volume of water, 522 700 km^3/year, was taken from Koutsoyiannis, 2020a). In contrast, CO_2 is well mixed as it has a much higher residence time, of a few years (specifically, 4 years according to Koutsoyiannis, 2024b)[5].

The thesis expressed in this paper is that none of these anthropogenic additions to the hydrological and carbon cycle drives climate. On the other hand, both H_2O and CO_2 are important elements of climate and their quantities and fluxes are determined by natural processes, with the human factor being rather negligible. Both are elixirs of life and in this respect, they act complementary to each other. Thus, it may be pointless to compare them to each other. Yet this comparison is the main focus of this paper, as lately, the scientific efforts to study each of them have been inversely proportional to their respective importance.

By its definition by UNESCO (1964), hydrology is the science that deals with the waters of the Earth, and its domain covers the entire history of the cycle of water on the Earth. Water is a critical element of life and of climate as well. While climate has become a hot topic and its research a top priority, it is odd that hydrology has lost importance, as evident from the abundance of papers examining climate change impacts on water and applying model projections for the future based on CO_2 emission scenarios. This misses the fact that water is the key element on Earth in driving climate and that the hydrological cycle is self-ruling rather than a feedback or impact of another cycle—namely the carbon cycle, which has also been downgraded to an issue governed by human carbon emissions (the 4% of the total).

By emphasizing the relative importance of water in climate, in comparison to carbon dioxide, this paper tries to show that the picture of Earth's climatic system may have been distorted and to reinstate the importance of water and hydrology (and its branch of hydrometeorology) in climate. The paper is made as a stand-alone and therefore it includes a synopsis of the related theoretical concepts and a model (Section 2 and Appendices A and B). Its foundation is not only theoretical but also empirical, utilizing observed data (Section 3). By combining the model and data, it derives simple macroscopical empirical relationships representing the greenhouse effect as accurately as the detailed model whose results are based upon (Section 4). These relationships are tested against observational data (Section 5) and their simple and analytical expressions, which enable extraction of partial derivatives, allow the comparison of the effect of water relative to other greenhouse gases (Section 6). The findings are put in a more general context (Section 7) and allow drawing relevant conclusions (Section 8).

2. Theoretical Background

The typical quantification of the abundance of a specific gas X in a gas mixture is given by its concentration, defined in terms of mole fraction as:

$$[X] := \frac{n_X}{n_{\mathrm{TOT}}} = \frac{N_X}{N_{\mathrm{TOT}}} \tag{1}$$

where n_X and n_{TOT} are the numbers of moles of the gas X contained in a specified volume and the total amount of moles of all constituents in the same volume, and N_X and N_{TOT} are the respective number of molecules; note that $n_X = N_X/N_A$, where $N_\mathrm{A} = 6.022\times10^{23}$ mol^{-1} is the Avogadro constant (and likewise for n_{TOT}). Additional metrics are discussed in Appendix A. The simple metric in Equation (1) is sufficient to quantify noncondensing greenhouse gases, such as CO_2,

[5] This can also be verified by estimates of the Intergovernmental Panel on Climate Change (IPCC) report (Masson-Delmotte et al., 2021), namely its figure 5.12. Specifically, we obtain 870 Gt / (226.9 Gt/year) = 3.8 years, where the total mass of atmospheric CO_2, 870 Gt was taken from the IPCC report, while the atmospheric inflow mass, 226.9 Gt/year, is taken from Koutsoyiannis et al. (2023).

with concentration (denoted as [CO_2]) only slightly varying geographically on long time scales. However, in the case of water vapour, its concentration varies substantially in space and time, and its vapour pressure, e_a, has a thermodynamic upper limit, the saturation water vapour pressure, which is a function, $e(T_a)$, of temperature, T_a. Therefore, we need a more sophisticated framework of quantification, which is again summarized in Appendix A.

Accordingly, the quantification of the greenhouse effect due to the presence of water vapour in the atmosphere is more demanding than that due to CO_2. However, there is a very rich experience for this quantification as it has been necessary for routine calculations of evapotranspiration, which represents a substantial component of the hydrological balance—and also the most intractable and difficult to measure. Evaporation calculations are also most essential for agricultural irrigation practice. The details of this quantification are presented in Appendix A. The related macroscopic formulae for the clear-sky LW radiation flux are based on two variables, the temperature, T_a, and the water vapour pressure, e_a, and a single value of each of them near the Earth's surface. This clearly reflects the fact that it is the water vapour that determines the greenhouse effect on Earth's atmosphere, contrary to the public perception that this is CO_2. Remarkably, the latter does not appear at all in the related formulae. Koutsoyiannis and Vournas (2024) demonstrated that, indeed, there is no need to involve [CO_2] in these calculations as the observations in a century-long period, in which the rise of [CO_2] was substantial, there was no discernible effect on the greenhouse effect.

However, for reasons explained in the Introduction, we seek to quantify the contribution of CO_2 to the greenhouse effect and compare it to that of water vapour. In this, we need to enrol detailed modelling of the spectroscopic properties of the atmosphere. Also, while the formulae of Appendix A are useful for the downwelling radiation, they do not quantify the outgoing radiation at the top of the atmosphere (TOA). For those tasks, we may use detailed spectroscopic models.

There are several databases of spectroscopic parameters and codes that perform detailed modelling of radiation in the atmosphere. Of these, here we use the MODerate resolution atmospheric TRANsmission model, or MODTRAN (Berk et al. (1987, 2008, 2014), which has been extensively validated in its over 30-year history, and serves as a community standard atmospheric band model. It simulates the emission and absorption of infrared radiation in the atmosphere, and particularly the effect of wavelength-selective greenhouse gases on Earth's LW radiation flux.

The specific implementation used is that of the University of Chicago, readily provided as an interactive web application[6]. The application is based on five different locality cases, which differ most significantly in their temperature, water vapour and ozone profiles, as specified in Appendix B. The application offers default values of several characteristics for each locality profile but also allows modifying these values (e.g., by offsetting temperature and holding fixed either the water vapour pressure or the relative humidity, or by multiplying the water vapour scale by a constant). Finally, in addition to the clear-sky conditions, it enables the use of several different cloud types, as will be described in Section 4.2.

A typical graphical output of the MODTRAN application is seen in Figure 1. This is for the standard tropical atmospheric profile, also in comparison to the case that the standard [CO_2] of 400 ppm is replaced by that of 800 ppm, where the difference is difficult to discern. The effect of the different greenhouse gases is also marked in the figure. It is clear that the effect of H_2O dominates, particularly in the downwelling radiation. Note that, according to Clark (2024, Fig. 19), 95% of the downwelling radiation originates from within the first 2 km layer and approximately half originates from the first 100 m layer above the surface.

As the MODTRAN web application only models the longwave radiation, in a case where the

[6] MODTRAN Demo, http://modtran.spectral.com/modtran_home (accessed 19 February 2024). Additional web applications can be found in other sites, such as MODTRAN Infrared Light in the Atmosphere. https://climatemodels.uchicago.edu/modtran/ (accessed 19 February 2024).

shortwave (SW) radiation was needed in this study, this was estimated by another model, RRTM (standing for Earth's Energy Budget), again available as a web application by the University of Chicago[7]. This simulates both LW and SW radiation fluxes, both upward and downward.

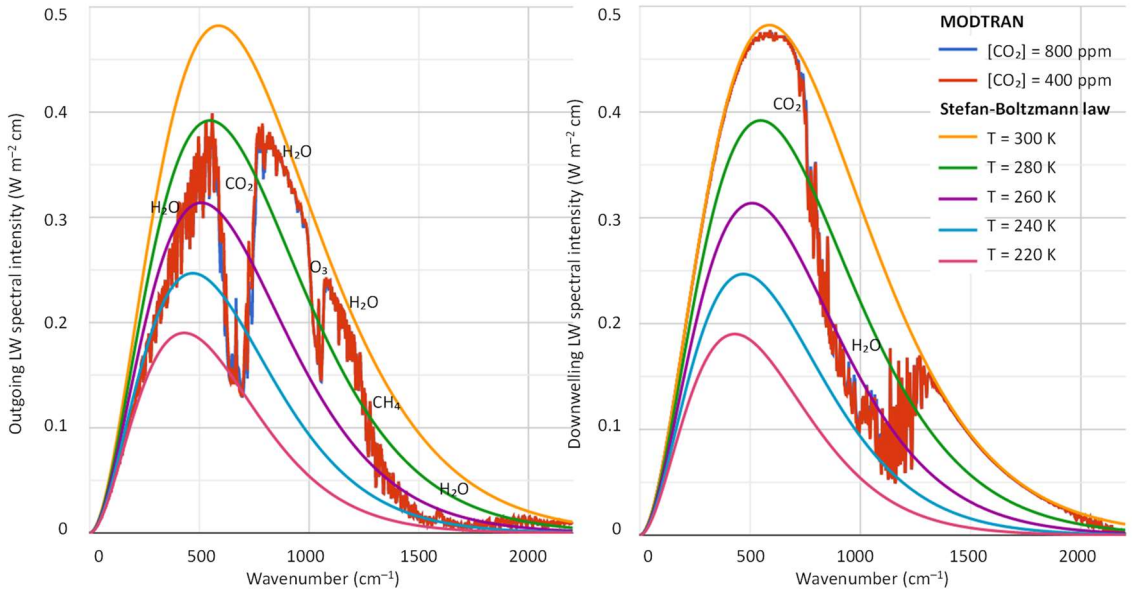

*Figure 1: Output of the MODTRAN model for the standard, cloud free, tropical atmospheric profile, in comparison to the case that the standard [CO_2] of 400 ppm is replaced by that of 800 ppm: (**left**) outgoing radiation corresponding to the level of 100 km above the ground; (**right**) downwelling radiation at zero level. The ground temperature is 299.7 K (26.55 °C) and the total outgoing and downwelling LW flux are, respectively, 298.52 and 369.26 W/m² for [CO_2] = 400 ppm, and 295.129 and 371.14 W/m² for [CO_2] = 800 ppm (differences: –3.36 and 1.88 W/m²). The gases mostly affecting LW radiation are noted for the respective wavenumbers. Graph generated from https://climatemodels.uchicago.edu/modtran/.*

3. Data

To compare MODTRAN results to observed radiation profiles in the atmosphere, we need radiosonde data. While radiosondes are routinely made in several hundreds of sites across the world, they typically measure temperature, humidity, pressure and wind. Radiation radiosonde measurements are rare, yet it is useful to make at least a single comparison to get a general idea. Here we use a couple of radiosondes from a day and a night flight on 23 September 2011, in cloud-free conditions, at the aerological station in Payerne, Switzerland (6.9440° E, 46.8130°, +491 m a.s.l.). In these, in-situ measurements of downward and upward radiation fluxes were taken through the troposphere and into the stratosphere, exceeding 32 km of altitude. They were presented by Philipona et al. (2012) in graphical form in their figure 2, which was digitized here to recover the measurements.

For the downwelling LW radiation flux, there have been numerous measurements at specific sites for more than a century, which are presented in Koutsoyiannis and Vournas (2024). These were the basis for the derivation of the empirical or semiempirical formulae for the calculation of the downwelling radiation flux, discussed in Section 2 and Appendix A. Considering that these formulae reflect the data that they were based upon, here we use the formulae, instead of the data, for comparisons with MODTRAN.

Information for the radiation fluxes at the top of the atmosphere (TOA), including the LW fluxes, are provided by satellite instruments. These are available only for the 21st century from the

[7] RRTM Earth's Energy Budget, https://climatemodels.uchicago.edu/rrtm/ (accessed 19 February 2024).

ongoing project Clouds and the Earth's Radiant Energy System (CERES), a part of NASA's Earth Observing System, designed to measure both solar-reflected and Earth-emitted radiation from the TOA (in CERES defined at the altitude of 20 km) to the surface.

The specific product used here is the CERES SSF1deg monthly averaged TOA LW radiative fluxes at a 1°-regional grid, constant-meteorology-temporally-interpolated (Wielicki et al., 1996; Doelling et al., 2013, 2016). The TOA fluxes are provided for clear-sky and all-sky conditions. Both these observational data are available online[8] and were retrieved here for their entire time span of complete years, i.e., from January 2001 to December 2022 from the Terra platform. The same CERES product provides information on clouds, which was also retrieved (monthly averaged for both day and night).

In addition, the CERES project provides LW fluxes for the surface, both downwelling and upgoing, through the product CERES_EBAF_Ed4.2, where EBAF stands for "Energy Balanced and Filled" (Kato et al., 2018; Loeb et al., 2018). However, these are computed gridded values rather than observational data. They are publicly available[9] and were also retrieved here.

The CERES data are associated with considerable uncertainties. According to CERES (2023), the combined regional all-sky LW flux uncertainty is 2.4 W/m² and the daily regional all-sky LW diurnal uncertainty is 8 W/m². According to CERES (2021, Table 6.1), the uncertainties in the 1°×1° regional monthly TOA fluxes are 4.6 W/m² for clear sky and 2.5 W/m² for all sky. In addition, as also noted in CERES (2021), with the most recent CERES instrument calibration improvements, there still is a net imbalance of ~4.3 W/m², much larger than the expected observed ocean heating rate which CERES assumes to be ~0.71 W/m². The latter value is not far from that of Trenberth et al. (2009), who give the net absorbed energy at 0.9 W/m^2. However, according to the calculations by Koutsoyiannis (2021), the latter imbalance value, again inferred from ocean heating data, is lower, 0.37 W/m². The EBAF dataset adjusts the observations in view of the above inconsistencies. All this information suggests that the observational uncertainties are far too high to allow calculations of Earth's imbalance and of temporal climatic changes, yet they are quite useful for the very scope of this study, which is not related to energy flux imbalances.

Additional atmospheric variables used here, namely temperature and water vapour pressure, are taken from the ERA5 and NCEP/NCAR Reanalyses at a monthly scale. ERA5 stands for the fifth-generation atmospheric reanalysis of the European Centre for Medium-Range Weather Forecasts (ECMWF; ECMWF ReAnalysis). Its data are publicly available for the period 1940 onwards at a spatial resolution of 0.5°. NCEP/NCAR stands for Reanalysis 1 by the National Centers for Environmental Prediction (NCEP) and the National Center for Atmospheric Research (NCAR). Its data are publicly available from 1948 to the present at a horizontal resolution of 1.88° (~ 210 km). Both data sets can be retrieved from the Climexp platform[10] and from the Physical Sciences Laboratory platform of the US National Oceanic and Atmospheric Administration (NOAA)[11]. Finally [CO_2] data were retrieved for the most well-known station, Mauna Loa, again from the Climexp platform.

The gridded CERES SSF1deg TOA LW data are presented in Figure 2, averaged over the period of observations. The cloud information (cloud area fraction) of the same data product is shown in Figure 3. The zonal distribution of the LW radiation data are shown in Figure 4, along with that of temperature, and, as expected, the distributions of the two variables are similar.

---

[8] CERES_SSF1deg_Ed4.1 Subsetting and Browsing, https://ceres-tool.larc.nasa.gov/ord-tool/jsp/SSF1degEd41Selection.jsp (accessed 19 February 2024).

[9] CERES_EBAF_Ed4.2 Subsetting and Browsing, https://ceres-tool.larc.nasa.gov/ord-tool/jsp/EBAF42Selection.jsp (accessed 19 February 2024).

[10] Climate Explorer: https://climexp.knmi.nl/ (last access: 19 February 2024).

[11] WRIT: Monthly Timeseries: NOAA Physical Sciences Laboratory, https://psl.noaa.gov/cgi-bin/data/atmoswrit/timeseries.pl (accessed 19 February 2024).

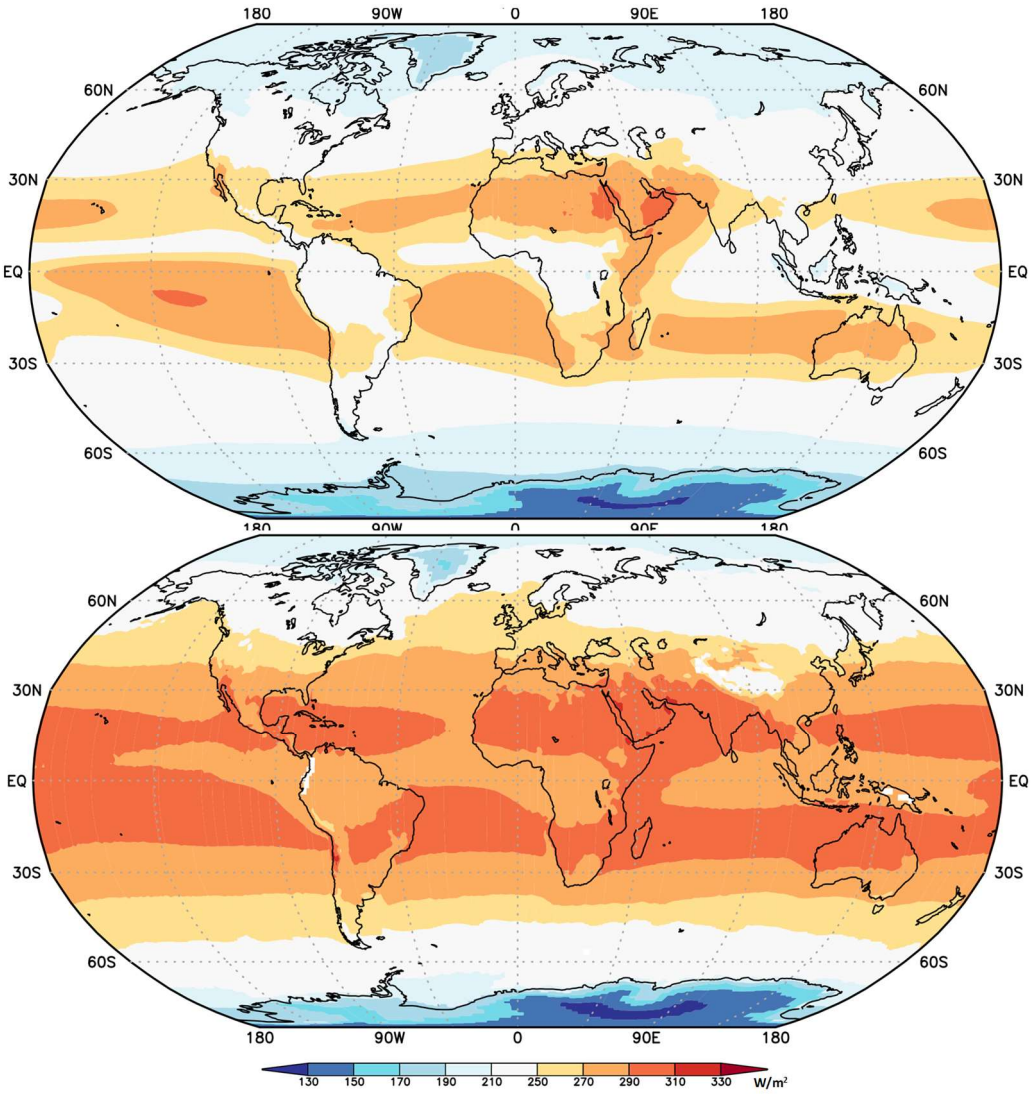

*Figure 2: Geographical distribution of outgoing LW radiation averaged over the period of 2000 – 2022 as given by the CERES data: (**upper**) all sky; (**lower**) clear sky. Data retrieved from [https://ceres-tool.larc.nasa.gov/ord-tool/jsp/SSF1degEd41Selection.jsp;](https://ceres-tool.larc.nasa.gov/ord-tool/jsp/SSF1degEd41Selection.jsp) graph generated by https://climexp.knmi.nl.*

Figure 5, constructed from the data of Figure 4, shows that the torrid zone (between 23.4° S and 23.4° N) contributes 43% of Earth's outgoing LW radiation flux, and together with the two temperate zones (between 23.4° and 66.6° S and N) radiates 94% of the total, leaving only 6% for the frigid zones (between 66.6° and 90° S and N).

Figure 6 better depicts the relationship of outgoing LW radiation flux and surface temperature, for each month of the 22 years of data availability separately, but areally averaged over geographical zones of 15° latitude. This graph allows important observations. First, the individual monthly values align very well with the average zonal distribution. Second, the relationship between temperature and outgoing LW radiation appears to be linear at most part of the graph. One would expect a 4th-power relationship, based on the Stefan-Boltzmann law (see Appendix A, Equation (A9)), but clearly this is not the case. The deviation has been explained as an emergent property of an atmosphere whose greenhouse effect is dominated by a condensable gas, namely water vapour (Koll and Cronin, 2018). Third, at the high end of temperature variation, around 300 K, there appears a stagnancy, or even regression of radiation with respect to temperature. This behaviour is observed in the tropics, where the maximum ocean surface temperature does not exceed 300 K. Evaporation, tropical clouds and thunderstorms actively regulate the temperature in this area blocking further temperature rise (Eschenbach, 2010; Clark, 2013a,b).

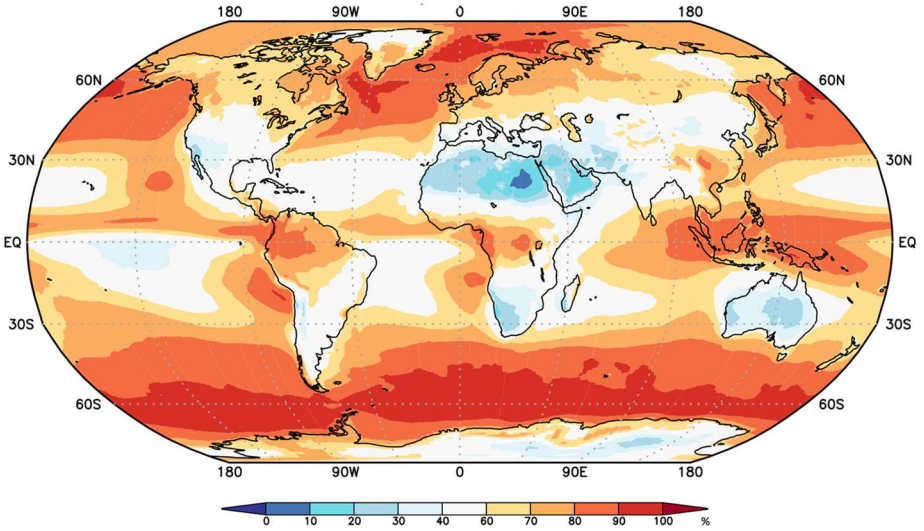

Figure 3: Geographical distribution of cloud area fraction averaged over the period of 2000 – 2022 as given by the CERES data. Data source and graph generation as in Figure 2.

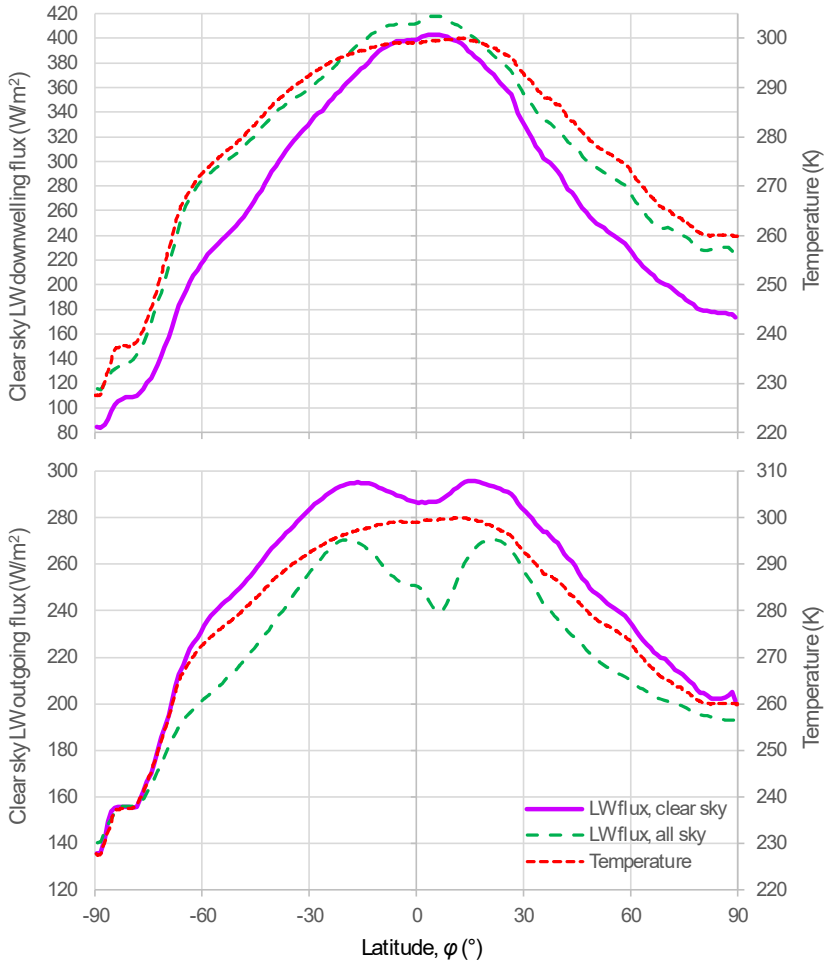

*Figure 4: Zonal distribution of LW radiation averaged from 2000 to 2022 as given by the CERES data: **(upper)** downwelling; **(lower)** outgoing; the temperature zonal distribution, as given by ERA5 Reanalysis is also plotted. Radiation data retrieved from https://ceres-tool.larc.nasa.gov/ord-tool/jsp/SSF1degEd41Selection.jsp for outgoing radiation and https://ceres-tool.larc.nasa.gov/ord-tool/jsp/EBAF42Selection.jsp for downwelling radiation; temperature data from ERA5 Reanalysis retrieved from https://climexp.knmi.nl.*

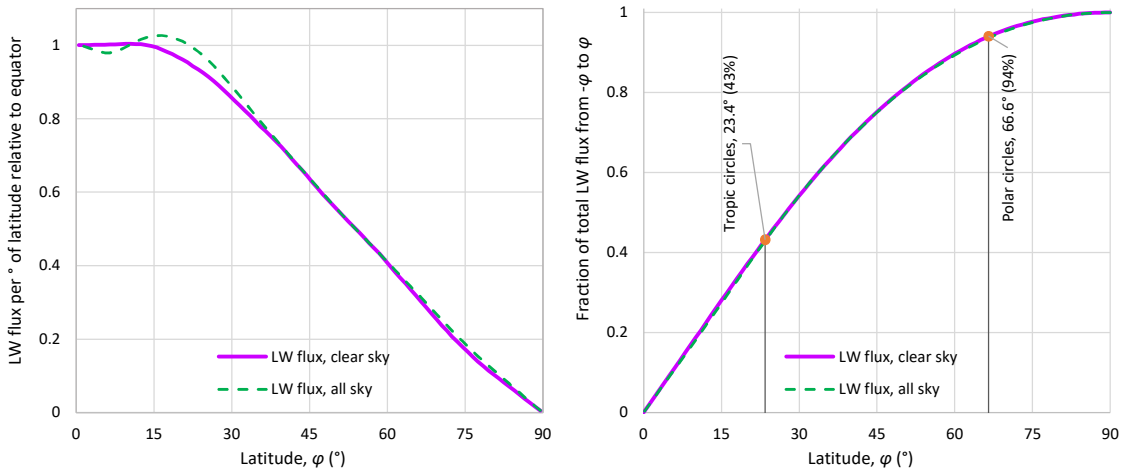

*Figure 5: Graphical depictions of the relative intensity of outgoing LW radiation averaged over the period of 2000 – 2022 as given by the CERES data, as a function of the latitude; (**left**) ratio of intensity at latitude φ (average for S and N) to that at the equator; (**right**) cumulative flux between latitudes φ S and φ N to the total outgoing radiation.*

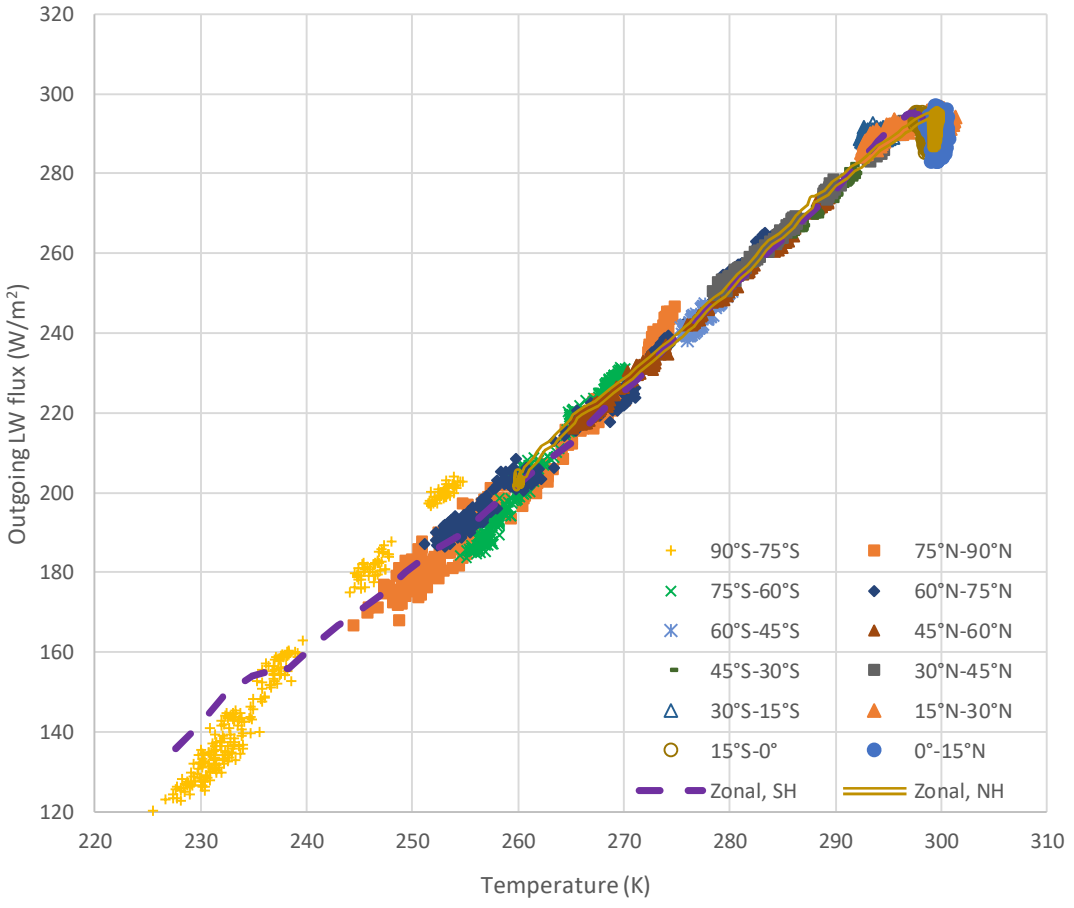

Figure 6: Depiction of monthly variability of outgoing LW radiation, as given by the CERES data; each point is the monthly value, spatially averaged over a geographical zone of 15° latitude, during the period of 2000 – 2022; the zonal distributions (temporal averages for the entire period as in Figure 4) are also shown for each hemisphere (SH and NH).

4. Macroscopic Relationships

4.1 Clear-sky Relationships

Faithful to Dooge's (1986) spirit of "looking for hydrologic laws", i.e., simple macroscopic laws for phenomena whose details are complex, this section tries to establish relationships between the downwelling and outgoing LW radiation fluxes with the variables that influence them, namely, temperature, water vapour pressure, carbon dioxide concentration and cloudiness. To this aim, it primarily uses MODTRAN outputs and also cloudiness information.

A series of systematic MODTRAN runs around the values of the standard tropical profile, i.e., $[CO_2]$ = 400 ppm and for surface T = 299.7 K and e_a = 19 hPa, with ranges of 200 – 800 ppm for $[CO_2]$, ±2 K for T and ±10% for e_a, gave the results shown in contour graphs in Figure 7 for the downwelling LW flux and in Figure 8 for the outgoing flux. Both figures suggest that the relationships among the involved variables are simple and that macroscopic representations are possible. Figure 7 shows a linear effect of e_a and a logarithmic one of $[CO_2]$ on the variation of the downwelling LW flux. In addition, it shows that a ±10% change in e_a has a larger effect than a doubling or halving of $[CO_2]$. Similar are the results of Figure 8, but with smaller differences in the effects of the two factors.

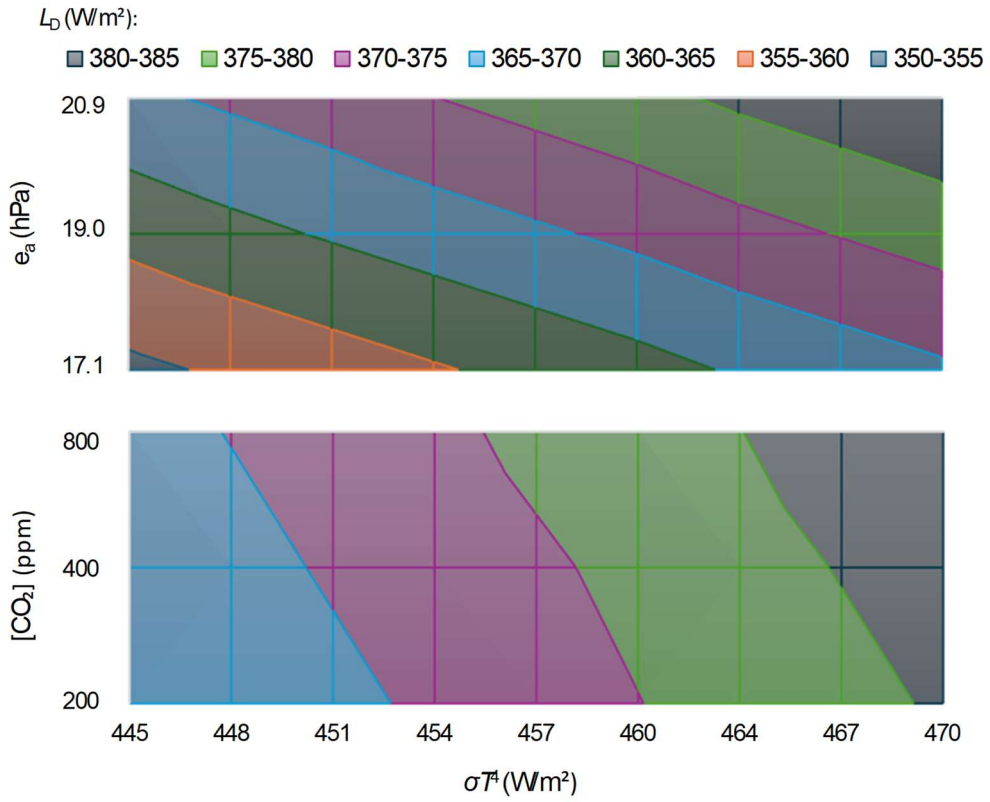

*Figure 7: Changes in the downwelling LW radiation, L_D, as calculated by MODTRAN, due to changes in temperature (converted to blackbody radiation, σT^4), and (**upper**) water vapour pressure (e_a) and (**lower**) carbon dioxide concentration ($[CO_2]$). The calculations were made for the tropical profile, no clouds and default other settings. For the upper graph it was assumed $[CO_2]$ = 400 ppm and for the lower graph e_a = 19 hPa. Notice that the scale of the vertical axis is linear in the upper graph (with range ±10% of the central value) and logarithmic in the lower graph (with range from half to twice the central value).*

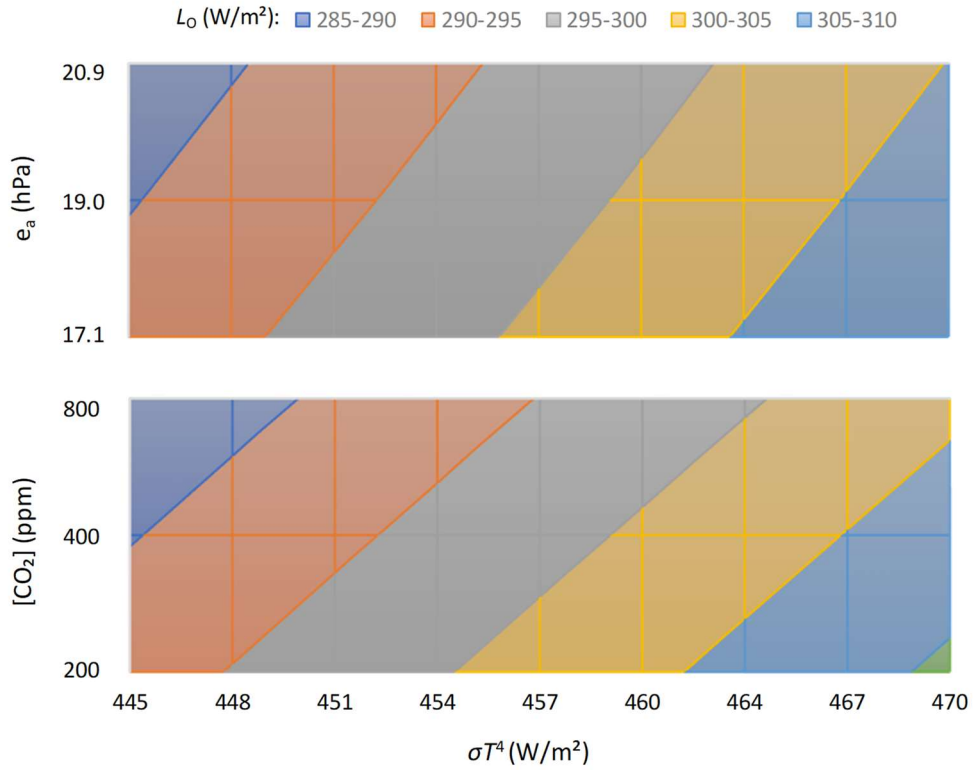

Figure 8: As in Figure 7 but for the outgoing LW radiation, L_O.

Based on these preliminary results, several mathematical expressions were formulated and fitted. The following equation was found to be the best for both the downwelling and outgoing flux, L_D and L_O, respectively:

$$L_{\mathrm{D,O}} = L^* \left(1 + \left(\frac{T}{T^*}\right)^{\eta_T} \pm \left(\frac{e_\mathrm{a}}{e_\mathrm{a}^*}\right)^{\eta_e}\right)\left(1 \pm a_{\mathrm{CO_2}} \ln\frac{[\mathrm{CO_2}]}{[\mathrm{CO_2}]_0}\right)(1 \pm a_C C) \qquad (2)$$

with $[\mathrm{CO_2}]_0$ = 400 ppm. This includes two groups of parameters to be optimized, namely (a) dimensional, L^*, T^*, and e_a^* with units $[L]$, $[T]$, and $[e_\mathrm{a}]$, respectively, and (b) dimensionless η_T, η_e, $a_{\mathrm{CO_2}}$and a_C. Excepting the last one, referring to the cloud area fraction, C, and discussed in Section 4.2, all others were optimized based on clear-sky MODTRAN results, and their values are contained in Table 1.

Table 1: Fitted parameters of Equation (2) for ranges of temperature 247.2 to 309.7 K (–26.0 to 36.6 °C), water vapour pressure 1.08 to 20.9 hPa, and CO_2 concentration 200 to 800 ppm.

	Sign†	L^* (W/m²)	T^*(K)	e_a^* (hPa)	$[\mathrm{CO_2}]_0$ (ppm)‡	η_T	η_e	$a_{\mathrm{CO_2}}$	a_C§
Downwelling, L_D	+	27	181	6.36	400	4.5	1	0.015	0.34
Outgoing, L_O	–	1	55	0.00302	400	3.5	0.5	0.015	0.15

† *Specific sign to replace ± in Equation (2).*
§ *These are global values; for values of outgoing radiation per geographical zone see Figure 13.*
‡ *Not necessary to optimize.*

As seen in Table 2, the performance measures of the fitting are very good and hence the equation is a good macroscopic representation of the MODTRAN results. The good performance is also seen graphically in Figure 9 for downwelling flux and Figure 10 for outgoing flux.

Table 2: Performance indices of Equations (2) (with parameters as in Table 1) and (3), fitted for ranges of temperature 247.2 to 309.7 K (–26.0 to 36.6 °C), water vapour pressure 1.08 to 20.9 hPa, CO_2 concentration 200 to 800 ppm, and clear sky.

Equation, variable	Range of L (W/m^2)	RMSE† in L (W/m^2)	NSE§ of L (%)	RMSE† in relative error $(L^e - L)/L$ (%)	Maximum absolute relative error $\lvert L^e - L\rvert/L$ (%)
(2), downwelling, L_D	140.0 – 419.5	1.3	99.97	0.5	1.9
(2), outgoing, L_O	170.6 – 351.1	1.3	99.79	0.7	1.9
(3), outgoing, L_O from L_D	170.6 – 351.1	3.6	99.24	1.5	4.5

† *Root mean square error.*
§ *Nash-Sutcliffe efficiency (defined to be the difference from 1 of the ratio of the mean model square error to the variance of the variable that is modelled).*

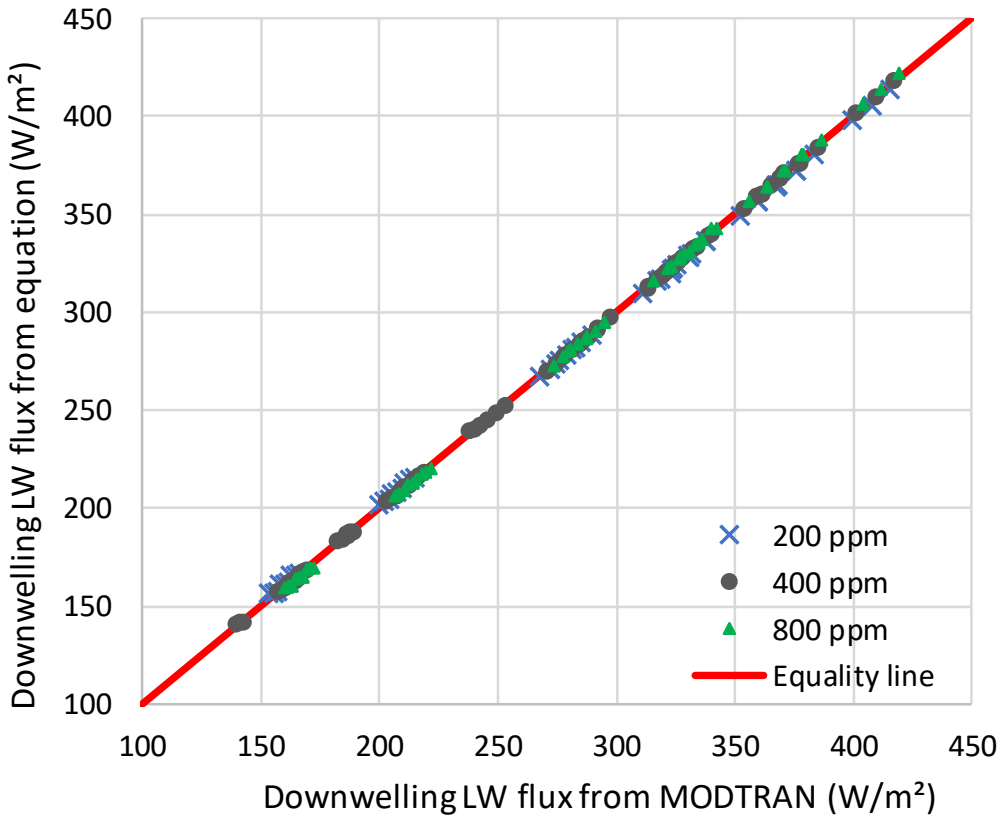

Figure 9: Comparison of downwelling LW radiation flux, L_D, as computed by MODTRAN and by Equation (2).

For completeness, an additional equation was formulated, which directly relates the outgoing to the downwelling radiation. It is very simple:

$$L_O = L_s - \frac{L_D}{2} + 40\ \mathrm{W/m^2} \tag{3}$$

where to calculate the surface radiation flux L_s the emissivity was taken $\varepsilon_s = 0.97$. The performance of Equation (3) is also good, albeit inferior to that of Equation (2), as seen in Table 2 and Figure 11. This equation shows that the outgoing and downwelling fluxes are closely (and negatively) correlated to each other.

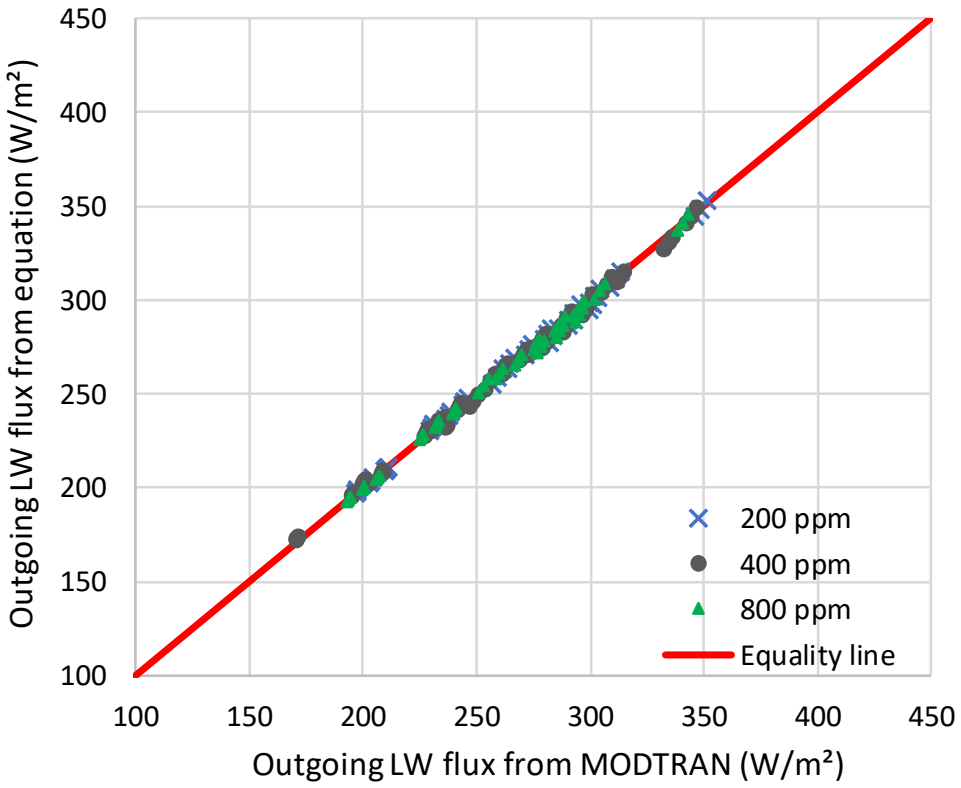

Figure 10: Comparison of outgoing LW radiation flux, L_O, as computed by MODTRAN and by Equation (2).

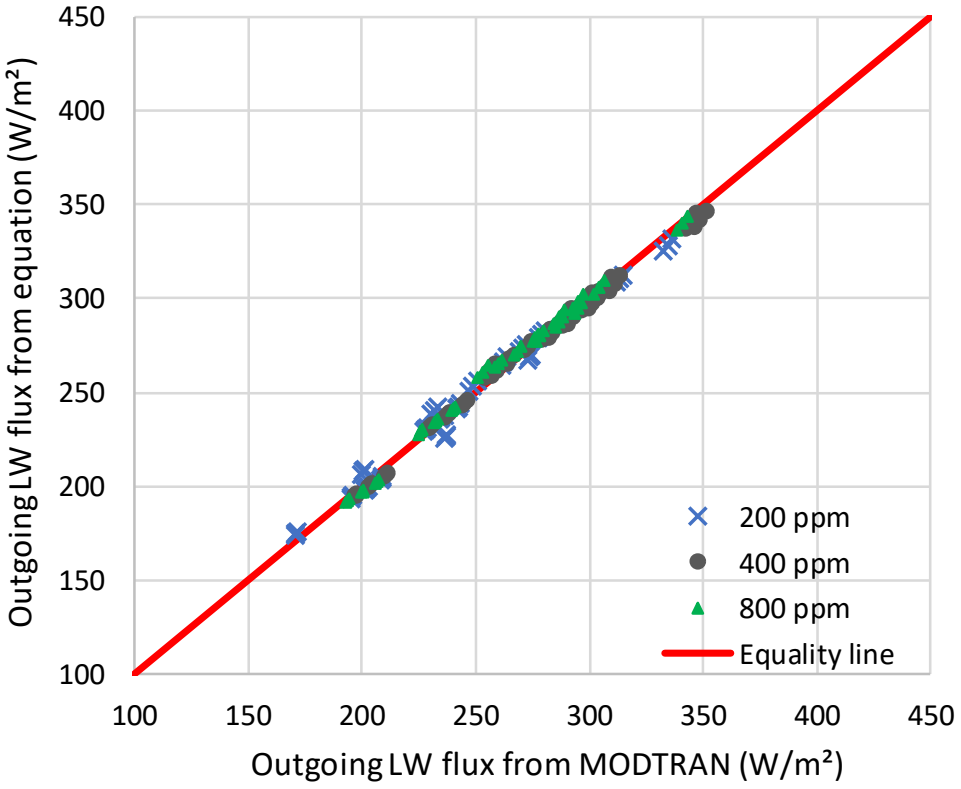

Figure 11: Comparison of outgoing LW radiation flux, L_O, as computed by MODTRAN and by Equation (3), based on the downwelling flux, L_D.

4.2 Effect of Clouds

MODTRAN offers the possibility to model different types of clouds, in addition to clear-sky conditions. Figure 12 shows an example for cumulus clouds and the tropical profile. In particular, it shows that Equation (2) with $(1 - a_C C) = 0.904$ (standing for the ratio of outgoing radiation under cloudy sky to that of clear sky) also represents well the case of cumulus clouds without changing the parameters. Similar performance appears for other types of clouds, but with different ratios, which are shown in Table 3 for the different types of clouds and locality profiles.

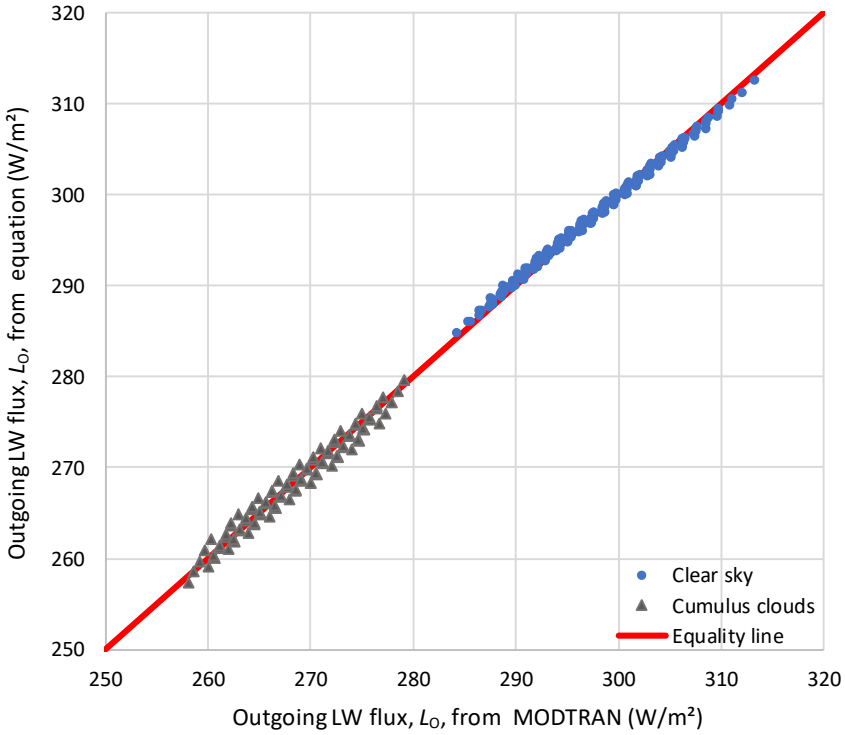

Figure 12: Comparison of outgoing LW radiation flux, L_O, as computed from MODTRAN and from Equation (2), fitted only for the tropical profile and for T = 299.7 ± 2 K, e_a = 19 ± 1.9 hPa, and [CO_2] range of 200 – 800 ppm. The parameters of Equation (2) were reoptimized for these ranges, and the values T^* = 56.2 K and $e_a^* = 0.00683$ hPa were found, while all others remained the same as in Table 1. The case of cumulus clouds is also plotted in the graph, with abscissae as derived by MODTRAN and ordinates equal to the values of Equation (2) for clear sky multiplied by 0.904.

Table 3 *Ratios of outgoing LW radiation under cloudy sky to that for clear sky, for the indicated types of clouds and locality profiles, as determined by MODTRAN for default settings (the lowest value is highlighted in bold).*

Locality profile → Cloud type ↓	Tropical	Midlatitude summer	Subarctic summer	Midlatitude winter	Subarctic winter
Cumulus	0.904	0.899	0.889	0.910	0.95
Altostratus	0.901	0.896	**0.887**	0.907	0.948
Stratus	0.966	0.973	0.962	0.973	1.016
Stratus/Stratocumulus	0.939	0.945	0.931	0.950	0.989
Nimbostratus	0.98	0.984	0.977	0.984	1.024
Standard Cirrus	0.93	0.939	0.957	0.95	0.974
NOAA Cirrus	0.937	0.945	0.963	0.956	0.98

However, it is important to test whether these ratios agree with observed ones. From the CERES data sets, the global average LW radiation flux for the entire observation period, 2001 – 2022, is $L_O^{CS} = 268.2$ W/m² for clear sky and $L_O^{AS} = 239.5$ W/m² for all sky, and give a ratio of 0.892. On

the other hand, the global average cloud area fraction, again calculated from the CERES data, is $C = 0.671$. We assume that the following approximation holds:

$$\frac{L_{\mathrm{O}}^{\mathrm{AS}}}{L_{\mathrm{O}}^{\mathrm{CS}}} = 1 - a_{\mathrm{O}} C \tag{4}$$

from which we find $a_{\mathrm{O}} = (1 - 0.892) / 0.671 = 0.161$. For $C = 1$, we would have $L_{\mathrm{O}}^{\mathrm{AS}} / L_{\mathrm{O}}^{\mathrm{CS}} = 0.839$. Comparing the latter value to those in Table 3, we understand that the MODTRAN model severely underestimates the effect of clouds, as even the least value of the ratio in the Table (0.887 for altostratus clouds and the subarctic summer profile) is too high in view of an average of 0.839. Therefore, to model the effect of clouds we use the CERES data rather than the MODTRAN results, based on the simple relationships:

$$L_{\mathrm{O}}^{C} = L_{\mathrm{O}}(1 - a_C C), \qquad L_{\mathrm{D}}^{C} = L_{\mathrm{D}}(1 + a_C C) \tag{5}$$

where L_{O} and L_{O}^{C} denote the outgoing LW radiation flux for clear sky and cloudiness C, respectively (and likewise for the downwelling, L_{D} and L_{D}^{C}), and a_C is a dimensionless parameter, which may take different values for different situations. These relationships are already incorporated in Equation (2). To determine the parameter a_C for the outgoing LW radiation, we investigate the CERES data (clear and all sky, and cloud fraction, globally and in the five different geographical zones, as shown in Figure 13.

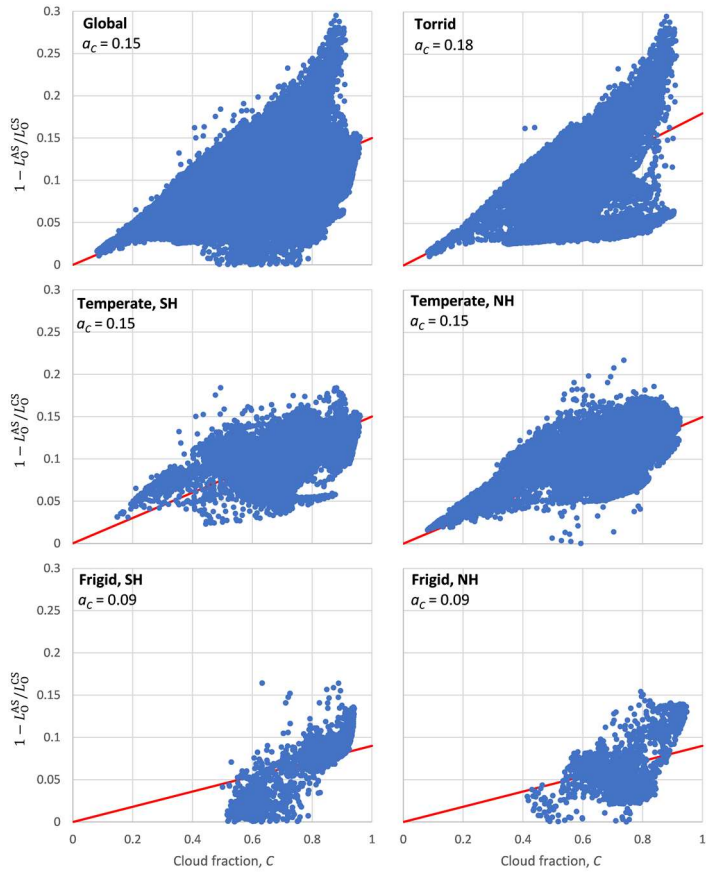

Figure 13: Effect of clouds to outgoing radiation, expressed as $1 - L_O^{AS}/L_O^{CS}$, i.e. the deviation from 1 of the ratio of longwave radiation for all sky (L_O^{AS}) to that for clear sky (L_O^{CS}), vs. the cloud fraction, C. The slopes of homogenous linear regressions, a_C are also shown. Each plotted point corresponds to one of the 64 800 grid points of the CERES grids of clear-sky and all-sky radiation (Figure 2), and cloud area fraction (Figure 3), where the average over the period 2001-2022 was taken.

The resulting a_C values are also shown in Figure 13 and vary from 0.18 in the torrid zone to 0.09 in the frigid zones. Notable is the large spread of the observations, with a variation range of 0 to about twice the estimated mean slope (i.e., $1 - L_O^{AS}/\, L_O^{CS}$ from 0 to 0.30). For a detailed deterministic modelling, this spread would not be acceptable, but in a macroscopic modelling within stochastics, Figure 13 provides useful and utilizable information.

The data used in this study do not allow direct estimation of a_C for downwelling flux and thus we use values from literature. Dingman (1994, p. 189) suggested a value of 0.4, Jacobs (1978, p. 108) estimated a value of 0.33 and Lhomme et al. (2007) a value of 0.34. (This could be also taken as 0.37 as the formula in their equation (13) can be written as is $L_D^C/L_D = 1.03 + 0.34\, C$, which for $C = 1$ yields $L_D^C/L_D = 1 + 0.37$.) Of these values, here we use $a_C = 0.34$ as this value was based on the most extensive data set and is the most recent. Other researchers give different formulae (Brutsaert, 1991, p.142; Carmona et al., 2014; Wong et al., 2023), but here we preferred the simplest linear formulation.

5. Testing of Model Results

5.1 Radiation Flux Profiles

As already mentioned (Section 3), the most appropriate way to test the validity of a model that determines the LW radiation, such as MODTRAN, would be to compare its results to observed radiation profiles. As described in Section 3, here we make a single comparison to get a general idea, using the two radiosondes launched on 23 September 2011 at Payerne, Switzerland, and reported in the study by Philipona et al. (2012), whose LW radiation profiles were digitized here. As reported in the study, the surface-emitted LW upward radiation was about 445 W/m² during the day, with a remarkably strong decrease during the first 1 km, and 380 W/m² during the night. A surface temperature of 11 °C (284.2 K) is reported in the study for 23 September 2011, without clarifying whether this corresponds to the day or night radiosonde. Using MODTRAN with the standard midlatitude summer profile, we find that at the altitude of +0.5 km, the values of 445 W/m² and 380 W/m² are achieved for a temperature offset of +5.5 K (297.5 K at +0.5 km) and −6.2 K (285.8 K at +0.5 km, close to the reported 284.2 K), respectively. However, the former temperature offset gives too high temperature at higher altitudes, inconsistent with the observed strong decrease across the first 1 km. Therefore for the comparison of the day profile with MODTRAN we did not use any temperature offset, while for the night case we assumed an offset of –6.8 K (285.1 K, midway of the values 284.2 K and 285.8 K).

Figure 14 depicts the radiosonde profiles, compared with the MODTRAN results obtained with the above assumptions. For the night radiosonde, there is a good agreement, yet the differences between observations and MODTRAN results are ±25% for the downward flux and ±4% for the upward flux. For the day radiosonde, the differences are substantial, particularly above 7 km. Philipona et al. (2012) attribute these differences to the thermal longwave radiation from the Sun—a plausible interpretation. Excepting the latter factor, we may deem that MODTRAN represents the relevant processes satisfactorily.

5.2 Downwelling Radiation

As already mentioned, we use the empirical or semi-empirical formulae of downwelling radiation to test the MODTRAN results. These formulae are expressed in terms of emissivity $\varepsilon_a = L_D/\sigma T_a^4$ (Appendix A). Figure 15 shows that the emissivity calculated by the macroscopic relationship of Equation (2) perfectly agrees with that directly calculated by MODTRAN, with a Nash-Sutcliffe efficiency NSE = 99.9%. As seen in Figure 16, the agreement is not so good if we compare MODTRAN's emissivity with those of the formulae in Appendix A. The best agreement (NSE = 61.6%) is seen for Prata's Equation (A14) followed by Brutsaert's Equation (A12) (NSE = 39.5%) and the FAO Penman-Montieth's Equation (A19) (NSE = 1%). The Brunt / Penman Equation

(A17) gives a NSE < 0, meaning that a single value equal to the mean performs better than the relationship in representing the compared data.

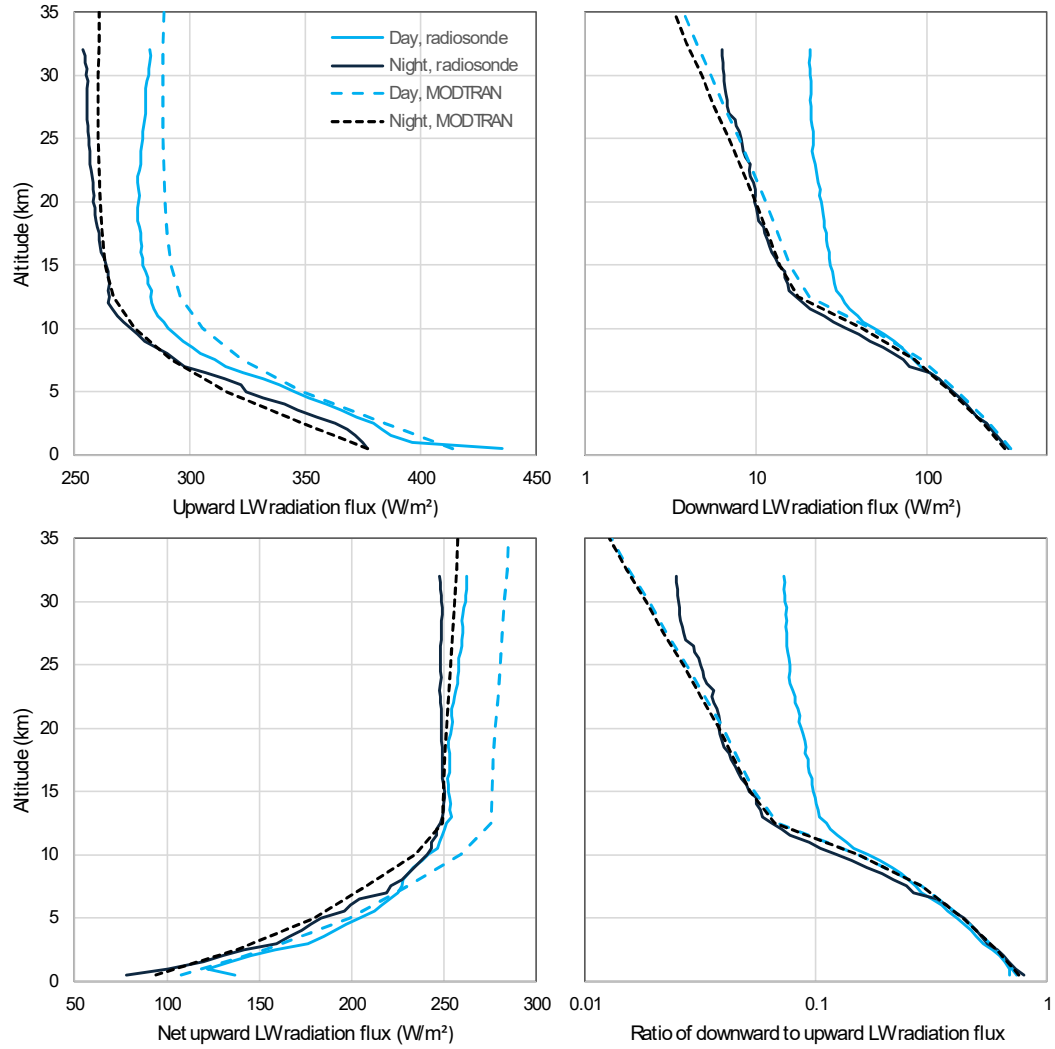

Figure 14: Comparison of LW radiation components calculated by MODTRAN to radiosonde measurements by Philipona et al.(2012).

Note that if the group of points corresponding to subarctic winter with temperatures lower than 270 K is excluded, Brutsaert's equation has the best performance of all, with a NSE of 75%. Overall, if we assume that the empirical or semi-empirical formulae are closer to reality than MODTRAN because they are based on data and if we exclude the subarctic winter data (and the Brunt / Penman equation) we conclude that MODTRAN underestimates the downwelling radiation flux.

Another comparison is made in Figure 17 for the downwelling LW radiation flux vs. temperature, as calculated by MODTRAN and the CERES EBAF zonal distribution shown in Figure 4. For the former, all five locality profiles are used with default settings as well as with temperature offsets from the default values of up to ±25 K. We recall that CERES EBAF data are not actually measurements but computed results. Yet the graph suggests a tendency of MODTRAN to underestimate the downwelling radiation, a finding similar to that in the comparison with the emissivity formulae.

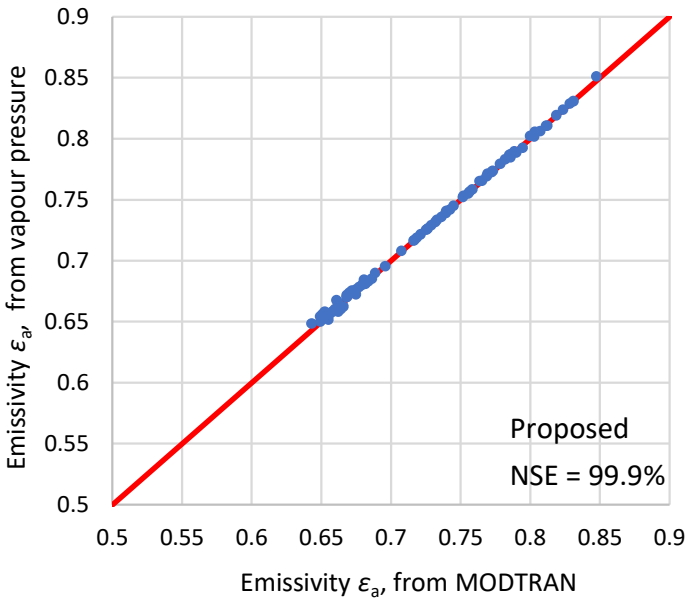

Figure 15: Comparison of emissivity calculated by MODTRAN to that calculated by Equation (2).

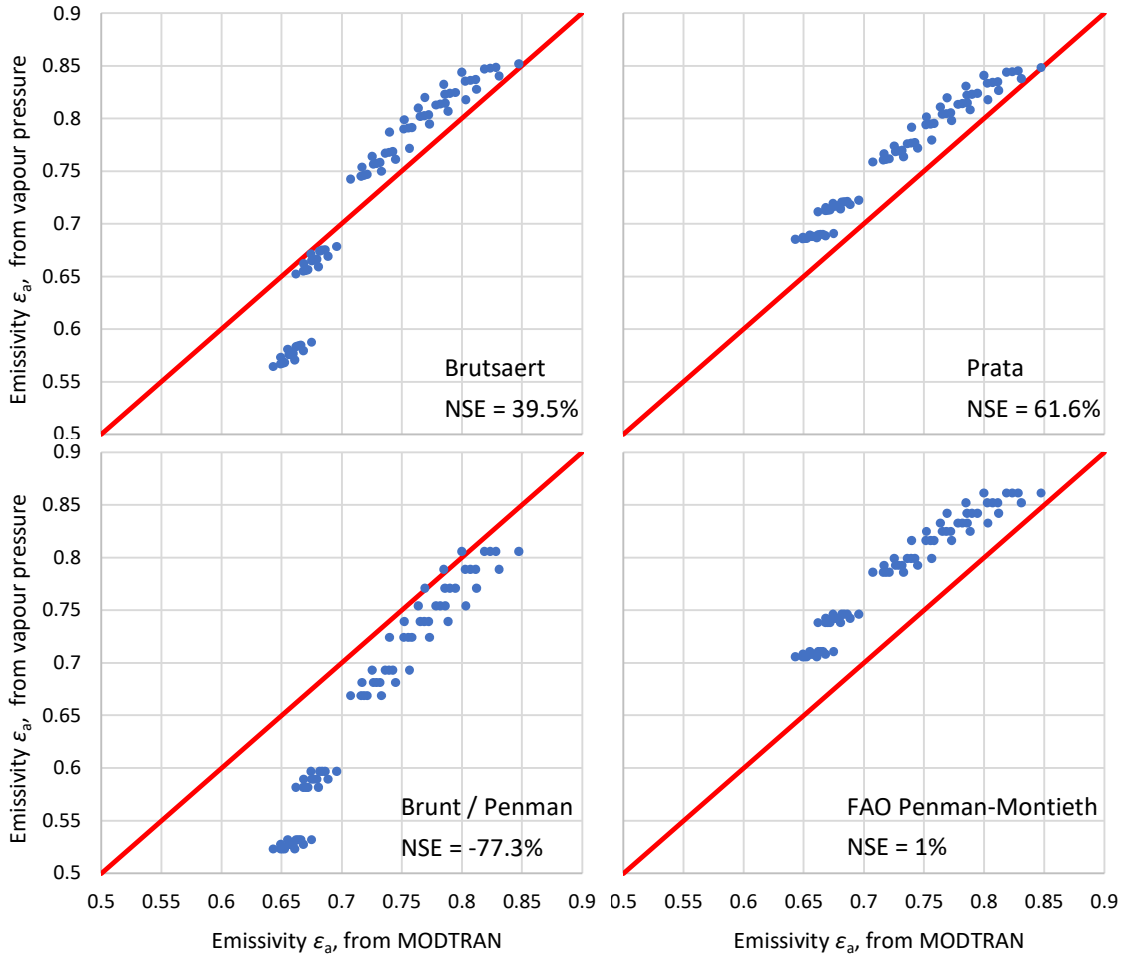

Figure 16: Comparison of emissivity calculated by MODTRAN to that calculated by each of the indicated formulae; the Nash-Sutcliffe efficiency (NSE) is also shown for each case.

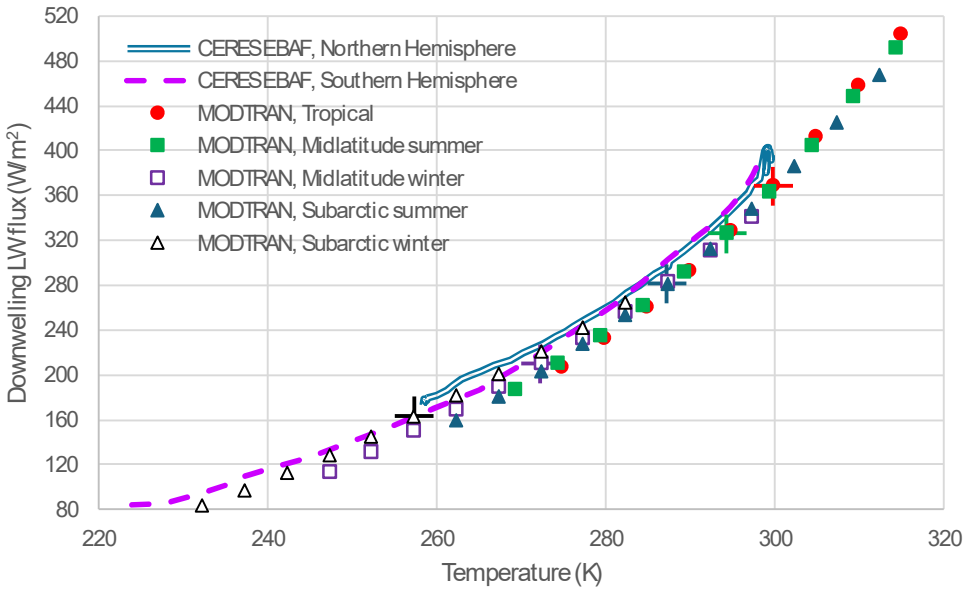

Figure 17: Downwelling LW radiation flux vs. temperature, as calculated by MODTRAN for the five indicated locality profiles and default settings (points with crosses) as well as with temperature offsets from the default values of up to ±25 K (all other points), in comparison to the CERES EBAF zonal distribution shown in Figure 4.

5.3 Outgoing Radiation

For the outgoing radiation, a comparison similar to that in Figure 17 is made. It is presented in Figure 18 and is now stronger and more meaningful, as the CERES outgoing LW flux is observed, rather than a model output. The graph shows that at the default temperature values of each of the MODTRAN profiles, there is almost perfect agreement between CERES data and MODRTAN results, and this is also extended for negative temperature offsets in MODRTAN. However, for positive temperature offsets, MODRTAN overestimates the flux.

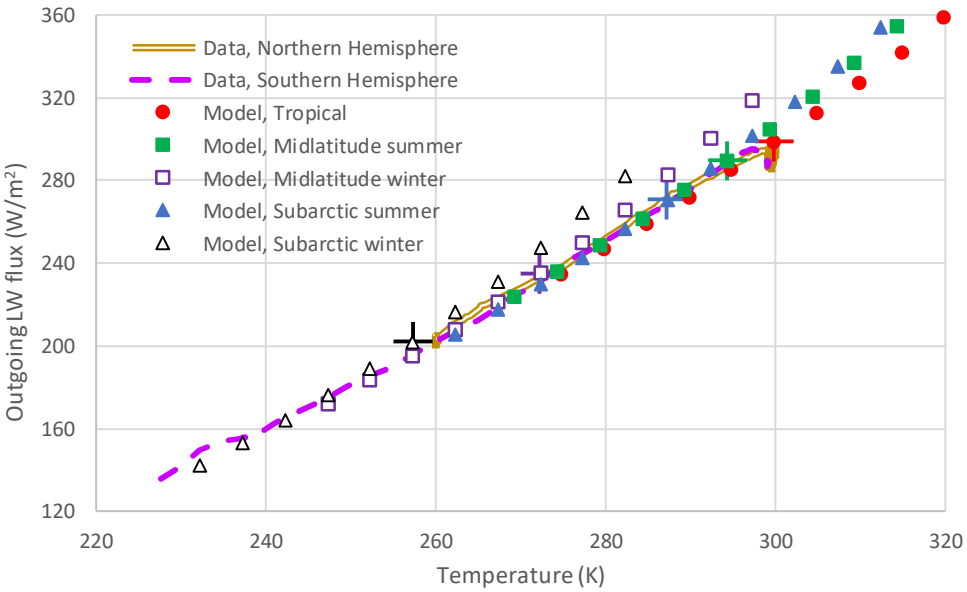

Figure 18: Outgoing LW radiation flux vs. temperature, as calculated by MODTRAN for the five indicated locality profiles and default settings (points with crosses) as well as with temperature departing from the default values by up to ±25 K (all other points), in comparison to the observed zonal distribution (CERES SSF1) as shown in Figure 4 and Figure 6.

As another test, we use time series of meteorological variables and [CO_2] for the 22 years of CERES data availability averaged over the torrid zone, which are shown in Figure 19.

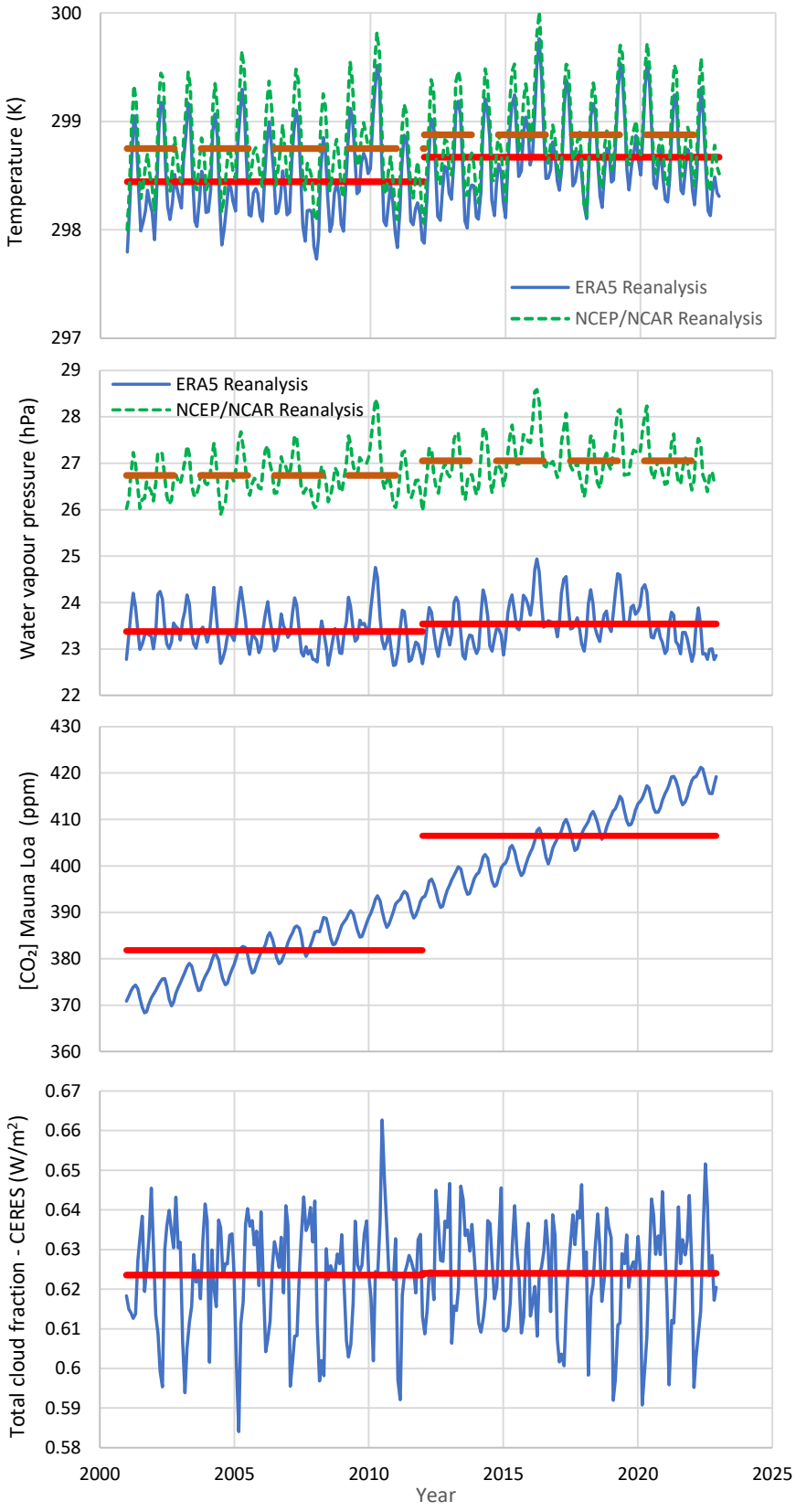

Figure 19: Time series of the indicated variables averaged over the torrid zone. The values plotted are monthly averages, while the 11-year averages are also plotted in thicker (red or dark red) lines.

For temperature and water vapour pressure, both ERA5 and NCEP/NCAR reanalyses data are used, which, as shown in the graphs, have differences from each other, particularly in the latter variable. Based on these time series and Equation (2), the model results, which correspond to MODTRAN, are calculated and plotted in Figure 20. In the upper panel of the Figure, substantial differences are seen in the mean levels of the clear-sky LW outgoing radiation, both between the time series of the two reanalyses and the latter with the CERES data. These can be attributed mostly to uncertainty in reanalyses data and their representation of reality, as indicated in the differences between the two. If we exclude the effect of the mean level differences, the cross-correlation coefficients with the CERES data are reasonable, i.e. 0.67 for ERA5 and 0.69 NCEP/NCAR.

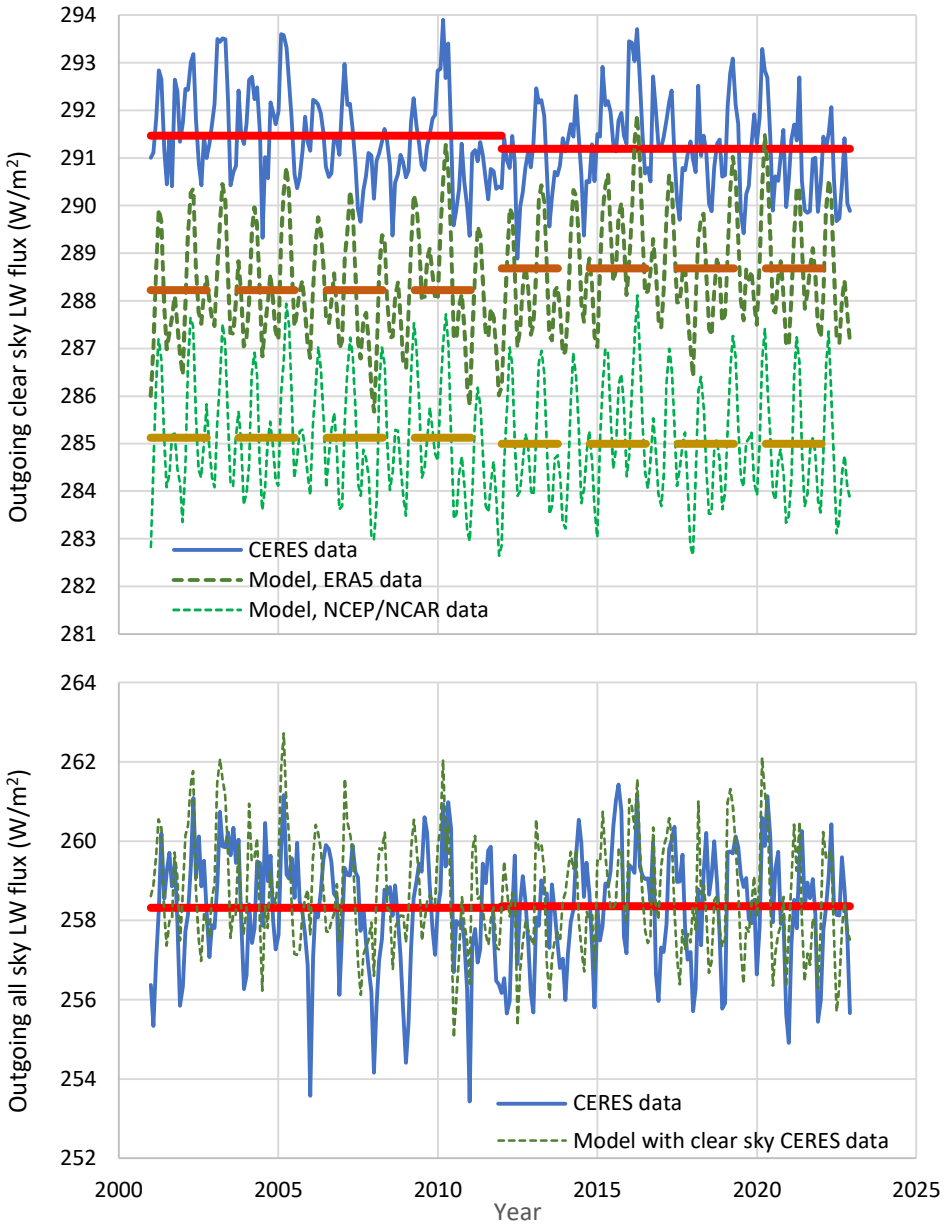

*Figure 20: **(upper)** Time series of outgoing clear-sky LW radiation flux, averaged over the torrid zone, as given by CERES data and as predicted by Equation (2) with temperature, water vapour and [CO_2] data from the ERA5 and NCEP/NCAR Reanalyses. **(lower)** Time series of outgoing all-sky LW radiation flux, averaged over the torrid zone, as given by CERES data and as predicted by the CERES clear-sky data and Equation (2) with CERES cloud area fraction. The values plotted are monthly averages, while the 11-year averages are also plotted in thicker (red or dark red) lines.*

In the lower panel of Figure 20, we use the CERES clear-sky time series, as shown in the upper panel, and multiply it by the quantity $(1 - a_C C)$ of Equation (2), with $a_C = 0.18$ (the value of the torrid zone) and cloudiness C as in the time series of the lowest panel of Figure 19. The attained results compare well with the all-sky CERES time series in terms of mean level, even though the cross-correlation between the two plotted time series (–0.15) does not suggest correspondence of the individual monthly values.

In both Figure 19 and Figure 20, the average values of the time series are shown for two 11-year subperiods, 2001 – 2011 and 2012 – 2022. It is seen that there were increases in the second period in all variables (very large in CO_2 and very slight in all-sky outgoing radiation) except in the clear-sky radiation, where a slight decrease (–0.08 W/m^2) is seen. It is interesting to investigate if the latter decrease is explained by MODTRAN. The results of the related calculations are shown in Table 4. Using any of its default profiles, MODTRAN results in an increase of outgoing clear-sky LW radiation (from +0.38 to +0.60 W/m^2), opposite to what is seen in the CERES data.

Table 4 *Comparison of observed data and MODTRAN results for the average conditions of each of the indicated two periods. The observed data are global averages. The MODTRAN results are for the average observed temperature and [CO_2] of each period, and for the same water vapour scales in the two periods, estimated so as to (approximately) match the outgoing clear-sky LW flux of CERES for the first period, while holding fixed relative humidity for the two periods.*

Period →	2001-11	2012-22	Difference
Observations (averages over each period)			
Temperature from ERA5 (K)	287.21	287.49	+0.28
[CO_2] from Mauna Loa (ppm)	381.83	406.48	+24.65
Outgoing TOA (20 km) clear-sky LW from CERES (W/m^2)	268.33	268.27	–0.08
Outgoing clear-sky LW radiation by MODTRAN at 20 km altitude (W/m^2)			
Tropical profile, water vapour scale 0.82	268.34	268.72	+0.38
Midlatitude summer profile, water vapour scale 1.08	268.34	268.78	+0.44
Midlatitude winter profile, water vapour scale 1.14	268.28	268.78	+0.50
Subarctic summer profile, water vapour scale 2.56	268.31	268.91	+0.60

The above results from CERES data, which are for the torrid zone only, are similar to those for global averages, presented by Koutsoyiannis and Vournas (2024; Appendix B). The latter study also examined SW radiation data and found a decrease in total outgoing radiation, which is consistent with the increased atmospheric temperature. This decrease in outgoing radiation can hardly be attributed to increased [CO_2] but it can be related to water vapour and cloud profiles. The effect of CO_2 is trumped by the effect of clouds, which is consistent with the major role of water on climate and the minor one of CO_2.

5.4 Final Assessment

The above tests illustrate the high uncertainties not only in the CERES LW radiation data, but also in the other atmospheric variables, and the relationships among them and the LW radiation, as represented in MODTRAN. The uncertainties do not allow accurate representation of quantities calculated as differences between different variables or between the same variables in different periods, which would be required for attribution of changes. On the other hand, the macroscopic behaviour of MODTRAN seems consistent with what is observed for clear sky, and therefore MODTRAN is suitable for the scope of this paper, which is the investigation of the relative importance of carbon dioxide and water in the greenhouse effect, as detailed in the next section. As regards clouds, MODTRAN seems to underestimate their effect, but by using the cumulus or altostratus cloud conditions, we get results close to reality for average all-sky conditions.

6. Comparison of H_2O and CO_2

6.1 Imaginary-world Conditions

Investigating imaginary-world conditions seems pointless, yet we include it for the reasons explained in the Introduction—the fact that several popular narratives are based on imaginary-world conditions. The imaginary-world conditions we examine are the most extreme ones, starting from the case that [CO_2] is totally absent in the atmosphere and ending in the case where the atmosphere is made up entirely of CO_2. Extreme ranges are also examined for other greenhouse gases, including water vapour.

Figure 21 compares detailed MODTRAN outputs for the default case of the tropical profile, with [CO_2] = 400 ppm (and T = 299.7 K, L_0 = 298.49 W/m², water vapour scale = 1; red curves), compared to two cases in which CO_2 is totally absent (blue curves). In the left panel, the water vapour is kept at the same level as in the default case. In order for the outgoing radiation to retain its default value (L_0 = 298.49 W/m²), the temperature must be lowered by 15 K (T = 284.7 K). Notably, by also zeroing water vapour, to match the total outgoing LW flux of the red curve (L_0 = 298.49 W/m²), the temperature should be lowered by 28.5 K (T = 271.2 K, a case not shown in the figure but easily imagined in the middle between the smooth curves of 260 and 280 K). The right panel shows that the temperature can remain at its default value (T = 299.7 K) if the water vapour scale is increased to 1.3, accompanied by cumulus clouds. Note that the 30% increase in the water vapour scale does not violate thermodynamic laws, as the vapour pressure remains below the thermodynamic limit. Therefore, assertions that the terrestrial greenhouse effect would collapse without CO_2 (see Introduction) are false.

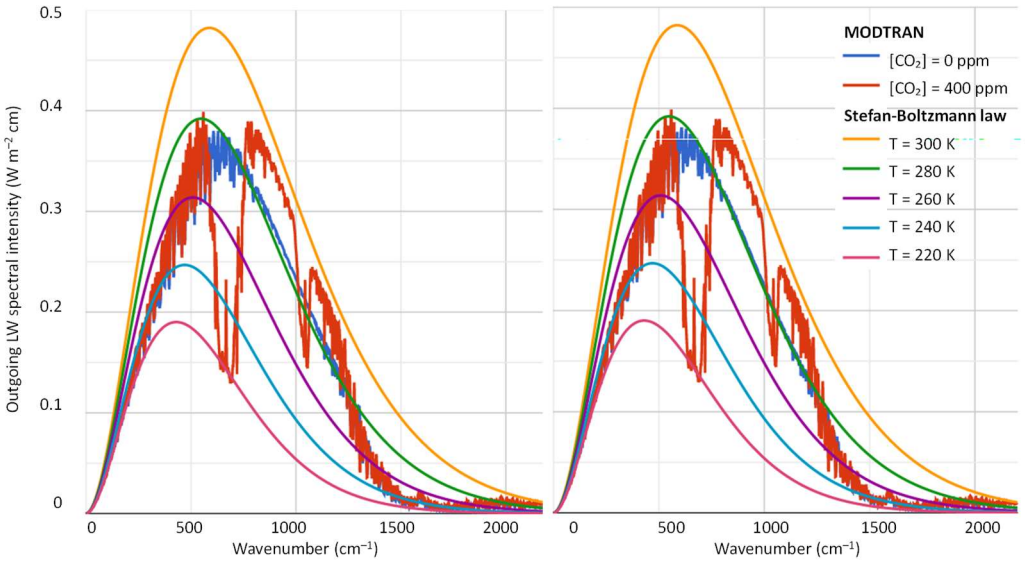

*Figure 21: Output of the MODTRAN model, with the red curves in both panels produced for default settings (for the standard tropical atmospheric profile; T = 299.7 K; [CO_2] = 400 ppm; L_0 = 298.49 W/m²), and the blue curves produced for zero concentrations of all greenhouse gases except water vapour, assuming constant relative humidity and conditions such as to match the total outgoing LW flux of the red curves, namely: **(left)** temperature lower than default by 15 K (T = 284.7 K); **(right)** temperature equal to the default (T = 299.7 K) but water vapour scale increased to 1.3, accompanied by cumulus clouds.*

The fact that the greenhouse effect would not collapse without CO_2 is also shown in Figure 22 (left panel), which gives a more macroscopic picture for both downwelling and outgoing LW flux, under constant temperature equal to that of the standard tropical atmospheric profile (T = 299.7 K) and zero concentrations of all greenhouse gases except water vapour. It is seen that even without any change in the water vapour profile, the difference of LW radiation flux from the value at

the default settings of [CO_2] = 400 ppm is only –3%. With a 10% increase of the water vapour and zero [CO_2], the downwelling radiation matches that for [CO_2] = 400 ppm.

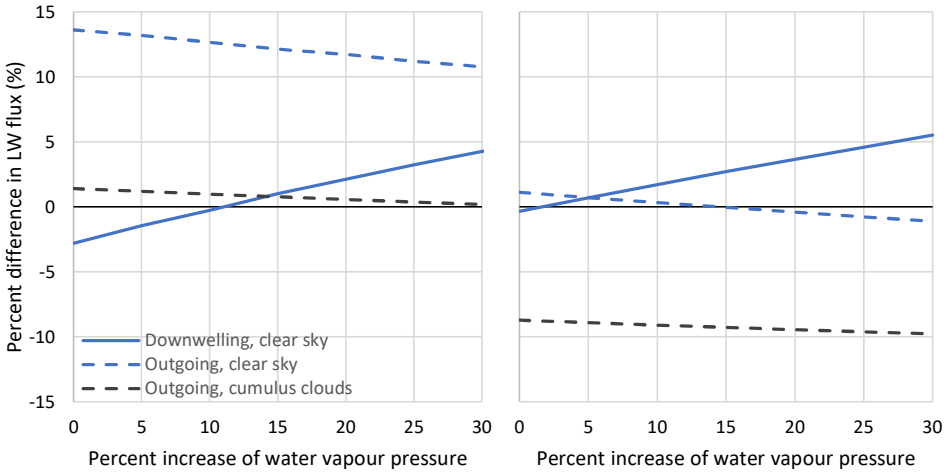

*Figure 22: Difference of LW radiation flux from the values at the default settings of the standard tropical atmospheric profile (T = 299.7 K; [CO_2] = 400 ppm; L_D = 369.26 W/m²; L_O = 298.49 W/m²), as calculated by MODTRAN for the cases of (**left**) zero concentrations of all greenhouse gases except water vapour, assuming constant relative humidity and (**right**) as in left but with [CO_2] = 200 ppm.*

Additional imaginary-world conditions are shown in Table 5. It can be seen there that by removing the entire quantity of atmospheric CO_2 we can achieve the same level of greenhouse effect, as produced by [CO_2] = 400 ppm and zero water vapour, with only 0.15% of the current H_2O level in terms of upward and downward LW heat flux at the surface, or 4% in terms of the outgoing LW heat flux at 100 km altitude. On the contrary, it is impossible to approach the values of the greenhouse effect achieved by H_2O alone in the atmosphere at the current level, by removing it and replacing it with CO_2. Even in an atmosphere entirely composed of CO_2 (i.e. 1 000 000 ppm or 2500 times the current CO_2 concentration), we cannot approach the greenhouse values achieved by the current level of atmospheric H_2O alone. On the other hand, we can easily achieve the greenhouse effect level of an atmosphere entirely composed of CO_2 with an atmosphere free of CO_2 and with only 20% of the current atmospheric H_2O for the downwelling radiation.

Table 5: Results of MODTRAN calculations for tropical profile and temperature at zero altitude of either 288 K (the value of current global temperature used by Brutsaert, 1975) or 299.7 K (the standard value of temperature at zero altitude of the tropical profile) and for extreme (imaginary-world) cases of greenhouse gas concentrations.

[CO_2] relative to the default value of 400 ppm	Water vapour scale relative to the default tropical profile	Other greenhouse gases concentration relative to default	Downward LW heat flux at surface (W/m²)	Upward LW heat flux at surface (W/m²)	Outgoing LW radiation flux at 100 km altitude (W/m²)
1	1	1	325.6 (369.3)*	381.5 (446.5)	249.5 (298.5)
1	1	0	324.0 (366.8)	381.5 (446.5)	256.7 (307.1)
0	0	0	1.7 (2.2)	380.3 (445.3)	379.0 (443.7)
1	0	0	68.2 (80.9)	380.3 (445.3)	340.7 (400.4)
2500†	0	0	215.7 (259.0)	381.5 (446.8)	257.1 (302.2)
0	0.0015	0	78.8 (90.0)	380.3 (445.3)	366.4 (449.6)
0	0.04	0	157.8 (183.3)	380.6 (445.6)	340.7 (399.7)
0	0.2 (0.27)*	0	212.5 (259.7)	380.9 (445.9)	319.3 (370.2)
0	1	0	319.7 (358.9)	381.5 (446.5)	284.7 (339.1)
0	2.2 (2.6)	0	372.1 (438.3)	381.8 (447.1)	257.7 (302.6)

* The values without and with parentheses correspond to a temperature at zero altitude of 288 K and 299.7 K, respectively. When there is no parenthesis in the column of water vapour scale, the same scale is assumed for both cases.
† In this case the atmosphere is entirely composed of CO_2 (2500 × 400 = 1 000 000 ppm = 1).

For completeness, we note that MODTRAN does not modify the temperature profile in the case that water vapour is removed. It assumes a temperature gradient of 6.5 K/km, as in the standard atmosphere, or lower. However, without water vapour, the temperature gradient would be the dry adiabatic one, i.e. 9.8 K/km (see Figure 25 discussed in Section 7), which signifies another effect of water vapour on the atmospheric processes. And of course, without water vapour, clouds would not exist and the surface cooling effect would be larger.

6.2 Realistic Conditions

Leaving aside the imaginary-world cases of an atmosphere without CO_2 or one made up entirely of CO_2, we may assume a realistic minimum value of $[CO_2]$ of the order of 200 ppm. Redrawing the left panel of Figure 22 under this minimal value, instead of zero, we get what appears in the right panel. It is obvious that, in comparison to the $[CO_2]$ level of 400 ppm, the differences are small and can be easily counterbalanced by slight changes in water vapour pressure.

Another view of the same is provided by Figure 23, where the differences from the $[CO_2]$ level of 400 ppm for two cases, doubling or halving this level, are presented. While in Figure 22 at zero altitude the temperature is fixed at $T = 299.7$ K and the water vapour pressure is varying, in Figure 23 the water pressure is fixed at its default value (19 hPa) and the temperature is varying (by offsetting the default value) over a wide range, 50 K. The differences are of the order of 1% and do not reach 2%.

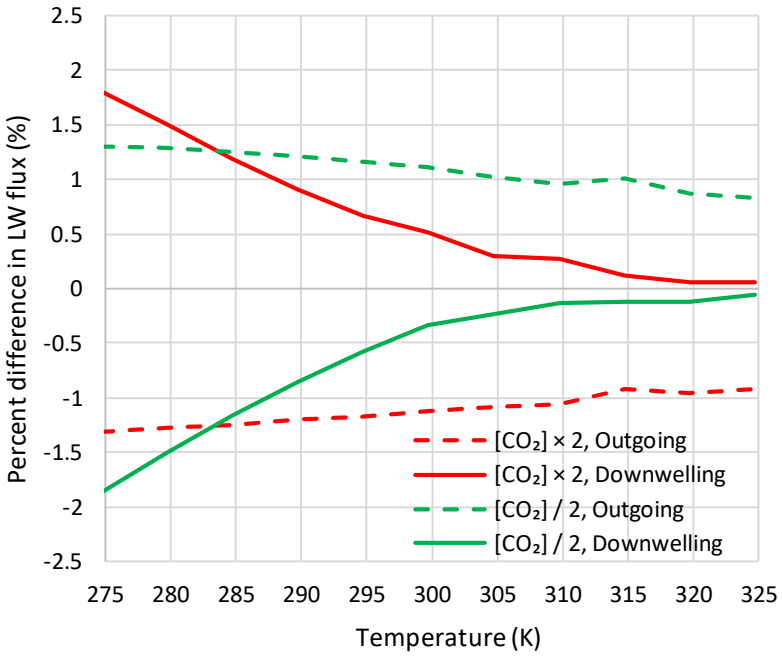

Figure 23: Difference of LW radiation flux for the indicated conditions of $[CO_2]$ from the respective values at the default settings of the standard tropical atmospheric profile (T = 299.7 K; $[CO_2]$ = 400 ppm; L_D = 369.26 W/m²; L_O = 298.49 W/m²), as calculated by MODTRAN.

While the above graphs are suggestive of the low importance of $[CO_2]$ in realistic real-world conditions, here we propose a more advanced method to quantify its relative importance in a more general and systematic manner. Let L be a quantity of interest—in our case the LW radiation flux—that depends on several factors F_i, the explanatory variables. To determine the relative importance of each of the factors F_i, we consider the relative change $\delta L/L$ produced by a relative change $\delta F_i/F_i$ in the factor F_i and we take the ratio:

$$\frac{\delta L}{L} \Big/ \frac{\delta F_i}{F_i} = \frac{\delta L}{\delta F_i} \frac{F_i}{L} \tag{6}$$

As δF_i becomes small, the ratio $\delta L/\delta F_i$ tends to the partial derivative $\partial L/\partial F_i$ and hence the above quantity becomes

$$\frac{\partial L}{\partial F_i} \frac{F_i}{L} = \frac{L'_{F_i} F_i}{L} =: L^{\#}_{F_i} \tag{7}$$

where $L'_{F_i} := \partial L/\partial F_i$ is the partial derivative of L with respect to F_i and $L^{\#}_{F_i} := \partial \ln L/\partial \ln F_i$ is the partial log-log derivative (LLD) of L with respect to F_i. Details about the properties of the LLD are given in Koutsoyiannis (2023, p. 97).

Considering all explanatory variables, the total differential is

$$\mathrm{d}L = \sum_i \frac{\partial L}{\partial F_i} \mathrm{d}F_i \tag{8}$$

and hence

$$\mathrm{d}(\ln L) = \frac{\mathrm{d}L}{L} = \sum_i \frac{\partial L}{\partial F_i} \frac{F_i}{L} \frac{\mathrm{d}F_i}{F_i} = \sum_i L^{\#}_{F_i} \frac{\mathrm{d}F_i}{F_i} = \sum_i L^{\#}_{F_i} \mathrm{d} \ln F_i \tag{9}$$

The partial LLDs, $L^{\#}_{F_i}$, reflect the relative importance of each F_i. For illustration, let us consider a quantity L affected by two factors F_1 and F_2. A small relative change $\delta F_1/F_1$ in F_1, equal to a, without any change in F_2, will result in a change of the dependent quantity L equal to $(\delta L/L)_1 = L^{\#}_{F_1} \delta F_1/F_1 = L^{\#}_{F_1} a$. Likewise, a small relative change $\delta F_2/F_2$, in F_2, again equal to a, without any change in F_1 will result in a change of $(\delta L/L)_2 = L^{\#}_{F_2} a$. Hence,

$$\frac{(\delta L/L)_1}{(\delta L/L)_2} = \frac{L^{\#}_{F_1}}{L^{\#}_{F_2}} \tag{10}$$

which means that the relative change in the quantity of interest due to changes in the explanatory variable is proportional to the partial LLD. Hence, Equation (9) allows the decomposition of the relative change $\mathrm{d}L/L$ due to the relative change $\mathrm{d}F_i/F_i$ of each of the different explanatory variables. Apparently, if the system studied is nonlinear (as most natural systems are), the partial LLDs are not constant. In this case, we must first specify a point of interest (with its coordinates F_i) and then calculate the partial LLDs for this point. The method is quite general and can be applied to any point of interest.

Now, Equation (2) allows analytical determination of the log-log derivatives and hence the relative importance of each of the factors $F_i \in \{T, e_\mathrm{a}, [\mathrm{CO_2}], C\}$. This is made in Table 6. MODTRAN also includes other greenhouse drivers with minor importance, i.e. CH_4, tropospheric ozone, stratospheric ozone, and freon, which were not modelled in the above analyses. To calculate their bulk contribution, we increased each of the default values in MODTRAN by 5% ($\delta \mathrm{AO}/\mathrm{AO} = 0.05$, where AO stands for "all other"), calculated $\delta L/L$ by MODTRAN for the tropical and subarctic summer profile (for comparisons), and applied Equation (6) to calculate $L^{\#}_{\mathrm{AO}}$, which resulted in values also included in Table 6; the relatively high value in the outgoing flux is primarily due to the influence of the stratospheric ozone.

It can be readily found using the values in Table 6, that the relative importance of water vapour over [CO_2] is 0.207/0.015 = 13.8 times for the downwelling flux, and $(-0.136)/(-0.015) = 9.1$ times for the outgoing flux. The relative importance of clouds over [CO_2] is 0.186/0.015 = 12.4 times for the downwelling flux and (–0.112)/(–0.015) = 7.5 times for the outgoing flux. In other words, each of the related factors, water vapour and clouds, is an order of magnitude more

important than [CO₂] in terms of the greenhouse effect.

Considering all above factors, Equation (9) is written as

$$\mathrm{d}(\ln L) = L_T^{\#}\mathrm{d}(\ln T) + L_{e_\mathrm{a}}^{\#}\mathrm{d}(\ln e_\mathrm{a}) + L_{[\mathrm{CO_2}]}^{\#}\mathrm{d}(\ln[\mathrm{CO_2}]) + L_C^{\#}\mathrm{d}(\ln C) \tag{11}$$

The first term in the righthand side, $L_T^{\#}$, is by far the most important factor determining the LW flux. The other terms describe the greenhouse effect. Excluding the first term, i.e., setting $\mathrm{d}T = \mathrm{d}(\ln T) = 0$, Equation (11) allows breakdown of the relative importance of the different greenhouse drivers. This is presented in Figure 24, where the compound importance of water vapour and clouds is 95% and 87% for the downwelling and outgoing radiation, respectively, while that of [CO₂] is 4% and 5%, respectively.

Table 6: Relative changes of LW radiation fluxes at standard conditions, equal to the global averages, T = 288.6 K, e_a = 15.2 hPa, $[CO_2]$ = 400 ppm, C = 0.671, as calculated analytically and numerically by Equation (2).

Case of relative change	Relative change expression	Numerical value of relative change	
		Downwelling flux	Outgoing flux
$L_T^{\#}$	$\dfrac{\eta_T \left(\frac{T}{T^*}\right)^{\eta_T}}{1 + \left(\frac{T}{T^*}\right)^{\eta_T} \pm \left(\frac{e_\mathrm{a}}{e_\mathrm{a}^*}\right)^{\eta_e}}$	3.18	4.44
$L_{e_\mathrm{a}}^{\#}$	$\dfrac{\pm\eta_e \left(\frac{e_\mathrm{a}}{e_\mathrm{a}^*}\right)^{\eta_e}}{1 + \left(\frac{T}{T^*}\right)^{\eta_T} \pm \left(\frac{e_\mathrm{a}}{e_\mathrm{a}^*}\right)^{\eta_e}}$	0.207	–0.136
$L_{[\mathrm{CO_2}]}^{\#}$	$\dfrac{\pm a_{\mathrm{CO_2}}}{1 \pm a_{\mathrm{CO_2}} \ln \frac{[\mathrm{CO_2}]}{[\mathrm{CO_2}]_0}}$	0.015	–0.015
$L_C^{\#}$	$\dfrac{\pm a_C C}{1 \pm a_C C}$	0.186	–0.112
$L_{\mathrm{AO}}^{\#}$	(see text)	0.006	–0.023

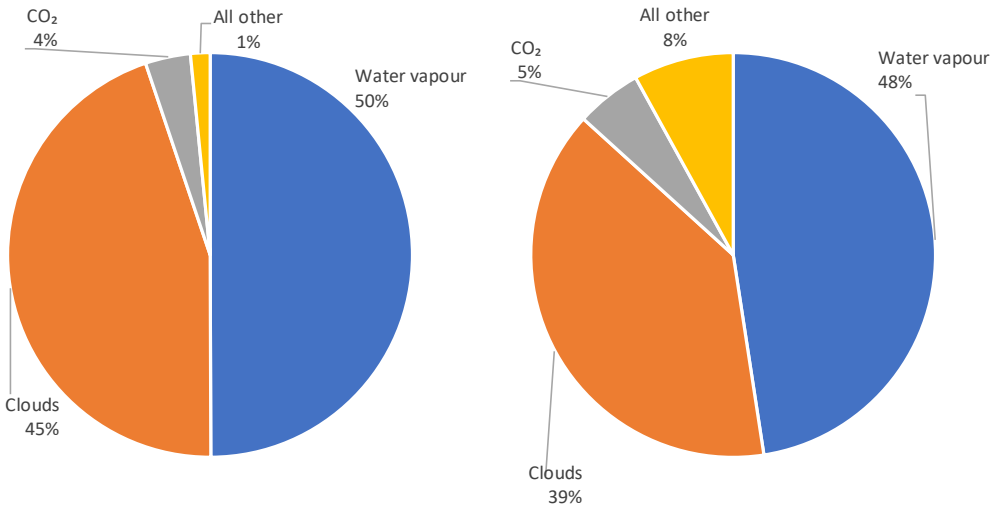

*Figure 24: Contribution of the greenhouse drivers to the LW radiation fluxes, **(left)** downwelling and **(right)** outgoing.*

As Equation (11) is a direct quantification of the greenhouse effect, it provides a means to make simple calculations, which help develop our intuition without resorting to untransparent climate

models. To illustrate this, we consider the example of a relative change in $[CO_2]$ equal to $a = \delta[CO_2]/[CO_2] = \delta \ln[CO_2]$, while the total outgoing LW radiation is constant (i.e. there is no change in the solar constant and the SW radiation process). If there is no change in water vapour and clouds, then this change will be counterbalanced by a temperature increase. Equation (11) with constants as in Table 6, will give $0 = 4.44\,\delta(\ln T) + 0 - 0.015\alpha + 0$ or $\delta(\ln T) = (0.015/4.44)a \approx a/300$. That is, a change of 30% in $[CO_2]$ will result in 0.1% change in T—roughly 0.3 K. If the change in $[CO_2]$ is counterbalanced by a change in water vapour without a change in temperature and clouds, then Equation (11) will give $0 = 0 - 0.136\,\delta(\ln e_a) - 0.015\alpha + 0$ or $\delta(\ln e_a) = -(0.015/0.136)a \approx -a/9$. That is, a change of 30% in $[CO_2]$ can be counterbalanced by a change of about –3% in water vapour pressure. Such calculations do not take into account the interdependence of the different variables, yet they are useful to discern the relative importance in changes thereof.

The above results differ substantially from those of Lacis et al. (2010) and Schmidt et al. (2010), who, using a different methodology, attributed 75% to water vapour and clouds and 19% to CO_2. Our results are closer to an example given by Brooks (1952), in which the contribution of the CO_2 bands is about 1:8 compared to water vapour, without considering the clouds. They are even closer to the results of Harde (2014), who presented exhaustive (line-by-line) spectroscopic calculations based on the detailed representation for high-resolution transmission molecular absorption database HITRAN (2008; a compilation of spectroscopic parameters that a variety of computer codes use to predict and simulate the transmission and emission of light in the atmosphere) and confirmed the domination of water and clouds in the absorption of both the SW and LW radiation. Specifically, Harde found that only about 4% and 3.5% of the total of SW and LW radiation absorption, respectively, can be allocated to carbon dioxide, taking into account the overlap of its spectrum with that of the water vapour (and other greenhouse gases).

For completeness it must be noted that clouds also affect the planet's albedo and the incoming solar radiation, reducing it, but such an analysis is outside the scope of this paper, which is focused on the greenhouse effect. In addition, as already noted, the explanatory variables are not independent from each other. For example, absence of water vapour entails absence of clouds. Additionally, according to the mainstream narrative, an increase of $[CO_2]$ results in increase of water vapour (with the mainstream regarding it to be a feedback of CO_2). But these dependencies, whether true (water vapour – clouds) or not (CO_2 – water vapour, regarded as a feedback) do not invalidate the methodology. The results in Table 6 have been produced for average conditions prevailing in the present atmosphere. If these conditions change because of the dependencies or any other reasons, the partial LLDs should be evaluated at a new point of the vector of explanatory variables.

In this respect, it is useful to estimate the changes that the increase of $[CO_2]$ in a century, from 300 to 420 ppm, may have caused. The results produced by Equation (2), as well as those by direct run of MODTRAN, for this specific increase are shown in Table 7. The former are deemed more reliable than the latter as they are based on a generalized equation representing all conditions, while the latter is based on a specific locality profile, namely midlatitude summer profile (and altostratus clouds for the cloudy case). The change in the downwelling radiation is estimated at 0.5% or lower, which could not be discerned by observations, thus confirming the finding by Koutsoyiannis and Vournas (2024). The change in the outgoing radiation is estimated also at 0.5% (but with a negative sign) or lower (compare also with Salby, 2012, p. 249), which also could not be discerned by observations. Table 7 also shows the expected results for the case that $[CO_2]$ increases to 800 ppm. Now the change in the LW radiation flux is higher, 1.5%, and again could hardly be detected macroscopically by measurements in the future, in case that indeed $[CO_2]$ reaches 800 ppm.

Our results in Table 7 are comparable to those of van Wijngaarden and Happer (2020) (corroborated in de Lange et al., 2022), who, using the HITRAN database and satellite data, concluded that a doubling of CO_2 concentration (from 400 to 800 ppm) would result in a 3 W/m^2 decrease of radiation flux in the top of the atmosphere, which translates to –1.1%. The results in Table 7

are also comparable with those by Harde (2017; tables 2, 4, 5) even though the latter study differs in the assumptions and the computational approach.

Table 7 *Relative changes of LW radiation fluxes at standard conditions, equal to the global averages, T = 288.6 K, e_a = 15.2 hPa, C = 0.671 (or C = 0 for clear sky), and with the indicated values of [CO₂] as calculated analytically and numerically by Equation (2). In parentheses are the values directly calculated by MODTRAN assuming midlatitude summer profile matching the above values of T and e_a, and altostratus clouds for the cloudy case.*

[CO₂] increase	Sky	Downwelling, L_D			Outgoing, L_D		
		ΔL_D	L_D mean*	% change	ΔL_O	L_D mean*	% change
From 300 to 420	Cloudy	1.93	382.4	0.5%	–1.18	235.1	–0.5%
		(0.31)	(374.1)	(0.1%)	(–1.00)	(238.0)	(–0.4%)
From 300 to 420	Clear	1.57	311.3	0.4%	–1.32	261.5	–0.5%
		(0.79)	(309.6)	(0.3%)	(–1.32)	(265.7)	(–0.5%)
From 300 to 800	Cloudy	5.63	384.2	1.5%	–3.45	234.0	–1.5%
		(0.63)	(374.3)	(0.2%)	(–2.89)	(237.0)	(–1.2%)
From 300 to 800	Clear	4.59	312.8	1.2%	–3.84	260.2	–1.5%
		(2.45)	(310.5)	(0.8%)	(–3.89)	(264.4)	(–1.5%)

* *Geometric mean.*

7. Discussion and Further Results

In light of the above results, we may revisit Lacis et al.'s (2010) statements quoted in the Introduction, leaving aside the fact they refer to imaginary world conditions. Specifically, even if we removed the CO_2 from the atmosphere, again there would be new emissions from volcanos and outgassing from the oceans, even if the biosphere was also removed. In the relatively recent glacial periods, covered by Vostok proxy data, the CO_2 concentration did not fall below 180 ppm. This value is perhaps the absolute low for the entire history of Earth. What would disappear from Earth in the imaginary-world case of CO_2 removal is not the greenhouse effect but life as we know it. For plants may not survive at CO_2 levels below 150 ppm (Gerhart and Ward, 2010) while without the photosynthesis performed by plants, the entire biosphere would collapse. On the opposite side, the increase in CO_2 is beneficial for plant growth. As recently reported and as a result of the recent increase, global greening is an "indisputable fact", and even its rate has increased slightly (Chen et al., 2024).

Furthermore, the notion of the effective temperature used by Lacis et al. is problematic because the temperature field of the Earth as a whole is not thermodynamically representable by a single temperature and the radiation from Earth deviates from a black body distribution, which is used to define the effective temperature (Essex et al., 2007). Moreover (and leaving aside this caveat), even the 10% of the current atmospheric value of water vapour for $T_S = T_E$, given in the quoted statement by Lacis et al., would produce a greenhouse effect and hence would imply the inequality $T_S \neq T_E$, thus leading to the absurd. That greenhouse effect would not be 10% or close to it, but closer to its current magnitude. Indeed, according to Brutsaert's equation (A12), for T_E/T_S = 255/288 (with 288 K being the current average temperature used by Brutsaert) and vapour pressure ratio of e_E/e_S = 0.1, the resulting emissivity ratio $\varepsilon_E/\varepsilon_S$ would be $(0.1 / (255/288))^{1/7} = 0.73$. An emissivity $e_E > 0$ means that we would again have the greenhouse effect produced by water vapour. (See also Table 5 and its discussion in Section 6.1.) And even in an "*icebound Earth state*", thermodynamics implies the presence of water vapour in the atmosphere, due to sublimation. Remarkably, though, geological evidence presented by Veizer (2005, 2011, 2012) suggests the presence of running water as far back as we have a record, up to 3.8 or even 4.2 billion years, despite the much smaller solar irradiance (the so-called faint young sun puzzle). All these imply that the argument is mistaken and so is the popular result that is being widely reproduced—now even by chatbots.

The distinction between feedbacks and forcings, also appearing in the quoted statements by Lacis et al., is problematic. Both H_2O and CO_2 have always been present on Earth and both are greenhouse gases, with the difference being that the former is much more abundant in the atmosphere and determinant for the greenhouse effect, as already demonstrated. Calling CO_2 forcing and H_2O feedback is like claiming that the tail wags the dog.

Water has more roles in climate than examined above. The greenhouse effect slows down the rate of Earth's cooling by LW radiation. However, Earth's surface cooling and its reaction, i.e., the atmosphere's warming, is not only due to LW radiation. According to Trenberth et al. (2009), the contribution of the LW radiation is 396 – 333 = 63 W/m^2, a value generally consistent with the results of this paper. This low value is due to the action of greenhouse gases, and, as we have seen, it is dominated by the presence of water vapour in the atmosphere. However, the greatest contribution to Earth's surface cooling, namely 80 W/m^2 (Trenberth et al., 2009; Koutsoyiannis, 2021), is due to the latent heat from evaporation (phase change of water from liquid to gaseous phase).

Surface cooling and atmosphere warming are reflected in the vertical profile of the net upgoing radiation flux, seen in Figure 25. Here the SW radiation was also considered, calculated by RRTM. The net radiation minus the absorbed SW radiation in the atmosphere is increasing with altitude. In the long term, as the energy is not stored in the atmosphere, the total heat transfer should be the same at all altitudes. The deficit of heat transfer in low altitudes is recovered by the transfer of sensible and latent heat, which warm the atmosphere. Figure 26 shows diagrammatically the contribution of each of these mechanisms to Earth's cooling and the atmosphere's warming.

Interestingly, heat exchange by evaporation (and hence the latent heat transfer from the Earth's surface to the atmosphere) is the Earth's natural locomotive, with the total energy involved in the hydrological cycle being 1290 ZJ/year, corresponding to an energy flux density of 80 W/m^2. Compared to human energy production, the total energy of the natural locomotive is 2100 times higher than that of humanity's locomotive (Koutsoyiannis, 2021). Notably, evaporation is a negative feedback of the climate as increased temperature causes evaporation to increase (cf. simplified equation (5) in Tegos et al., 2015). This increases the latent heat, which tends to lower the temperature, making evaporation a strong stabilizer for the climate (Harde, 2014, 2017; Clark, 2024, figure 32), a fact also reflected in Figure 6.

In addition to regulating the LW radiation flux and the latent heat flux, water vapour and clouds also regulate the SW radiation and Earth's albedo. Other properties of water, as listed in Koutsoyiannis (2021), are also determinants for climate. First is its unique property of existing on Earth in *all three phases* and in different formations, with spectacular differences among them in properties related to climate. Remarkable is its *abundance* on Earth, as only the part that is in turbulent motion amounts to 1.34×10^9 Gt (not counting quantities that are stored in the soil, ground and glaciers), 260 times larger than the total mass of the atmosphere. The *turbulent motion* of water, which is intrinsically uncertain, generates climatic phenomena at all scales, from large-scale coupled ocean-atmosphere fluctuations, such as the El Niño–Southern Oscillation (ENSO), Atlantic Multidecadal Oscillation (AMO) and Interdecadal Pacific Oscillation (IPO), to regional droughts and floods. The high specific heat (or *heat capacity*) of water, particularly in its liquid phase, combined with its abundance, makes water the climatic thermostat of the Earth, i.e., the element that determines the heat storage and through it the climate of the Earth. The high *specific latent heat* of vaporization (calculated from Equation (A5)) combined with the water occurrence on Earth in all three phases, makes water the thermodynamic regulator of climate. Finally, the fact that water is a universal solvent makes it an *elixir of life*, complementary to the CO_2 which is the other elixir of life, as through photosynthesis it is responsible for the organic matter on which life on Earth is based.

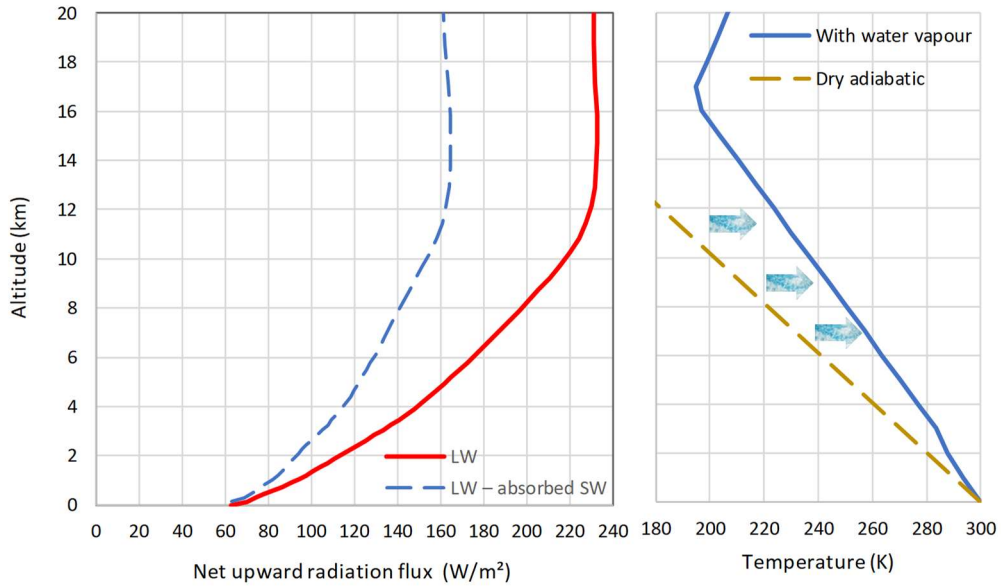

*Figure 25: **(left)** Vertical profile of net LW radiation flux for default conditions and standard tropical atmospheric profile (T = 299.7 K; $[CO_2]$ = 400 ppm; L_D = 369.26 W/m²; L_O = 298.49 W/m²), as calculated by MODTRAN, and its difference from the net SW profile, as calculated by the RRTM Earth's Energy Budget (https://climatemodels.uchicago.edu/rrtm/). **(right)** MODTRAN's standard tropical atmospheric profile of temperature, compared with the dry adiabatic profile (with a gradient of 9.8 K/km); the arrows indicated the heating of the atmosphere due to the latent heat released by condensation of water vapour, accumulated over elevation.*

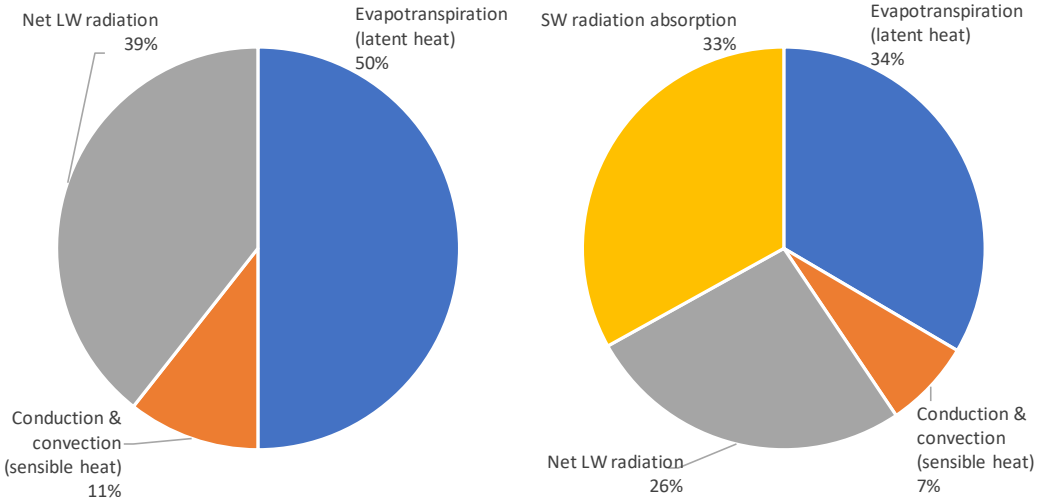

*Figure 26: Contribution of **(left)** the three mechanisms responsible for the cooling of Earth's surface and **(right)** the four mechanisms responsible for the warming of Earth's atmosphere, based on the global energy balance by Trenberth et al. (2009).*

Thus, the biosphere strongly depends on both CO_2 and H_2O. In particular, the presence of water determines the type and extent of ecosystems. In turn, the ecosystems affect climate at large through the carbon and oxygen cycles (where the vast majority of the CO_2 and O_2 emissions are products of life, through respiration and photosynthesis, respectively), and their contribution to the water cycle (transpiration) and in the carbon and energy cycles (photosynthesis). Humans, as part of the biosphere, also interact with water and climate, affecting them and being affected by them. Excluding human influences, the processes of the biosphere determine the vast majority (96%) of CO_2 emissions and partly, in the terrestrial part, the emission of H_2O by the transpiration process. And as Koutsoyiannis and Kundzewicz (2020), Koutsoyiannis et al. (2023) and

Koutsoyiannis (2024b) have shown, it is the relationship between temperature and biosphere that has determined the recent increase in the atmospheric [CO_2].

Considering all these facts, it is stunning that the whole "climate project", including climate modelling, is based on hypotheses and scenarios about human CO_2 emissions.

8. Conclusions

According to the calculations presented here and the depiction of the results in Figure 24, the contribution of CO_2 to the greenhouse effect is 4% – 5%. Human CO_2 emissions represent 4% of the total, which means that the total human contribution to the enhancement of the greenhouse effect is 0.16% to 0.20% —a negligible effect. Irrespective of the origin of the increase of [CO_2] in the last century, its contribution to the greenhouse effect is about 0.5%, below any threshold to make it observable. In contrast, water (including clouds) contributes to the atmospheric greenhouse effect by 87% to 95%. The physical background that makes water, in its different phases, to have the strongest impact on the radiation in the atmosphere and CO_2 to have a weak contribution are explained, with detailed spectroscopic calculations, by Harde (2013, 2014). In addition, 50% of Earth's cooling and atmosphere's warming is due to water (against 39% due to LW radiation, which again is dominated by water—Figure 26).

Common arguments trying to amplify the importance of human carbon emissions are that these accumulate in the atmosphere and that they cause temperature to rise. The former argument is mistaken as the atmosphere does not have any mechanism to separate the incoming CO_2 according to its origin, and to accumulate that part that comes from humans. Also, the second argument has been refuted by showing, using both paleoclimatic proxies and modern instrumental CO_2 and temperature time series, that temperature changes precede CO_2 changes and thus the CO_2 increase cannot be a cause of the temperature increase (Koutsoyiannis and Kundzewicz, 2020; Koutsoyiannis et al., 2022a,b, 2023; Koutsoyiannis, 2024a).

Given these recent developments, the case of the magnified importance of CO_2, and particularly the human emissions thereof, appears to be a historical accident in scientific terms, that was exploited in non-scientific terms. If we return to science, the proper path is to improve hydrology and stochastics to better understand and model climate. For climate is mostly hydrology in terms of its driving physical mechanisms (as articulated here) and mostly stochastics in terms of its proper mathematical representation (as implied by its very definition; cf. Koutsoyiannis 2021, 2023).

Appendix A: Quantification of Greenhouse Gases and of Longwave Radiation

The typical quantification of the abundance of a specific gas X in a gas mixture is given by the simple metric in Equation (1). Another metric is provided by the mass fraction:

$$q_X = \frac{M_X}{M_{\mathrm{TOT}}} = \frac{\rho_X}{\rho_{\mathrm{TOT}}} = \frac{m_X n_X}{m_{\mathrm{TOT}} n_{\mathrm{TOT}}} = \frac{m_X}{m_{\mathrm{TOT}}}[X] \tag{A1}$$

where M_X and M_{TOT} are the mass of the gas and the total mass of all constituents at a specified volume V, ρ_X and ρ_{TOT} are the respective densities ($\rho_X = M_X/V, \rho_{\mathrm{TOT}} = M_{\mathrm{TOT}}/V$), and m_X and m_{TOT} are respective molar masses (in units of mass per mole).

The partial pressure of X, p_X, provides another quantification. Under the ideal gas law and the above equation, we find:

$$p_X = \frac{\rho_X R_* T}{m_X} = \frac{\rho_{\mathrm{TOT}} R_* T}{m_{\mathrm{TOT}}}[X] = p_{\mathrm{TOT}}[X] \tag{A2}$$

where $R_* = 8.314$ J K^{-1} mol^{-1} is the universal gas constant and T is the temperature.

As an example, we consider the atmosphere in standard conditions at mean sea level, i.e., $p \equiv p_{\mathrm{TOT}} = 1013.25$ hPa, T = 15 °C = 288.15 K, $\rho_{\mathrm{TOT}} = 1.225$ kg/m^3. The molar mass of the mixture is $m_{\mathrm{TOT}} = \rho_{\mathrm{TOT}} R_* T / p_{\mathrm{TOT}} = 28.96$ kg/kmol. Considering CO_2 as the specific gas of interest, with molar mass $m_{\mathrm{CO_2}} = 44.01$ kg/kmol, at concentration [CO_2] = 400 ppm, we find that $q_{\mathrm{CO_2}} = (m_X / m_{\mathrm{TOT}})\,[X] = 607.8$ ppm and $p_{\mathrm{CO_2}} = p_{\mathrm{TOT}}[X] = 0.4$ hPa.

For the water vapour in the atmosphere, whose partial pressure by convention is denoted as e_{a}, the concentration varies substantially in space and time. The mass fraction, known as specific humidity, is found, after algebraic manipulations, to be:

$$q = \frac{\varepsilon e_{\mathrm{a}}}{p - (1-\varepsilon) e_{\mathrm{a}}} \tag{A3}$$

where ε is the ratio of the molecular mass of water to that of the mixture of gases in the dry air, i.e., ε = 18.016/28.966 = 0.622. As an example, for a typical value of $e_{\mathrm{a}} = 15$ hPa (see Section 6.2) and standard atmospheric conditions as above, we find q = 9.3‰ and [H_2O] = 14.9‰ (almost 40 times higher than in the above typical example of CO_2).

The water vapour pressure has a thermodynamic upper limit, the saturation water vapour pressure, which is a function of the temperature, T:

$$e(T) = e_0 \exp\left(\frac{\alpha}{R T_0}\left(1 - \frac{T_0}{T}\right)\right)\left(\frac{T_0}{T}\right)^{(c_{\mathrm{L}} - c_p)/R} \tag{A4}$$

where (T_0, e_0) are the coordinates of the triple point of water ($T_0 = 273.16$ K, $e_0 = 6.11657$ hPa), $R := R_*/m$ is the specific gas constant of water vapour ($R = 461.5$ J kg^{-1}K^{-1}), c_p is the specific heat at constant pressure of the water vapour ($c_p = 1884.4$ J kg^{-1} K^{-1}), c_{L} is the specific heat of the liquid water ($c_L = 4219.9$ J kg^{-1} K^{-1}), and $\alpha := \xi R/k = \xi N_{\mathrm{A}}$, with k the Boltzmann's constant, and ξ is the amount of energy required for a molecule to move from the liquid to gaseous phase. The parameter α is related to the latent heat of vaporization, Λ:

$$\alpha = \Lambda_0 + (c_L - c_p) T_0 = \Lambda + (c_L - c_p) T \tag{A5}$$

which is valid for any T, where at the triple point $\Lambda_0 = 2.501 \times 10^6$ J kg^{-1}. By substitution of the various constants in (A4), the following form of the equation is derived (first presented in Koutsoyiannis, 2012):

$$e(T_{\mathrm{a}}) = e_0 \exp\left(24.921\left(1 - \frac{T_0}{T_{\mathrm{a}}}\right)\right)\left(\frac{T_0}{T_{\mathrm{a}}}\right)^{5.06}, \quad T_0 = 273.16\ \mathrm{K}, e_0 = 6.11657\ \mathrm{hPa} \tag{A6}$$

This is a very accurate form of the celebrated Clausius-Clapeyron equation, which was recently rederived in a pure stochastic context by maximizing the entropy, i.e., the uncertainty, in a single water molecule (Koutsoyiannis, 2014, 2023). Notably, the maximization of uncertainty at the microscopic level yields a law that at the macroscopic level is nearly deterministic.

For completeness, we also produce the equation for the saturation water pressure over ice. In this case, it suffices to replace in Equation (A4) the specific heat of liquid water c_{L} with that of ice, c_{I}, and the latent heat of vaporization with that of sublimation, resulting in a constant α_{I} to substitute for α. Following Ambaum (2020), we adopt the value $c_{\mathrm{I}} = 2097$ J kg^{-1} K^{-1} and hence $(c_{\mathrm{I}} - c_p)/R = 0.461$. Optimizing the average relative square error from benchmark values provided by Murphy and Koop (2005; Appendix C) for temperatures 150 to 273.16 K, we find $\alpha_{\mathrm{I}}/RT_0 = 22.812$. Hence, the equation for the saturation water pressure over ice becomes:

$$e_{\mathrm{I}}(T_{\mathrm{a}}) = e_0 \exp\left(22.812\left(1-\frac{T_0}{T_{\mathrm{a}}}\right)\right)\left(\frac{T_0}{T_{\mathrm{a}}}\right)^{0.461}, \quad T_0 = 273.16\ \mathrm{K}, e_0 = 6.11657\ \mathrm{hPa} \tag{A7}$$

A state in which the vapour pressure e_{a} is lower than the saturation pressure $e(T)$ is characterized by the relative humidity:

$$U := \frac{e_a}{e(T)} = \frac{e(T_{\mathrm{d}})}{e(T)} \tag{A8}$$

which serves as a formal definition of both the relative humidity U and the dew point T_{d}.

The longwave radiation flux, L, from a body (measured as energy per unit time and unit area, typically $\mathrm{W/m^2}$) at temperature T (measured in kelvins) is described by the Stefan-Boltzmann law:

$$L = \varepsilon\sigma T^4 \tag{A9}$$

where ε is the emissivity of the body (dimensionless, with $\varepsilon = 1$ for a black body radiator) and σ is the Stefan–Boltzmann constant, a fixed physical constant that is related to other fundamental physical and mathematical constants by

$$\sigma = \frac{2\pi^5 k^4}{15c^2h^3} = 5.67\times10^{-8}\ \mathrm{W\,m^{-2}\,K^{-4}} \tag{A10}$$

Here, π is the ratio of a circle's circumference to its diameter, k is the Boltzmann's constant, h is the Planck's constant, and c is the speed of light in vacuum.

At the Earth's surface, the three LW radiation fluxes of interest are: (a) L_{s}, emitted by the surface (solid or liquid) directed upward, (b) L_{D}, emitted by the atmosphere directed downward, and (c) L_{n}, the net emission. These are given as:

$$L_{\mathrm{s}} = \varepsilon_{\mathrm{s}}\sigma T_{\mathrm{s}}^4, \qquad L_{\mathrm{D}} = \varepsilon_{\mathrm{a}}\sigma T_{\mathrm{a}}^4, \qquad L_{\mathrm{n}} = L_{\mathrm{s}} - L_{\mathrm{D}} \tag{A11}$$

where in the last equation a minor term of reflected upward longwave radiation has been neglected. The temperature of the surface, T_{s}, is well defined and the emissivity ε_{s} is close to 1, usually taken $\varepsilon_{\mathrm{s}} = 0.97$. However, in the atmosphere the temperature varies substantially and the quantity L_{D} is the integration of the radiation process across the entire atmosphere.

The theoretical basis for such integration is described by Goody (1964). Based on this theoretical basis and some assumptions on the atmospheric profiles (nearly standard atmosphere), Brutsaert (1975) was able to express analytically (by integration) the atmospheric radiation L_{a} near the surface for clear sky, and eventually find the effective emissivity as a function of the atmospheric temperature, T_{a}, taken at a level near Earth's surface, and the partial pressure of water vapour, e_{a}, taken at the same level:

$$\varepsilon_{\mathrm{a}} = 1.24\left(\frac{e_{\mathrm{a}}/\mathrm{hPa}}{T_{\mathrm{a}}/\mathrm{K}}\right)^{1/7} \tag{A12}$$

He also proposed a simplification by fixing T_{a} to the average Earth's temperature near the surface, i.e. to 288 K, whence Equation (A12) becomes

$$\varepsilon_{\mathrm{a}} = 0.553(e_{\mathrm{a}}/\mathrm{hPa})^{1/7} \tag{A13}$$

A modification of the Brutsaert's Equation (A12) was proposed by Prata (1996), which is expressed as:

$$\varepsilon_\mathrm{a} = 1 - (1 + w)\exp\left(-\sqrt{1.2 + 3.0w}\right), \qquad w := 46.5\frac{e_\mathrm{a}/\mathrm{hPa}}{T_\mathrm{a}/\mathrm{K}} \tag{A14}$$

with w representing the atmospheric water content (most commonly known with the misnomer 'precipitable water'), found by linear regression on radiosonde data and expressed in cm. We may observe that for $e_\mathrm{a} = 0$, Brutsaert's equation (A12) results in zero emissivity, while Prata's Equation (A14) has a nonzero minimum of $\varepsilon_\mathrm{a} = 0.67$ and, in this way, it describes the non-condensing greenhouse gas contribution to emissivity.

Decades earlier, empirical relationships of the same type (and with nonzero minimum) had been proposed, among which the earliest, most celebrated and most popular is that by Brunt (1932, 1934):

$$\varepsilon_\mathrm{a} = 0.526 + 0.065\sqrt{e_\mathrm{a}/\mathrm{hPa}} \tag{A15}$$

Furthermore, Brunt (1954), using several data sets, fitted the mathematical expression

$$\varepsilon_\mathrm{a} = a + b\sqrt{e_\mathrm{a}/\mathrm{hPa}} \tag{A16}$$

and found different values of the coefficients a and b for each data set. An average fitting for all cases is:

$$\varepsilon_\mathrm{a} = 0.44 + 0.08\sqrt{e_\mathrm{a}/\mathrm{hPa}} \tag{A17}$$

With Penman's (1948) celebrated paper on evaporation, this quantification became an essential part of hydrological practice in calculating evaporation. Essentially, Penman used Brunt's Equation (A17), also assuming that $T_\mathrm{s} = T_\mathrm{a}$ and $\varepsilon_\mathrm{s} = 1$. Indeed, it can be readily seen that Penman's (1948) original equation (numbered (7) in his paper), which for clear sky conditions reads

$$\frac{L_\mathrm{n}}{\sigma T_\mathrm{a}^4} = 0.56 - 0.08\sqrt{e_\mathrm{a}/\mathrm{hPa}} \tag{A18}$$

is a direct result of Brunt's Equation (A17) and these assumptions, even though Penman (1948) did not make a distinction between the two components seen in Equation (A11).

Later Penman's equation was complemented by Monteith (1965) to estimate the water requirements of crops, thus shaping what has been called the Penman-Monteith method. This became a standard of the Food and Industry Organization (FAO), initially in the version by Doorenbos and Pruitt (1977) and later in the version by Allen et al. (1998). In both versions, the downwelling longwave radiation (again assuming that $T_\mathrm{s} = T_\mathrm{a}$ and $\varepsilon_\mathrm{s} = 1$) is calculated as

$$\varepsilon_\mathrm{a} = 0.66 + 0.044\sqrt{e_\mathrm{a}/\mathrm{hPa}} \tag{A19}$$

Subsequently, a large variety of similar empirical relationships were proposed by several researchers, critical reviews of which can be found in Carmona et al. (2014), Guo et al. (2019) and Wong et al. (2023), to mention the most recent.

Appendix B: MODTRAN locality profiles

MODTRAN implements five different locality profiles, which differ in their temperature, H_2O and O_3 profiles. The profiles most relevant to this study are depicted Figure A1[12]. By comparison with zonal temperature distributions analogous to that in Figure 4, but separately for summer and

[12] Additional information can be found in "The 6 model atmospheres in MODTRAN", accessed 19 February 2024, http://modtran.spectral.com/static/modtran6/html/help_atmosphere_model.html

winter, we infer that the tropical profile corresponds roughly to the equator, but is representative for the entire torrid zone (between 23.4° N or S), the midlatitude profile corresponds to a latitude at about 45° N or S, and the subarctic profile at about the latitude of polar circles (66.6° N or S). In addition, MODTRAN includes the 1976 U.S. Standard Atmosphere temperature profile, which provides an effective median for the set of locality profiles; this was not used in this study.

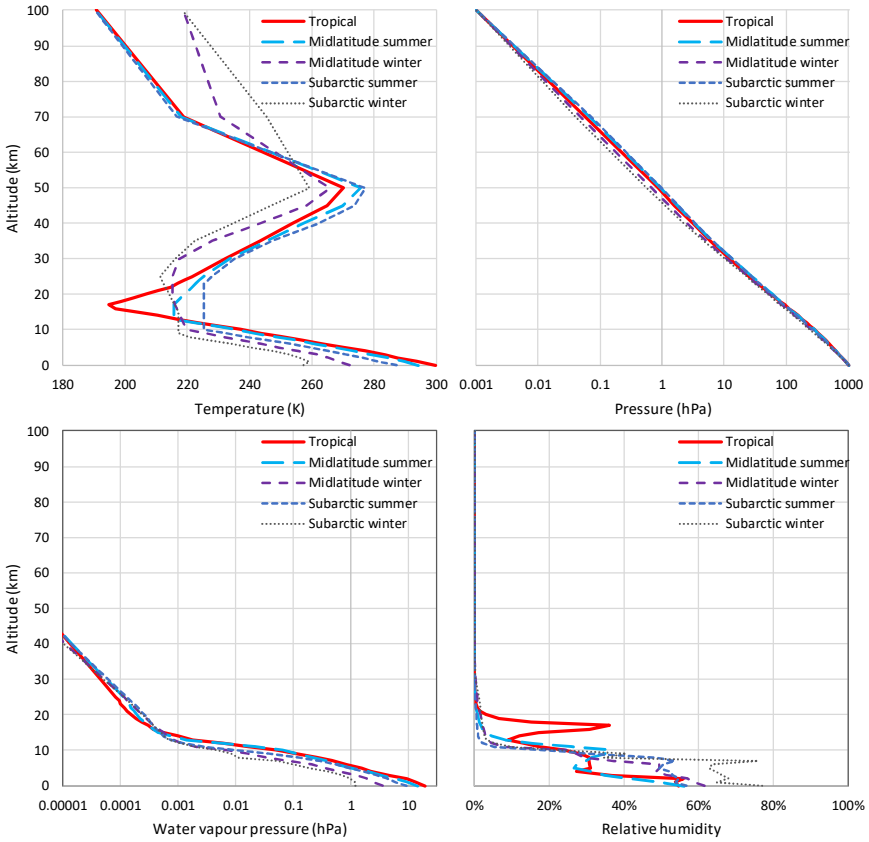

Figure A1: Standard profiles of the indicated variables used in MODTRAN.

Figure A2 depicts a characteristic example of MODTRAN output profiles upward, downward and net LW radiation flux across the atmosphere for the tropical profile and default settings. Above the level of 20 km, the downward LW radiation is very low and the upward LW radiation, total or net, is almost constant.

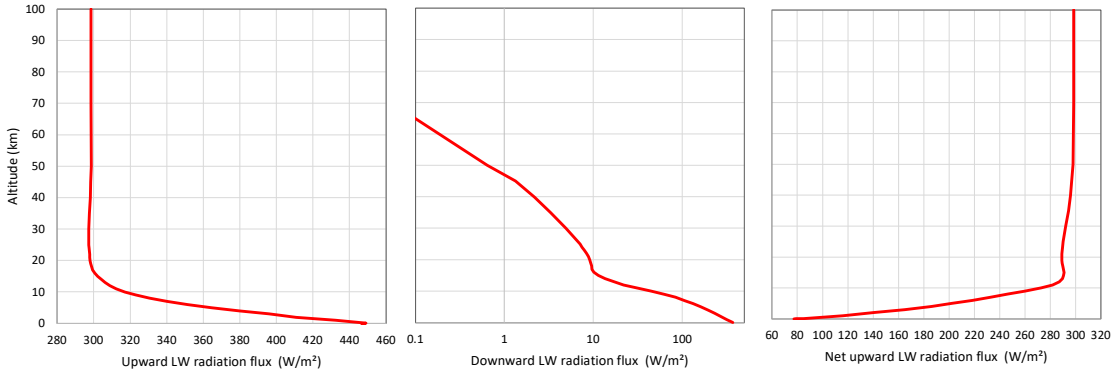

Figure A2: Profiles of the indicated variables resulting from MODTRAN for the tropical profile and default settings.

Supplementary Information

Earlier review comments from other journals, which did not accept the paper, are posted as Supplementary Information, along with the replies to comments and exchanges with editorial offices (see: https://scienceofclimatechange.org/wp-content/uploads/Dog_and_Tail_SI_ocred.pdf).

Funding

This research received no funding but was conducted out of scientific curiosity.

Guest-Editor: H. Harde; Reviewers: anonymous.

Data Availability Statement

This research uses no new data. The data sets used have been retrieved from the sources described in detail in the text.

Conflicts of Interest

I declare that I have no competing financial interests or personal relationships that could have appeared to influence the work reported in this paper.

Acknowledgements

I am grateful to the colleagues and organizations who have put their huge data sets online along with the data processing and computational systems they have developed. These include the CERES data, the ERA5 and NCEP/NCAR Reanalyses, the CLIMEXP data and software platform, and the MODTRAN and RRTM software systems.

I thank the Editor Hermann Harde and an anonymous reviewer for their comments and the favourable assessment of my paper.

I thank Richard Cina for his constructive suggestions on the first draft of the paper and Ariane Loening for editorial corrections. I am grateful to William Happer for his encouragement and his helpful comments on an earlier draft of the paper.

I thank an anonymous reviewer of a predecessor paper (Koutsoyiannis and Vournas, 2024), whose critical comments made it necessary to delve into the topic examined in the present paper. The brief reply to those review comments was not included in the predecessor paper in order not to distract its focus. Yet it constituted the springboard to produce this paper.

I acknowledge three rejections of this paper. The first was by *Hydrological Sciences Journal* with a unanimous decision of all five editors (Attilio Castellarin, Stacey Archfield, Aldo Fiori, Riddhi Singh, Konstantinos Soulis) without review. The second by the MDPI *Hydrology* by a decision by the Editor-in-Chief Ezio Todini, based on a unanimous recommendation for rejection by four anonymous reviewers. The third was by an anonymous editor of *Hydroecology and Engineering*. The latter journal's staff invited the paper, and before its submission (but after its posting as a preprint) informed me that they "believe in the importance of diverse perspectives in scientific discourse". After its submission, they initially accepted it with major revisions. After I addressed or rebutted the review comments, they eventually rejected it. As I believe that the prehistory of rejections is very informative and confirms the assertions I made in the Introduction, I have compiled all the review materials and editorial exchanges into a lengthy document published as Supplementary Information.

References

Allen RG, Pereira LS, Raes D, Smith M. 1998: *Crop Evapotranspiration – Guidelines for Computing Crop Water Requirements*. FAO Irrigation and Drainage Paper 56, Food and Agriculture Organization of the United Nations, Rome, https://www.fao.org/3/X0490E/x0490e00.htm

(accessed 25 August 2023).

Ambaum MHP, 2020: *Accurate, simple equation for saturated vapor pressure over water and ice,* Q. J. R. Meteorol. Soc., 146, 4252–4258. doi:10.1002/qj.3899

Berk A, Bernstein LS, Robertson DC, 1987: *MODTRAN: A Moderate Resolution Model for LOWTRAN*, Scientific Report No. 1; Air Force Geophysics Laboratory, Air Force Systems Command, United States Air Force: Hanscom Air Force Base, Massachusetts, USA, https://apps.dtic.mil/sti/pdfs/ADA185384.pdf (accessed 19 February 2024).

Berk A, Acharya PK, Bernstein LS, Anderson GP, Lewis P, Chetwynd JH, Hoke ML, 2008: *Band model method for modeling atmospheric propagation at arbitrarily fine spectral resolution*, U.S. Patent #7433806.

Berk A, Conforti P, Kennett R, Perkins T, Hawes F, van den Bosch J. 2014: *MODTRAN6: A Major Upgrade of the MODTRAN Radiative Transfer Code*, Proc. SPIE, 9088, 90880H. doi:10.1117/12.2050433.

Biermann F, Abbott K, Andresen S, Bäckstrand K, Bernstein S, Betsill MM, Bulkeley H, Cashore B, Clapp J, Folke C, et al., 2012: *Navigating the anthropocene: improving earth system governance*, Science, 335, 1306–1307.

Brooks FA, 1952: *Atmospheric radiation and its reflection from the ground*, J. Atmos. Sci., 9, 41–52.

Brunt D. 1932: *Notes on radiation in the atmosphere*, I. Q. J. R. Meteorol. Soc., 58, 389–420.

Brunt D, 1934: *Physical and Dynamical Meteorology*, Cambridge University Press: Cambridge, UK,; 411 pp., https://archive.org/details/in.ernet.dli.2015.215092 (accessed 25 August 2023).

Brutsaert W, 1975: *On a derivable formula for long-wave radiation from clear skies*, Water Resour. Res., 11, 742–744.

Brutsaert W, 1991: *Evaporation into the Atmosphere: Theory, History and Applications*, Springer Science & Business Media: Dordrecht, Netherlands,; 299 pp.

Carmona F, Rivas R, Caselles V, 2014: *Estimation of daytime downward longwave radiation under clear and cloudy skies conditions over a sub-humid region*, Theor. Appl. Climatol., 115, 281–295.

CERES, 2021: *CERES_EBAF_Ed4.1 Data Quality Summary*, Version 3 (Updated 12/9/2021). (accessed 15 February 2024).
https://ceres.larc.nasa.gov/documents/DQ_summaries/CERES_EBAF_Ed4.1_DQS.pdf

CERES, 2021: *CERES_SSF1deg_Hour/Day/Month_Ed4A Data Quality Summary*, Version 2 (Updated 8/4/2023), (accessed 15 February 2024).
https://ceres.larc.nasa.gov/documents/DQ_summaries/CERES_SSF1deg_Ed4A_DQS.pdf

Chen X, Chen T, He B, Liu S, Zhou S, Shi T, 2024: *The global greening continues despite increased drought stress since 2000*, Glob. Ecol. Conserv., 49, e02791.

Clark R, 2013a: *A dynamic, coupled thermal reservoir approach to atmospheric energy transfer Part I: Concepts*, Energy and Environment, 24 (3-4), 319-340, doi: 10.1260/0958-305X.24.3-4.319.

Clark R, 2013b: *A dynamic, coupled thermal reservoir approach to atmospheric energy transfer Part II: Applications*, Energy and Environment, 24 (3-4), 341-359, doi: 10.1260/0958-305X.24.3-4.341.

Clark R, 2024: *A Nobel Prize for Climate Modeling*, Science of Climate Change, 4 (1), 1-73, doi: 10.53234/scc202404/17.

de Lange CA, Ferguson JD, Happer W, van Wijngaarden WA, 2022: *Nitrous oxide and climate*,

arXiv, arXiv:2211.15780, https://arxiv.org/abs/2211.15780 (accessed 25 August 2023).

Dingman SL, 1994: *Physical Hydrology*, Prentice Hall, Upper Saddle River, New Jersey, USA.

Doelling DR, Loeb NG, Keyes DF, Nordeen ML, Morstad D, Nguyen, C.; Wielicki, B.A.; Young, D.F.; Sun, M, 2013: *Geostationary enhanced temporal interpolation for CERES flux products*, J. Atmos. Ocean. Technol., 30, 1072–1090, doi: 10.1175/JTECH-D-12-00136.1.

Doelling DR, Sun M, Nguyen LT, Nordeen ML, Haney CO, Keyes DF, Mlynczak PE, 2016: *Advances in geostationary-derived longwave fluxes for the CERES synoptic (SYN1deg) product*, J. Atmos. Ocean. Technol., 33, 503–521, doi: 10.1175/JTECH-D-15-0147.1.

Dooge JC, 1986: *Looking for hydrologic laws*, Water Resour. Res., 22, 46S–58S.

Doorenbos J, Pruitt WO, 1977: *Guidelines for Predicting Crop Water Requirements*, FAO Irrigation and Drainage Paper 24, Food and Agriculture Organization of the United Nations, Rome, https://dokumen.tips/download/link/fao-irrigation-and-drainage-paper-24.html (accessed 25 August 2023).

Eschenbach W, 2010: *The thunderstorm thermostat hypothesis*. Energy and Environment, 21 (4), 201-200, doi: 10.1260/0958-305X.21.4.201.

Essex C, McKitrick R, Andresen B, 2007: *Does a global temperature exist?* J. Non-Equilibrium Thermodynamics, 32 (1), 1-27, doi: 10.1515/JNETDY.2007.001.

Gerhart LM, Ward JK, 2010: *Plant responses to low [CO2] of the past*, New Phytol., 188, 674–695.

Goody RM, 1964: *Atmospheric Radiation*, Oxford University Press, Oxford, UK; New York, NY, USA, 436 pp.

Guo Y, Cheng J, Liang S, 2019: *Comprehensive assessment of parameterization methods for estimating clear-sky surface downward longwave radiation*, Theor. Appl. Climatol., 135, 1045–1058.

Harde H, 2013: *Radiation and heat transfer in the atmosphere: a comprehensive approach on a molecular basis*, International Journal of Atmospheric Sciences, 2013(1), http://dx.doi.org/10.1155/2013/503727.

Harde H, 2014: *Advanced two-layer climate model for the assessment of global warming by CO2*, Open Journal of Atmospheric and Climate Change, 1 (3), https://web.archive.org/web/20160429061756/ http://www.scipublish.com/journals/ACC/papers/download/3001-846.pdf.

Harde H, 2017: *Radiation transfer calculations and assessment of global warming by CO2*, Int. J. Atmos. Sci., 9251034, 1-30, https://doi.org/10.1155/2017/9251034.

Harde H, 2022: *How much CO_2 and the sun contribute to global warming: Comparison of simulated temperature trends with last century observations,* Science of Climate Change, 2(2), 105-133, https://doi.org/10.53234/scc202206/10.

Howe N, 2020: *'Stick to the science': when science gets political,* Nature, doi: 10.1038/d41586-020-03067-w.

Jacobs JD, 1978: *Radiation climate of Broughton Island*, In Energy Budget Studies in Relation to Fast-Ice Breakup Processes in Davis Strait, Barry RG, Jacobs JD, Eds.; Inst. of Arctic and Alp. Res. Occas. Paper no. 26; University of Colorado: Boulder, USA, 105–120, https://www.colorado.edu/instaar/node/963 (accessed 13 February 2024).

Kato S, Rose FG, Rutan DA, Thorsen TE, Loeb NG, Doelling DR, Huang X, Smith WL, Su W, Ham S-H, 2018: *Surface irradiances of Edition 4.0 Clouds and the Earth's Radiant Energy System (CERES) Energy Balanced and Filled (EBAF) data product*, J. Clim., 31, 4501–4527, doi: 10.1175/JCLI-D-17-0523.1.

Koll, DDB, Cronin, TW, 2018: *Earth's outgoing longwave radiation linear due to H_2O greenhouse effect*, PNAS, 115 (41), 10293-10298, doi: 10.1073/pnas.1809868115.

Koutsoyiannis D, 2012: *Clausius-Clapeyron equation and saturation vapor pressure: simple theory reconciled with practice*, Eur. J. Phys., 33, 295–305. doi:10.1088/0143-0807/33/2/295

Koutsoyiannis D, 2014: *Entropy: from thermodynamics to hydrology*, Entropy, 16, 1287–1314, doi: 10.3390/e16031287.

Koutsoyiannis D, 2020a: *Revisiting the global hydrological cycle: is it intensifying?*, Hydrol. Earth Syst. Sci., 24, 3899–3932, doi: 10.5194/hess-24-3899-2020.

Koutsoyiannis D, 2020b: *Rebuttal to review comments on "Revisiting global hydrological cycle: Is it intensifying?"*, Hydrol. Earth Syst. Sci. Discuss., doi: 10.5194/hess-2020-120-AC1, https://hess.copernicus.org/preprints/hess-2020-120/hess-2020-120-AC1-supplement.pdf (accessed 2022-02-13).

Koutsoyiannis D, 2021: *Rethinking climate, climate change, and their relationship with water*, Water, 13, 849, doi: 10.3390/w13060849.

Koutsoyiannis D, 2023: *Stochastics of Hydroclimatic Extremes – A Cool Look at Risk*, Edition 3, Kallipos Open Academic Editions, Athens, 391 pp, doi: 10.57713/kallipos-1.

Koutsoyiannis D, 2024a: *Stochastic assessment of temperature – CO_2 causal relationship in climate from the Phanerozoic through modern times,* Mathematical Biosciences and Engineering, 21 (7), 6560–6602, doi: 10.3934/mbe.2024287.

Koutsoyiannis D, 2024b: *Refined reservoir routing (RRR) and its application to atmospheric carbon dioxide balance*, Water, 16 (17), 2402, doi: 10.3390/w16172402.

Koutsoyiannis D, Kundzewicz ZW, 2020: *Atmospheric temperature and CO_2: Hen-or-egg causality?*, Sci, 2, 72, doi:10.3390/sci2040077.

Koutsoyiannis D, Mamassis N, 2021: *From mythology to science: the development of scientific hydrological concepts in the Greek antiquity and its relevance to modern hydrology*, Hydrology and Earth System Sciences, 25, 2419–2444, doi: 10.5194/hess-25-2419-2021.

Koutsoyiannis D, Onof C, Christofides A, Kundzewicz ZW, 2022a: *Revisiting causality using stochastics: 1. Theory*, Proc. R. Soc. A, 478, 20210835, doi: 10.1098/rspa.2021.0835.

Koutsoyiannis D, Onof C, Christofides A, Kundzewicz ZW, 2022b: *Revisiting causality using stochastics: 2. Applications*, Proc. R. Soc. A, 478, 20210836, doi: 10.1098/rspa.2021.0836.

Koutsoyiannis D, Onof C, Kundzewicz ZW, Christofides A, 2023: *On hens, eggs, temperatures and CO2: Causal links in earth's atmosphere*, Sci, 5, 35, doi:10.3390/sci5030035.

Koutsoyiannis D., Vournas C, 2024: *Revisiting the greenhouse effect—a hydrological perspective*, Hydrol. Sci. J., 69, 151–164, doi: 10.1080/02626667.2023.2287047.

Lacis AA, Schmidt GA, Rind D, Ruedy RA, 2010: *Atmospheric CO2: Principal control knob governing Earth's temperature*, Science, 330, 356–359.

Lhomme JP, Vacher JJ, Rocheteau A, 2007: *Estimating downward long-wave radiation on the Andean Altiplano*, Agric. For. Meteorol., 145, 139–148.

Li X, Peachey B, Maeda N, 2024: *Global warming and anthropogenic emissions of water vapor*, Langmuir, 40 (14), 7701-7709.

Loeb NG, Doelling DR, Wang H, Su W, Nguyen C, Corbett JG, Liang L, Mitrescu C, Rose FG, Kato S, 2018: *Clouds and the Earth's Radiant Energy System (CERES) Energy Balanced and Filled (EBAF) Top-of-Atmosphere (TOA) Edition-4.0 Data Product*, J. Clim., 31, 895–918, doi: 10.1175/JCLI-D-17-0208.1.

Lupia A, 2023: *Political endorsements can affect scientific credibility*, Nature, 615, 590-591, doi:

10.1038/d41586-023-00799-3.

Masson-Delmotte V, Zhai P, Pirani A, Connors SL, Péan C, Berger S, Caud N, Chen Y, Goldfarb L, Gomis MI, et al. (Eds.), 2021: IPCC, *Climate Change 2021: The Physical Science Basis*, Contribution of Working Group I to the Sixth Assessment Report of the Intergovernmental Panel on Climate Change, Cambridge University Press, Cambridge, UK; New York, NY, USA, 2391 pp.

Miskolczi F, 2023: *Greenhouse gas theories and observed radiative properties of the Earth's atmosphere*, Sci. Clim. Change, 3, 232–289, doi: 10.53234/scc202304/05.

Monteith JL, 1965: *Evaporation and environment*, Symposia of the Society for Experimental Biology, 19, 205–234.

Murphy, D.M.; Koop, T, 2005: *Review of the vapor pressures of ice and supercooled water for atmospheric applications*, Q. J. R. Meteorol. Soc., 131, 1539–1565.

Nature Editorial, 2023: S*hould Nature endorse political candidates? Yes — when the occasion demands it*, Nature, 615, 561, doi: 10.1038/d41586-023-00789-5.

Nikolov N., Zeller K, 2017: *New insights on the physical nature of the atmospheric greenhouse effect deduced from an empirical planetary temperature*, Model. Environ. Pollut. Climate Change, 1, 1000112, doi: 10.4172/2573-458X.1000112.

Peachey B, 2006: *Mitigating human enhanced water emission impacts on climate change*, In 2006 IEEE EIC Climate Change Conference, doi: 10.1109/EICCCC.2006.277221.

Penman HL, 1948: *Natural evaporation from open water, bare soil and grass*, Proc. R. Soc. Lond. A Math. Phys. Eng. Sci., 193, 120–145.

Philipona R, Kräuchi A, Brocard E, 2012: *Solar and thermal radiation profiles and radiative forcing measured through the atmosphere*, Geophys. Res. Lett., 39, L13806, doi: 10.1029/2012GL052087.

Prata AJ, 1996: *A new long-wave formula for estimating downward clear-sky radiation at the surface*, Q. J. R. Meteorol. Soc., 122, 1127–1151.

Salby ML, 2012: *Physics of the Atmosphere and Climate*, Cambridge University Press, New York, NY, USA.

Schmidt GA, Ruedy RA, Miller RL, Lacis AA, 2010: *Attribution of the present-day total greenhouse effect*, J. Geophys. Res., 115, D20106.

Searle JR, 1984: *Minds, Brains and Science*, Harvard University Press: Cambridge, MA, USA.

Sherwood SC, Dixit V, Salomez C, 2018: *The global warming potential of near-surface emitted water vapor*, Environmental Research Letters, 13 (10), 104006.

Tegos A, Malamos, N, Koutsoyiannis D, 2015: A parsimonious regional parametric evapotranspiration model based on a simplification of the Penman–Monteith formula, Journal of Hydrology, 524, 708-717, doi: 10.1016/j.jhydrol.2015.03.024.

Trenberth KE, Fasullo JT, Kiehl J, 2009: *Earth's global energy budget*, Bull. Am. Meteorol. Soc., 90, 311–324, doi:10.1175/2008BAMS2634.1.

UNESCO (United Nations Educational, Scientific and Cultural Organization) 1964: *Final Report, International Hydrological Decade, Intergovernmental Meeting of Experts*, UNESCO/NS/188; UNESCO House: Paris, https://unesdoc.unesco.org/images/0001/000170/017099EB.pdf (accessed 15 February 2024).

van Wijngaarden WA, Happer W, 2020: *Dependence of Earth's thermal radiation on five most abundant greenhouse gases*, arXiv, arXiv:2006.03098, https://arxiv.org/abs/2006.03098 (accessed 25 August 2023).

Veizer J, 2005: *Celestial climate driver: a perspective from four billion years of the carbon cycle*,

Geoscience Canada, 32, 13-28.

Veizer J, 2011: *The role of water in the fate of carbon dioxide: implications for the climate system*, In 43rd Int. Seminar on Nuclear War and Planetary Emergencies, Ragaini R (Ed.). World Scientific, 313-327, doi: 10.1142/8232.

Veizer J, 2012: *Planetary temperatures/climate across geological time scales*, In International Seminar on Nuclear War and Planetary Emergencies—44th Session: The Role of Science in the Third Millennium, 287-288.

Wielicki BA, Barkstrom BR, Harrison EF, Lee III RB, Smith GL, Cooper JE, 1996: *Clouds and the Earth's Radiant Energy System (CERES): An Earth observing system experiment*, Bull. Amer. Meteor. Soc., 77, 853-868, doi: 10.1175/1520-0477(1996)077<0853:CATERE>2.0.CO;2

Wong RY, Tso CY, Jeong SY, Fu SC, Chao CY, 2023: *Critical sky temperatures for passive radiative cooling*, Renewable Energy, 211, 214-226.

Zhang FJ, 2023: *Political endorsement by Nature and trust in scientific expertise during COVID-19*, Nature Human Behaviour, 7(5), 696-706, doi: 10.1038/s41562-023-01537-5.

OPEN ACCESS

Klimarealistene
Vollsveien 109
1358 Jar, Norway
ISSN: 2703-9072

Correspondence:
frans.schrijver@gmail.com

Vol. 4.2 (2024)
pp. 79-88

Impact of global greening on the natural atmospheric CO_2 level

Frans J. Schrijver

Independent Scientist, Hattem, Netherlands

Abstract

In this study we investigate the impact of greening on the Earth in terms of gross primary production (GPP) on the natural atmospheric CO_2 level. The total mass of CO_2 in the atmosphere is equal to the yearly amount of CO_2 that leaves the atmosphere (down flux), multiplied by the average time CO_2 remains in the atmosphere (residence time). The biological processes of photosynthesis and respiration are by far the most important components of the fluxes to and from the atmosphere. Since the preindustrial period the down flux has increased by 29% and the residence time by 16%. Together they fully explain the recent CO_2 rise, without assuming different behaviors for human-generated CO_2 compared to natural CO_2 and without the need for an ad-hoc model with multiple residence times. Based on the changes in the biosphere under the influence of higher temperatures, the present CO_2 level can be regarded as a natural level, so much larger than the assumed 280 ppmv. The current total GPP is probably not extraordinary, which makes it unlikely that the ice core records of Antarctica provide an accurate representation of the historical levels.

Keywords: CO_2, atmosphere, greening, GPP, climate

Submitted 2024-10-01, Accepted 2024-11-15, https://doi.org/10.53234/scc202411/02

1. Introduction

Global greening refers to the observed increase in the amount of green vegetation, such as plants and trees, across the planet. Long-term satellite records revealed a significant global greening of vegetated areas since the 1980s. In this contribution we refer to greening in terms of the increase in gross primary production (GPP), the rate of carbon fixation by photosynthesis. Global terrestrial gross primary production has gone up by more than 30% since 1900 (Haverd *et al.*, 2020; Lai *et al.*, 2024). Multiple studies have identified the growing atmospheric CO_2 concentration and climate warming as important drivers of this greening, with other factors being notable at the regional scale (Zhu *et al.*, 2016; Piao *et al.*, 2019; Chen *et al.*, 2022). A similar effect has been observed in the oceans, where increased levels of dissolved CO_2 lead to more photosynthesis by phytoplankton (Riebesell *et al.*, 2007).

Biological processes, particularly photosynthesis and respiration, have a dominant effect on the fluxes to and from the atmosphere. The impact of global greening on the atmospheric CO_2 level is therefore crucial in understanding the global carbon cycle and the causes of the CO_2 rise as measured in the last 65 years. Understanding the possible mitigating effects of forestation on the CO_2 level is also important. The CO_2 fertilization has been largely considered as an enhanced land carbon sink. By storing large amounts of carbon in the form of biomass, vegetation sequesters

carbon. Therefore, an increase in vegetation is generally considered as a process in which CO_2 greenhouse gas is removed from the atmosphere, partly mitigating human emissions.

It is true that especially new vegetation is a net sink, however this does not mean that an increased level of vegetation automatically leads to a lower CO_2 concentration. For the impact on the atmospheric CO_2 concentration it is not sufficient to look at the short-term effect of a single flux. One also has to consider the impact of this change on the longer term and on other fluxes in the carbon cycle. We believe that the current way in which the global carbon budget is determined is not suitable for properly assessing the impact of changes in the fluxes.

The conventional approach to examining the carbon cycle and explaining changes in atmospheric CO_2 levels is based on bookkeeping. Typically, the current CO_2 concentration is accounted for by aggregating the annual differences between the amount of CO_2 entering and leaving the atmosphere over an extended period of time, starting in 1750. This is, for example, the method used in the annual determination of the Global Carbon Budget (Friedlingstein *et al.*, 2023). The CO_2 level change in each year is explained by summing the human emissions from different sources and natural emissions from land and oceans, and subtracting natural absorptions from land and oceans. The conclusions are however colored by the all-determining assumption that without human perturbation, the natural inflows and outflows are always in perfect balance with each other. This leads to the conclusion that every year roughly half of the human-produced CO_2 accumulates in the atmosphere, while the other half is absorbed by the land and oceans.

A major problem with this approach is the high degree of uncertainty and inaccuracy of both the natural flows to and from the atmosphere and the size of the carbon reservoirs in the oceans and on land. In the calculation of the Global Carbon Budget only the increase in atmospheric concentration and annual human emissions are accurately known. The natural flows to and from the atmosphere are not directly related; rather, they have different causes and occur at different times and/or places. Most of the CO_2 is transformed into other carbon compounds on land and in the sea through complex and chaotic processes. The amount of CO_2 stored in the oceans and on land is so large that relatively little CO_2 uptake or release cannot be measured. An annual change of the carbon mass in the oceans of only 0.013% is enough to explain the full 5 PgC/yr increase of the CO_2 level. A small imbalance, even for many years, is quite possible and would have no noticeable impact on the subsurface reservoirs. Thus, we cannot measure the natural fluxes with sufficient precision, nor can we assume that influx and outflux are in balance. Summarizing the results over a long period of time makes the problem even worse. The inaccurate bookkeeping method makes it impossible to draw conclusions about the impact of human emissions on the increase of CO_2 in the atmosphere.

2. Method

In this study we investigated the causes of the increase in CO_2 concentration by examining the changes in fluxes and residence times since the preindustrial period. The mass in the atmosphere is equal to the total yearly absorption (down flux), multiplied by the average time that the CO_2 remains in the atmosphere (residence time). Changes in the down flux and residence time are therefore directly related to changes in the atmospheric concentration. An explanation of why both the down flux and the residence time have increased could provide a better understanding of the recent changes in the CO_2 concentration and more generally in the global carbon cycle.

Here we assume that CO_2 in the atmosphere behaves like a first-order container system, where the rate of outflow is proportional to the mass within the container. This behavior is true for all gases in the atmosphere, including CO_2; however, the IPCC and many others make an exception for excess CO_2, meaning CO_2 that is not part of the normal natural cycle, but has been added to the system by humans. While the residence time of natural CO_2 is approximately 4 years, a much longer residence time is used for human CO_2: *'The removal of human-emitted CO_2 from the atmosphere by natural processes will take a few hundred thousand years (high confidence)'*

(IPCC, 2015, p. 469). This leads to the conclusion that approximately 45% of human CO_2 accumulates in the atmosphere.

Several studies have indicated that this exception is illogical and incorrect and that the use of multiple residence times makes no sense, as the atmosphere can be regarded as a well-mixed container and that nature cannot distinguish between different sorts of CO_2 based on their origin. Fluctuations in the natural cycle due to seasonal effects or volcanic eruptions are often greater than the amount of excess CO_2 from human emissions in one year, which makes it impossible to conclude whether the CO_2 is 'excess' or 'natural' (Segelstad, 1998; Harde, 2017, 2019; Salby and Harde, 2021). In this study, we will not directly address this exception or the use of multiple residence times for excess CO_2, as our analyses are at first based solely on natural changes in CO_2 fluxes with no excess CO_2 involved. The description of the atmospheric carbon cycle with only natural flows as a first order system is, as far as we know, undisputed.

For our analysis, two processes are important: first, the buffering capacity of the oceans. The atmosphere, which acts as a container for CO_2, interacts with the land and oceans, which hold a significantly larger amount of carbon. Oceans are by far the largest carbon stock. The oceans contain far more carbon than would be predicted solely from gas solubility. Based on Henry's Law, CO_2 in the atmosphere is in equilibrium with dissolved CO_2 in the water. The vast majority of dissolved CO_2 reacts with water to form carbonic acid, which breaks down into bicarbonate and carbonate ions (and other carbonate complexes), that cannot exchange with the atmosphere. As the carbon mass in the oceans (Dissolved Inorganic Carbon) is approximately 50 times greater than that in the atmosphere, this set of equilibrium reactions enables the oceans to buffer changes in the atmospheric CO_2 concentration. A perturbation such as a single emission or absorption will affect only the short-term CO_2 concentration. With a relatively short residence time of approximately four years, most of the perturbation is eventually neutralized by this process (Stallinga, 2023).

A second important element for understanding the impact of global greening on the atmospheric CO_2 level, is the fact that the large fluxes to and from the atmosphere are primarily the result of interactions with the terrestrial and oceanic biospheres, based on photosynthesis and respiration. Due to the direct influence of the sun on the process of photosynthesis, the net in- and out-fluxes exhibit great diurnal and annual fluctuations. At night, respiration-related emissions predominate, but during the day, a significantly greater photosynthetic flux leads to net absorption. Additionally, the seasonal cycle of carbon is influenced by the growth and decay of vegetation. In spring and summer photosynthesis predominates, during which CO_2 is absorbed from the atmosphere. During fall and winter much of the absorbed CO_2 is released back into the atmosphere. At a constant residence time the atmospheric CO_2 level is proportional to the magnitude of the down flux. Alterations in sunlight-driven biological fluxes are, therefore, critical to the increased CO_2 levels.

Given that we are interested in the impact of greening over a period of decades and centuries, we can exclude processes with a much longer time frame, such as exchanges with sediments and rocks and the Earth's interior.

3. The impact of greening

The greening of the Earth leads to an increase in natural absorption: more trees/phytoplankton means more photosynthesis and thus more absorption. The increased absorption is reflected in Figure 1, which shows the most important atmospheric CO_2 levels and fluxes from 1750 (IPCC, 2021) and 2022 (Friedlingstein *et al.*, 2023). The atmospheric residence time for each year was calculated by dividing the CO_2 mass by the total absorption in that year. The uncertainty of the natural fluxes and residence times is estimated at ±20% (IPCC, 2015). The concentration in the atmosphere has increased by approximately 50% since 1750 (blue background). This growth is a combination, on the one hand, of the 29% increase in absorption from 167 to 216 PgC/year (green

background) and, on the other hand, of the 16% increase in the residence time from 3.5 years to 4.1 years (orange background). Column I shows the original data. Column II shows the impact on the CO_2 level, only based on the increased fluxes. Column III shows the impact if only the residence time would have changed, so without global greening.

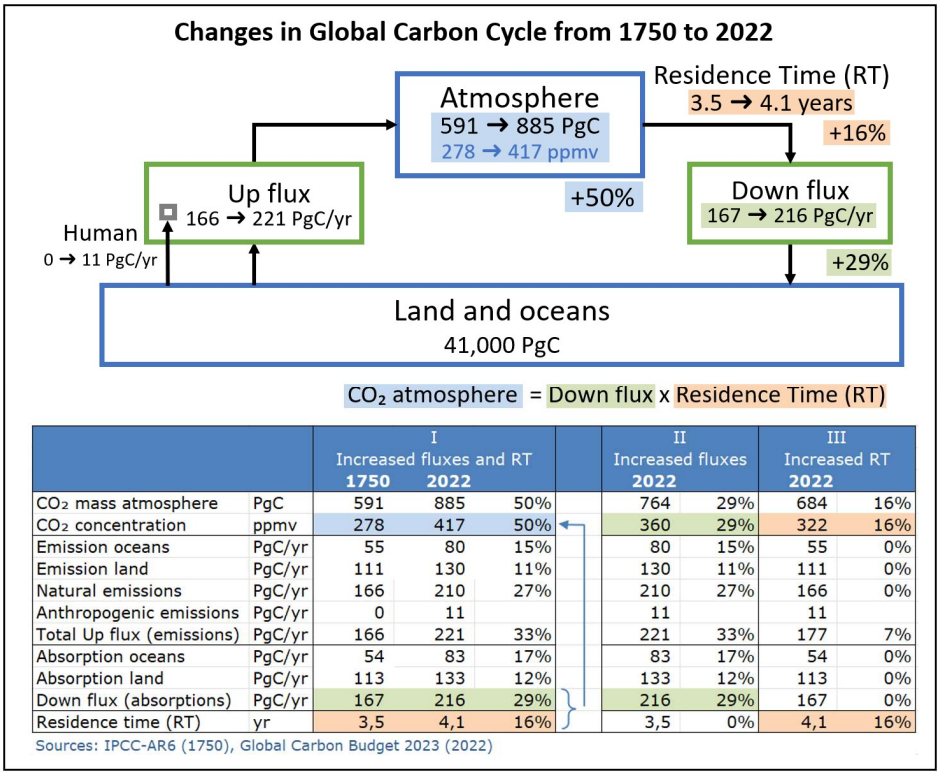

		I Increased fluxes and RT 1750	2022			II Increased fluxes 2022		III Increased RT 2022	
CO_2 mass atmosphere	PgC	591	885	50%		764	29%	684	16%
CO_2 concentration	ppmv	278	417	50%		360	29%	322	16%
Emission oceans	PgC/yr	55	80	15%		80	15%	55	0%
Emission land	PgC/yr	111	130	11%		130	11%	111	0%
Natural emissions	PgC/yr	166	210	27%		210	27%	166	0%
Anthropogenic emissions	PgC/yr	0	11			11		11	
Total Up flux (emissions)	PgC/yr	166	221	33%		221	33%	177	7%
Absorption oceans	PgC/yr	54	83	17%		83	17%	54	0%
Absorption land	PgC/yr	113	133	12%		133	12%	113	0%
Down flux (absorptions)	PgC/yr	167	216	29%		216	29%	167	0%
Residence time (RT)	yr	3,5	4,1	16%		3,5	0%	4,1	16%

Sources: IPCC-AR6 (1750), Global Carbon Budget 2023 (2022)

Figure 1: An overview of the most important CO_2 levels and fluxes from 1750 and 2022. Columns I show the original data, including their percentual change. Columns II show the impact on the CO_2 concentration with only global greening. Columns III show the impact on the CO_2 concentration without global greening. (IPCC, 2021; Friedlingstein et al.*, 2023).*

The 29% increase of the down flux alone indicates that greening of the Earth contributes to an increase in the atmospheric concentration. Due to more vegetation, the absorption flow has increased from 167 PgC/yr to 216 PgC/yr. The growth of the downward flux since the preindustrial period is only possible if the upward flux has increased more than that. Based on the historic levels and fluxes, we can conclude that this is the case. The total emissions have increased by 33%, from 166 to 221 PgC per year, which is also much more than the growth in the anthropogenic emissions alone.

Given the facts that the fluxes to and from the atmosphere are largely determined by the biological processes and that the atmosphere can be regarded as a first order container, in general we can conclude that the CO_2 level is directly related to the biological activity of the Earth. In Figure 2 we have given a simplified illustration of this mechanism, with CO_2 in the atmosphere presented as water in a reservoir (also acting as a first order process).

To understand the long-term impact of greening on the natural CO_2 concentration we assume the following two (hypothetical) steady states.

1. A stable situation with a constant concentration of ~280 ppmv, as assumed to be the case before any human influence. In this situation the total respiration is equal to total photosynthesis (GPP). As the down flux is proportional to the concentration, it follows that also the GPP is stable, so no greening or browning.

2. A stable situation similar to 1, but with a larger total GPP, so more greenness. This could be the result of more favorable conditions with respect to e.g. temperature, water availability and nutrition. The GPP level is supposed to be stable long enough so that the total respiration is again equal to the total photosynthesis, but at a higher level. As the concentration is proportional to the down flux, the concentration is now also at a higher level.

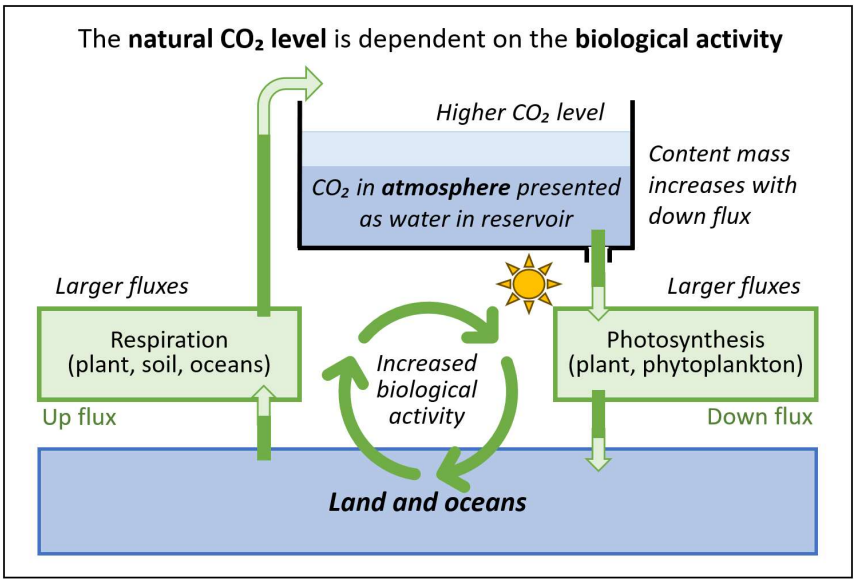

Figure 2: This simplified illustration demonstrates the importance of the Earth's biological activity for the natural CO_2 level in the atmosphere. Larger fluxes due to an increase in the yearly photosynthesis and respiration will lead to more CO_2 in the atmosphere (and vice versa).

This illustrates that in steady state situations with photosynthesis and respiration in balance, the level of greenness, in terms of GPP, defines the CO_2 level in the atmosphere. A larger GPP is only possible if also the CO_2 concentration is at a higher level.

During a period of greening that leads to the transition from state 1 to state 2, the increase in photosynthesis per year is larger than the resulting respiration, as the respiration partly lags the photosynthesis. The respiration increases, partly immediately by plant respiration, partly at later stages when leaves and other biomass degenerate. This delay qualifies new vegetation as a net sink.

The concentration can only increase if the up flux is larger than the down flux, so the greening alone cannot be the initial cause of the increasing concentration. Following correct bookkeeping, an increase of the concentration is only possible if in some period of time the sum of the total respiration and any other emission is larger than the total photosynthesis. This is apparently the case in the past decades given the yearly increase if the CO_2 mass in the atmosphere of approximately 5 PgC. Although new vegetation is a net sink, it is nevertheless an important element in the rising CO_2 concentration, as it leads to a structural increase in respiration. Ultimately greening can lead to a new steady state situation with larger up and down fluxes and a higher atmospheric concentration.

The greening of the Earth is mostly the result of the increased CO_2 concentration, but estimates show large variations from 44% (Chen *et al.*, 2022) to 74% (Zhu *et al.*, 2016) and 86% (Haverd *et al.*, 2020). Other factors include climate warming and nitrogen deposition. This means that the CO_2 concentration can be characterized as positive feedback for greening. If the atmospheric CO_2 level increases for any reason, this can lead to more greening. The extent to which this happens, however, will depend on many (local) circumstances.

Increased greenness, along with a higher concentration of atmospheric CO_2, imply that both the biosphere and the atmosphere contain more carbon than there was originally. This change could be the result of a net flux from the oceans and soil due to higher temperatures (Lee, 2011; Palmer et al., 2019). Another possible explanation involves the ocean's buffer capacity, which results from the combined equilibrium reactions of Henry's Law and the carbonate system. A reduction in concentration due to more absorption is in time compensated by increased emissions from the oceans. During the transition phase to a higher GPP level, the atmosphere and biosphere apparently behave as a net sink and the oceans and soil as a net source of CO_2.

The 16% change in residence time from 3.5 to 4.1 years indicates a nonlinear behavior of the carbon system, where the ratio of the atmospheric carbon mass and the down flux has increased over the years. Therefore, a greater partial pressure is needed for the same uptake rate. There could be many causes for this behavior, but satellite observations indicate that it can be related to constraining factors in the fertilization. CO_2 is just one limiting factor of photosynthesis; other factors include phosphorus, nitrogen, and water availability. With increasing CO_2 levels, the fertilization may be slowed down, due to the constraining effect of soil nutrients and soil water (Wang *et al.*, 2020). So, the increase in residence time can at least partly be linked to the increased greenness of the Earth. The larger residence time can also be connected to the reduced solubility of CO_2 in the oceans, which is generally inversely proportional to temperature. Several studies have suggested that higher temperatures due to climate warming result in not only more emissions, but also reduced absorption with a consequently longer residence time (Essenhigh, 2009; Harde, 2017, 2019). It is evident that further research into the various underlying mechanisms and interactions is necessary to enhance our understanding of this part of the increase in CO_2 levels.

4. Potential causes

Although the greening of the Earth since the preindustrial period developed parallel with the CO_2 level in the atmosphere, it was not the initial cause of this increase. Several studies have indicated that global warming since the Little Ice Age was the main initial driver of increased CO_2 levels (Humlum, Stordahl and Solheim, 2013; Harde, 2019; Koutsoyiannis, 2024b). Since 1750 the average global temperature has increased by approximately 1.1 K (IPCC, 2021) which has led to more emissions from the ocean and, more importantly, from the soil (Lee, 2011; Palmer *et al.*, 2019). This means that the great impact of global greening on CO_2 is closely related to the controlling role of climate warming in explaining the increased carbon dioxide level in the atmosphere. A higher temperature not only increases emissions from soil and oceans, it has also a direct positive impact on global greening and reduces the solubility of CO_2 in the oceans. The impact of temperature on the CO_2 level is supported by investigations of the causal relationship showing that changes in CO_2 concentrations are not the cause of temperature changes; rather, changes in temperature can potentially cause variations in CO_2 levels across all time scales (Koutsoyiannis *et al.*, 2023).

Based on the obvious impact of global greening on the CO_2 level, e.g., as observed in the seasonal cycles, we think that the present paradigm that human emissions are the sole cause of the increasing CO_2 level is untenable. The increased down flux observed since preindustrial times due to greening of the Earth leaves no other conclusion then that most of the CO_2 increase has a natural cause. In the present widely accepted hypothesis excess CO_2, that is CO_2 emitted on top of the natural equilibrium, accumulates partly in the atmosphere and remains there for a very long time. It is argued that there is a relatively short residence time of 4.1 years for natural CO_2, and multiple (much longer) residence times for excess CO_2 (IPCC, 2015). As previously mentioned, there is no physical justification for assuming multiple residence times for a part of the CO_2 in the uncompartmentalized well-mixed atmosphere, nor can we explain why a perturbation of human CO_2 would lead to a change in residence time.

However, we think there is no need for an ad-hoc model to describe the behavior of excess CO_2 in the atmosphere. Temperature induced global greening explains the observed CO_2 rise well, without the need for any extraordinary assumptions. The increase in GPP due to more greening can fully explain the observed increase of the down flux, and the constraining factors in the CO_2 fertilization combined with the reduced solubility of CO_2 in the oceans are plausible explanations for the observed increase in residence time. The close interaction of the expanding biosphere and higher temperatures is described in detail in a mathematical framework based on reservoir routing. Without any ad-hoc assumptions the results of this framework are in excellent agreement with real-world data (Koutsoyiannis, 2024a).

Assuming the same behavior for excess CO_2 as for natural CO_2, the contribution of human activities to the increase in CO_2 can be estimated based on its contribution to the down flux. A stable level of 9.6 PgC per year for fossil CO_2 (Friedlingstein *et al.*, 2023) leads to an almost equal down flux. With a residence time of 4.1 year, it has resulted in an increase of almost 40 PgC in the atmosphere, or 19 ppmv. This finding is consistent with the more accurate estimate of 4.3% of the concentration (i.e., 38 PgC or 18 ppmv in 2022) based on actual historical emissions (Harde, 2019). Under the influence of the positive feedback from the CO_2 fertilization, the effective contribution to the CO_2 increase may have been higher.

An important element of the present hypothesis is land use change, such as deforestation and the conversion of forests into agricultural land. This change is regarded as a form of emission similar to the burning of fossil fuels. This is true when the carbon stored in trees is released into the atmosphere, which represents 1.3 PgC/yr in 2022 (Friedlingstein *et al.*, 2023). On the other hand, deforestation has also led to a 4.4% reduction in the global terrestrial GPP of 130 PgC/yr (Krause *et al.*, 2022), and thus a relatively smaller down flux of approximately 5.7 PgC/yr, and a smaller CO_2 concentration. The combined contribution to the down flux due to the release of carbon from deforestation and the resulting reduction in GPP, can together be estimated at -4.4 PgC/yr. With a residence time of 4.1 years, this contribution has been responsible for 18 PgC less in the atmosphere, or -9 ppmv.

5. Conclusions

It may seem contradictory that the greening of the Earth is associated with a higher concentration in the atmosphere. After all, plants absorb more CO_2 from the atmosphere. But global greening is being initiated by and combined with global warming. Higher temperatures have direct effects on greening and on the emissions from soil and oceans. Greening is not the initial cause, but it leads to a larger down flux and ultimately also to a larger up flux. An increase in the fluxes to and from the atmospheric container results in a higher level, so we can say that the combination of global warming and global greening has led to more CO_2 in the atmosphere. The greater down flux since 1750 explains 29% of the 50% increase in CO_2, and the longer residence time could well be the result of constraining factors in the CO_2 fertilization combined with the reduced solubility of CO_2 in the oceans. This confirms that natural factors play a dominant role in increasing CO_2 concentrations, while human factors have only a limited influence.

In the present thinking about the carbon cycle there is no difference of opinion about the first order behavior for the natural carbon dioxide fluxes to and from the atmosphere. It is therefore remarkable that the growth of these fluxes is not considered as a viable explanation for the increased atmospheric concentration. The only reason we can think of this almost trivial aspect as being neglected is the bias of the human liability, which results from the flawed bookkeeping method that is used for the global carbon budget.

The quantifications in this study are based on the numbers as presented in Figure 1. Especially for the year 1750 the accuracy of the data is questionable. The atmospheric concentration in that year is based on ice core proxies from Antarctica, and the down flux is based on model calculations by the IPCC. Both are subject to considerable uncertainty. It is obvious that a more

detailed modeling based on the changes in fluxes at different time frames is necessary to obtain a more accurate understanding of all the causes and interactions involved. However, an increase in the down flux of approximately 30% is in line with the results of the previously mentioned studies on global greening, which makes it evident that global greening is directly related to the increase in CO_2. It is likely that the overall increase of the CO_2 level can be attributed to the interplay between global warming and greening, with a relatively small anthropogenic contribution, without the need to presume a special behavior for excess CO_2 or the use of an ad-hoc model with multiple residence times in the well-mixed atmosphere.

The supposed CO_2 level of ~280 ppmv from before the Industrial Revolution is often used as a baseline for comparing current and projected CO2 concentrations, and as a reference point for assessing human-induced climate change. Due to the dominant role of natural changes in the biosphere under the influence of higher temperatures, one can conclude that the present CO_2 concentration can be regarded as a 'natural' level. The present atmospheric CO_2 level matches with the actual greenness of the Earth and is much larger than 280 ppmv. If we exclude human contribution to the down flux due to the use of fossil fuels, the natural equilibrium rate would still be well above 400 ppmv (2024).

Our conclusion that the natural atmospheric CO_2 level depends on the greenness of the Earth is at odds with the suggested stable CO_2 level from the ice core proxies of Antarctica. These proxies suggest that the natural equilibrium concentration has been stable for a very long time: between 260 and 280 ppmv in the last 10,000 years and between 180 and 290 ppmv in the past 800,000 years (Bereiter *et al.*, 2015). However, it is improbable that there have been no fluctuations in the Earth's GPP over the past 800,000 years, or that the GPP has ever been as high as it is today. It is for example estimated that 10,000 years ago, shortly after the end of the last glacial, the area of the globe covered with forests was approximately 50% larger than in 2018 (Ellis, Beusen and Goldewijk, 2020; Ritchie and Roser, 2024). The average GPP from forests is 29% larger than from grassland and 10% larger than from cropland, which indicates a greater CO_2 down flux and hence a higher atmospheric concentration than today (Krause *et al.*, 2022).

Although ice core measurements are incredibly valuable for providing trend information on CO_2 levels, temperature and other parameters, we have reason to believe that the absolute measured CO_2 values are much lower than the original concentrations, due to the dissolvement of CO_2 from the capsulated air in firn and ice into water (Jaworowski, 2007). Ice core reconstructions also give a very flattened representation, in which only slow changes are visible. In the data recorded over the past 800,000 years, a single observation in an ice layer represents a period of 10s to many 100s of years (up to 5000 years). Short fluctuations, even with much higher concentrations, are therefore not visible. Unlike the ice core records, direct measurements taken between 1800 and 1960 and proxies from plant stomata show much greater values and more variations, which is more in line with what could be expected from our findings (Kouwenberg, 2003; Beck, 2021).

The impact of global greening on the atmospheric CO_2 concentration has important implications for the present policy to mitigate climate change. Due to the relatively large impact of natural factors the human contribution to the increase in CO_2 is much smaller than presently assumed. With a single residence time for all carbon dioxide in the atmosphere the human contribution based on fossil fuels is approximately 4.3% or 18 ppmv. This contribution will not further increase if the human emissions are stabilized at the present level, and even the most rigorous net zero scenario can have only a very limited impact.

Competing interests

The author declares that he has no conflict of interest.

Chief-Editor: H. Harde, **Reviewers**: anonymous.

Acknowledgements

We thank Prof. Wouter Keller, Prof. Demetris Koutsoyiannis and Prof. Hermann Harde for their helpful comments on the manuscript.

References

Beck, E.-G., 2021: *Reconstruction of Atmospheric CO_2 Background Levels since 1826 from Direct Measurements near Ground*, SCC, 2.2, pp. 148–211. https://doi.org/10.53234/scc202112/16.

Bereiter, B. *et al.*, 2015: *Revision of the EPICA Dome C CO_2 record from 800 to 600 kyr before present*, Geophysical Research Letters, 42(2), pp. 542–549. https://doi.org/10.1002/2014GL061957.

Chen, C. *et al.*, 2022: *CO_2 fertilization of terrestrial photosynthesis inferred from site to global scales*, Proceedings of the National Academy of Sciences of the United States of America, 119(10), p. e2115627119. https://doi.org/10.1073/pnas.2115627119.

Ellis, E.C., Beusen, A.H.W. and Goldewijk, K.K., 2020: *Anthropogenic Biomes: 10,000 BCE to 2015 CE*, Land, 9(5), p. 129. https://doi.org/10.3390/land9050129.

Essenhigh, R.H., 2009: *Potential Dependence of Global Warming on the Residence Time (RT) in the Atmosphere of Anthropogenically Sourced Carbon Dioxide*, Energy & Fuels, 23(5), pp. 2773–2784. https://doi.org/10.1021/ef800581r.

Friedlingstein, P. *et al.*, 2023: *Global Carbon Budget 2023*, Earth System Science Data, 15(12), pp. 5301–5369. https://doi.org/10.5194/essd-15-5301-2023.

Harde, H., 2017: *Scrutinizing the Carbon Cycle and CO_2 Residence Time in the Atmosphere*, Global and Planetary Change, 152, pp. 19–26. https://doi.org/10.1016/j.gloplacha.2017.02.009.

Harde, H., 2019: *What Humans Contribute to Atmospheric CO_2: Comparison of Carbon Cycle Models with Observations*, Earth Sciences, 8(3), p. 139. https://doi.org/10.11648/j.earth.20190803.13.

Haverd, V. et al., 2020: *Higher than expected CO_2 fertilization inferred from leaf to global observations*, Global Change Biology, 26(4), pp. 2390–2402. https://doi.org/10.1111/gcb.14950.

Humlum, O., Stordahl, K. and Solheim, J.-E., 2013: *The phase relation between atmospheric carbon dioxide and global temperature*, Global and Planetary Change, 100, pp. 51–69. https://doi.org/10.1016/j.gloplacha.2012.08.008.

IPCC, 2015: *Climate change 2014: synthesis report: contribution of working groups I, II and III to the Fifth Assessment Report of the Intergovernmental Panel on Climate Change. Ipcc*, Cop. https://www.ipcc.ch/assessment-report/ar5/.

IPCC, 2021: *Climate Change 2021: The Physical Science Basis. Contribution of Working Group I to the Sixth Assessment Report of the Intergovernmental Panel on Climate Change*. Cambridge, United Kingdom and New York, NY, USA: Cambridge University Press. https://doi.org/10.1017/9781009157896.

Jaworowski, Z., 2007: *CO_2: The greatest scientific scandal of our time*, 21st CENTURY Science & Technology. http://21sci-tech.com/Articles%202007/20_1-2_CO2_Scandal.pdf.

Koutsoyiannis, D. et al., 2023: *On Hens, Eggs, Temperatures and CO_2: Causal Links in Earth's Atmosphere*, Sci, 5(3), p. 35. https://doi.org/10.3390/sci5030035.

Koutsoyiannis, D., 2024a: *Refined Reservoir Routing (RRR) and Its Application to Atmospheric Carbon Dioxide Balance*, Water, 16(17), p. 2402. https://doi.org/10.3390/w16172402.

Koutsoyiannis, D., 2024b: *Reservoir routing and its application to atmospheric carbon dioxide balance*. https://doi.org/10.20944/preprints202405.0420.v1.

Kouwenberg, L., 2003: *Application of conifer needles in the reconstruction of Holocene CO_2 levels*. Utrecht: Universiteit Utrecht. https://dspace.library.uu.nl/bitstream/handle/1874/243/full.pdf.

Krause, A. et al., 2022: *Quantifying the impacts of land cover change on gross primary productivity globally*, Scientific Reports, 12(1), p. 18398. https://doi.org/10.1038/s41598-022-23120-0.

Lai, J. et al., 2024: *Terrestrial photosynthesis inferred from plant carbonyl sulfide uptake*, Nature, 634(8035), pp. 855–861. https://doi.org/10.1038/s41586-024-08050-3.

Lee, J.-S., 2011: *Monitoring soil respiration using an automatic operating chamber in a Gwangneung temperate deciduous forest*, Journal of Ecology and Environment, 34, pp. 411–423. https://doi.org/10.5141/jefb.2011.043.

Palmer, P.I. et al., 2019: *Net carbon emissions from African biosphere dominate pan-tropical atmospheric CO_2 signal*, Nature Communications, 10(1), p. 3344. https://doi.org/10.1038/s41467-019-11097-w.

Piao, S. et al., 2019: *Characteristics, drivers and feedbacks of global greening*, Nature Reviews Earth & Environment, 1, pp. 1–14. https://doi.org/10.1038/s43017-019-0001-x.

Riebesell, U. et al., 2007: *Enhanced biological carbon consumption in a high CO_2 ocean*, Nature, 450(7169), pp. 545–548. https://doi.org/10.1038/nature06267.

Ritchie, H. and Roser, M., 2024: *The world has lost one-third of its forest, but an end of deforestation is possible*, Our World in Data [Preprint]. https://ourworldindata.org/world-lost-one-third-forests (Accessed: 27 September 2024).

Salby, M. and Harde, H., 2021: *Control of Atmospheric CO_2 Part I: Relation of Carbon 14 to the Removal of CO_2*. Classica Forlag AS. https://doi.org/10.53234/scc202112/12 (Accessed: 27 March 2023).

Segelstad, T., 1998: *Carbon cycle modelling and the residence time of natural and anthropogenic atmospheric CO_2: on the construction of the 'Greenhouse Effect Global Warming' dogma*, European Science and Environment Forum (ESEF), Cambridge, England. https://www.researchgate.net/publication/237706208.

Stallinga, P., 2023: *Residence Time vs. Adjustment Time of Carbon Dioxide in the Atmosphere*, Entropy, 25(2), p. 384. https://doi.org/10.3390/e25020384.

Wang, S. et al., 2020: *Recent global decline of CO_2 fertilization effects on vegetation photosynthesis*, Science, 370(6522), pp. 1295–1300. https://doi.org/10.1126/science.abb7772.

Zhu, Z. et al., 2016: *Greening of the Earth and its drivers*, Nature Climate Change, 6, pp. 791–795. https://doi.org/10.1038/nclimate3004.

OPEN ACCESS

Science of Climate Change
Vollsveien 109
NO-1358 Jar
Norway

***ISSN**: 2703-9072*

Correspondence: ah@on.nl

Vol. 4.2(2024)

pp. 89-113

Greenhouse Feedbacks are Intrinsic Properties of the Planck Feedback Parameter

Ad Huijser

Abstract

The idea that our climate reacts differently to anthropogenic forcings than to natural instabilities through the phenomenon of "feedbacks", seems widespread. This paper shows that climate feedbacks are not effects induced by forcings, but in fact "constitute" our climate. Independent from the origin of a disturbance, our climate will always respond according to the Planck feedback parameter λ_{PL}. This is not the "basic feedback" of our climate as often quoted, but just the difference between the Surface feedback parameter λ_S and the sum of Climate feedbacks λ_{FB}, according to $\lambda_{PL} = -(\lambda_S - \lambda_{FB})$. The Surface feedback parameter λ_S is coupled to the Stefan-Boltzmann relation and holds for any planet. The sum of Climate feedbacks λ_{FB} on the other hand, is an intrinsic property of our Earth' specific atmosphere/surface combination. It describes our climate's reaction to surface temperature changes, governed by water in all its possible forms of aggregation. These findings are supported by analyzing 23 years of incoming- and outgoing radiation data at the Top of the Atmosphere from NASA's CERES program. This also shows that the observed temperature trend can only be for about 40% attributed to Greenhouse gas forcings.

Keywords: Greenhouse effect; radiative forcing; climate sensitivity; climate feedbacks.

Submitted 2024-04-08; Accepted as Debate Paper on 2024-11-25, see Comment of the Editorial Board, https://doi.org/10.53234/scc202411/03

1. Introduction

The development of very complex Ocean Coupled-Global Circulation Models (GCMs) has become a domain of climate science that can hardly be followed nor checked by non-insiders. Fortunately, we can still apply basic physics as expressed in Energy Balance Models (EBMs) in analyzing climate-change data that are available.

EBMs are excellent tools to demonstrate and explain the way our climate works. They are based on the notion that at the Top of the Atmosphere (TOA) no thermal processes such as convection, but only radiation fluxes play a role. The radiation balance between incoming short wavelength (SW) radiation and outgoing long wavelength (LW) radiation at TOA sets the equilibrium temperature at the surface. EBMs are 1-D models that only yield atmosphere specific results. For global averages often the US Standard Atmosphere is being used, and in that respect, EBMs are not at all comparable to the very sophisticated 3-D GCMs. Simulations with GCMs dominate already for years the field of climate science. In particular they are being used in forecasting climate change under the influence of anthropogenic forcings.

Contrary to the pure numerical output of GCM's, EBMs allow us, in spite of other shortcomings due to their simplicity, to derive analytical expressions that give much more insight in the relationships between surface temperature and changes in our climate system. One of the most basic analytical relations derived, for instance lets us calculate the ultimate temperature change due to a forced radiation-imbalance at TOA. As an example, a sudden change in the Solar constant

by about 0.35 % would create an imbalance of 3.3 W/m^2, thus forcing todays Earth's set-point temperature to shift by only 1 ºC [6].

Not many will question this relation governed by the so-called Planck feedback parameter, nor its outcome. Accordingly, an identical temperature change should also occur for a similarly sized change in the imbalance by a forcing from anthropogenic origin, *e.g.* by doubling of the CO_2-concentration. Already more than 50 years ago, scientists from NASA's Goddard Institute for Space Science (NASA/GISS) Rasool & Schneider (1971) [1] came to the same conclusion. For the effect of doubling the CO_2-concentration in our atmosphere, they calculated an increase of only 0.8 ºC, even taking the effect of the so-called "Water-vapor feedback" into account. The latter is an important addition. Our climate is not constant, and changes in surface temperature have their impact on our atmosphere's behavior. In particular, the abundantly available water in all possible forms within our climate system plays a dominant role in these phenomena.

More modern studies applying the most detailed spectroscopic data by Van Wijngaarden & Happer (2021) [2] and also calculations with the on-line climate program MODTRAN [3] show similar results: about 1 ºC for doubling of the CO_2-concentration in our atmosphere. However, todays most sophisticated, 6th generation (CMIP6) of GCMs deliver much higher values for such anthropogenic global warming scenarios. Those outcomes are the foundation under the climate policies developed by the UN-International Panel on Climate Change (IPCC) [4] and are embraced by governments around the globe. The large discrepancies between these 1-D calculations and the outcomes of these sophisticated 3-D GCMs are generally explained in terms of these climate feedbacks, changes in our atmosphere triggered by temperature changes at the surface. From a physics point of view, those feedbacks should exist, and they appear in many analyses of climate data or models, *e.g.*in Sherwood *et al*. (2020) [5]. It is commonly accepted in climate science to regard these feedbacks as add-ons to the earlier mentioned Planck feedback parameter which is seen as fundamental to any climate system. Here is a quote from a university's climate course [6]: "*The Planck feedback is the most basic and universal climate feedback, and is present in every climate model. It is simply an expression of the fact that a warm planet radiates more to space than a cold planet*".

Now the question arises: why would this Planck feedback parameter not already contain these feedback effects? If that parameter perfectly explains the warming from a forcing in the short wavelength channel, why would warming from a forcing by Greenhouse gasses (GHGs) that interferes with the long wavelength channel, trigger a completely different behavior in effects that should primarily, if not solely, be attributed to all the water in our climate system?

Nevertheless, this idea of climate feedbacks is the generally accepted narrative in explaining the large climate sensitivities as calculated by GCMs. Climate feedbacks have also been introduced in EBMs, be it on an *ad hoc* basis by just enhancing the Planck feedback parameter [6]. But is that justified? Time for a reassessment by an EBM-analysis of the Greenhouse effect.

2. The Greenhouse effect

The Greenhouse effect, the interaction between our atmosphere and the long wavelength outgoing radiation keeps our Earth livable. The effect is not just about "obstructing" the outgoing radiation that cools our planet, but also about redistributing vertical energy flows, both radiant as well as thermal fluxes. There are a number of ways to express this Greenhouse effect *G*. Within the concept of forcings to quantify the AGW-hypothesis *i.e.,* global warming due to Anthropogenic Greenhouse gas emissions, we apply here the definition of Raval & Ramanathan (1989) [7]:

$$G = LW_{UP} - LW_{OUT} \quad (1)$$

This relation expresses the difference between the upwelling longwave length radiation LW_{UP} from the surface as determined through the Stefan-Boltzmann relation by the surface temperature T_S, and the outgoing longwave length radiation LW_{OUT} at the Top of Atmosphere (TOA). In balance LW_{OUT} equals the incoming shortwave radiation from the Sun at TOA: SW_{IN}.

In the AGW-hypothesis, an increase in Greenhouse gasses (GHGs) like CO_2, has an obstructing effect expressed as a forcing that leads directly to warming. A higher temperature however, leads also to an increase in water evaporation from the surface. That goes with an increase in the Latent Heat flow. The thermal energy-flux (Latent- plus Sensible Heat) from the surface to higher levels in the atmosphere by-passes the obstructing effect for the upwelling long wavelength radiation, thus reducing the Greenhouse effect. But at the same time, this evaporation also leads to more water-vapor in the atmosphere. Water-vapor is a strong Greenhouse gas itself and therefore adds to it. Water-vapor and Lapse Rate feedback, but also Cloud feedback, are typically affecting the outgoing (cooling) Long Wavelength LW-channel. However, Cloud feedback and surface temperature dependent changes in Surface Albedo [4] are also affecting the incoming (warming) Short Wavelength SW-channel. It is certainly interesting to know how, and if these various feedbacks add to, or reduce the warming effect of Greenhouse gasses. However, for the following discussion we do not need those details. We just accept that all these feedbacks exist.

3. Feedbacks

With the present increase in GHG's like CO_2 due to human activities, we change the major radiation components in the LW-channel by about 1% only and therefore, we can handle changes in Greenhouse effects as (small) perturbations. This also holds for the additional forcings from a change in the Greenhouse effect by a surface temperature increase as induced by the forcing ΔF_{GHG} from extra Greenhouse gasses. As shown above, we have various climate feedbacks acting at the same time. Accordingly, the sum of all these temperature-induced changes in G can be expressed as:

$$\Delta G = \frac{\partial G}{\partial T_S} \Delta T_S \quad (2)$$

As climate related effects seldom occur instantaneously, differential changes are here denoted by Δ-symbols to reflect differences after a finite time interval Δt. In first order, the surface temperature dependency of the Greenhouse effect $\frac{\partial G}{\partial T_S}$ can be regarded as a single, constant climate feedback parameter γ. So, for the "integral" effect of a forcing on the surface temperature due to adding GHGs, we have to add to the direct forcing ΔF_{GHG} also this Greenhouse feedback effect. There might be other, yet unknown forcings in the LW-channel active as well, so for completeness we define $\Delta F_{LWC} = \Delta F_{GHG} + \Delta F_X$ which leads together with (2) to:

$$\Delta G = \Delta F_{LWC} + \gamma \Delta T_S \quad (3a)$$

The radiation imbalance at TOA due to a (stepwise) forcing ΔF_{LWC} will ultimately be fully compensated by a surface temperature increase ΔT_S (at $t \rightarrow \infty$), but the change in the Greenhouse effect ΔG will remain after the new equilibrium has set. Both increases, in GHG-concentration as well as in surface temperature, yield permanent changes in the atmosphere, and thus in the Greenhouse effect. As we will show later on, this relative change in G is even for a large forcing as from $2xCO_2$, still less than 3 %. So, neglecting second order effects in climate feedbacks as assumed earlier, remains allowed.

Although the incoming radiation from the Sun SW_{IN} will not be directly affected by the increase in CO_2-concentration, temperature induced feedbacks like changes in cloudiness and surface albedo do influence the incoming Solar flux. In a similar way as defining the climate feedback effect in the LW-channel we can write this feedback effect in the SW-channel as:

$$\Delta SW_{IN} = \Delta F_{SWC} + \alpha \Delta T_S \qquad (3b)$$

with $\alpha = \frac{\partial SW_{IN}}{\partial T_S}$. Like γ in the LW-channel, α is assumed constant, again neglecting second order effects. The integral climate feedback λ_{FB} for our entire climate system is the sum of the climate feedbacks in the warming (SW) and those in the cooling (LW) channel *i.e.,* $\lambda_{FB} = \alpha + \gamma$. For completeness, we have added in (3b) the change in the SW-channel due to a primary forcing ΔF_{SWC}, similar to the GHG-forcing in the LW-channel. For instance, it can take care of changes in the Solar constant, but also for forcings that are typically acting in the SW-channel like aerosols through a.o. cloud formation. Those latter will also affect the LW-channel, which is the reason to use ΔF_{LWC} and not just ΔF_{GHG} in (3a). Both forcings, F_{SWC} and F_{LWC} are regarded unique to their respective channels (hence their subscript SWC and LWC, respectively). Nevertheless, they might contain channel cross-effects as *e.g.*, the influence from clouds.

4. A begin-to-end-state scenario for the enhanced Greenhouse effect

With the above definitions, let us assume for $t < 0$ that our climate is in equilibrium. This climate state can be characterized by $T_{S,0}$ due to the incoming Solar radiation $SW_{IN,0}$. The Stephan-Boltzmann (S-B) relation links the upwelling long wavelength radiation LW_{UP} from the Earth' surface with emissivity ε, to its surface temperature T_S through the S-B-constant σ:

$$LW_{UP} = \varepsilon \sigma T_S^4 \qquad (4)$$

As LW_{OUT} equals the incoming Solar flux SW_{IN} at TOA in equilibrium, the (begin-state) Greenhouse effect G_0 for $t < 0$ is given by combining (1) and (4) as:

$$G_0 = LW_{UP,0} - LW_{OUT,0} = \varepsilon \sigma T_{S,0}^4 - SW_{IN,0} \qquad (5)$$

At t = 0 we now inject some extra CO_2 into the atmosphere yielding a stepwise forcing ΔF_{GHG} which will immediately lower LW_{OUT} by that amount. Next, the climate will relax to a new equilibrium ($t \rightarrow \infty$) by an increase in surface temperature ΔT_S needed to restore LW_{OUT} to the level of the incoming Solar flux $SW_{IN,1} = SW_{IN,0} + \Delta SW_{IN}$. Applying (3b) we can now write this new (end-state) equilibrium for the Greenhouse effect as:

$$G_1 = LW_{UP,1} - LW_{OUT,1} = \varepsilon \sigma T_{S,1}^4 - (SW_{IN,0} + \Delta F_{SWC} + \alpha \Delta T_S) \qquad (6)$$

As $T_{S,1} = T_{S,0} + \Delta T_S$ we get for small changes in a first order approximation:

$$G_1 - G_0 = \Delta G = 4\varepsilon \sigma T_{S,0}^3 \Delta T_S - \alpha \Delta T_S - \Delta F_{SWC} \qquad (7)$$

Obviously, (7) should be equal to (3a) as derived earlier for the permanent change in G due to the forcing from extra GHG's <u>*plus*</u> the climate feedbacks expressed by $\gamma \Delta T_S$ from the permanent surface temperature increase ΔT_S. After reshuffling and writing the sum of <u>*all*</u> feedbacks in both SW- and LW-channels as $(\alpha + \gamma) = \lambda_{FB}$, this equality can be rewritten into:

$$(\lambda_S - \lambda_{FB}) \Delta T_S = \Delta F_{SWC} + \Delta F_{LWC} \qquad (8)$$

Here, we introduce the Surface feedback parameter λ_S as:

$$\lambda_S = 4\varepsilon \sigma T_S^3 = 4LW_{UP}/T_S \qquad (9)$$

defined in analogy (but omitting the minus-sign) with the Planck feedback parameter λ_{PL}:

$$\lambda_{PL} = -4SW_{IN}/T_S \tag{10}$$

Ad hoc corrections of this Planck feedback parameter by climate feedbacks, as already mentioned in the introduction, is often expressed (see *e.g.* [6]) in a similar expression for the temperature increase due to a forcing from an increase in GHGs analogous to (8). In that case, the AGW-hypothesis based on GHGs-only, also assumes that $\Delta F_{LWC} = \Delta F_{GHG}$ and $\Delta F_{SWC} = 0$ leading to:

$$(-\lambda_{PL} - \lambda_{FB})\Delta T_S = \Delta F_{GHG} \tag{11}$$

Just forgetting the "minus"-sign in front of the Planck feedback parameter λ_{PL} due to its definition as a genuine feedback parameter, and it is clear that this (11) differs fundamentally from (8) as derived here. Textbooks regard λ_{PL} as our climate's fundamental feedback parameter, whereas λ_S plays that role in (8). Many, including the IPCC, are treating this Planck feedback parameter as a genuine, independent feedback next to the others such as Water-vaper and Cloud feedback in their reports [4]. For planets with an atmosphere like the Earth, the Surface feedback λ_S is not equal to $-\lambda_{PL}$. Deciding whether (8) or (11), is correct, boils down to answering the question: "*are climate feedbacks part and parcel of the Planck feedback parameter, yes, or no?*"

N.B.: Equation (11) is often visualized and/or mathematically derived by using an electronic analogon of an operational amplifier with a feedback-loop. This logical and powerful concept is discussed in Appendix A, including its "Achillis' heel": the choice for the "open-loop gain".

5. Mutual feedback dependencies

According to textbooks, the Planck feedback parameter λ_{PL} "translates" changes in the incoming radiation into changes in T_S as is easily derived from an EBM analysis [6]:

$$-\lambda_{PL}\Delta T_S = \Delta SW_{IN} \tag{12}$$

In that sense, λ_{PL} is the parameter that controls our climate's "setpoint" for the average surface temperature T_S at a given level of the Solar constant. Averaged over the Earth' disc as seen from the Sun, the Solar constant is about 340 W/m^2 bringing an average flux $SW_{IN} \approx 240$ W/m^2 into our climate system. In today's climate, that leads to a T_S of about 288 K.

The begin-to-end-state-scenario from Section 4 can also be used to derive (12) for a step-wise change in the incoming Solar flux SW_{IN}, with a forcing ΔF_{SWC} in the shortwave channel at $t = 0$. When due to just a change in the Solar constant, there is no extra forcing in the LW-channel as the atmosphere's GHG-concentration remains constant, *i.e.* $\Delta F_{LWC} = 0$. The permanent change in Greenhouse effect according to (3a) between begin- and end-state is then given by $\Delta G = \gamma\Delta T_S$. In the SW-channel we triggered $\alpha\Delta T_S$, but as $\gamma\Delta T_S$ in the LW-channel, this is just part of the natural response of what (12) describes. That leads straightforwardly from (8) to an expression similar to (12),

$$(\lambda_S - \lambda_{FB})\Delta T_S = \Delta F_{SWC} \tag{13}$$

The time response of the various components involved as described above for scenarios with GHG- and SW_{IN}-forcings that are equal in size, are schematically depicted in Fig. 1a and 1b. The temperature response represented is equal in both cases. The same holds for the radiation imbalance $N = SW_{IN} - LW_{OUT}$. That is of course, not a real surprise as our climate's reaction should be equal to any forcing at TOA, independent from its origin.

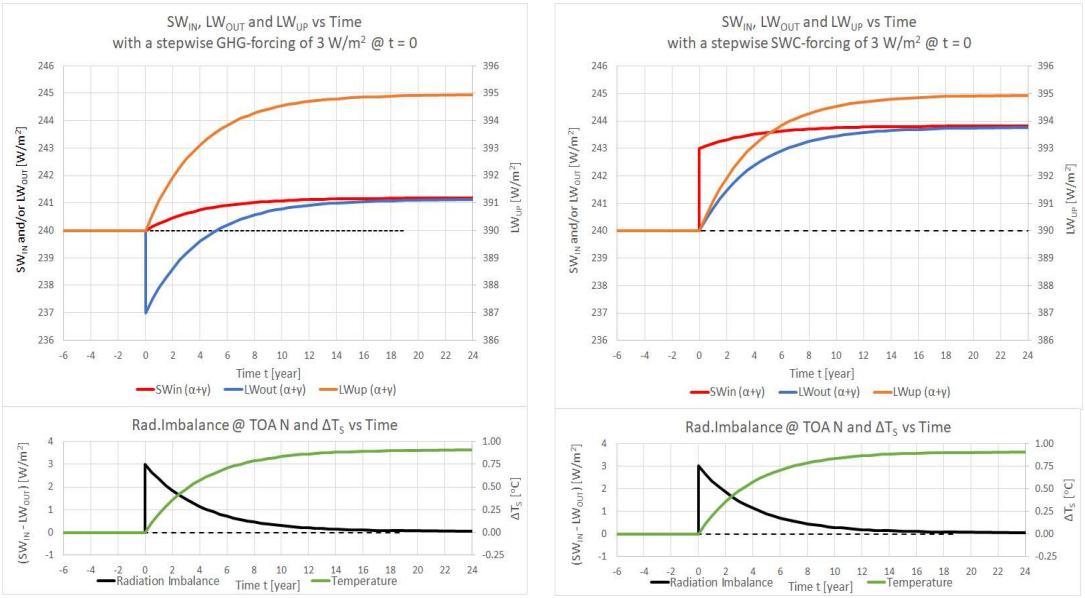

***Figure 1a and b**. Time-line of the relevant radiation components and Surface Temperature for a step-wise 3 W/m² forcing of the radiation imbalance at t = 0. On the left-hand side (a) in case of adding a GHG that is directly affecting LW_{OUT}; on the right-hand side (b) from changing the incoming Solar radiation that is directly affecting SW_{IN}. The applied climate relaxation time τ = 4 years, and for the sum of total climate feedbacks λ_{FB} = 2.2 W/m²/K the split is made in α = 1.3 and γ = 0.9 W/m²/K for the SW- and LW-channels, respectively. For the actual division between α and γ, see Section 8.*

Important to note here, is the effect of climate feedbacks on the time-lines in Fig. 1. Where the time dependencies for SW_{IN}, and LW_{OUT} in Fig. 1a and 1b are very sensitive to the distribution of feedbacks over the SW- and the LW-channels, as given by α and γ, we see that the time-line of the Radiation Imbalance N seems insensitive to this distribution of feedbacks. The reason is due to the fact that climate feedbacks are not independent (external) drivers like the forcings from adding GHGs or changes in Solar irradiation. They are "responses" of our climate to induced temperature changes. In fact, climate feedbacks slow down the speed with which our climate regains its balance, thus affecting the climate relaxation time τ. In that way, they allow more energy ($\tau\Delta F$) to enter the system and hence their "amplifying" effect on the final temperature increase. But the maximum radiation imbalance at TOA is just given by the total of primary forcings $(\Delta F_{SWC} + \Delta F_{LWC})$, and will not be further increased by these "internal" climate feedbacks.

Equation (12) in the expression with $\Delta SW_{IN} = \Delta F_{SWC}$ and (13) as derived, are two equations for the same relation between the surface temperature increase ΔT_S, and a change in Solar forcing without changing the atmospheric composition with extra CO_2. Combining them by eliminating ΔF_{SWC} and ΔT_S delivers a very important relation for the three feedbacks involved:

$$-\boldsymbol{\lambda_{PL}} = (\boldsymbol{\lambda_S} - \boldsymbol{\lambda_{FB}}) \qquad (14)$$

First of all, this relation indeed confirms the earlier expressed idea that **climate feedbacks are *part and parcel* of the Plank feedback parameter**. Secondly, this relation also fulfills the obvious requirement that the Earth without an atmosphere, *i.e.* $\lambda_{FB} = 0$, demands as a consequence of the Stefan-Boltzmann relation that $-\lambda_{PL} = \lambda_S$. In this case expressed as: $\lambda_S \Delta T_S = \Delta SW_{IN}$, which relates temperature changes to changes in Solar constant and/or changes in Surface Albedo only. Next to (14), that last condition simply proves that expressions like (11) cannot be correct. They do not at all adequately describe the warming of a planet without an atmosphere *i.e.*, without climate feedbacks in the form of λ_{FB},

We defined ΔF_{SWC} and ΔF_{LWC} as forcings unique to their respective channel. From spectroscopic data we can assume that GHG-forcings will not, or hardly affect the SW-channel. The effect from Aerosols through their influence on cloud formation could be a forcing acting on both channels. A growing SW-flux would then lead to a growing LW_{OUT} *i.e.,* a negative forcing in G. As proposed already in Section 3, it therefore makes sense to express the forcing in the LW-channel as $\Delta F_{LWC} = (\Delta F_{GHG} + \Delta F_X)$. Inserting (14) into (8) leads to the general expression between temperature change and the sum of forcings ΔF_{TOT} as:

$$-\boldsymbol{\lambda_{PL}\Delta T_S} = \boldsymbol{\Delta F_{SWC} + \Delta F_{LWC}} = \boldsymbol{\Delta F_{TOT}} \tag{15}$$

What (15) shows, next to the additional term from effects in the SW-channel, is that we better regard λ_{FB} as being "*our most basic and universal climate feedback*". The Planck feedback λ_{PL} is not an independent parameter at all. It is just the difference of two "genuine" ones: the Surface feedback that holds for all planets, and the Greenhouse feedback λ_{FB} that is specific for a planet's atmosphere/climate system. It makes $-1/\lambda_{PL}$ more the parameter that characterizes a planet's climate sensitivity to forcings given its atmospheric/climatic composition that differentiate it from a bare solid body. This notion implies that in relations like (11) with $(-\lambda_{PL} - \lambda_{FB})$, feedbacks are in fact, counted twice: a first time as already embedded in λ_{PL} and a second time in the "additional" term λ_{FB}. That makes quite a difference in the calculated effect of Greenhouse gasses.

Separate discussions about climate sensitivity and feedbacks are fruitless as they are discussing one and the same set of phenomena. If we would build up the Earth's climate system starting from a bare planet, we would start with a single feedback mechanism being that of a (near) Black Body radiator. The climate sensitivity would then be $1/\lambda_S$ as defined in (9). Without clouds, the incoming Solar radiation would be larger than today. Adding the atmosphere/biosphere of today's Earth in small steps *i.e.,* adding forcings due to water such as water-vapor and clouds as well as forcings from non-condensable Greenhouse gasses like CO_2, will increase the surface temperature. At the same time, we are creating a climate that step by step will show a stronger reaction to those temperature changes due to the growing effect of climate feedbacks. When we have finally created today's Earth system, the climate sensitivity has increased to the present value $-1/\lambda_{PL} = 1/(\lambda_S - \lambda_{FB})$. At the same time, the integral feedback for the entire system has been gradually decreased due to the feedbacks of the atmosphere, inducing extra warming. Doubling now the CO_2-concentration will certainly change our climate's reaction a little bit further, but with the present rate of adding CO_2 by burning fossil fuels, that change in feedbacks is extremely small. The Planck feedback parameter as given by (10) changes by the increase in SW_{IN} and T_S. According to the CERES-data [8] the relative change in SW_{IN} over the last 2 decennia, is less than $3 \cdot 10^{-4}$/year and in T_S about $7 \cdot 10^{-5}$/year. Moreover, they change in the same positive direction thus creating a relative change in λ_{PL} of less than 0.2 ‰/year. It is amazing that with all the various feedbacks involved, our climate's reaction to forcings is just governed by such a stable factor.

6. Numerical implications

With average values from CERES-data [8] we can calculate the various components and show what a difference (14) makes in our climate sensitivity within the AGW-hypothesis. According to (9) and (10) those data yield $\lambda_S = 5.52$ W/m^2/K and $\lambda_{PL} = -3.33$ W/m^2/K, respectively. Through (14) we calculate for the sum of all feedback parameters $\boldsymbol{\lambda_{FB}}$ **= +2.19 W/m^2/K.** This is "spot on" in comparison with the "*most likely*" value of $+2.2 \pm 0.6$ W/m^2/K from GCM-calculations that the IPCC published in their most recent AR6-report [4]. Not a surprise given the analysis above, but the wide range in the IPCC value shows the enormous scatter in the calculated results of the

various GCMs that exist. That must be a reflection of the immaturity of these models. We also see that large scatter in IPCC's reported climate sensitivities as derived from CMIP6-GCMs: 0.9 $\pm$ 0.2 K/W/m^2 [4]. Or, in Equilibrium Climate Sensitivity (ECS) terms for the ultimate warming from doubling the CO_2-concentration, in the range of 2.5 – 4 ^oC.

The "real" climate sensitivity from (8) or (15) however is only $\mathbf{-1/\lambda_{PL} = 0.3\ K/W/m^2}$. In comparison with a climate sensitivity as calculated by (11) and apparently also today's climate science as with IPCC's "reality", this gives a value $-1/(\lambda_{PL} + \lambda_{FB}) \approx 0.9$ K/W/m^2. It indeed supports the GCM-derived values, but as we have shown above, that "agreement" seems to be based on counting the influence of climate feedbacks twice.

That GCMs deliver in average adequate values for the sum of feedbacks, is not that remarkable at all. It can be obtained independently of time by varying the surface temperature in these models. Atmospheric models applied are apparently very realistic. A similar methodology should also deliver an adequate climate sensitivity, and indeed, GCMs deliver a proper value for the Planck feedback parameter as well [4]. Running GCMs over a long period of time and deriving from the calculated temperature trend a climate sensitivity that is not near the inverse of the Planck feedback parameter, only demonstrates that GCMs are still not good enough to forecast our future climate. As shown by Frank (2019) [9] GCMs are like weather-models based on the same physics, very sensitive to error propagation. Nevertheless, IPCC's narrative around climate feedbacks has so far been a very effective argument in "explaining" these discrepancies (see also Appendix A).

From the analysis above, it is clear that values for climate sensitivity and climate feedbacks are not "free to choose" parameters in our climate system, but prescribed by the setpoint of it. That climate-setpoint, characterized by T_S is fully determined by the combination of the Solar flux SW_{IN} and the atmospheric composition. However, when $-\lambda_{PL}$ is fixed and T_S is reasonably well measured, the climate forcing F has to be a given, according to (15). The fact that people come up, based on a mix of measurements of temperatures and estimates of forcings, with climate sensitivities that differ substantially from $-1/\lambda_{PL}$ can only hint to the conclusion that our knowledge about all the forcings active in our climate, is far from complete. To prove that statement as well as the validity of the thesis that the climate sensitivity is given by the inverse of the Planck feedback parameter, we can make use of the above observations. In spite of the 3x difference in climate sensitivity, the value for the total of climate feedbacks λ_{FB} is identical. So, the sum of those climate feedbacks cannot be a factor of dispute in such an analysis. With (3a) and (3b) we created tools to analyze more than 20 years of measurements of incoming and outgoing radiation through NASA's CERES-program [8]. The sum of forcings that we can derive in that way from experimental data should then be consistent with the total forcing that we derive through (15); or in case the IPCC is correct, at or close to those derived through (11).

7. Dynamics of Climate change

Although (15) gives a clear picture of the effect of forcings, it is often stated in view of the inertia of our climate system that it cannot be used to analyze actual observation. Certainly not for the relatively short period since when we observe our climate extensively from space as through the CERES-program [8]. Next to that, our climate is more complex than the model used so far where the surface acts as a well-defined interface. To use those CERES-data, we need a dynamic model that describes warming as a result of time-dependent forcings. We also need a better understanding of how and where the heat that the Solar radiation delivers, is stored. We can derive such a model by starting from the total energy balance where the flux difference at TOA between incoming and outgoing energy must equal the thermal change of the entire Earth (climate) system:

$$N(t) = SW_{IN}(t) - LW_{OUT}(t) = C(t)\frac{dT_S(t)}{dt} + T_S(t)\frac{dC(t)}{dt} \quad (16)$$

with *C(t)* being the heat capacity of the Earth-system per unit surface area. The term $T_S \frac{dC(t)}{dt}$ takes care of the fact that the Earth is a "water-planet" with all three states of aggregation for its most important Greenhouse gas H_2O: ice, water and water-vapor, all abundantly present in our climate system at the same time. Consequently, water with high specific (latent) heat between its various phases, must play a significant role in the energy balance. That last term in (16) not only represents the latent heat, but also the storage of heat in the deep ocean. With over 70 % covered by water, most energy absorbed at the Earth's surface ends up in the oceans. SW-radiation penetrates, depending on its wavelength, about a hundred meters deep or more. Its majority is absorbed in the so called *mixed-layer* that interacts with the atmosphere, but some reaches the deeper layers where it gets isolated from atmospheric interaction. This *mixed layer* is a 75-100 m thick layer with a reasonable homogeneous sea-surface temperature (SST) due to mixing by wind- induced waves and surface turbulence. In fact, it determines the value of *C* in (16), the heat capacity that plays the determining role in today's observations of Global warming. The heat capacity of our atmosphere is only about 2 % of that of the *mixed layer*, but this capacity is again only about 2 % of the total heat capacity of all the oceans together.

Below the mixed layer the temperature drops very quickly with a steep gradient, which is "pushing" a small part of the absorbed heat from SW_{IN} into deeper layers. It will there be isolated from the *mixed layer* and cannot participate in the heat-exchange at the surface anymore. It is the reason that today's radiation imbalance $N \approx 0.9$ W/m^2 as determined from the trend in Ocean Heat Content (*dOHC/dt),* is much larger than zero [13]. The dynamic behavior of the radiation balance *N(t)* that is subject to a small forcing *F(t)* pushing it out of its equilibrium N_0, can be described by a universally applicable expression:

$$\frac{dN(t)}{dt} = \frac{dF(t)}{dt} - \frac{(N(t) - N_0)}{\tau} \quad (17)$$

It shows, in case of a "free" system out of balance *i.e.,* for *dF(t)/dt = 0,* that *N(t)* will in time relax back to its equilibrium N_0 with a characteristic time constant τ. In fact, it describes the curves in Fig. 1a and b where the climate system has been brought out of balance by a step-wise forcing ΔF at $t = 0$, with $dF(t)/dt = 0$ for $t \neq 0$. For simplicity we have set in those examples $N_0 = 0$, whereas N_0 is in fact the radiation imbalance equilibrium at TOA at which no temperature change occurs without external forcings. This amount of excess heat entering the climate system without causing a temperature change, is not necessarily constant in time. Not even over such short periods of time as applied here in the analysis of 23 years of CERES-data. First of all, it is proportional to the incoming Solar flux. Of this 240 W/m^2, only about 1 W/m^2 goes into N_0, so changes in SW_{IN} as observed, will have very little effect. As almost all of the stored energy in our climate ends up in the oceans, N_0 is dominated by effects in the oceans. Examples are a.o., changes in the flow-patterns of ocean currents, in the penetration depth of light or in salinity. Given the huge thermal capacity of the oceans, changes will be trend-wise small, so all those effects can be regarded as perturbations of N_0. Thus, these changes will end up in (17) as part of the term *dF(t)/dt* and being related to the SW-channel, as part of the sum of forcings F_{SWC} in (3b).

As already explained earlier in discussing Fig. 1, feedbacks have no effect on the radiation imbalance other than increasing the characteristic relaxation time τ. According to (17), the dynamic offset $(N(t) - N_0)$ will then just be somewhat larger than without feedbacks. As the relaxation time is an intrinsic property of our climate, we would not be able to identify this effect in analyzing experimental data [21]. But feedbacks and thus τ, do influence the climate sensitivity

as the derivation of (15) has shown. In the dynamic situation it does not differ, which is directly visible from the left-hand side equality of (16) when expanding the SW- and LW-channel components by applying (3a) and (3b). After compacting this with (14), we get the dynamic version of (15):

$$-\lambda_{PL}\Delta T_S = \Delta F_{LWC} + \Delta F_{SWC} - \Delta N = \Delta F_{TOT} - \Delta N \qquad (18)$$

for changes over a finite period Δt. The difference of (18) compared to (15) is in ΔN. At equilibrium, as applied in sections 5 and 6 with $\Delta t \rightarrow \infty$, this last term will vanish. However, if we apply (18) to determine the climate sensitivity from the CERES-observations, the change ΔN at TOA over the applied period is an essential component to correct for.

This relationship between changes in surface temperature ΔT_S, the sum of forcings in both LW- and SW-channels and a change in radiation imbalance ΔN as expressed in (18) is comparable to the expression $\lambda \Delta T_S = (\Delta F - \Delta N)$ as used by Lewis & Curry (2015) [10]. In their case, however, it was applied to determine λ, that they regarded contrary to this work, as an unknown parameter. From the observed temperature changes and their estimates about the total forcings in both the LW- and SW-channels over a long period of time, they estimated $1/\lambda \approx 0.5$ K/W/m^2. That analysis already falsifies the popular narrative of the AGW-hypothesis where all global warming is attributed to the increase in GHGs, in particular from the emission of CO_2 from the abundant use of fossil fuels. The analysis by Lewis & Curry yields considerably lower climate sensitivities than IPCC's *most likely* value of about 0.9 K/W/m^2 (see Section 6). But their value is still much larger than the 0.3 K/W/m^2 of the inverse of the Planck feedback parameter $-1/\lambda_{PL}$ of this work.

N.B. Given the fixed period used later on with $\Delta t = 23$ years, and the linear approximations of trends as drawn in Fig. 2, we can in expressions like (3) to (15) and (18), either apply the Δ-format for the period Δt or the $\Delta/\Delta t = d/dt$-format for these 23-years trends. For example: these 23-year trends are written as dF/dt or $d/dt(F_{SWC}+F_{LWC})$. True time dependent time-derivatives ($dt \rightarrow 0$) are expressed as $dF(t)/dt$. In the following analyses it must be clear what is being used.

8. Climate relaxation times

Equation (18) in Section 7 should be comparable to (17) with the sum of forcings in both radiation-channels $F_{TOT} = (F_{SWC} + F_{GHG})$. This implies that:

$$-\lambda_{PL}\frac{dT_S}{dt} = \frac{(N - N_0)}{\tau} \qquad (19)$$

This is equal to the logical expression $C\, dT_S/dt = (N - N_0)$ for the heating of the *mixed layer* with capacity C, a relaxation time $\tau = -C/\lambda_{PL}$ and assuming a homogeneous temperature T_S. That relaxation time τ is an important characteristic for the dynamics of climate change. Since the heat-capacity of our climate can in first order be regarded constant and coupled to the heat capacity of the *mixed layer*, the relaxation time becomes an indicator for the climate sensitivity. Based on the analysis of Ocean Heat Content (OHC)-data, Schwartz (2007) [11] concluded to $\tau = 5 \pm 1$ year resulting in a climate sensitivity of 0.3 ± 0.14 K/W/m^2, close to the $-1/\lambda_{PL}$ of this study.

In case one would still have doubts about such a result, a more general relation between relaxation time and climate sensitivity $1/\lambda$ would anyhow be: $\tau \sim 1/\lambda$. With the large climate sensitivities according to GCM-calculations as used by the IPCC and given in Section 6, we are automatically confronted with much longer climate relaxation times than we observe. Data from measurements by satellites since early 2000 as shown in Fig. 2, show large fluctuation in the major radiation components with time characteristics in the order of a few years, rather than decades. If we assume

the thickness of the ocean *mixed layer* to be 75 – 100 m, the heat-capacity C would be 3 – 4x10^8 J/m^2/K. The Planck feedback parameter λ_{PL} = – 3.3 W/m^2/K, would yield relaxation times of 3 – 4 years, close to Schwartz' analysis [11]. The observations in Fig. 2, support this outcome with fast variations in amplitude that are about as large as the total change over the entire period. In contrast, IPCC's high climate sensitivities $1/\lambda \approx 0.9$ K/W/m^2 would imply relaxation times of 9 – 12 years. With those relaxation times, the data related to the outgoing LW-channel in Fig. 2 such as LW_{UP} *and* LW_{OUT} would have rendered almost featureless.

With $\tau << \Delta t$, a short relaxation time helps in analyzing the "only" 23-years of CERES-data. As important in this analysis is, the almost constant time-derivative in anthropogenic forcing $dF_{GHG}(t)/dt$ equalling its long-term trend dF_{GHG}/dt over at least the last 4 decennia [12,18]. Absolute values in surface temperature do trail forcings, but in a *steady state* characterized by variables with constant trends, (16), (17) and (18) can be used without an explicit correction for time delays. Trends in surface temperature and radiation components can indeed be regarded as being constant over the 23-year period of the CERES-data, as illustrated in Fig. 2. So, in the next analysis applying period-averaged trends instead of absolute changes over longer periods of time is justified and sufficiently accurate. It is tempting to apply the above equations also to the "wiggles" seen in Fig. 2. That however, requires detailed knowledge about our climate's dynamics and could easily lead to unjustified conclusions.

9. Quantifying the feedback parameters α and γ

For a proper analysis of the CERES-data we need to quantify γ for the LW-channel and α for the sum of feedbacks in the SW-channel. The most important feedbacks according to IPCC AR6 [4] are Surface Albedo feedback, Cloud feedback, Water-vapor feedback and Lapse Rate feedback effects. The first two are acting in the SW-channel, and have according to IPCC AR6 a *most likely* value of +0.35 $\pm$ 0.25 and 0.42 $\pm$ 0.52 W/m^2/K for the Albedo and net Cloud feedback, respectively. Together they span quite a broad range from "no" feedback at all, to one as high as 1.5 W/m^2/K. The Albedo feedback must be positive, as melted snow due to higher temperatures will uncover less reflecting ground. G*reening* of our planet could also yield a positive change in Albedo, but it will be difficult to simply couple the observed greening either to the temperature change, or to an increase of CO_2. For clouds, the average warming or cooling effect is less obvious. In the Tropics more clouds certainly yield cooling *i.e.,* net negative feedback. SW_{IN} is there considerably larger than LW_{OUT} and therefore, more sensitive to cloud change. At higher latitudes, we can expect the opposite with $LW_{OUT} > SW_{IN}$.

In spite of all those uncertainties, these IPCC AR6 values are the only realistic estimates around, representing *state of the art* climate knowledge and modelling. Water vapor feedback in the LW-channel, also the largest feedback component of all, can be calculated with reasonable accuracy from spectroscopic data. Applying the Clausius-Clapeyron relation for the temperature dependent growth in moisture by the on-line climate model MODTRAN [3] yields values around 1.5 – 1.8 W/m^2/K for Water-vapor feedback, depending on the Relative Humidity. This is close to the *most likely* 1.30 $\pm$ 0.17 W/m^2/K from IPCC AR6 [4] where it is corrected for some negative feedback from the accompanying change in Lapse Rate for which MODTRAN cannot be tweaked through its user-interface. With λ_{FB} = 2.2 W/m^2/K from this work, but also as *most likely* value from IPCC AR6, this would leave about 0.9 W/m^2/K for the sum of Surface Albedo- and net Cloud feedback.

For estimating both α and γ we start here from this IPCC AR6 *most likely* value for Water-vapor + Lapse Rate (WV/LR) feedback of 1.30 W/m^2/K as argued above. The Cloud feedback is a net value as clouds influence both channels. For the division in its contributions to α and γ we use

their channel-specific Cloud Radiative Effects (CREs). CREs are derived from the difference between the radiation components at TOA in either a *clear-sky* or an *all-sky* situation. CERES data provides an SW-CRE and LW-CRE of 45.2 and 25.6 W/m^2, respectively. That implies that this net Cloud feedback parameter of +0.42 W/m^2/K contributes +0.97 W/m^2/K to α and –0.55 W/m^2/K to γ. The latter, when combined with the WV/LR feedback, yields a value for $\gamma \approx 0.75$ W/m^2/K. With $\lambda_{PL} = 2.2$ W/m^2/K as the result of (14) and also being IPCC AR6' *most likely* value, this implies that $\alpha \approx 1.45$ W/m^2/K for the feedback in the SW-channel.

Those estimates might be regarded as realistic. Deliberately, the margins of error in the quoted values have not been carried forward in these calculations. They would have allowed almost any combination of α and γ as long as they add up to 2.2 W/m^2/K. Therefore, we started from the Water-vapor feedback. With "only" $\pm$ 15 % error margin, it has by far the best-known value. We could have avoided that extensive analysis by simply stating: $\alpha = \gamma = 1.1$ W/m^2/K. Climate reactions are not SW- or LW-channel specific: unforced relaxation to equilibrium always runs along the process described by $N(t) - N_0 = \Delta N \exp(-t/\tau)$ (as in Fig. 1). Nature does not split up its reaction to regain equilibrium into SW- and/or LW-specific actions. It is supposed to always follow the most efficient path to do so, depending on the local situation. That must also be the case for natural fluctuations where deviations from equilibrium without explicit forcings can happen in either channel and at any place. The "internal forcings" that drive this rebalancing process contain either α or γ, or a combination of both as (3a) and (3b) show. If we cannot see any difference in reaction to regain balance between SW- and LW-specific fluctuations, it is hard to image that when averaged over all circumstances and all places, the outcome will value-wise not yield $\alpha \approx \gamma$. In the end, separate values only determine the most efficient distribution of feedback related forcings over both channels, not their total value. For the climate sensitivity, this choice does not matter at all, as λ_{FB} is determined by $(\alpha + \gamma)$. It just triggers an intriguing question about those channel-specific feedbacks: "are they indeed actively balanced by nature to keep $\alpha = \gamma = \lambda_{FB}/2$?". It might very well be possible with clouds as common factor in both channels and where nature creates clouds in endless varieties depending on local circumstances. In the following analysis of CERES-data, we apply both options: this "intuitive" $\alpha = \gamma$, as well as their estimates according to IPCC AR6 values, as derived above.

10. The applied CERES-EBAFv4.2 data

In Fig. 2 the major radiation data, measured under both *all-sky* and *clear-sky* conditions, from the CERES-EBAFv4.2 database [8] have been plotted as Centered Moving Annual Averages (CMAA) including trendlines. As for this analysis only trends are used, data are plotted with arbitrary offsets to capture all in one plot. This CERES-program started early 2000. The full *Solar*-flux S_0, the short wavelength reflected SW_{OUT} and the long wavelength emission LW_{OUT}, are from true radiation measurements by satellites at TOA, with good *all globe* coverage. SW_{IN} and the imbalance N are derived from these data. LW_{UP} and its related Black Body temperature T_S (or *vice versa*), must come from other sources. *Clear-sky* data are added to show the effect of clouds. However, one should be very careful to apply those data in calculations, except for the later-on used Cloud Radiative Effect (CRE). Those data as in Fig. 2 are derived from cloud-free areas embedded in the climate setting of an *all-sky* system. Obviously, true *clear-sky* measurements should come from a cloud-free Earth in (near) thermal equilibrium. But that climate does not exist.

Radiation measurements, in particular in the far-infrared wavelengths are in an absolute sense not better than within a few W/m^2. So, we cannot determine the absolute radiation imbalance *N(t)* with sufficient accuracy. The reference value used for the imbalance in the CERES data has been derived from trends in the Ocean Heat Content [13] with its own specific inaccuracies. Fortunately, absolute values are not important in the next analyses. Radiation trends as being used here, are much more trustworthy due to regular internal calibration of the sensors in the satellites. Trend values are of course dependent on the chosen period. But doing that consistently for multiples of 12-month periods (in Fig. 2: 2000/8 – 2023/7) allow for proper mutual comparisons.

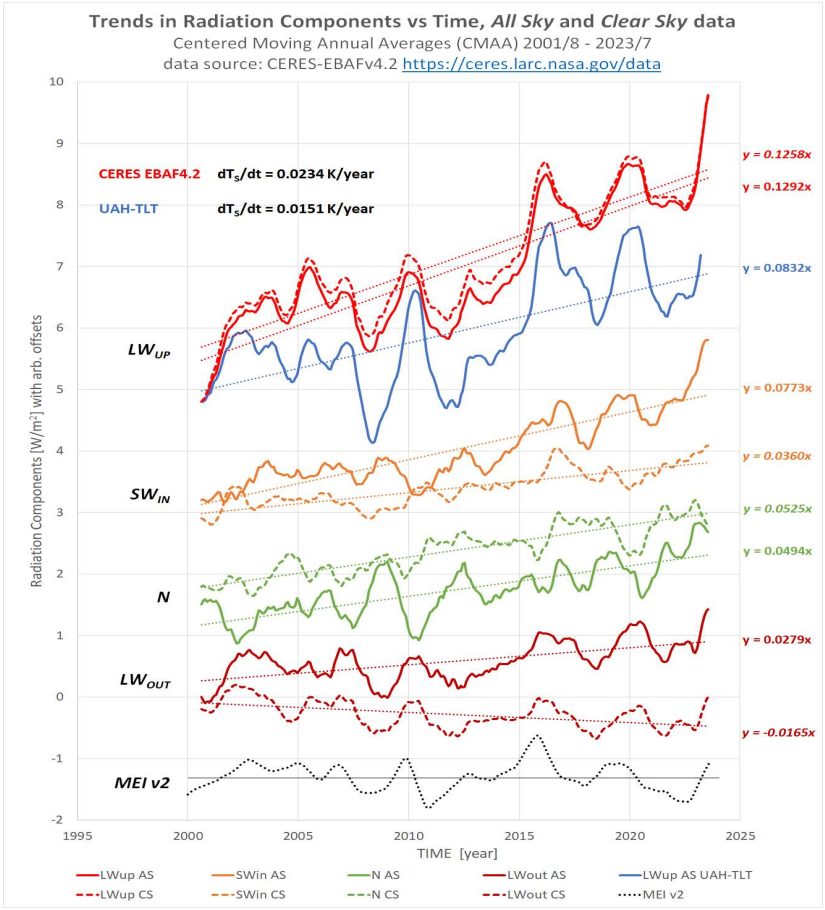

Figure 2. *Major radiation components, as Centered Moving Annual Averages of the monthly, globally averaged CERES EBAFv4.2-data 2000/8-2023/7, all-sky (solid lines) as well as clear-sky conditions (dashed lines, trends in italics) [8]. The UAH-TLT surface temperature series are transformed into LW_{UP}-data with λ_S = 5.52 W/m^2/K. The respective trends in W/m^2/year over the 23 full year period, are shown next to the curves and used in the text. One of the possible causes for the wiggles in the various components next to the forcings from the SW-channel, are El Niño/La Niña oscillations as represented by the CMAA of the ENSO-MEIv2-index [21] shown for comparison.*

There is no reason to dispute these CERES radiation data, except for those that are derived through atmospheric models with the applied temperature series, like the surface radiation components in the CERES database. In a recent update from CERES-EBAFv4.1 to v4.2 [8] the temperature data have been substantially changed with an increased trend over the applied period from about 0.019 to 0.023 K/year, matching now more or less the HadCRUTv5 temperature series [14]. The discrepancy with the also commonly quoted satellite-based UAH-TLT series [15] with a trend of around 0.015 K/year has therefore become rather large. This latter temperature series of the lower Troposphere with a real global coverage by satellites through measurements of Oxygen micro-wave-emission-bands of the atmosphere, is regarded by many as the most realistic trend in the

development of the global average temperatures [16]. Why NASA took the opposite route *i.e.*, towards the HadCRUTv5 ground-station-based temperature series, suffering from Urbanization effects [17] and with a lot of interpolations and adaptations via climate models (*e.g.* homogenization), is unclear. The following analyses are dependent on those trends, so for an objective assessment both are applied and differences discussed.

11. Analyzing the SW- and LW-channels

The main tool to analyze the SW-channel is (3b) in its trend-format. Independently from any choice of climate sensitivity $1/\lambda$, it "translates" the observed trend in SW_{IN} into a value for the trend dF_{SWC}/dt in the SW-channel forcing. For the latter, a value of 0.0516 W/m^2/year is calculated using the temperature trend dT_S/dt = 0.0234 K/year from CERES-EBAF4.2. The temperature trend of 0.0151 K/year of the UAH-TLT series [15], as also shown in Fig. 2, results in dF_{SWC}/dt = 0.0607 W/m^2/year. Those results are for $\alpha = \gamma$. All other results for different parameter sets, including those calculated for the IPCC-based α and γ values as from Section 9, are summarized in row #4 of Table 1.

Table 1. *Summary of the analysis of the CERES-radiation data as presented and discussed in Sections 11 & 12 (see text for details; rows #4, #5 and #9 are colored according to the relevant components in Fig. 2).* ***Row #6****, the sum $d/dt(F_{SWC} + F_{LWC})$ of the, via (3b) and (3a) derived forcing-trends in the respective SW- and LW-radiation channels,* ***should be compared to row #9****, the total climate forcing-trend dF_{TOT}/dt as calculated from the radiation imbalance N through the generic form of (18) ($\lambda dT_S/dt + dN/dt$). The first sum is insensitive to the applied climate sensitivity, whereas the derived dF_{TOT}/dt, highly depends on that choice. A similar comparison can be made when the calculated dF_{LWC}/dt is replaced by the forcing trend dF_{GHG}/dt (row #7). The last 2 blocks of 3 columns each, are the calculated forcings for the various options applied. The colored part contains the various numbers to compare, in particular the larger, bold printed ones. The last column (specific parameters in bold) scores by far the best in all aspects.*

	Parameter(s)	Units	Applied trends	Eq.#	Based on IPCC-AR6 $\lambda = (-\lambda_{PL} - \lambda_{FB})$			Based on this work $\lambda = (\lambda_S - \lambda_{FB})$		
1	**Climate sensitivity 1/λ**	K/W/m²			**0.90**			**0.30**		
2	**Temperature trend**	K/y	CERES 4.2 UAH-TLT		0.0234	0.0151	0.0234	0.0151	0.0234	**0.0151**
3	**Channel feedbacks**	W/m²/K	1.45 / 0.75 *vs* α = γ = 1.1	α / γ	1.1 / 1.1	1.45 / 0.75	1.45 / 0.75	1.45 / 0.75	1.1 / 1.1	**1.1 / 1.1**
4	**SW-channel: dF_{SWC}/dt**	W/m²/y	dSW_{IN}/dt = 0.0773	3b	0.0516	0.0554	0.0434	0.0554	0.0516	0.0607
5	**LW-channel: dF_{LWC}/dt**	W/m²/y	dLW_{OUT}/dt = 0.0279	3a	0.0753	0.0440	0.0835	0.0440	0.0753	0.0387
6	**$d(F_{SWC} + F_{LWC})/dt$**	W/m²/y	SW + LW forcings	3a+3b	***0.1269***	***0.0994***	***0.1269***	**0.0994**	***0.1269***	**0.0994**
7	**$d(F_{SWC} + F_{GHG})/dt$ dF_{GHG}/dt = 0.037**	W/m²/y	SW + GHG forcings	3b	0.0887	0.0925	0.0805	**0.0925**	0.0887	**0.0978**
8	Reference equation to determine total forcing			18	$\frac{dF_{TOT}}{dt} = \lambda \frac{dT_S}{dt} + \frac{dN}{dt}$					
9	**Imbalance N: dF_{TOT}/dt**	W/m²/y	dN/dt = 0.0494	18	***0.0754***	***0.0662***	***0.0754***	**0.0997**	***0.1274***	**0.0997**

A similar analysis for the LW-channel is done using (3a) which independently from any choice of climate sensitivity, "translates" the observed trends in LW_{UP} *and* LW_{OUT} into a value for the trend dF_{LWC}/dt in the LW-channel forcing. For $\alpha = \gamma$, and applying NASA's temperature trend of 0.0234 K/year, we calculate dF_{LWC}/dt = 0.0753 W/m^2/year. That value is very high compared to

the forcing rate of GHGs that we can expect. This $dF_{GHG}/dt \approx 0.037$ W/m^2/year can be derived from the trend in the logarithm of CO_2-equivalent concentration [18] of the AGGI-database [12] and the 3.9 W/m^2 ERF for doubling of the CO_2-concentration from IPCC AR6 [4]. With the UAH-TLT temperature trend of 0.0151 K/year we calculate $dF_{LWC}/dt = 0.039$ W/m^2/year, which seems to be more in line with the expected GHG-forcings. It would more or less eliminate the existence of "other" LW-channel forcings introduced as F_X in (3a). Certainly, a more likely result as GHGs are supposed to be the dominant factor for the changes in the LW-channel. With that argument, the high dF_{LWC}/dt value from applying NASA's temperature trend disqualifies that temperature series almost immediately. Again, all results for the various combinations used in analyzing the LW- channel are summarized in Table I, for this case in row #5.

12. Analyzing the Radiation Imbalance N

In analyzing the radiation imbalance N with (18), not the climate feedbacks α and γ, but the integral climate sensitivity $1/\lambda$ is becoming the important discriminator. Here we take the two clearly opposite options. Apply the Plank feedback parameter of –3.3 W/m^2/K (0.30 K/W/m^2 for the climate sensitivity) according to this paper as in (14), or accept IPCC's $\lambda = (-\lambda_{PL} - \lambda_{FB}) = 1.1$ W/m^2/K (0.90 K/W/m^2 as climate sensitivity used in Table 1). For both cases we can calculate the trend in the total forcing dF_{TOT}/dt by using the observed trend dN/dt.

As a next step, we compare that value for the calculated integral forcing to the sum of the two channel-specific forcings as derived in Section 11. In this case the various values for α and γ are of no interest. According to Section 11, the sum $dF_{SUM}/dt = (dF_{SWC}/dt + dF_{LWC}/dt)$ should be either **0.0994** or **0.1269** W/m^2/year, depending on the 0.0151 K/year or the 0.0234 K/year reference. Those sums are for the various parameter combinations summarized in row #6 of Table 1.

The bottom row #9 of Table 1 shows for the various parameter sets all the dF_{TOT}/dt-values as calculated with (18). The 0.0662 and 0.0754 W/m^2/year for those matching situations when using IPCC's climate sensitivity of 0.9 K/W/m^2 ($\lambda = 1.1$ W/m^2/K), are in both $\{\alpha,\gamma\}$-combinations about 40 % off from the sum of forcings $(dF_{SWC}/dt + dF_{LWC}/dt)$ based on the same data and parameters. Not a very convincing result which justifies the conclusion: **climate sensitivities as promoted by the IPCC cannot adequately replicate the CERES-data**.

With $1/\lambda = -1/\lambda_{PL} = 0.3$ K/W/m^2 according to this paper, we get **0.0997** and **0.1274** W/m^2/year for the two different temperature series. These numbers match almost perfectly with the "sum of forcings" of the separate channels (all in **bold** fonts above). The assumption that the LW-channel forcing should be close to the GHG forcing, also allows for an alternative comparison: $(dF_{SWC}/dt + dF_{GHG}/dt)$, the forcing trend in the SW-channel plus the (estimated) forcing trend for the GHGs. That alternative sum is shown in row #7 of Table 1. It makes clear why the UAH-TLT series, as earlier mentioned, is chosen here as our "preferred" temperature trend. Together with the Planck feedback parameter it simply yields the best possible match with the CERES radiation data. The differences are so small that this match cannot be the result of a lucky coincidence.

Now, we can also judge the differences between a choice for $\alpha = \gamma$ versus one with the IPCC AR6-based $\alpha = 1.45$ W/m^2/K and $\gamma = 0.75$ W/m^2/K. As stated, this difference is not in the total forcing dF_{TOT}/dt via the analysis of dN/dt, but in its distribution over the channels. As GHG-forcings most probably dominate the LW channel, the calculated forcing hinges on the value for γ. The two "green" colored columns in Table 1 for the "best" combinations with $1/\lambda = 0.3$ K/W/m^2 and $dT_S/dt = 0.0151$ K/year, are showing the differences for both options. From the CERES-data the derived value of 0.039 W/m^2/year for the $\alpha = \gamma$ options is not only closer, but even very close to the earlier mentioned $dF_{GHG}/dt \approx 0.037$ W/m^2/year. It gives credit to the choice for $\alpha = \gamma =$

$\lambda_{FB}/2$, but doesn't prove its correctness. It does indicate that the calculated value for γ = 0.75 W/m^2/K is most probably too small. When we stick to the WV/LR-feedback parameter of 1.3 W/m^2/K, it points to a net Cloud feedback parameter around 0.15 W/m^2/K in case $\alpha = \gamma$. This is considerably lower than the 0.42 W/m^2/K as being the center of the IPCC AR6 value range. As a consequence, this yields a larger Surface Albedo feedback parameter of about 0.65 W/m^2/K.

For a complete comparison, all results and important parameters are summarized in Table 1, including row #7 with $dF_{SUM}/dt = (dF_{SWC}/dt+dF_{GHG}/dt)$ as derived from (3b) and from the AGGI-database plus the ERF value for CO_2-doubling from IPCC AR6 [4].

13. Discussion

The analyses in Sections 11 and 12 show, that independent from the value for the GHG-forcing, the CERES-data for the trends in SW_{IN} and LW_{OUT} can only be quantitively matched with forcings in both SW- and LW-channel plus a climate sensitivity at, or close to the inverse of the Planck feedback parameter. With that climate sensitivity, even the various temperature trends applied, does not change this conclusion. This sufficiently proves the thesis of this paper that climate feedbacks are part and parcel of the Planck feedback parameter.

The major reason to reject the temperature series in NASA's CERES database is the high forcing in the LW-channel needed to justify its high trend in T_S. With NASA's choice, the measured LW_{OUT}-trend requires a forcing with $dF_{LWC}/dt \approx 0.075$ W/m^2/year, which is far off from $dF_{GHG}/dt \approx 0.037$ W/m^2/year as estimated for the forcing from Greenhouse gasses. Moreover, it is hard to imagine forcings in the LW-channel with a similar positive trend in strength as from GHGs. Changes in cloud area as seen in the CERES-data with a small decreasing trend, yields even a negative forcing trend in the LW-channel, making such positive forcing(s) *highly unlikely*. Most probably, ΔF_X as introduced in (3a) "for completeness", is either negligible or non-existing.

All combination of parameters, even including the high climate sensitivity promoted by the IPCC, ask for a substantial contribution from a positive forcing trend in the SW-channel in the order of 0.045 to 0.060 W/m^2/year. Often, the positive trend in SW_{IN} is attributed to the effect of Cloud- and Surface Albedo feedbacks. The sum of feedbacks in the SW-channel accounts for only 1.1*0.0151 ≈ 0.017, or in case α = 1.45 about 0.022 W/m^2/year in dSW_{IN}/dt. When just the temperature change due to GHG-forcings is considered, the related feedback effects in the SW-channel can only explain about 10 % of the observed trend in SW_{IN}. That debunks the myth that the observed growth in SW_{IN} is a by-product of GHG-forcings. As temperature dependent effects are considered to be part of the natural climate feedbacks, the source of this large SW-forcing has to be found in non-temperature related effects. For the SW-channel, that can range from effects in clouds, contrails, absorption or scattering in the atmosphere and/or from changes in surface absorption from a.o. urbanization, change of land use and natural greening or desertification. Or, as already mentioned in Section 7 related to (17), changes in N_0 are due to changes in the ocean.

14. Clouds and Albedo

CERES data also contain cloud area measurements with a 23-year trend of about –0.019 %point/year. With an average cloud area of 67 % and an SW-CRE of 45.2 W/m^2, this trend translates into a forcing trend in the SW-channel of about +0.013 W/m^2/year. That is by far not enough to explain the calculated SW-forcing trend dF_{SWC}/dt of 0.061 W/m^2 as given in Table 1. It is just about the expected effect from Cloud feedback in the SW-channel which we calculated

to be between 0.010 – 0.015 W/m^2/year, depending on the SW-channel specific Cloud feedback parameter. In fact, we must be happy with this observation. In case this cloud-area change could have explained the SW-channel forcing, the observed trend in the LW-channel would not match. Positive forcing in the SW-channel due to diminishing cloud-area, would have created a negative forcing in the LW-channel proportional to the ratio of LW- and SW-CRE of about 0.57. This dF_{SWC}/dt of 0.061 W/m^2/year would thus have induced a negative forcing dF_X/dt in the LW-channel of about –0.034 W/m^2/year. The calculated dF_{LWC}/dt of Table 1 (row #5) would then have pointed to a much larger GHG-forcing in the LW-channel than assumed. One can certainly question the exact figure for the strength of doubling the CO_2-concentration ΔF_{2xCO2}, but a substantially higher forcing trend from GHGs is *highly unrealistic* [18].

However, the average values for the respective CREs are not conclusive in ruling out major effects from clouds. As earlier mentioned, CREs are latitude sensitive due a changing ratio between SW_{IN} and LW_{OUT} from the Equator to the Poles. Cloud characteristics such as Top of Cloud (TOC) temperature and TOC-height, change with latitude as well. CREs calculated per percent-point cloud-change (% cc) averaged per degree latitude from the 1°x1°-gridded CERES-data, show around the equator a NET-CRE of about –0.15 W/m^2/%cc. At mid latitudes on the Northern Hemisphere this is about –0.45 W/m^2/%cc *i.e.*, a factor 3 larger. So, without changes in the total cloud area, changes in the lateral distribution are quite well capable to create substantial radiation imbalances. GHG-forcing trends of about 0.03 W/m^2/year, could simply be matched or compensated by 0.1 %cc/year cloud-exchange between mid-latitudes and Tropics. And those lateral changes of 2 %cc over the last two decades did occur as we can see in Fig. 3b.

Rather than to focus on cloud changes, it makes for the forcing in the SW-channel more sense to look to the Albedo change. In the end, it is the Albedo (and of course the Sun) that determines SW_{IN}. As the CERES data show, the Albedo of 0.291 has changed considerably since 2000, with a trend of –0.00023/year. Although less than 1 ‰ per annum, 340 W/m^2 averaged Solar constant S_0 creates *by definition* exactly this measured dSW_{IN}/dt = 0.0773 W/m^2/year. Of course, this value contains "everything" from the contributions which we can reasonably quantify as Surface Albedo- and Cloud feedback, to any other effect such as changes in cloudiness that affect the Albedo. Those "other effects" add up to the calculated SW-channel forcing with a trend dF_{SWC}/dt ≈ 0.061 W/m^2/year, or about 80 % of dSW_{IN}/dt. As the absorption of Sunlight at the surface is the determining factor in warming, a first contribution could come from the change in Surface Albedo.

Although direct Sunlight is for 2/3rd obscured by clouds, it will have significant effects on all absorbed light, and thus on Global Warming. It also can be the major cause of the relatively high slope dSW_{IN}/dt for the *clear-sky* measurements as displayed in Fig. 2. Unfortunately, we cannot easily distinguish Surface Albedo forcings from forcings due to changes in the radiation imbalance N_0 as determined by the oceans. Without a clear split up between both effects, translating these *clear-sky* data into an *all-sky* contribution is almost impossible. That Albedo changes are not evenly spread globally, is shown in Fig. 3. In its left-hand side panel (a), we show the latitude averaged CERES-data for the Albedo changes, at TOA as well as at the surface between 5-years averaged periods, 18 years apart. This difference is therefore a reasonable proxy for the effect after 18 years of the trends as shown in Fig. 2. We also show the latitude averaged SW_{IN}. The similarities are striking, but not one-to-one identical. Cloud area change, in the same way depicted in the right-hand side panel (b) of Fig. 3, might account for the differences. But we should not forget that the increase in the latitude averaged surface temperature is for about 60 % determined by this SW_{IN} profile. Cloud feedback as the supposed prime cause of cloud-area change is therefore mostly caused by SW_{IN}, not the other way around. It is clear from Fig. 3 that

the Northern Hemisphere suffers much more from heating through Albedo changes than anywhere else on the Globe. In particular, Western- and Southern Europe are exposed to a much higher Solar influx. For comparison with the effect from GHGs, we have added in both panels also the change in GHG-forcing over that period with a level of $\Delta F_{GHG} = 18*0.037 \approx 0.67$ W/m^2. That forcing must indeed be rather evenly distributed over the globe as CO_2 is a well mixed gas in our atmosphere. It makes clear that in the most urbanized areas of the world, forcing from the Sun ($\Delta F_{SWC} \approx 0.8\ \Delta SW_{IN}$) is considerably larger than forcing from the emission of Greenhouse gasses. This work is not denying Anthropogenic Global Warming through the emission of GHGs, but the IPCC narrative attributing all warming to it, is clearly not at all explaining the real issues.

The data in Fig. 3 for the Southern Hemisphere offer an interesting reference as it resembles almost a true "water-planet". The Albedo @ TOA has changed such that dSW_{IN}/dt is of the order of 0.05 W/m^2, close to the observed average global trend. However, also here without a significant change in Surface Albedo as observed on the Northern half. As stated earlier, changes in the global averages for N_0 and for the Surface Albedo are difficult to separate. However, for large area of ocean waters, that is different, as Surface Albedo changes from a water surface are not very likely. By lack of other options this implies that the majority of the forcings creating this growth in SW_{IN} on the Southern Hemisphere are related to changes in N_0 *i.e.,* changes in the oceans. There is no reason to expect that this will be different on the Northern Hemisphere.

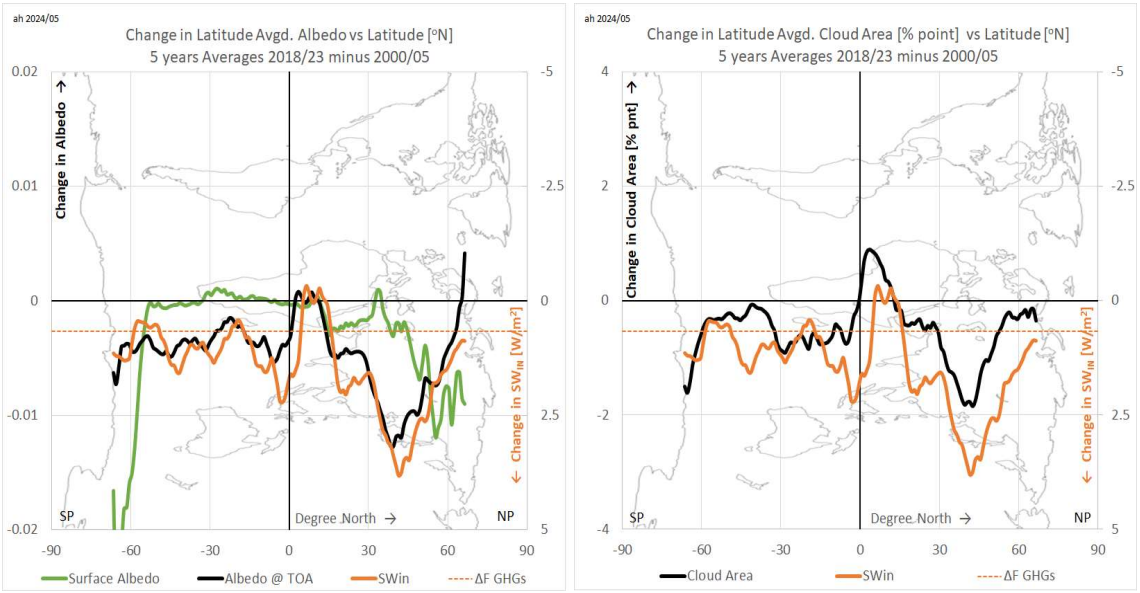

Figure 3a and b. *Changes over time for 1°-latitude averaged CERES-data showing Albedo at TOA and Surface (left-hand panel) or Cloud Area (right-hand panel) in comparison to the incoming Solar flux SW_{IN} (orange). Changes shown are obtained by subtracting 5-years averages for the periods 2018/8-2023/7 and 2000/8-2005/7. ΔSW_{IN} is shown "reversed", as a lower Albedo or less clouds yield a higher SW_{IN}. The 18-years change in the forcing from well-mixed GHGs of about 0.67 W/m^2, is shown (dashed) in relation with the forcings from the incoming Solar. For the Southern Hemisphere both are about equal in importance, but for the Northern Hemisphere the Solar forcing clearly dominates the observed warming trends/change. Data as shown are limited to the area between the two polar circles as the CERES-data during the polar nights, are not always complete/usable in deriving proper averages.*

The causes for the very large Albedo changes at mid latitudes on the Northern Hemisphere which are absent on the Southern part, are however less clear. Given the above, they are most likely related to land area. Explosive urbanization after WW II must certainly have affected surface absorption of Sunlight. Clean Air acts at the end of the last century in the industrialized Western World, might have had permanent effects as well. The closing of many coal-fired power plants

and transferring heavy industries to the Far East helped in reducing emissions of all sort. At the same time, it also led to a cleaner air and an increased brightening. Its overall net effect had most probably feed forward effects on warming. As we simply do not know that net effect, blaming fossil fuel emissions for all that warming since the '80-ies of the 20th century, offers an easy way out. As temperatures and CO_2 concentrations both are rising measurably fast, the AGW hypothesis sounds very plausible. Moreover, from a physics point of view, such a relation should also exist, as also shown here. Calling it "Global Warming", however, is simply misleading. Sold already for years as an undisputable "fact", nobody questions that statement anymore. This paper shows that it is even less than half of the truth. And how "global" is that warming really?

14. A final check on Global Warming

In Section 3, the proposed concept behind the analysis of the CERES-data had been worked out with the expressions in (3a) and (3b). Those ended up in (15) or (18) by adding dynamics. The essence of this all, just describes how our climate is continuously in motion to maintain the overall radiation balance expressed by the basic equation $SW_{IN} = LW_{OUT}$ (for simplicity the offset N_0 in relation to the OHC-trend is left out). In that balancing act, the surface and with that, the surface temperature T_S is the link between both radiation channels. It can be made visible by the CERES data through this balance equation in its rudimentary form in **bold**:

$$\Delta LW_{UP} = \boldsymbol{\lambda_S \Delta T_S = \Delta SW_{IN} + \Delta G} = \Delta F_{TOT} + \lambda_{FB} \Delta T_S \qquad (20)$$

The left-hand side equality is according to the S-B relation. The right-hand side is simply the sum of (3a) plus (3b) *i.e.*, the sum of all primary forcings and all their climate feedbacks. As discussed in the earlier analyses, feedbacks are part of both ΔSW_{IN} and ΔLW_{OUT}, and only through (3a) and (3b) we could address them individually. Checking (20) against the CERES data can be done without that kind of knowledge, as we simply plot ($\Delta SW_{IN} + \Delta G$) against ΔT_S. This is shown in Fig. 4 in a less commonly used approach. The ratio between the color scales for both plots equals $\lambda_S = 5.5$ W/m^2/K, so that the colors in both maps match when (20) holds. Differences between the two pictures are the local imbalances, independent from the choice for the temperature series [19]. That choice might influence both pictures in an equal way, but it is not expected that the lateral distribution for both series will be much different. The overall similarity will anyhow remain striking. More so, as this analysis of the radiation balance at TOA seems to works more local than

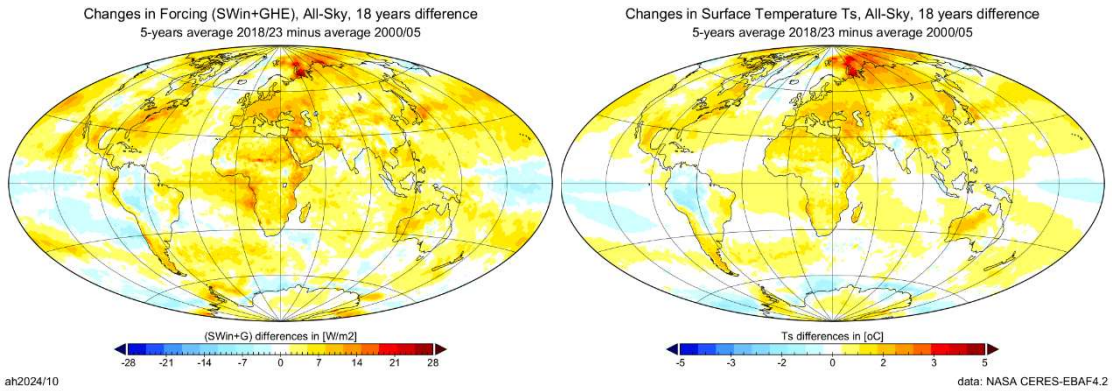

Figure 4. *Changes over time for the gridded CERES-data by subtracting 5-years averages, 18 years apart (same periods as in used in Fig. 3). On the left-hand side changes are shown in the sum of incoming Solar flux SW_{IN} and the Greenhouse Effect G ($\Delta SW_{IN} + \Delta G$), representing the sum of all climate forcings ΔF_{TOT} and climate feedbacks $\lambda_{FB}\Delta T_S$. The right-hand side features the changes in the surface temperature ΔT_S. For easy comparison, color scales are adjusted according to the Surface feedback parameter of about 5.5 W/m^2/K according to (20) (see Section 4 and definition through (9)).*

anticipated. Winds and wind patterns should play an important role in the surface temperatures by lateral movements of heat. Not much of that is seen in Fig. 4 other than that some heat generated around the Equator apparently ends up at higher latitudes.

Anyhow, Fig. 4 shows that "Global Warming" is clearly less global than often suggested. Moreover, the majority of warming ($\geq$ 60 %) is due to the forcings from incoming Solar, leaving less than 40 % for the warming from Greenhouse gasses. These prime forcings in the SW-channel due to changes in the Albedo, are from a combination of local changes in the atmosphere, changes at surface level and from changes in the oceans. With their very constant, slowly increasing level, forcings form well-mixed Greenhouse gasses must form a kind of evenly spread "background level". We also see areas with a clear trend in cooling, implying that GHGs cannot play a too dominant role in the observed warming. Nevertheless, IPCC maintains its CAGW-narrative, and climate alarmists will simply shuffle those "*other forcings*" automatically under the heading "*anthropogenic origin*". This might even be partially true, as effects from urbanization or more in general, change in land use do affect the important Surface Albedo. However, those effects are most probably non-reversible, and certainly not vanishing with "Net-Zero emission" initiatives. Also effects from melting of snow and ice from feedbacks, often "sold" as long-term effects from CO_2-emissions, are in fact highly over-emphasized. Sea ice coverage and glacier length are also part of long term natural cycles, as history has shown. Melting Polar caps are frequently used for scaring people with the effects of this GHG-related "Catastrophic Global Warming". Climate-model based predictions of ice free polar waters well before 2020, have meanwhile proven to be wrong. Even twice as much warming by Solar forcings added to the effect from Greenhouse gasses, could not melt it all.

Changes in the oceans affecting N_0, are more difficult to link to anthropogenic causes. As long as we do not know "what" exactly is causing these "*other forcings*", we will not know "how" to counter them. Only when understood, we can address the questions "is it needed?", "is it possible?" and most importantly "is it doable and at what price?". From the ratio between SW- and LW-channel forcings as shown in Table 1, we must conclude that from the total warming we experienced since 2000, just 40 % can be blamed on GHGs, in particular CO_2 emissions from burning fossil fuels. As this study shows, it is not the absolute amount, but the trend we should watch in forecasting future warming. The GHG contribution from a forcing that has shown already a stable trend for 40 years, will soon start to decline. Fossil emissions are in first approximation, proportional to the size of the world population. Growth thereof is coming to an end by 2060-2070. Together with "Net-Zero"-drives, it will bring the growth in emissions to an end. But even if we could achieve $dF_{GHG}/dt = 0$ soon, we could still be confronted with this present 0.061 W/m^2/year from increasing Solar radiation. This warms our planet anyhow, with a rate of dT_S/dt = 0.061/3.3 ≈ 0.02 K/year, or with 2 ºC/century still well above the Paris-agreement. And for how long will that continue?

Fortunately, given some historic perspective, we should not be too scared. The well known Central England Temperature (CET) series based on "real" thermometer-measurements since 1659 [20] shows several long-lasting, pre-industrial *i.e.,* "natural" fluctuations with warming- and cooling rates as high as 0.5 ºC/decennium. Obviously higher warming- (but also cooling) rates than we experience today. Fortunately, all those "natural" disturbances of our climate also stopped after 3 to 5 decennia and turned into the opposite direction. It is therefore not unthinkable that also these Sun-driven, *natural* phenomena of warming we experience today, will end not too long from now.

14. Conclusions

1. This analysis shows that the argument, of climate feedbacks as used by the IPCC to justify the high climate sensitivity values as derived from GCMs and which are the foundation under their alarmistic messages about the danger of future warmings due to CO_2 emissions, is flawed.
2. Climate feedbacks exist, even with a total value as quoted in IPCC's latest AR6 report. But as shown here, climate feedbacks are already part and parcel of the Planck feedback parameter λ_{PL} and cannot change our natural climate sensitivity – $1/\lambda_{PL}$ a second time.
3. Energy Balance equations as derived in this work, are fully supported by experimental data from NASA's CERES program or *vice versa*, the CERES-measurements of the radiation components at TOA can be trend-wise fully explained by these Energy Balance equations. This experimental evidence clearly demonstrates the validity of $-1/\lambda_{PL}$ as our climate's sensitivity to radiative forcings.
4. Our climate sensitivity in terms of the Equilibrium Climate Sensitivity ECS is therefore around 1 °C for $2xCO_2$; about a factor of 3 smaller than the ECS-values of 2.5 – 4 °C and more. These high values are the results of GCMs and applied by the IPCC in their projections for the catastrophic effects of anthropogenic global warming (CAGW).
5. This analysis shows that based on "best fits" to all radiation data and the reasonably well-known forcings from GHGs, the UAH-TLT temperature series with a trend of 0.015 K/year are much more credible than the 0.023 K/y series as used by NASA in their processing of CERES measurements or from the HadCRUTv5 series. High warming trends might be tuned to better fit the AGW narrative and the IPCC-preferred value for climate sensitivity in a GHG-only scenario. With a much smaller sensitivity and SW-channel forcings at play, this analysis shows that those high warming rates do not match the CERES radiation data in combination with the GHG-forcing trends known.
6. From the analysis of CERES data, it is clear that the largest forcing(s) occur in the SW-channel. They are adding about 80 % to the observed growth-trend in the incoming Solar flux SW_{IN}. Cloud area changes due to the Cloud feedback effect by GHG-induced warming can only explain around 10 % of the observed growth rate.
7. Albedo changes due to a variety of phenomena have to explain these SW-channel forcings responsible for the majority of the observed dSW_{IN}/dt. We cannot exclude that part of these Albedo changes have an anthropogenic origin such as urbanization and change of land use. Southern Hemisphere data indicate, however, a dominant effect from forcings linked to changes in the oceans. Without clear causes linked to human activities, we have to regard theses forcings as being primarily due to "natural" fluctuations in our climate.
8. The here determined forcing trends from the CERES data indicate in average, a 3:2 ratio for the amounts of warming that can be attributed to these "natural" Solar-related effects *versus* the effects from Greenhouse gasses. In practical terms: **from the 0.35 °C global warming since 2000, 0.14 °C is caused by Greenhouse gasses primarily from CO_2-emissions, but the majority of it, 0.21 °C comes from the increased Sunshine**. With the observed Albedo changes, in particular above land at the Northern Hemisphere, these ratios can easily become as high as 5:1. In most of the Southern Hemisphere this ratio is closer to 1:1 depending on data over oceans or land.

9. All conclusions above imply that in addition to these unrealistically high climate sensitivities, IPCC's claims that natural causes are negligible, are also far from reality. Analyses in this work all point to the same conclusion: the AGW hypothesis, nowadays often referred to as "Climate Change", with an alarmistic message about high warming rates caused by burning fossil fuels, is for whatever reason, highly inflated. Part of that inflation is apparently due to the outcome of sophisticated Global Circulation Climate Models projecting way too high warming rates from anthropogenic forcings. Future scenarios of an unlivable planet unless we stop burning fossil fuels and end emitting CO_2 immediately, are in IPCC's own terminology: "*highly unlikely*".

Funding: No funding received, nor asked for**.**

Guest Editor: Stein Storlie Bergsmark, **Reviewers**: Anonymous

Comment of Editorial Board: It is the philosophy of this journal, to give authors a platform for new approaches and their interpretations, even when they are in contradiction to established climate science considerations. This also holds, when one of the reviewers or a member of the Editorial Board sees a conflict in the author's approach. Such a contribution is accepted for publication, as long as it is in agreement with fundamental physical principles, but it is classified as Debate Paper, to point to an extraordinary interpretation or result of a paper, worthy of discussion.

References

1. Rasool S. & Schneider S. (1971), *Atmospheric Carbon Dioxide and Aerosols: Effects of Large Increases on Global Climate*, Science, Vol. 173, 138-141 https://doi.org/10.1126/science.173.3992.138
2. Van Wijngaarden W. & Happer W. (2021), *Relative Potency of Greenhouse Molecules*, https://doi.org/10.48550/arXiv.2103.16465
3. MODTRAN on-line climate model: https://climatemodels.uchicago.edu/modtran/
4. Climate Change (2021), *The Physical Science basis IPCC WG 1*, 6th Assessment Report Technical Summary TS3.2 pg.93-97, http://www.ipcc.ch/report/ar6/wg1
5. Sherwood S.C. *et al* (2020), *An Assessment of Earth's Climate Sensitivity Using Multiple Lines of Evidence*, Reviews of Geophysics, Vol. 58, 1-92, https://doi.org/10.1029/2019RG000678
6. See for instance the on-line climate course from the University of Albany NY, https://www.atmos.albany.edu/facstaff/brose/classes/ATM623_Spring2015/Notes/index.html
7. Raval A. & Ramanathan V. (1989), *Observational determination of the greenhouse effect*, Nature, Vol. 342, 758-761, https://doi.org/10.1038/342758a0
8. NASA-CERES *project*, https://ceres.larc.nasa.gov/data.
9. Frank P. (2019), *Propagation of Error and the Reliability of Global Air Temperature Projections,* Front. Earth Sci. 7:223, https://www.frontiersin.org/articles/10.3389/feart.2019.00223/full

10. Lewis, N. & Curry, J. (2015), *The implications for climate sensitivity of AR5 forcing and heat uptake estimates.* Clim Dyn **45**, 1009–1023 https://doi.org/10.1007/s00382-014-2342-y

11. Schwartz, S. E. (2007), *Heat capacity, time constant, and sensitivity of Earth's climate system,* J. Geophys. Res., 112, https://doi.org/10.1029/2007JD008746

12. https://data.giss.nasa.gov/modelforce/ or in more detail: https://gml.noaa.gov/aggi/aggi.html

13. https://www.ncei.noaa.gov/products/climate-data-records/global-ocean-heat-content

14. https://www.metoffice.gov.uk/hadobs/hadcrut5/data/HadCRUT.5.0.2.0/download.html

15. https://www.nsstc.uah.edu/climate/index.html

16. For a good overview of the various temperature trends, their quality, pro's/con's, etc., see https://www.climate4you.com/ "global temperatures"

17. Spencer R. & Christy J. (2024), *Urban Heat Island Effects in U.S. Summer Surface Temperature Data, 1880-2015,* submitted to JAMC in October 2023. For content see: https://www.drroyspencer.com

18. With regard to the forcing and forcing trend from all GHGs, there can hardly be any doubt about the measurements of the concentration since around 1960 [22]. For this analysis, the concentrations in GHGs are summed as CO_2-equivalent: C_{GHG} [12]. For this analysis, the trend is important which is described by $d/dt(ln[C_{GHG}]) = 0.0066$ [ppm], a value that describes the trend since 1980 very well. The forcing trend $dF_{GHG}/dt = 0.0066/\ln 2 * \Delta F_{2xCO2}$. Various values for ΔF_{2xCO2} exist: IPCC's estimated ERF value of 3.9 W/m^2 [4], 3.0 W/m^2 form modern calculations [2], or the experimental value of 2.65 W/m^2 from 17 years of satellite-based spectroscopic data [23]. These latter two values are for cloudless *clear sky* situations. It is expected that *all sky* values for ΔF_{2xCO2} will be even lower, as CO_2 under clouds will hardly influence LW_{OUT} in a direct way.

19. Unfortunately, there is no public access to the gridded data for the UAH-TLT series. Although with a different average trend, they are not expected to have a very different lateral distribution globally than temperatures from the CERES-dataset.

20. https://www.metoffice.gov.uk/hadobs/hadcet/

21. https://psl.noaa.gov/enso/mei/

22. NOAA Global Monitoring Laboratory: https://gml.noaa.gov/ccgg/trends/

23. Rentsch C. (2021), *Radiative forcing by CO_2 observed at top of atmosphere from 2002 to 2019 (v2)*, https://doi.org/10.48550/arXiv.1911.10605 or https://essopenarchive.org/users/283962/articles/607772-radiative-forcing-by-co-observed-at-top-of-atmosphere-from-2002-2019

Appendix A

Climate feedbacks and the Planck feedback parameter

Our climate system is a so-called "setpoint-controller" where the incoming- and outgoing radiation fluxes are being matched by various internal changes affecting a.o., our planetary albedo, the amount of moisture in the atmosphere and last but not least, the surface temperature. In today's climate science with its prime focus on the increasing temperature as a result of our atmosphere's growing CO_2-concentration linked to the abundant burning of fossil fuels, this complex control-process is often simplified by using a control scheme as in Fig. A1. It depicts an operational amplifier with an open-loop gain (or better: transfer-function) $-1/\lambda_{PL}$ and a temperature-driven feedback-loop through a transfer-function λ_{FB}. A radiative forcing ΔF at *TOA* from increasing CO_2-levels, thus results in a change ΔT_S in the surface temperature of our planet. Without any feedbacks ($\lambda_{FB} = 0$), we get $\Delta T_S = -\Delta F/\lambda_{PL}$ and with feedbacks a temperature increase $\Delta T_S = -\Delta F/(\lambda_{PL} + \lambda_{FB})$. This relation is identical to equation (11) as discussed in this paper. For the *closed-loop* system, it is clear that in case $\lambda_{FB} > 0$ *i.e.,* a positive feedback "amplifies" the forcing effect, thus resulting in a larger ΔT_S than without.

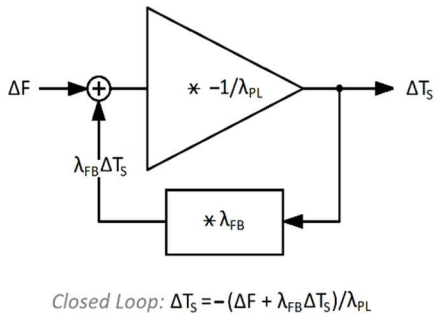

Figure A1. *The often-used electronic analogon for our climate's surface temperature reaction ΔT_S to an external forcing ΔF at TOA. The main process, or "open-loop" gain is characterized by the transfer function $-1/\lambda_{PL} \approx 0.3$ W/m²/K. The sum of the various climate feedbacks $\lambda_{FB} \approx 2.2$ W/m²/K are fed back to the input via a feedback-loop. This translates the output temperature change into a forcing $\lambda_{FB}\Delta T_S$, which is then added to the input ΔF. Accordingly, this circuit gets a "closed-loop" gain of $-1/(\lambda_{PL} + \lambda_{FB}) \approx 0.9$ W/m²/K, suggesting a 3x higher climate sensitivity than without feedbacks. However, this is the result of erroneously applying the Planck feedback parameter as the "open-loop" gain of our climate.*

This amplification of climate feedbacks increasing the climate sensitivity depends however, also on the *open-loop* gain of this op-amp. In standard climate science literature, the *open-loop* gain used, is the inverse of the Planck feedback parameter: $-1/\lambda_{PL}$. That stems from the definition of the Planck feedback parameter. This expresses the reaction of the surface temperature T_S on a change in the radiation imbalance N at TOA (Top of the Atmosphere), under the condition that "nothing else changes", *i.e.* $1/\lambda_{PL} = -\partial T/\partial N$ in order to assure that no feedbacks can influence this particular climate sensitivity. That should make $-1/\lambda_{PL}$ by definition the *open-loop* gain of this climate-analogon as in Fig. A1. One derives λ_{PL} from a forcing ΔSW_{IN} by a small increase in the Solar constant. In that way, we don't change anything to our climate as for instance adding extra CO_2 would do. It is then easily shown for this particular case that one can express the temperature change as $\Delta T_S = -\Delta SW_{IN}/\lambda_{PL}$, with the Planck feedback parameter $\lambda_{PL} = -4\,SW_{IN}/T_S$.

However, it is an illusion to think that feedbacks do not act in this, as "*open-loop*"-declared climate. Indeed, "we" did not change anything to the system, but to keep thermal equilibrium, our climate-system did change itself in accommodating ΔT_S. As a matter of fact, *a temperature change will always lead to a redistribution of water* in our climate system. That includes: changing the amount of water-vapor in the atmosphere, the amount and distribution of clouds, the Lapse Rate and the ice and snow cover. These are our climate feedbacks!! **Any climate system containing condensable Greenhouse gasses as water-vapor, can (and will) never reach equilibrium after a change in temperature, without internal changes**. So, this model climate system in which "nothing changes" doesn't exist. Declaring this $-1/\lambda_{PL}$ to be the *open-loop* gain of our climate control-system as depicted in Fig. A1, is simply *wrong and totally misleading*. This climate analogon in Fig. A1 looks convincingly "logic", but has no meaning without a proper choice for the *open-loop* climate response.

Our climate system's *open-loop* gain is nothing more than that of a bare "dry" Earth without an atmosphere. Any other climate system with water in its various forms of aggregation, will always show feedbacks. In essence, feedbacks "constitute" our climate. Accordingly, Fig. A1 can be "fixed" by applying the *open-loop* response of a bare planet characterized by the Stefan-Boltzmann feedback $1/\lambda_S$. The *closed-loop* gain is then given by $1/(\lambda_S - \lambda_{FB})$. Through the relation $-\lambda_{PL} = (\lambda_S - \lambda_{FB})$ *as derived in Section 4,* $\Delta T_S = \Delta F/(\lambda_S - \lambda_{FB}) = -\Delta F/\lambda_{PL}$ *as in equation* (8). But now under the practical condition that "we" do not change anything in the climate system.

In a more generic way this explanation is validated in this paper using the scenario in section 4 describing the effects from a step-wise external forcing going from **one thermal equilibrium to the other thermal equilibrium**. That leads to the conclusion that **the inverse of the Planck feedback parameter is our universal climate sensitivity to forcings that also accounts for all climate feedbacks related to the vast amount of water in our climate.**

OPEN ACCESS

Klimarealistene
Vollsveien 109
1358 Jar, Norway
ISSN: 2703-9072

Correspondence:
zak@chemi.muni.cz

Vol. 4.2 (2024)
pp. 114-116

Question About 280 ppm CO_2 Background Level

A Note to the Comment of F. Engelbeen

Zdirad Žák

Department of Chemistry, Masaryk University

Brno, Czech Republic

Abstract

The late Ernst-Georg Beck wrote a rather controversial but very interesting article titled *"Reconstruction of Atmospheric CO_2 Background Levels since 1826 from Direct Measurements near Ground* ", published in this journal (Beck, 2022) that raised several comments, the most extensive being from Engelbeen (2023). However, he repeats the same objections (Engelbeen 2007) he had already raised to Beck's (2007) first paper. On the other hand, he missed some logical consequence of his arguments.

Keywords: Chemical analysis, historical CO_2 levels

Submitted 2024-06-10, Accepted 2024-07-22. https://doi.org/10.53234/SCC202407/20

1. Introduction

In his comment to E.-G. Beck's paper (Beck 2022) Ferdinand Engelbeen raises the same objections as he did to the first paper of E.-G. Beck,"180 Years of Atmospheric CO_2 Gas Analysis by Chemical Methods". He objects namely to reliability of historical chemical analyses and to an existence of increased CO_2 levels in 1940 – 1943. This latter objection has already been commented by others (Solheim 2023). Surprisingly, F. Engelbeen does not comment the outcome of Beck's paper – the reconstruction of historical CO_2 levels.

2. Chemical Analysis

Chemical analyses may not be the most sensitive procedures, but they are definitely reliable and give true values. They determine directly the substances (by weighting, titration etc.) while instrumental methods, often very sensitive, determine the substances from their properties – absorption, emission of a radiation etc. However, this objection of F. Engelbeen makes no sense at all – until to the sixties chemical methods were the only available means of analysis. On the other hand, F. Engelbeen has not realized that doubting reliability of chemical analysis may have an interesting logical consequence: If historical chemical analyses of CO_2 levels are not reliable, then the values used by G. S. Callendar (Callendar 1940, 1958) to determine a pre-industrial concentration of atmospheric carbon dioxide are also unreliable and, as a consequence, the Callendar's value of 290 ppm (today 280 ppm) cannot be true!

3. Reconstruction of historical CO_2 levels

What surprises me the most, is the lack of any comment to the results of Beck's reconstruction of

CO_2 levels in the span of 134 years 1826 – 1960. The results are summarized in the table reproduced from Beck 2022:

Table 11. Annual CO_2 MBL estimations from 1826 to 1960 from direct measurements

1	2	3	1	2	3	1	2	3	1	2	3	1	2	3
1826	364.50	72.90	1856	335.20	33.52	1886	299.00	8.97	1916	323.40	9.33	1946	336.00	47.04
1827	359.00	71.80	1857	337.00	33.70	1887	302.80	9.08	1917	321.00	10.20	1947	338.00	47.32
1828	358.00	70.80	1858	335.20	33.35	1888	300.00	9.00	1918	317.00	10.46	1948	328.40	45.98
1829	339.00	67.80	1859	333.50	33.50	1889	300.80	6.02	1919	320.20	10.44	1949	316.00	9.48
1830	339.90	67.98	1860	331.80	33.30	1890	302.40	6.05	1920	323.40	10.43	1950	308.85	9.27
1831	340.80	102.24	1861	330.10	33.10	1891	308.10	9.24	1921	305.80	3.07	1951	314.50	9.44
1832	341.70	102.51	1862	328.40	32.90	1892	311.30	9.34	1922	289.40	2.90	1952	314.50	6.29
1833	342.60	102.78	1863	326.70	32.70	1893	310.00	6.30	1923	305.10	3.02	1953	318.90	6.36
1834	343.50	103.05	1864	325.00	32.50	1894	317.00	9.51	1924	330.00	3.20	1954	321.90	6.44
1835	344.40	103.32	1865	310.00	31.00	1895	305.00	9.15	1925	321.30	3.18	1955	318.80	6.38
1836	345.30	103.59	1866	301.20	9.04	1896	313.80	9.41	1926	321.90	3.22	1956	320.50	6.41
1837	346.20	103.86	1867	300.00	9.00	1897	312.00	9.36	1927	327.00	5.89	1957	320.20	6.43
1838	347.10	104.13	1868	298.00	8.94	1898	317.30	9.52	1928	327.00	6.54	1958	318.40	6.37
1839	348.00	174.00	1869	290.00	8.70	1899	313.60	9.41	1929	328.00	6.56	1959	317.80	6.36
1840	347.00	173.50	1870	291.00	8.73	1900	307.50	9.23	1930	328.00	6.56			
1841	341.50	170.75	1871	300.00	9.00	1901	311.50	9.35	1931	329.25	6.58			
1842	336.00	168.00	1872	313.90	9.42	1902	305.90	9.18	1932	326.40	4.90			
1843	325.00	162.50	1873	311.00	9.33	1903	306.50	9.19	1933	328.00	4.89			
1844	328.50	164.25	1874	317.50	9.52	1904	305.50	9.17	1934	331.00	4.96			
1845	332.10	166.05	1875	324.00	9.72	1905	307.00	9.21	1935	357.00	5.36			
1846	335.60	167.80	1876	311.00	9.33	1906	306.00	9.18	1936	349.50	6.99			
1847	339.30	169.65	1877	298.00	8.94	1907	307.10	9.23	1937	354.00	7.08			
1848	319.90	63.98	1878	303.50	9.11	1908	306.50	9.26	1938	354.00	7.08			
1849	330.00	66.00	1879	309.90	9.30	1909	303.30	7.75	1939	382.40	5.74			
1850	330.00	66.00	1880	300.00	9.00	1910	307.80	7.72	1940	376.50	5.65			
1851	323.60	64.72	1881	309.00	9.27	1911	308.20	7.69	1941	376.00	5.64			
1852	325.30	65.06	1882	312.00	9.36	1912	318.50	15.21	1942	379.50	15.18			
1853	328.30	65.66	1883	312.00	9.32	1913	329.00	9.24	1943	383.00	15.32			
1854	331.60	66.32	1884	312.00	9.36	1914	327.15	9.35	1944	367.30	14.69			
1855	333.50	66.70	1885	303.50	9.11	1915	325.30	9.46	1945	352.00	14.08			

1: year; 2: CO_2 MBL estimation; 3: ±error (ppm) of method

As follows from the table, only 6 CO_2 concentrations have values less than 300 ppm, 29 have 300 - 310 ppm, 57 have between 310 – 320 ppm, and 45 have more than 320 ppm. And, moreover, the values hold a nearly flat level with only random variations, except higher levels (>340ppm) before 1840 and a peak 1935-1945 (>350ppm). The level 1826-1900 is 322.67 and 1901-2000 is 331.38 ppm, which is a growth rate of only 2.6%.

Callendar (1940,1958) published two papers summarizing some historical data of carbon dioxide levels. The data published in 1940 (Callendar 1940) give an average of 300 ppm, the data published in 1958 (Callendar 1958) yield an average of 291 ppm for the 19th century values and 322 ppm for the 20th century, joined average being 307 ppm. Both concentrations 300 ppm and 307 ppm fit well with Beck's findings.

Now an important question arises. Has not already come the time to change our mind about 280 ppm?

Co-Editor: Prof. J.-E. Solheim.

References

Beck, E.-G. 2007: 180 Years of Atmospheric CO_2 Gas Analysis by Chemical Methods, Energy and Environment, Vol .18, Issue 2, pp. 259-282
https://doi.org/10.1177/0958305X0701800206

Beck, E.-G. 2022: Reconstruction of Atmospheric CO_2 Background Levels since 1826 from Direct Measurements near Ground, Science of Climate Change, Vol 2.2. pp. 148-211
https://doi.org/10.53234/scc202112/16

Callendar, G. S. 1940: Variation of the amount of carbon dioxide in different air currents, Quart. J. of the Meteor. Soc. 66 (1940), 395-400.

Callendar, G. S. 1958: On the amount of carbon dioxide in the atmosphere. Tellus 10, 243-248. https://doi.org/10.3402/tellusa.v10i2.9231

Engelbeen F. 2008: Historical CO_2 measurements compiled by the late Ernst Beck, http://www.ferdinand-engelbeen.be/klimaat/beck_data.html

Engelbeen, F. 2023: About Historical CO_2 Levels. Discussion of Direct Measurements near Ground since 1826 by E.-G. Beck, Science of Climate Change Vol. 3.2 (2023), 190-208, https://scienceofclimatechange.org

Solheim, J.-E. 2023: More Comments to Engelbeen's Discussion Paper. Science of Climate Change, Vol. 3. pp. 219-222
https://doi.org/10.53234/SCC202304/22